THE UNIVERSITY OF CHICAGO

TOPOLOGICAL PHASES AND EXACTLY SOLUBLE LATTICE MODELS

A DISSERTATION SUBMITTED TO
THE FACULTY OF THE DIVISION OF THE PHYSICAL SCIENCES
IN CANDIDACY FOR THE DEGREE OF
DOCTOR OF PHILOSOPHY

DEPARTMENT OF PHYSICS

BY
CHIEN-HUNG LIN

CHICAGO, ILLINOIS
DECEMBER 2015

To my parents

TABLE OF CONTENTS

LIST OF FIGURES vii

LIST OF TABLES ix

ACKNOWLEDGMENTS x

ABSTRACT xi

1 INTRODUCTION 1
  1.1 Gapped quantum phases 1
  1.2 Topological phases 2
  1.3 Symmetry protected topological phases 4
  1.4 Exactly soluble lattice models 6
  1.5 Overview of the thesis 8

2 2D TOPOLOGICAL PHASES AND EXACTLY SOLUBLE LATTICE MODELS 11
  2.1 Introduction 11
  2.2 Summary of results 14
    2.2.1 Construction of lattice models 14
    2.2.2 Braiding statistics and Chern-Simons description 15
    2.2.3 Characterizing the realizable phases 16
  2.3 String-net models 17
    2.3.1 General string-net models 17
    2.3.2 Abelian string-net models 19
    2.3.3 String-net condensation 20
  2.4 String-net wave functions 21
    2.4.1 Local rules ansatz 22
    2.4.2 String-net conventions and γ, α 24
    2.4.3 Example of computing a string-net amplitude 27
    2.4.4 Self-consistency conditions 29
    2.4.5 Gauge transformations 30
  2.5 String-net Hamiltonians 33
    2.5.1 Definition of the Hamiltonian 33
    2.5.2 Properties of the Hamiltonian 37
  2.6 Quasiparticle excitations 39
    2.6.1 String operator picture 39
    2.6.2 Constructing the string operators 40
    2.6.3 Path independence constraint 43
    2.6.4 Labeling scheme for quasiparticle excitations 46
    2.6.5 Braiding statistics of quasiparticles 48
    2.6.6 Expressing braiding statistics in terms of $F(a, b, c)$ 54
  2.7 Quasiparticle statistics of general abelian string-net models 55
    2.7.1 $\mathbb{Z}_N$ string-net models 55

2.7.2 $\mathbb{Z}_{N_1} \times \cdots \times \mathbb{Z}_{N_k}$ string-net models . . . 59
2.8 Chern-Simons description . . . 62
2.9 Characterizing the phases that can be realized by string-net models . . . 65
2.9.1 Braiding statistics and K-matrix characterizations . . . 65
2.9.2 Examples of realizable and non-realizable phases . . . 68
2.9.3 Characterization in terms of gapped edges . . . 70
2.10 Examples . . . 72
2.10.1 $\mathbb{Z}_2$ string-net model . . . 72
2.10.2 $\mathbb{Z}_3$ string-net model . . . 75
2.10.3 $\mathbb{Z}_4$ string-net model . . . 76
2.10.4 $\mathbb{Z}_2 \times \mathbb{Z}_2$ string-net model . . . 78
2.11 Conclusion . . . 80

3 3D TOPOLOGICAL PHASES AND EXACTLY SOLUBLE LATTICE MODELS 82
3.1 Introduction . . . 82
3.2 Models . . . 86
3.2.1 Hilbert space for the models . . . 86
3.2.2 Ground state wave functions . . . 87
3.2.3 Sheared cubic lattice . . . 87
3.2.4 Hamiltonians . . . 89
3.2.5 Properties of the Hamiltonians . . . 95
3.2.6 Solving the models . . . 96
3.2.7 Particle-like and loop-like excitations . . . 97
3.3 Excitations and the associated creation operators . . . 98
3.3.1 General picture for string and membrane operators . . . 98
3.3.2 String and membrane operators for H_0 . . . 100
3.3.3 String and membrane operators for H_1 . . . 103
3.3.4 Labeling scheme for loop excitations . . . 117
3.4 Braiding statistics of excitations . . . 119
3.4.1 Braiding two charges . . . 119
3.4.2 Braiding a charge and a vortex loop . . . 120
3.4.3 Braiding two vortex loops . . . 122
3.4.4 Three-loop braiding . . . 125
3.5 Conclusion . . . 132

4 3D SPT PHASES AND EXACTLY SOLUBLE LATTICE MODELS . . . 134
4.1 Introduction . . . 134
4.2 Two kinds of paramagnets with $\mathbb{Z}_2 \times \mathbb{Z}_2$ symmetry . . . 136
4.2.1 Hilbert space for the models . . . 136
4.2.2 Sheared cubic lattice . . . 137
4.2.3 Definition of models . . . 138
4.2.4 Properties of models . . . 141
4.3 Coupling the Ising models to $\mathbb{Z}_2 \times \mathbb{Z}_2$ gauge field . . . 143
4.4 Excitations and the associated creation operators . . . 147
4.4.1 String and membrane operators for $\tilde{H}_0$ . . . 148

4.4.2 String and membrane operators for $\tilde{H}_1$ 150
4.5 Braiding statistics of excitations 152
4.5.1 Implication of three-loop braiding statistics 155
4.6 Protected surface modes and the three-loop braiding statistics 156
4.7 Conclusion 161

5 CONCLUSION 163
5.1 Summary of results 163
5.2 Future directions 164

A APPENDICES FOR CHAPTER 2 166
A.1 Motivation for γ and α 166
A.2 Derivation of self-consistency conditions 168
A.3 Local unitary transformations and gauge equivalence 171
A.4 Graphical representation of the Hamiltonian 172
A.5 Showing $B_{p_1}^{s_1}$ and $B_{p_2}^{s_2}$ commute 174
A.6 Properties of the Hamiltonian (2.27) 177
A.7 Gapped edge states 179
A.8 Ground state degeneracy 182
A.9 Derivation of Eqs. (2.46, 2.47) 186
A.10 Exchange statistics 189

B APPENDICES FOR CHAPTER 3 194
B.1 Proving the identities (3.24,3.26,3.27) 194
B.2 Showing that the cylinder operators create braiding eigenstates 199
B.2.1 Connection between equation (3.46) and braiding eigenstates 199
B.2.2 Checking that f_b obeys equation (3.46) 203

C APPENDICES FOR CHAPTER 4 208
C.1 Ground state degeneracy 208
C.2 Showing that $|\Psi_1\rangle$ is short-range entangled 209
C.3 Mapping between spin models and membrane models 210

REFERENCES 214

LIST OF FIGURES

1.1 Braiding statistics of excitations . . . 3
1.2 Toric code model . . . 6
1.3 Gapped quantum phases . . . 8
1.4 Three-loop braiding process . . . 10

2.1 String-net picture . . . 17
2.2 Branching rules of string-nets . . . 18
2.3 A $\mathbb{Z}_4$ string-net configuration . . . 19
2.4 The pentagon identity . . . 30
2.5 Lattice spin model (2.27) . . . 34
2.6 The action of the string operator $W(P)$ along a path P . . . 42
2.7 Computation of mutual statistics from string operators . . . 48
2.8 A "local" vacuum state $|0_{\text{loc}}\rangle$ . . . 50
2.9 Computation of exchange statistics from string operators . . . 51

3.1 Two-loop and three-loop braiding processes . . . 85
3.2 The cubic lattice and its dual cubic lattice . . . 86
3.3 The sheared square and cubic lattices . . . 88
3.4 Intersections between a cube with membranes . . . 91
3.5 Definition of the functions m_c and n_c . . . 93
3.6 A picture representing the intersections drawn on a cylinder . . . 104
3.7 A typical picture representing the intersections drawn on an unlinked blue cylinder 105
3.8 Two typical pictures representing the intersections drawn on linked blue cylinders 110
3.9 A blue torus operator $M_b(S)$ acts on two slightly different membrane configurations. 115
3.10 The hopping algebra . . . 119
3.11 Braiding of a charge around a loop and one loop around another loop . . . 120
3.12 Three-loop braiding process . . . 126

4.1 The cubic lattice and its dual cubic lattice . . . 137
4.2 The sheared square and cubic lattices . . . 137
4.3 Intersections between red domain walls and a sheared cube . . . 139
4.4 Intersections between a cube and membranes . . . 140
4.5 Definition of the functions m_c and n_c . . . 141
4.6 Coupling the spin models to a $\mathbb{Z}_2 \times \mathbb{Z}_2$ gauge field . . . 144
4.7 Three-loop braiding process . . . 154
4.8 A sequence to show that three-loop braiding is equivalent to two-arch braiding . 159
4.9 A sequence to show that two-arch braiding is trivial . . . 161

A.1 Derivation of self-consistency conditions . . . 168
A.2 Showing $\alpha(a,b)\alpha(b,c)\alpha(b,a) = 1$ with $a+b+c=0$ . . . 170
A.3 Showing $[B_{p_1}, B_{p_2} = 0$ . . . 175
A.4 The lattice spin model in a disk geometry . . . 180
A.5 A 5×5 lattice on torus . . . 184
A.6 The sequence to show Eq. (2.49) . . . 186

A.7 The sequence to show Eq. (2.50) 188
A.8 Piece-connectedness and path independence of string operators 189
A.9 Piece-connectedness of string operators 191

B.1 An example of the 2D identity (B.8) 195

C.1 The unitary operator which transforms $|\Psi_0\rangle$ to $|\Psi_1\rangle$ 209

LIST OF TABLES

3.1 The values of f_b on four basic pictures on a unlinked blue cylinder 107

3.2 The values of f_b on four basic pictures on a blue cylinder linked with a red/blue base loop 111

ACKNOWLEDGMENTS

I want to sincerely thank my adviser, Michael Levin. Michael has many great impacts on me beginning with his class on many-body physics. I learned much from his well-organized lectures and new ways of thinking about physics. Many times, I was confused after class. He always clarified my confusion from different angles. I benefit a lot from his breadth of knowledge.

I feel so lucky to work with Michael. I am really grateful to Michael for introducing me to a new area of research. I am amazed by his creativity, unique way of doing physics and strong physical intuitions. He is always approachable and patient to answer my questions. Quite often when I was stuck by a problem, discussing with Michael was always helpful. He always came out with many new ideas to resolve the problem. His brilliant insights and originality make the research with him a great fun.

In addition to Michael, I also have the good fortune to work with Sankar Das Sarma, Jay Deep Sau, Rajdeep Sensarma, Krishnendu Sengupta, Ryan Barnett, So Takei and Victor Galitski on cold atoms and Majorana physics during the period at the University of Maryland. I am grateful to them for teaching me on different areas of physics.

I also like to thank Chenjie Wang, the post-doc of Michael, for many insightful discussions. He is kind and patient to answer my simple and naive questions. I am also glad to have many good friends in the graduate school, from whom I spent good times with: Ananta Poudel, Chien-Te Wu, Yung-Tsen Chen, Chih-Chieh Hsu, Harry Ha, Hsin-Yu Chen, Victor Lee, Shang-Huei Liang, Grace Lee, Sam Chunte Peng, Hsiu-Ming Tsai, Christopher Heinrich, Dung Nguyen Xuan, Wynton Moore, Matthew Low, Sergey Pershoguba, Xinghan Cai, Hoi-Yin Hui, and many others. Listing all of my friends would be an impossible task, but instead I will thank them collectively, without listing their names, for enriching my life.

Finally, I like to thank my parents, my aunts, my uncles, my siblings especially Tzu-Cheng. I thank them for their endless support and love. I owe everything to them.

ABSTRACT

In the past few years, the discovery of topological insulators has resurrected the study of exotic phases of matter beyond the Landau symmetry breaking paradigm. In this thesis, we focus on two particular classes of exotic phases, known as "topological phases" and "symmetry protected topological phases (SPT phases)" in 2D and 3D. Topological phases are generalizations of fractional quantum Hall liquids while SPT phases are generalizations of topological insulators. We investigate topological phases and SPT phases by constructing and analyzing appropriate exactly soluble lattice spin models. We address the following three questions: The first question involves a large class of exactly soluble lattice spin models called string-net models. It is known that string-net models can realize a large class of 2D topological phases, but it is unclear what topological phases can and can not be realized by these models. Thus our first question is: what are the most general topological phases that can be realized by string-net models? We find that a topological phase can be realized by a string-net model if and only if it supports a gapped edge, i.e. the edge can be gapped by suitable local interactions. In the second question we ask: how can we distinguish different 3D topological phases? While it is well known that 3D topological phases can be distinguished by the braiding statistics between particle and loop-like excitations, we construct two exactly soluble lattice models that demonstrate that we also have to consider the braiding statistics of loops with other loops. In the final part of the thesis, we derive a bulk-boundary correspondence for 3D SPT phases. More specifically, we prove that a particular exactly soluble lattice spin model has protected surface states using the fact that the vortex loop excitations in the bulk have non-trivial braiding statistics. We prove the result for a particular 3D exactly soluble lattice model, but our arguments apply more generally.

CHAPTER 1

INTRODUCTION

1.1 Gapped quantum phases

Matter can exist in various phases which originate from the different ways of organizing the constituents of materials. These phases can be classified into different universality classes each of which is characterized by certain universal quantities independent of microscopic details. Even at zero temperature, there are many distinct phases of matter which are called quantum phases. Quantum phases can be divided into two classes: gapless quantum phases and gapped quantum phases. The two classes are distinguished by the existence of the energy gap between the ground state and the excited states in the thermodynamic limit. In this thesis, we focus on gapped quantum phases.

So how do we study gapped quantum phases? Many years ago, the Russian physicist Lev Landau[57] developed a framework to understand phases of matter. The basic idea is that different phases correspond to different types of *symmetry-breaking*. Thus phases can be characterized by "order parameters" which measure the extent of symmetry breaking. The order parameter is the expectation value of some local operator which vanishes in an disordered phase but takes nonzero values in the ordered phase. Landau's symmetry breaking theory successfully describes many phases of matter from crystals and ferromagnets to superfluid and superconductors.

For many years, it was widely believed that the only gapped quantum phases were symmetry breaking phases. Thus to understand these gapped quantum phases, what one need to do is to apply Landau's theory in each particular case. However, the belief that all gapped quantum phases were symmetry breaking phases was disproved by the discovery of the fractional quantum Hall states.

1.2 Topological phases

In 1982, the fractional quantum Hall (FQH) effect was discovered by Tsui, Stormer, and Gossard[82]. They found that when a two dimensional electron gas is placed in a strong magnetic field at certain densities and field magnitudes, the Hall conductance shows a plateau with $\sigma_{xy} = \frac{e^2}{3}$. A year later, Laughlin[58] successfully explained the physics of the $\nu = \frac{1}{3}$ fractional quantum Hall liquid with a simple wave function. This wave function shows many unusual properties of the $\nu = \frac{1}{3}$ FQH state. First, the $\nu = \frac{1}{3}$ FQH state is a gapped quantum phase which contains quasiparticles with fractional charge $e/3$. Second, the quasiparticles have fractional statistics[5]. For example, if one exchanges two $e/3$ quasiparticles, the state gets a phase of $e^{i\pi/3}$. Third, if one puts this system on a torus, one finds three degenerate ground states[95]. Finally, the $\nu = \frac{1}{3}$ FQH state has gapless edge excitations[91]. These exotic properties can not be explained by Landau's theory of symmetry breaking. Indeed, the $\nu = \frac{1}{3}$ state is completely trivial from a symmetry-breaking perspective.

One may start to suspect that there are other FQH-like phases of matter beyond Landau's symmetry breaking paradigm. For example, it is possible to have a class of phases which share the same symmetry but are characterized by distinct fractional quasiparticles. This motivates a generalization of FQH states. In fact, since the discovery of the FQH state, researchers have searched for other fractional phases in nature and attempt to develop a new framework to describe them. These "fractional" gapped quantum phases are called "topological phases" [1][92, 95, 11].

In general, topological phases can occur in any spatial dimension $D > 1$. In this thesis, we will focus on topological phases in two and three dimensions. In two dimensions, topological phases are defined as *gapped quantum phases which support quasiparticles excitations with non-trivial braiding statistics.* In other words, the low energy localized excitations, quasiparticles, are typically anyons which exhibit fractional statistics. If one exchanges two

---

[1] This terminology is motivated by the fact that the low energy effective theories for these phases are the topological quantum field theories.

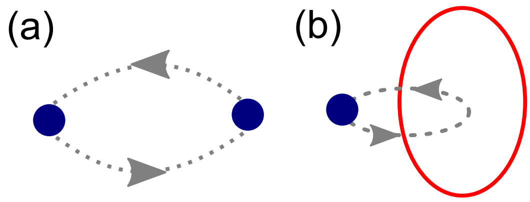

Figure 1.1: (a) Exchange statistics of two particles. (b) Braiding statistics between a particle and a vortex loop.

quasiparticles, the resulting phase, $e^{i\theta}$, is typically neither +1 (bosons) nor -1 (fermions) but something in between[59, 96, 5] (see Fig. 1.1 (a)). Moreover, if one braids one quasiparticle all the way around another, the state will acquire a nontrivial phase. This is in contrast to conventional phases of matter where excitations are either fermions or bosons.

One important implication of the nontrivial fractional statistics is that systems in a topological phase have degenerate ground states on torus. This property is especially useful for numerical studies to detect the topological order. If we take the system and wrap it into a torus and measure its energy spectrum, one will find the spectrum is still gapped and the ground state is now multiply degenerate. Importantly, this degeneracy is completely different from the degeneracy in the symmetry breaking phases. Instead, the degeneracy is robust against any local perturbation which breaks all the symmetries[92, 90, 95]. This topology dependent degeneracy reflects the nonlocal correlations and entanglement in topological phases.

In addition to FQH liquids, there are several physical systems which in principle can realize topological phases. One class of examples are frustrated quantum magnets. For instance, the spin-1/2 Heisenberg antiferromagnet on the 2D kagome lattice[97] is believed to support fractional statistics. Topological phases can also occur in non-interacting fermion systems, such as $p + ip$ superconductors[78], with vortices. In addition to experimental realizations, there are many theoretical lattice spin models such as the toric code[46] and the Kitaev honeycomb model[47] which also realize various topological phases.

The definition of topological phases in 3D is similar to the 2D case. Again, 3D topological phases are defined as gapped quantum phases which support excitations with *non-trivial braiding statistics.* However 3D topological phases can have not only particle-like excitations, quasiparticles, but also line-like excitations, vortex loops. Thus the non-trivial braiding statistics refers to the process of braiding a quasiparticle around a vortex loop (see Fig. 1.1(b)). In other words, if one braids a quasiparticle around a vortex loop, the state will acquire a nontrivial phases.

As in 2D case, the fractional statistics between particles and loops implies the existence of degenerate ground states if one puts the system on 3-torus. For example, the 3D toric code supports point-like charges and line-like flux loops with mutual braiding statistical phase $e^{i\pi}$. If one puts the system on 3-torus, the ground state will be 8-fold degenerate. In addition, many 2D topological phases can be generalized to three spatial dimensions such as the 3D generalization of the Kitaev honeycomb model[80] and the 3D fractional topological insulators[61].

1.3 Symmetry protected topological phases

It is natural to wonder: Are there any other gapped quantum phases beyond topological phases and symmetry breaking phases? Recently, the discovery of topological insulators[36, 77, 71] reveals another new type of gapped quantum phase. Topological insulators are band insulators with strong spin orbit interactions which have a bulk gap like an ordinary insulator but whose edge or surface has *protected* conducting states. The 2D topological insulator is also known as a “quantum spin Hall insulator”. This state was originally proposed to exist in graphene[44] and 2D semiconductor systems with strain[10]. It subsequently was predicted to exist[9] and was then experimentally observed[53] in HgCdTe quantum well systems. Soon after, the quantum spin Hall insulator state was generalized to three dimensions[29, 71, 79] and this phase was predicted in several real materials[28]. In 2008, Hsieh, et al.[37] reported the experimental discovery of the first 3D topological insulator in $\mathrm{Bi}_{1-x}\mathrm{Sb}_x$. What makes topological insulators special is that the edge or surface states are *protected* by time reversal symmetry and $U(1)$ charge conservation symmetry. In other words, the boundary states can not be gapped without breaking at least one of these symmetries either explicitly or spontaneously. Since topological insulators don't break any symmetries, and don't support any particles with nontrivial braiding statistics, they are examples of a new class of gapped phases which are distinct from symmetry breaking pases and topological phases.

More specifically, topological insulators are examples of a class of phases called "symmetry protected topological (SPT)" phases[27, 26, 73, 74, 81, 72, 32, 19, 20, 21, 17]. To define SPT phases, consider a general quantum many-body system which can be built of bosons/spins or fermions in any spatial dimension. A system is defined to be in a nontrivial SPT phase if it has four properties. The first property is that the system has a finite energy gap in the bulk. The second property is that the Hamiltonian is invariant under some set of symmetries, and none of these symmetries are broken spontaneously. This property makes SPT phases different from conventional symmetry breaking phases.

The third property is that *the ground state can be adiabatically connected to a trivial state if one or more of the symmetries are broken during the process.* By a "trivial state", we mean a product state (in the boson/spin case) or an atomic insulator (in the fermion case); by "adiabatically connected", we mean connected by varying a parameter in the Hamiltonian without closing the energy gap. This property implies that SPT phases do not support excitations with fractional statistics and thus sharply distinguishes SPT phases from topological phases.

The final property of an SPT phase is that *the ground state cannot be adiabatically connected to a trivial state without breaking one or more of the symmetries.*

The most important physical property of SPT phases is that they typically have robust gapless boundary modes like those of topological insulators[62, 21]. However we do not include this property in the definition.

SPT phases can be realized in any spatial dimension in both boson/spin and fermion systems. One of the most famous examples is the Haldane spin-1 antiferromagnetic chain[34].

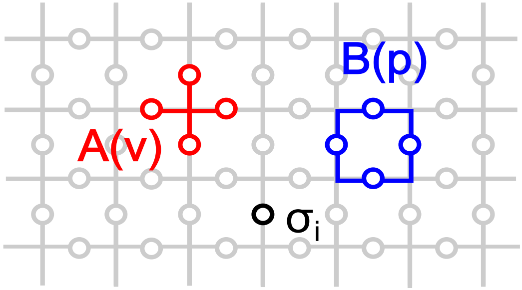

Figure 1.2: The toric code defined on a square lattice with spin-1/2 living on each link. The vortex operator $A(v)$ acts on four edges touching the vertex v and the plaquette operator $B(p)$ acts on four edges surrounding the plaquette p.

This spin chain is an example of a 1D bosonic SPT phase[32, 73, 74]. The Hamiltonian is gapped and its ground state is unique when the chain is closed, i.e. with periodic boundary condition. This state can not be transformed into a product state without breaking the $SO(3)$ spin rotational symmetry. Moreover, in the presence of the boundary, there is a dangling spin-1/2 at each of the two ends protected by $SO(3)$ symmetry. An other set of examples are the 2D and 3D topological superconductors[77] which are cousins of topological insulators. In contrast to topological insulators which have boundary modes protected by time reversal and charge conservation symmetry, topological superconductors have boundary modes protected by time reversal symmetry only.

1.4 Exactly soluble lattice models

Topological phases and SPT phases pose a basic challenge because their properties cannot be understood in terms of symmetry breaking or order parameters. Therefore, studying them requires new tools and approaches. One approach that proven to be useful is the construction of exactly soluble lattice models that realize these phases.

One of the simplest examples is the toric code model of Ref. [46]. This model is a spin-1/2 system where the spins live on the links of the square lattice (see Fig. 1.2). The

Hamiltonian is defined as

$$H = -\sum_{v} A(v) - \sum_{p} B(p) \tag{1.1}$$

with

$$A(v) = \frac{1 + \prod_{i \in v} \sigma_i^x}{2}, \quad B(p) = \frac{1 + \prod_{i \in p} \sigma_i^z}{2}. \tag{1.2}$$

Here the Hamiltonian consists of two sets of operators: the vortex operators $A(v)$ acting on four edges touching the vertex v and the plaquette operators $B(p)$ acting on four edges surrounding the plaquette p. The Hamiltonian has two key properties. First, the $A(v), B(p)$ operators are projectors:

$$A(v)^2 = A(v), \quad B(p)^2 = B(p). \tag{1.3}$$

The second property is that the $A(v), B(p)$ operators commute with one another:

$$[A(v), A(v')] = [B(p), B(p')] = [A(v), B(p)] = 0. \tag{1.4}$$

With these properties, one can solve the Hamiltonian exactly by simultaneously diagonalize $\{A(v), B(p)\}$. Further analysis of this model shows that the toric code supports quasiparticles with fractional statistics and realizes a topological phases with $\mathbb{Z}_2$ topological order.

As emphasized above in Eqs. (1.3,1.4), the key reason that the toric code is exactly soluble is that the Hamiltonian is *a sum of commuting projectors*. In this thesis, we will focus primarily on exactly soluble models of this kind, i.e. Hamiltonians which are sums of commuting projectors.

Why are these exactly soluble models important and useful? First, the topological properties of exactly soluble models apply to the whole phase. Second, they are exactly soluble so the results are exact and conclusive. In contrast, perturbative analysis or numerical computation may suffer certain uncertainty in their validity. Third, they are useful for giving intuition. As in the toric code model, one can see the properties of topological phases on the lattice explicitly. For example, one can derive the topological entanglement explicitly by

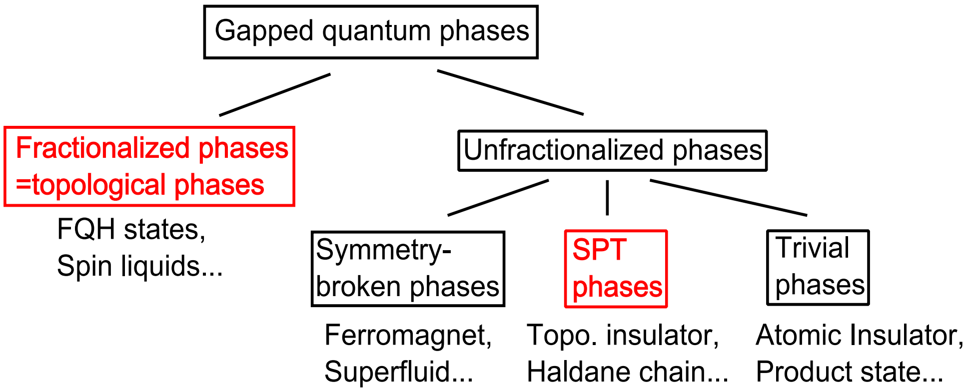

Figure 1.3: Gapped quantum phases are divided into topological phases, symmetry broken phases, SPT phases and trivial phases. In this thesis, we focus on the topological phases and SPT phases.

these models[64]. One can also study the properties of gapped boundaries of these models in a more concrete manner[48]. Moreover, some lattice models can help to find possible realizations of topological phases. For example, a easy-axis spin-1/2 Heisenberg antiferromagnet on the Kagome lattice[7] is closely related to exactly soluble models and its ground state is known to be a quantum spin liquid. This model is beneficial for experimentalists to find possible candidate materials to realize spin liquids. Finally, these models are useful for some numerical techniques. For example, the structure of exactly soluble lattice models leads to a remarkably simple way to express their grounds states as a tensor network[14].

1.5 Overview of the thesis

Gapped quantum phases can basically be divided into topological phases, symmetry broken phases, SPT phases and trivial phases [2](see Fig. 1.3). In this thesis, we focus on topological phases and SPT phases in 2D and 3D. We use exactly soluble models to investigate the universal properties associated with these phases.

Specifically, we address the following three questions. The first question involves a large

---

[2] Here we define gapped quantum phases modulo the long range entangled phases with no fractional statistics (which is called invertible topological order), such as integer quantum Hall liquids and the E_8 state which are characterized by nonzero chiral central charge in the edge.

class of exactly soluble lattice models called "string-net" models[65] which are generalizations of the toric code model. The string-net models realize a large class of 2D topological phases. An important question is to determine which topological phases can and cannot be realized by string-net models. Thus our first question is: what are the most general topological phases which can be realized by the string-net models and what physical property distinguishes the phases that can and cannot be realized? We answer this question for the case of abelian topological phases, namely those with abelian braiding statistics. We generalize the original string-net construction in Ref. [65] and find that an abelian topological phase can be realized by a string-net model if and only if the phase supports a gapped edge, i.e. its boundary with the vacuum can be gapped by suitable local interactions.

The starting point for the second question is a basic question: how can we tell whether or not two gapped Hamiltonians without symmetry belong to the same phase? This question has an appealing answer in the case of 2D systems. To determine whether two gapped 2D Hamiltonians belong to the same phase, we need to compare two pieces of data: (1) the braiding statistics of their quasiparticle excitations and (2) the thermal Hall conductance[42], or equivalently the chiral central charge[47] of the edge state. It is widely believed that two Hamiltonians can be adiabatically connected to one another without any symmetry constraints if and only if they have the same braiding statistics and the same thermal Hall conductance. In the 3D case, our understanding is much more limited. One way to attack the classification problem is to generalize the concept of quasiparticle braiding statistics to the 3D case. One complication in 3D is that many 3D Hamiltonians support loop-like excitations in addition to particles. Given this observation, we ask the second question: how can we distinguish/classify different 3D topological phases? In this thesis, we show that the three-loop braiding statistics is a necessary piece of data to distinguish 3D topological phases in addition to the braiding statistics of one particle around a loop and one loop around another loop. Here by three-loop braiding statistics we are referring to a process in which one loop is braided around another while both are linked to a third loop (see Fig. 1.4).

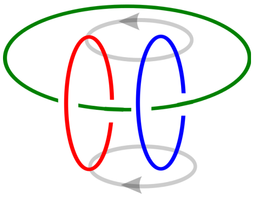

Figure 1.4: Three-loop braiding process. The gray curves show the paths of two points on the moving loop.

The starting point for the last question is a result of a previous work, Ref. [62]. In that paper it was proven that the edges of 2D SPT phases must be either gapless or symmetry-breaking. The argument was based on a connection between protected edges and the braiding statistics of vortex excitations in the bulk, after gauging the symmetry. One may naturally wonder whether there is a similar result involving the protected surface states of 3D SPT phases. In the last part of the thesis, we establish a similar result that relates protected surface states of 3D SPT phases to the three-loop braiding statistics of vortices in the bulk. We demonstrate this result by constructing two exactly soluble lattice spin models that can only be distinguished by their three-loop braiding statistics. We prove the result for a particular 3D exactly soluble lattice model, but the arguments apply more generally.

The thesis is organized as follows. In chapter 2, we generalize the original string-net models and examine the limitation of this construction by explicitly constructing all the possible abelian string-net models. In chapter 3, we construct two exactly soluble lattice spin models that demonstrate the importance of three-loop braiding statistics for the classification of 3D gapped quantum phases. In chapter 4, we discuss the bulk-boundary correspondence for 3D SPT phases. In the final chapter, we summarize our results and describe several future directions for research. Many of mathematical details can be found in the appendices. Most of the material in this thesis has been adapted from papers published elsewhere. In particular, chapters 2,3 were adapted from Refs. [66],[67].

CHAPTER 2

2D TOPOLOGICAL PHASES AND EXACTLY SOLUBLE LATTICE MODELS

2.1 Introduction

In recent years, it has become clear that the physics of gapped quantum phases of matter is much richer than was previously thought. One example of this richness is the large class of two dimensional quantum many body systems that support quasiparticle excitations with fractional statistics. These systems are known as "topological phases" of matter.[94]

Topological phases pose a basic challenge because their properties cannot be understood in terms of symmetry breaking or order parameters. Therefore, studying them requires new tools and approaches. One approach that proven to be useful is the construction of exactly soluble lattice models that realize topological phases. One of the simplest examples is the toric code model of Ref. [46]. This model is a spin-1/2 system where the spins live on the links of the square lattice. The reason that the toric code is exactly soluble is that the Hamiltonian is a sum of commuting projectors: $H = \sum_i P_i$ where $[P_i, P_j] = 0$.

An interesting aspect of the toric code model is that it can be mapped onto a model of closed loops or strings. Based on this observation, Ref. [65] generalized the toric code to a large class of exactly soluble "string-net" models. Like the toric code, string-net models are lattice spin models whose low energy physics is governed by effective extended objects.

String-net models can realize a large class of topological phases. For example, these models can realize all phases whose low energy effective theory is either (a) a gauge theory with finite gauge group or (b) a sum of two decoupled Chern-Simons theories with opposite chiralities.[65] At the same time, string-net models cannot realize *all* topological phases. In particular, they cannot realize any phase with a nonzero thermal Hall conductance[42] (or equivalently, nonzero chiral central charge[47]). This restriction follows from the fact that any Hamiltonian that is a sum of commuting projectors has a vanishing thermal Hall conductance. [1]

Given these facts, an important question is to determine which topological phases can and cannot be realized by string-net models. On a mathematical level, the answer to this question is at least partially understood: it has been argued that string-net models, when suitably generalized from the original construction of Ref. [65], realize all "doubled" phases — where "double" refers to a generalization of Drinfeld's quantum double construction.[48] However, the physical interpretation of this result is not clear. In other words, what physical property distinguishes the phases that can and cannot be realized?

In this chapter, we answer this question for a simple case, namely the case of abelian topological phases. Our analysis is based on an explicit construction: we systematically construct all string-net models that realize abelian topological phases. For each model, we compute the quasiparticle braiding statistics and ground state degeneracy, and we derive a low energy effective field theory that captures these properties. These effective theories are multicomponent $U(1)$ Chern-Simons theories.

From this analysis, we find necessary and sufficient conditions for when an abelian topological phase can be realized by a string-net model: we find that an abelian phase is realizable if and only if (i) it has a vanishing thermal Hall conductance and (ii) it has at least one Lagrangian subgroup. Here, a "Lagrangian subgroup"[45] $\mathcal{M}$ is a subset of quasiparticles with two properties. First, all the quasiparticles in $\mathcal{M}$ are bosons and have trivial mutual statistics with one another. Second, any quasiparticle that is not in $\mathcal{M}$ has nontrivial mutual statistics with at least one particle in $\mathcal{M}$.

Interestingly, the above conditions are identical to the conditions for an abelian topological phase to support a *gapped edge*.[60, 45] Thus, an alternative formulation of the criterion is that an abelian topological phase can be realized by a string-net model if and only if its

---

[1] The fact that the thermal Hall conductance/chiral central charge vanishes for a commuting projector Hamiltonian follows from the analysis of the chiral central charge given in appendix D.1 in Ref. [47]. Specifically, one can see that f in Eq. (159) vanishes for commuting projectors and therefore we can choose $h = 0$. It then follows that $c_- = 0$ in Eq. (160).

boundary with the vacuum can be gapped by suitable local interactions. We conjecture that this criterion generalizes to the non-abelian case. (see section 2.11)

As we are interested in investigating the scope of string-net models, it is important that we use the most general possible definition of these models. This issue is particularly relevant since several recent works[48, 52, 56] have described a modified formulation of string-net models which is more general than the original setup of Ref. [65]. Here we use another formulation of these models, which we believe is equally general to the one described in Refs. [48],[52],[56], at least for the abelian case we consider here. The main difference between our construction of string-net models and the original construction of Ref. [65] is that we introduce two new ingredients, γ, α, into the definition of these models. These new objects are related to $\mathbb{Z}_2$ and $\mathbb{Z}_3$ Frobenius-Schur indicators[47, 12] respectively, and they allow us to realize more general topological phases than Ref. [65]. We note that it is also possible to define general string-net models without introducing γ, α, as in Ref. [52], [56]. The trade-off is that the approaches of Ref. [52] [56] explicitly break the rotational symmetry of the lattice since they assume that all links are oriented along a preferred direction.

The topological phases that we construct are equivalent to the topological gauge theories of Dijkgraaf and Witten[23] with finite abelian gauge group G. The braiding statistics and other topological properties of these phases were analyzed previously by Propitius[76] using the quantum double construction. Our results for the braiding statistics agree with those of Propitius, but we obtain them using a more concrete approach in which we directly analyze braiding in our microscopic lattice models. This braiding analysis is similar to that of Mesaros and Ran[68] who derived braiding statistics from a lattice Dijkgraaf-Witten model using a ribbon algebra.

Explicit lattice models for Dijkgraaf-Witten gauge theories with general finite gauge group G were constructed in Refs. [38], [68]. We believe that the models we discuss here are closely related to the models of Refs. [38], [68]. However, since we work in the string-net formalism, our models can be generalized beyond Dijkgraaf-Witten gauge theories.[65]

The chapter is organized as follows. In Sec. 2.2, we outline our analysis and summarize our results. In Sec. 2.3, we review some basics of string-net models and define "abelian string-net" models. In Secs. 2.4,2.5, we construct ground state wave functions and lattice Hamiltonians for the abelian string-net models. We analyze the low energy quasiparticle excitations of these models in Sec. 2.6. In Sec. 2.7, we explicitly compute the quasiparticle braiding statistics for general abelian string-net models, and in Sec. 2.8 we derive multicomponent $U(1)$ Chern-Simons theories that capture these statistics. Finally, we characterize the phases that are realizable by abelian string-net models in Sec. 2.9. We illustrate our construction with concrete examples in Sec. 2.10. The mathematical details can be found in the appendices.

2.2 Summary of results

2.2.1 Construction of lattice models

The first step in our analysis is to systematically construct a large class of exactly soluble lattice models. The models we construct are a subset of string-net models called "abelian string-net" models. In these models, the string types are labeled by elements $a, b, c, ...$ of a finite abelian group G. The allowed branchings are triplets (a, b, c) such that $a + b + c = 0$. We focus on this subset of models because these are the most general string-net models with abelian quasiparticle statistics.

Each abelian string-net model is specified by two pieces of data: (1) a finite abelian group G, and (2) a collection of four complex-valued functions $(F(a, b, c), d_a, \alpha(a, b), \gamma_a)$ defined on G, obeying certain algebraic equations (2.18). The corresponding Hamiltonian (2.27) is a spin model where the spins live on the links of the honeycomb lattice and where each spin can be in $|G|$ states parameterized by elements of the group: $\{|a\rangle : a \in G\}$. Like the toric code,[46] the Hamiltonian is exactly soluble because it can be written as a sum of commuting projectors.

2.2.2 Braiding statistics and Chern-Simons description

The second step in our analysis is to construct the quasiparticle excitations in each of the abelian string-net models. We find that these models have $|G|^2$ topologically distinct quasiparticle excitations. The excitations can be labeled by ordered pairs (s, m) where $s \in G$, and m is a $1D$ representation of G. We think of the excitations of the form $(0, m)$ as "pure charges" and the excitations of the form $(s, 0)$ as "pure fluxes." General excitations can be thought of as flux/charge composites.

The most important property of the quasiparticle excitations are their braiding statistics. We find that the charges braid trivially with one another but have nontrivial mutual statistics with respect to the fluxes. Specifically, the phase associated with braiding a charge $(0, m)$ around a flux $(s, 0)$ is $\rho_m(s)$ where ρ_m denotes the $1D$ representation corresponding to m. In addition, we find that the flux excitations have nontrivial statistics with one another (2.88,2.89). (In fact, in some of the abelian string-net models, the fluxes have *non-abelian* statistics[76], though we restrict our attention to the subset of models that have only abelian quasiparticles).

We find that the quasiparticle braiding statistics can be described by a multicomponent $U(1)$ Chern-Simons theory of the form

$$L = \frac{K_{IJ}}{4\pi} \varepsilon^{\mu\nu\lambda} a_{I\mu} \partial_\nu a_{J\lambda}$$

with a different "K-matrix" (2.92) for each model. These Chern-Simons theories can be thought of as low energy effective theories for the abelian string-net models.

2.2.3 *Characterizing the realizable phases*

The abelian string-net models can realize many $U(1)$ Chern-Simons theories. For example, our models can realize time-reversal symmetric phases such as

$$K = \begin{pmatrix} 2 & 0 \\ 0 & -2 \end{pmatrix}.$$

In addition, we can also realize some phases that break time-reversal symmetry such as:

$$K = \begin{pmatrix} 2 & 0 \\ 0 & -8 \end{pmatrix}.$$

On the other hand, we find that we cannot realize other time-reversal breaking phases such as:

$$K = \begin{pmatrix} 2 & 0 \\ 0 & -4 \end{pmatrix}.$$

Given these examples, it is natural to wonder: what is the physical distinction between the phases that can and cannot be realized by string-net models? To answer this question, we derive three equivalent criteria for determining whether an abelian topological phase is realizable:

1. Braiding statistics criterion: an abelian topological phase is realizable if and only if it has a vanishing thermal Hall conductance and contains at least one Lagrangian subgroup (see introduction).

2. K-matrix criterion: an abelian topological phase is realizable if and only if its K-matrix has even dimension $2k \times 2k$, and there exist k integer vectors $\Lambda_1, ..., \Lambda_k$ satisfying $\Lambda_i K \Lambda_j = 0$.

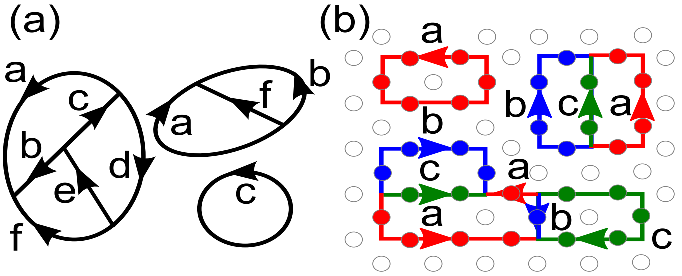

Figure 2.1: (a) String-nets in the continuum. Strings come in different types and carry orientation. They can branch and form string-nets. (b) String-nets on the lattice. The circles denote spins sitting on the links of the lattice. Spins can be in different states indicated by different colors. They organize to form different types of strings and branch as string-nets.

3. Edge state criterion: an abelian topological phase is realizable if and only if its boundary with the vacuum can be gapped by suitable interactions.

2.3 String-net models

In this section, we will define string-nets and string-net models and explain their basic structure. This material is essentially a review of the string-net formalism of Ref. [65] with the only difference being our treatment of string orientations. We also define "abelian string-net" models – a special class of string-net models which are the main focus of this chapter.

2.3.1 General string-net models

A *string-net* is a network of strings. The strings that form the edges of the network can come in different "types", and carry orientations. In this chapter, we will focus on trivalent networks – that is, each branch point or node in the network is connected to exactly 3 strings. Also, we will assume that the string-nets live in a two-dimensional space. Thus, for the purposes of this chapter, string-nets can be thought of as trivalent graphs with labeled and oriented edges, which live in the plane (see Fig. 2.1(a)). These trivalent graphs can live in the continuum, or (when we want a well-defined quantum theory) on a lattice.

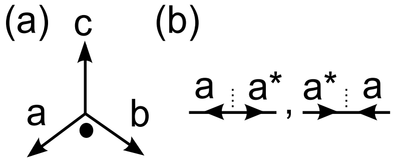

Figure 2.2: (a) The branching rules are defined with the convention that the 3 strings are all oriented outward. We will discuss the meaning of the black "dot" in section 2.4.2. (b) The branching rules for the null strings are defined so that $(a, b, 0)$ is allowed iff $b = a^*$.

A *string-net model* is a quantum mechanical model whose basic degrees of freedom are fluctuating string-nets. To specify a string-net model, one has to provide several pieces of data. First, one needs a finite set of string types $\{a, b, c \dots\}$. Second, one needs to specify a "dual" string type a^* for each string type a. The meaning of the dual string type is related to the string orientations: a string a with a given orientation corresponds to the same physical state as a string a^* with the opposite orientation – up to a phase factor which we will specify below. The final and most important piece of data are the "branching rules." The branching rules are the set of all triplets of string types $\{(a, b, c) \cdots\}$ which are allowed to meet at a point; these branching rules are specified with the convention that the 3 strings are all oriented away from the point where they meet (see Fig. 2.2(a)).

The above data specify the string-net Hilbert space: an orthonormal basis for the string-net Hilbert space is given by the set of all string-net configurations which satisfy the above branching rules. Note that in this Hilbert space, the spatial positioning of the string-net is important: two string-net configurations that are *geometrically* distinct correspond to orthogonal states, whether or not the configurations are *topologically* equivalent. On the other hand, two string-net configurations that are positioned identically in space, and differ only by reversing string orientations and replacing $a \to a^*$, are regarded as the same physical state up to a phase factor. These phases will be defined below.

As we will see, string-nets and string-net models can be realized in lattice spin-systems (see Fig. 2.1(b)). Usually for a weakly interacting spin system, the underlying spins can fluctuate independently and the physics is characterized by individual spins. However in some

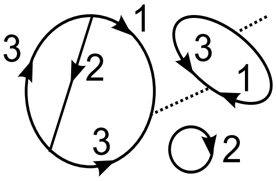

Figure 2.3: A typical string-net configuration for $\mathbb{Z}_4$ string-net model. Each string is labeled by the string types $\{0, 1, 2, 3\}$ and carries an orientation. The dotted line denotes the null string 0. At each vertex, strings can branch according to the $\mathbb{Z}_4$ branching rules.

spin models, energetic constraints can force the local spin degrees of freedom to organize into effective extended objects. In this case, the low energy physics of the spin system may be described by a string-net model, where the string-nets live on a lattice.

In order to discuss string-nets on a lattice, and also to simplify some of the mathematics below, it is convenient to include the "null" string type into the formalism. The null string type, denoted by 0, is equivalent to no string at all. This string type is self-dual: $0^* = 0$. The associated branching rule is that $(0, a, b)$ is allowed if $a = b^*$ (see Fig. 2.2(b)). Unlike the other strings, the orientation of the null string can be reversed without generating any phase factor. Therefore, we will often neglect the orientation of the null string and draw it as an unoriented dotted string.

2.3.2 Abelian string-net models

In this chapter we focus on a special class of string-net models associated with abelian groups. We call these models "abelian string-net models." To construct an abelian string-net model, one starts with a finite abelian group G and then follows a simple recipe. First, one labels the string types by the elements of the group $a \in G$, with the null string corresponding to the identity element 0. Second, one defines the dual string a^* using the group inverse: $a^* = -a$. Finally, one defines branching rules by:

$$(a, b, c) \text{ is allowed if } a + b + c = 0. \tag{2.1}$$

Here, the branching rules are defined with the convention that the 3 strings are all oriented outward (see Fig. 2.2(a)). Note that we use additive notation for the group operation.

We focus on this subset of string-net models because we believe that these are the most general models with abelian quasiparticle statistics — i.e. other branching rules always give models with at least one non-abelian quasiparticle. Although we do not have a proof of this conjecture, in section 2.9.3 we show that even if other branching rules could give abelian topological phases, they could not give any phases beyond those that we realize here. This result justifies our focus on models with the above structure (2.1).

To see an example of this construction, consider the group $G = \mathbb{Z}_4$. In this case, the corresponding abelian string-net model has four string types, including the null string: $\{0, 1, 2, 3\}$. The dual string types are $0^* = 0$, $1^* = 3$, $2^* = 2$, and $3^* = 1$. The branching rules are $\{(0, 0, 0), (0, 1, 3), (0, 2, 2), (1, 1, 2), (3, 3, 2)\}$. A typical string-net configuration for this model is shown in Fig. 2.3.

2.3.3 String-net condensation

To define a string-net model, one needs to specify both the Hilbert space and the Hamiltonian; so far we have focused entirely on the Hilbert space. Now let us imagine writing down a string-net Hamiltonian. A typical string-net Hamiltonian is a sum of a kinetic energy term and a string tension term. The kinetic energy term is off-diagonal in the string-net basis. This term gives an amplitude for the string-net states to move. On the other hand, the string tension term is diagonal in the string-net basis. This term gives an energy cost to large string-nets.

It is natural to expect that such a Hamiltonian can be in two phases depending on the relative size of the kinetic energy and string tension terms. One phase occurs when the string tension term dominates over the kinetic energy term. In that case, we expect that the ground state will contain only a few small strings. The other phase occurs when the kinetic energy term dominates over the string tension term. In that case, we expect that the ground state will be a superposition of many large string-net configurations. We call the former phase a “small string” phase and the latter phase a “string-net condensed phase.”

Following the physical picture of Ref. [65], we expect that string-net condensed phases are topologically ordered – that is, they support excitations with fractional statistics – while the small-string phases do not contain topological order. Therefore, our strategy for constructing topological phases will be to construct wave functions for string-net condensed phases. We will then construct exactly soluble Hamiltonians whose ground states are described by these wave functions, and we will verify that these exactly soluble models support excitations with fractional statistics.

2.4 String-net wave functions

In this section we construct wave functions for abelian string-net condensed phases. As in Ref. [65], the wave functions that we construct are special: they describe “perfect” string-net condensates with vanishing correlation length. Intuitively, these states can be thought of as fixed points under an RG flow. These states capture the universal long distance features of the corresponding phases without any of the complexities of the short distance physics. In section 2.5, we will show that these wave functions are ground states of exactly soluble string-net Hamiltonians, defined on a lattice.

Our construction of the string-net wave functions closely follows that of Ref. [65]. The only difference appears in section 2.4.2, where we describe our conventions for manipulating the “null” string and for dealing with string orientations. There we introduce two new objects, γ, α, that were not included in the original construction of Ref. [65]. Also, in section 2.4.4, our self-consistency conditions differ from the self-consistency conditions of Ref. [65], since we do not assume that F, d obey reflection symmetry.

2.4.1 Local rules ansatz

As in Ref. [65], we will not attempt to construct explicit ground state wave functions for string-net condensed phases. Instead, we will define the wave functions *implicitly* using local constraint equations. This approach has the advantage of allowing us to construct complicated wave functions that would be difficult to write down explicitly. In addition, this approach ensures that the wave functions we construct can be realized as ground states of *local* Hamiltonians.

More specifically, we use the following ansatz for constructing abelian string-net wave functions Φ. We assume that Φ obeys local constraint equations that take the following graphical form:

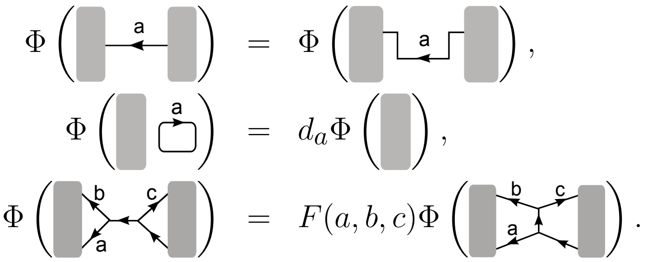

(2.2)

(2.3)

(2.4)

Here a, b, c are arbitrary string types (including the null string type) and the shaded regions represent arbitrary string-net configurations which are not changed. The d_a are complex numbers that depend on the string type a, while $F(a, b, c)$ is a complex number that depends on 3 string types a, b, c. For the moment, d_a and $F(a, b, c)$ can be arbitrary, but we will soon see that $d_a, F(a, b, c)$ have to satisfy certain algebraic equations (2.18-2.19) in order for our construction to work.

We now discuss the meaning of these local constraints or local rules. The first rule (2.2) has been drawn schematically. This rule says that two string-net configurations that can be continuously deformed into one another must have the same amplitude. Namely, the amplitude of a string-net configuration only depends on the topology of the configuration. The second rule (2.3) says that the amplitude of a string-net configuration containing a closed loop of string type a is equal to the amplitude of the same configuration *without* the closed loop, multiplied by a factor of d_a.

The third rule (2.4) is the most important one. This rule relates the amplitude of one string-net configuration to the amplitude of another configuration that differs from it by recoupling the strings joined at two adjacent vertices. The reader may notice that two strings have been left unlabeled on both sides of this equation. These labels are completely determined by the (abelian) branching rules and have been left out due to space constraints. Specifically, the label on the bottom right hand corner is $a + b + c$, while the middle labels are $a + b$ on the left hand side and $b + c$ on the right hand side.

The basic idea of equations (2.2 - 2.4), is that by applying these local rules multiple times, one can relate the amplitude of any string-net configuration to the amplitude of the vacuum or "no-string" configuration. [2] Then, using the convention that

$$\Phi(\text{vacuum}) = 1, \tag{2.5}$$

the amplitude of every configuration is fully determined. Thus, the rules determine the wave function completely once the parameters $d_a, F(a, b, c)$, etc. are given. We will give an example of such a computation below. However, before presenting this example, we need to explain our conventions for how to apply these rules, and some additional structure associated with these conventions.

It is worth emphasizing that the conventions we discuss below are the key *new* elements in our construction. While everything that we have discussed until this point can be thought of as a special case of the string-net construction of Ref. [65], the conventions described below allow us to go beyond Ref. [65].

---

[2] Here we assume the string-nets are defined in a disk geometry. In more complicated geometries, such as a torus, a general string-net configuration can be reduced to one of several basic configurations containing noncontractible loops. In such geometries, the wave function is not completely determined by the local rules. The existence of multiple, linearly independent wave functions obeying the local rules is an indication of a topological ground state degeneracy.

2.4.2 String-net conventions and γ, α

factors We begin with our conventions regarding the “null” string. In applying the above rules, one often encounters string-net configurations containing a null string with label $a = 0$. For example, when $b = c^*$, equation (2.4) gives:

$\Phi\Big($ 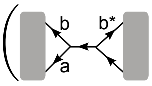 $\Big) = F(a,b,b^*)\Phi\Big($ 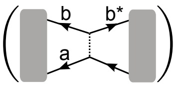 $\Big)$

or in bra-ket notation,

$\Big\langle$ 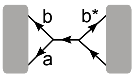 $\Big|\,\Phi\Big\rangle = F(a,b,b^*)\Big\langle$ 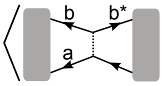 $\Big|\,\Phi\Big\rangle$

where the configuration on the right hand side contains a null string. In Ref. [65], it was assumed that these null strings could be freely erased, since the null string corresponds to the vacuum. This erasing of null strings was a key part of the local rule formalism, since it was what allowed us to reduce string-net configurations to the vacuum configuration, and thereby compute their amplitude. Here, we will also assume that null strings can be erased, but under more restricted circumstances.

Our rules for dealing with the null string are as follows. We will describe these rules using *bras* $\langle X|$ rather than *kets* $|X\rangle$ because it simplifies some of the notation below. First, null strings can be freely erased everywhere except near vertices with non-null strings. For example:

$\Big\langle$ 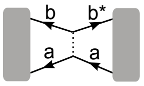 $\Big| = \Big\langle$ 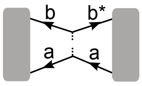 $\Big|$ (2.6)

Second, the “end” of a null string can be erased at any vertex where the two other strings at the vertex are oriented in the same direction:

$\Big\langle$ 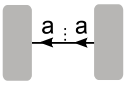 $\Big| = \Big\langle$ 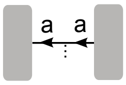 $\Big| = \Big\langle$ 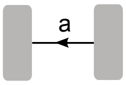 $\Big|.$ (2.7)

On the other hand, the end of the null string *cannot* be erased at vertices where the two other strings are oriented in opposite directions. Indeed, in this case, we need to keep careful track of the end of the null string, since "flipping" the null string from one side of the vertex to the other introduces a phase factor:

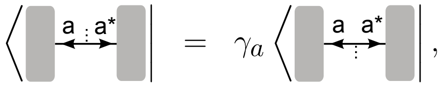

(2.8)

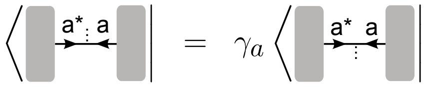

(2.9)

where γ_a is a complex number with modulus 1: $|\gamma_a| = 1$. Later we will see that γ_a can be chosen to be ± 1 without loss of generality. (We explain the motivation behind γ in appendix A.1.)

Our fourth rule is that the ends of the null strings can be erased in pairs according to:

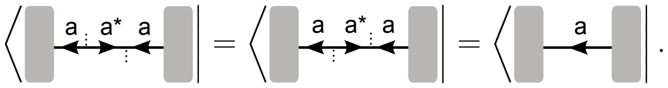

(2.10)

Finally, the ends of the null strings can be absorbed into vertices as follows:

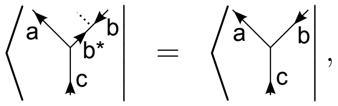

(2.11)

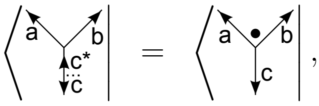

(2.12)

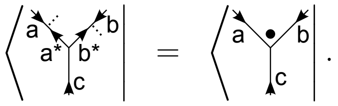

(2.13)

The last two rules (2.12 - 2.13) introduce another ingredient into our diagrammatical calculus: we can see that the vertices on the right hand side of Eq. (2.12) and Eq. (2.13) are decorated with dots. In general, we decorate all vertices that have three incoming or three outgoing legs with dots. The dots can be placed in any of the three positions near the vertex. Like the string orientations or the ends of the null strings, moving the position of the dot does not change the physical state, but it can introduce a phase factor (similar to γ_a). These phase factors are defined by

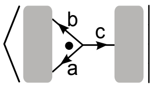

$= \alpha(a,b)\cdot$
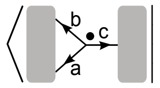

, (2.14)

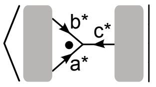

$= \alpha(a,b)\cdot$
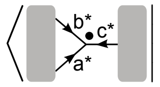

(2.15)

where $\alpha(a,b)$ is a complex number with unit modulus $|\alpha(a,b)| = 1$. Later we will see that $\alpha(a,b)$ can be chosen to be a third root of unity without loss of generality. (We explain the motivation behind α in appendix A.1.)

A few comments are in order here. First, we would like to mention that the phases γ_a and $\alpha(a,b)$ have an important mathematical meaning and are closely related to so-called $\mathbb{Z}_2$ and $\mathbb{Z}_3$ "Frobenius-Schur indicators" in tensor category theory[47, 12]. The key difference between the formalism in this chapter and that of Ref. [65], is that here we include the phase factors γ_a, and $\alpha(a,b)$, while the construction in Ref. [65] effectively assumed that $\gamma_a = \alpha(a,b) = 1$. Indeed, Ref. [65] did not keep track of dots or ends of null strings at all. Here, by allowing for more general γ_a and $\alpha(a,b)$, we are able to construct string-net models and topological phases that were inaccessible[39] to Ref. [65].

Second, we would like to mention that equations (2.10 - 2.13) are not particularly fundamental and merely represent a particular choice of conventions for how to relate different vertices to one another. There are other equally good conventions where these rules would include additional phase factors.

Another important point has to do with string orientations. As we mentioned in section 2.3.1, if two string-net configurations differ only by reversing string orientations and replacing labels by $a \to a^*$, then those two string-net configurations correspond to the same physical state, *up to a phase factor.* In Ref. [65], these phase factors were assumed to vanish. That is, in that work, it was assumed that the string orientations could be changed without introducing any phases. Here, we allow for nontrivial phase factors, as we find that they are important in realizing more general topological phases. In our formalism, the phase factors associated with reversing string orientations are completely determined by the parameters γ_a and $\alpha(a,b)$. For example, we have:

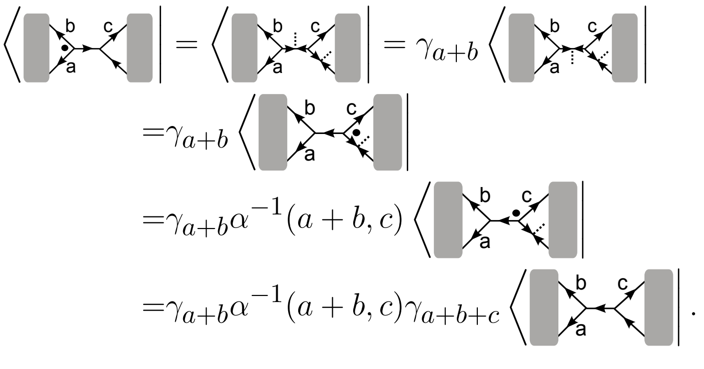

These phase factors play an important role in our diagrammatical calculus, especially when using (2.4). Indeed, in order to implement this rule, the string orientations have to match the orientations shown in (2.4), and it is often necessary to reverse the orientations of certain strings to achieve this matching. In general, this orientation reversal can be accomplished using manipulations similar to those shown above.

2.4.3 Example of computing a string-net amplitude

We now present an example of how the local rules (2.2 - 2.4) and the conventions (2.6 - 2.15) determine the amplitude of general string-net configurations. Before discussing the example, we first point out two useful relations:

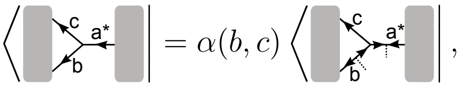

(2.16)

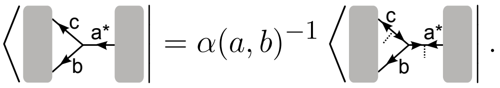

(2.17)

These relations allow us to change the orientations of vertices with one incoming string and two outgoing strings. Eqs. (2.16 - 2.17) are often useful when we need to reverse string orientations so that we can apply the local rule (2.4). They can be shown by considering

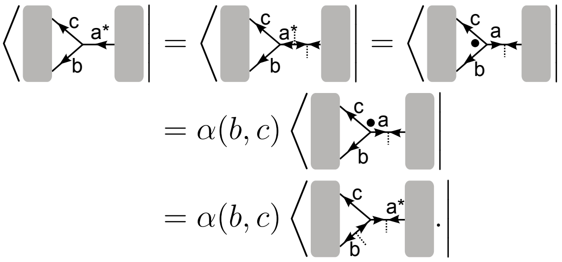

This shows (2.16). Similarly, by rotating the dot counterclockwise in the second step above, we can show (2.17).

Now let us consider the example:

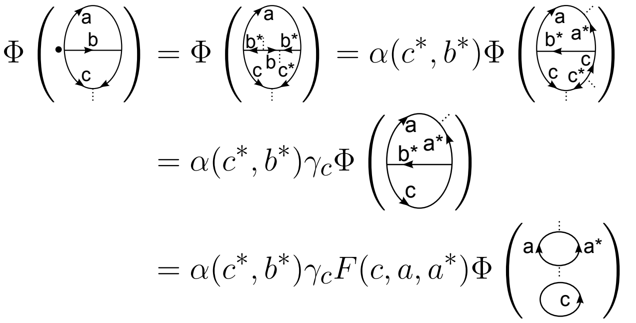

$$= \alpha(c^*, b^*)\gamma_c F(c, a, a^*)\gamma_{a^*} d_a d_{c^*} \Phi(\text{vacuum})$$

$$= \alpha(c^*, b^*)\gamma_c F(c, a, a^*)\gamma_{a^*} d_a d_{c^*}.$$

In the first step we convert both of the vertices to "basic" vertices which have one incoming and two outgoing strings. We then use Eq. (2.16) in the second step. Rules (2.8), (2.4) and (2.3) are then applied in sequence. Finally we use the normalization convention (2.5).

The above example is typical: in general, any string-net configuration can be reduced to the vacuum configuration by applying the above rules and conventions multiple times. In this way, these rules completely determine the wave function Φ.

2.4.4 Self-consistency conditions

We have seen that the rules (2.2 - 2.4) and the conventions (2.6 - 2.15) uniquely specify the wave function Φ. Accordingly, the wave function Φ is completely determined once the parameters $\{F(a,b,c), d_a, \alpha(a,b), \gamma_a\}$ are given. However, not every choice of parameters corresponds to a well-defined wave function. The reason is that for most choices of these parameters, the local rules/constraints are *not self-consistent* – that is, there are no wave functions Φ that satisfy them. In fact, only those $\{F, d, \gamma, \alpha\}$ that satisfy the following algebraic equations lead to self-consistent rules and a well-defined wave function Φ:

$$F(a+b,c,d) \cdot F(a,b,c+d) = \qquad (2.18a)$$

$$F(a,b,c) \cdot F(a,b+c,d) \cdot F(b,c,d),$$

$$F(a,b,c) = 1 \text{ if } a \text{ or } b \text{ or } c = 0, \qquad (2.18b)$$

$$d_a d_b = d_{a+b}, \qquad (2.18c)$$

$$\gamma_a = F(a^*, a, a^*) d_a, \qquad (2.18d)$$

$$\alpha(a,b) = F(a,b,(a+b)^*)\gamma_{a+b}. \qquad (2.18e)$$

We now explain why these conditions are necessary for self-consistency; we show that they are sufficient in appendix A.2. We begin with the first equation (2.18a). The origin of this condition can be understood by considering the sequence of manipulations shown in Fig. 2.4. We can see that the amplitudes of the string-net configurations (a) and (c) can be related to one another in two different ways: $(a) \to (b) \to (c)$ and $(a) \to (d) \to (e) \to (c)$. In order for these two relations to be consistent with one another, F must satisfy equation (2.18a), known as the "pentagon identity." The other conditions can be derived from similar consistency requirements (see appendix A.2).

In addition to equations (2.18), we will need to impose one more constraint on $\{F, d, \gamma\, \alpha\}$

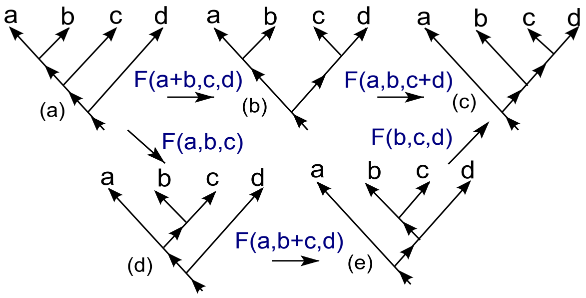

Figure 2.4: The amplitude of (a) can be related to the amplitude (c) in two different ways by the fusion rule (2.4). Self-consistency requires the two sequences of operation result in the same linear relations between the amplitudes of (a) and (c).

in order to construct a consistent string-net model:

$$|F(a,b,c)| = 1. \tag{2.19}$$

This constraint, known as the "unitarity condition", has a different origin from equations (2.18): it is not necessary for constructing a well-defined wave function Φ, but rather for constructing an exactly soluble Hamiltonian with Φ as its ground state. More specifically, we will see that (2.19) is important in ensuring that our exactly soluble Hamiltonians are *Hermitian* (see appendix A.6).

Readers that are familiar with Ref. [65] may notice that the self-consistency conditions (2.18), (2.19) appear different from the corresponding conditions in Eq. (9), (15) of Ref. [65]. Despite the apparent differences, it is possible to show that the two sets of conditions are equivalent — provided that $\alpha = \gamma = 1$ and d, F obey reflection symmetry, as assumed in Ref. [65].

2.4.5 Gauge transformations

In general, it is not so easy to find solutions to the conditions (2.18) and (2.19). However, once we have one solution $\{F, d, \gamma, \alpha\}$, we can construct an infinite class of other solutions

$\{\tilde{F}, \tilde{d}, \tilde{\gamma}, \tilde{\alpha}\}$ by defining

$$\begin{aligned}
\tilde{F}(a,b,c) &= F(a,b,c) \cdot \frac{f(a,b+c)f(b,c)}{f(a,b)f(a+b,c)}, \\
\tilde{d}_a &= d_a, \\
\tilde{\gamma}_a &= \gamma_a \cdot \frac{f(a,a^*)}{f(a^*,a)}, \\
\tilde{\alpha}(a,b) &= \alpha(a,b) \cdot \frac{f(b,(a+b)^*)f(a,a^*)}{f(a,b)f((a+b)^*,a+b)}.
\end{aligned} \tag{2.20}$$

Here $f(a,b)$ is any complex function with

$$|f(a,b)| = 1 \quad , \quad f(a,b) = 1 \quad \text{if } a \text{ or } b = 0.$$

Similarly, we can construct solutions by defining

$$\begin{aligned}
\tilde{F}(a,b,c) &= F(a,b,c), \\
\tilde{d}_a &= d_a \cdot g(a), \\
\tilde{\gamma}_a &= \gamma_a \cdot g(a), \\
\tilde{\alpha}(a,b) &= \alpha(a,b) \cdot g(a+b)
\end{aligned} \tag{2.21}$$

where $g(a)$ is any complex function with

$$|g(a)| = 1 \quad , \quad g(a+b) = g(a) \cdot g(b). \tag{2.22}$$

We will refer to (2.20),(2.21) as "gauge transformations" and we will say that $\{F, d, \gamma, \alpha\}$ and $\{\tilde{F}, \tilde{d}, \tilde{\gamma}, \tilde{\alpha}\}$ are "gauge equivalent" if they differ by such a transformation. As the name suggests, gauge equivalent solutions are closely related to one another. In fact, it is possible to show that if $\{F, d, \gamma, \alpha\}$ and $\{\tilde{F}, \tilde{d}, \tilde{\gamma}, \tilde{\alpha}\}$ are gauge equivalent solutions to (2.18), (2.19), then the corresponding wave functions $\Phi, \tilde{\Phi}$ can be transformed into one another by a *local unitary transformation* (See appendix A.3). Here, by a local unitary transformation we mean a unitary transformation that can be generated by the time evolution of a local Hamiltonian over a finite period of time. The existence of this local unitary transformation has an important physical meaning: it implies that Φ and $\tilde{\Phi}$ belong to the same quantum phase. [18, 31] Therefore, if we are primarily interested in constructing different topological phases, then we only need to consider one solution to (2.18,2.19) within each gauge equivalence class.

This freedom to make gauge transformations can be quite useful. For example, using the first gauge transformation (2.20), we can always transform γ so that

$$\gamma_a = \begin{cases} \pm 1, & \text{if } a = a^* \\ 1, & \text{otherwise} \end{cases} . \tag{2.23}$$

The second gauge transformation, parameterized by $g(a)$ is also quite useful. As we show in section 2.10, this transformation allows us, in many cases, to transform γ, α so that $\gamma_a = \alpha(a,b) = 1$.

Another gauge transformation which can simplify our models can be obtained by generalizing the conventions (2.12) and (2.13) to

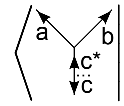

$= \beta(a,b)$

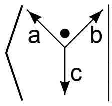

,

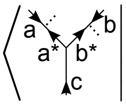

$= \beta(a,b)$

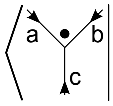

(2.24)

where $|\beta(a,b)| = 1$ are complex numbers with modulus 1. With this modification, the self-consistency condition (2.18e) becomes

$$\alpha(a,b) = \frac{\beta(b,c)}{\beta(a,b)} F(a,b,(a+b)^*) \gamma_{a+b}. \tag{2.25}$$

It is not hard to show that by choosing β appropriately, we can always transform α so that

$$\alpha(a,b) = \begin{cases} 1 \text{ or } \omega \text{ or } \omega^2, & \text{if } a = b = (a+b)^* \\ 1, & \text{otherwise} \end{cases} \tag{2.26}$$

where ω is a 3rd root of unity.

2.5 String-net Hamiltonians

In this section, we will construct a large class of exactly soluble lattice Hamiltonians that have the wave functions Φ as their ground states. The basic input for our construction is a finite abelian group G and a solution $\{F(a,b,c), d_a, \gamma_a, \alpha(a,b)\}$ to the self-consistency conditions, (2.18,2.19). Given this input, we will construct an exactly soluble Hamiltonian whose ground state $|\Phi_{latt}\rangle$ obeys the local rules (2.2 - 2.4) and (2.6 - 2.15) on the lattice. Our construction of this Hamiltonian is nearly identical to that of Ref. [65]. The only difference are the γ, α factors and the associated "dot" structure that were introduced in section 2.4.2.

2.5.1 Definition of the Hamiltonian

Let us first specify the Hilbert space for our model. The model is a generalized spin system, where the spins are located on the links of the 2D honeycomb lattice. Each spin can be $|G|$ different states which are labeled by elements of the group: $\{|a\rangle : a \in G\}$. When a spin is in state $|a\rangle$, we regard the link as being occupied by a string of type-a, oriented in certain direction. If the spin is in state $|0\rangle$, we think of the link as being occupied by the null string.

The Hamiltonian for our model is of the form

$$H = -\sum_I Q_I - \sum_p B_p. \tag{2.27}$$

Here, the two sums run over the sites I and plaquettes p of the honeycomb lattice. The

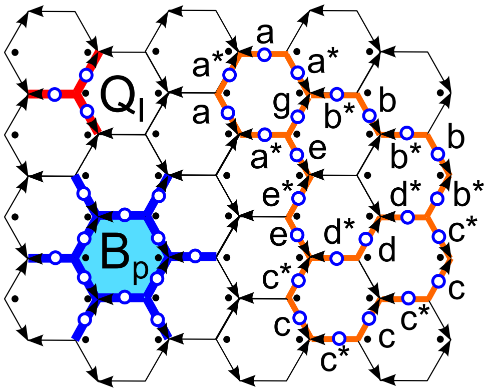

Figure 2.5: Lattice spin model (2.27). The Q_I operator acts on three spins on the links connected to vertex I, while the B_p operator acts on 12 spins on the links adjacent to the hexagonal plaquette p. The Q_I term constrains the string-nets to satisfy the branching rules while the B_p term provides dynamics for the string-nets. On the right is the typical ground state configuration. The $a = 0$ spin state corresponds to the vacuum or null string.

operator Q_I acts on the 3 spins adjacent to the site I :

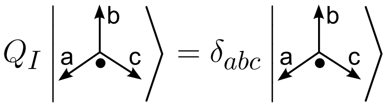

(2.28)

where

$$\delta_{abc} = \begin{cases} 1, & \text{if } a + b + c = 0 \\ 0, & \text{otherwise} \end{cases} \tag{2.29}$$

(See Fig. 2.5). We can see that the Q_I term penalizes states that don't satisfy the branching rules.

The operator B_p provides dynamics for the string-net configurations and makes them condense. The definition of this operator is more complicated. It can be written as a linear combination

$$B_p = \sum_{s \in G} a_s B_p^s \tag{2.30}$$

where B_p^s describes a 12 spin interaction involving the spins on the 12 links that are adjacent to the vertices of the hexagon p (See Fig. 2.5) and where a_s are some complex coefficients satisfying $a_{s^*} = a_s^*$. The operator B_p^s has a special structure, which we now describe. First, it annihilates any state that does not obey the branching rules at the 6 vertices surrounding the plaquette. Second, while it acts non-trivially on the inner 6 spins along the boundary of p, it does not affect the outer 6 spins at all. The outer spins are still important, however, because the matrix element of B_p^s between two inner spin configurations, $\langle g, h, i, j, k, l|$ and $|g', h', i', j', k', l'\rangle$ depends on the state of the outer spins, (a, b, c, d, e, f). These matrix elements are defined by

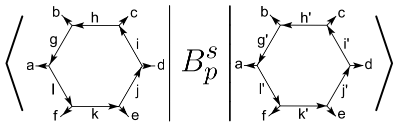

$$= B^{s,ghijkl}_{p,g'h'i'j'k'l'}(abcdef)$$

where

$$B^{s,ghijkl}_{p,g'h'i'j'k'l'}(abcdef) = \delta^{g+s}_{g'}\delta^{h+s}_{h'}\delta^{i+s}_{i'}\delta^{j+s}_{j'}\delta^{k+s}_{k'}\delta^{l+s}_{l'}$$
$$\cdot F_{s^*g'b} \cdot F_{s^*h'c} \cdot F_{s^*i'd} \cdot F_{s^*j'e} \cdot F_{s^*k'f} \cdot F_{s^*l'a}. \tag{2.31}$$

and $F_{abc} \equiv F(a, b, c)$. Note that the above expression is only valid if the initial and final states obey the branching rules, i.e. $h = b + g$, $h' = b + g'$, etc. If either state doesn't obey the branching rules, the matrix element of B_p^s vanishes.

An important point is that the above matrix elements are calculated for a particular orientation configuration in which the inner links are oriented cyclically. This choice of orientations leads to simple matrix elements, but unfortunately there is no way to extend this orientation configuration to the whole honeycomb lattice while preserving translational symmetry. If we instead choose the translationally invariant orientation configuration shown in Fig. 2.5, the matrix elements are modified as

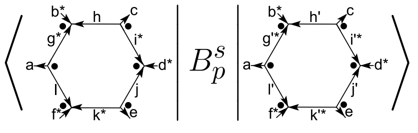

$$= \mathbf{B}^{s,ghijkl}_{p,g'h'i'j'k'l'}(abcdef)$$

with

$$\mathbf{B}^{s,ghijkl}_{p,g'h'i'j'k'l'}(abcdef) = B^{s,ghijkl}_{p,g'h'i'j'k'l'}(abcdef) \cdot \frac{\alpha_{g^*l}\alpha_{h'c}\alpha_{j^*i}\alpha_{k'f}\gamma_g\gamma_i\gamma_k}{\alpha_{g'^*l'}\alpha_{hc}\alpha_{j'^*i'}\alpha_{kf}\gamma_{g'}\gamma_{i'}\gamma_{k'}}. \tag{2.32}$$

The additional factors come from reversing the orientations on the g, i, k links.

Although the algebraic definition of B_p^s is complicated, there is an alternative graphical representation for this operator which is much simpler. It is convenient to describe this graphical representation in terms of the action of B_p^s on a bra $\langle X|$ rather than describing its action on a ket $|X\rangle$. In the graphical representation, the action of B_p^s can be understood as adding a loop of the type-s string around the boundary of p:

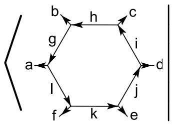

$B_p^s =$

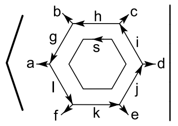

. (2.33)

To obtain matrix elements of B_p^s, we use the local rules (2.2 - 2.4) and (2.6 - 2.15) to "fuse" the string s onto the links along the boundary of the plaquette. That is, using these rules, we express

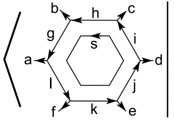

as the state

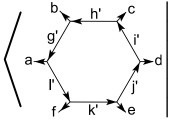

multiplied by some constant. This constant tells us the matrix element of B_p^s between the state

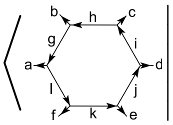

and the state

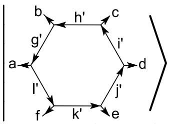

. In appendix A.4, we show that this prescription reproduces the formula in equation (2.31).

It is worth clarifying how exactly we use the local rules, especially since the first three rules (2.2 - 2.4) involve the wave function Φ. To be precise, we replace every rule of the form $\Phi(X) = \sum_i c_i \Phi(X_i)$ (i.e. 2.2 - 2.4) with a linear relation $\langle X| = \sum_i c_i \langle X_i|$. We then use these linear relations along with the linear relations (2.6 - 2.15) to fuse the string s onto the boundary of plaquette, and obtain the required matrix elements.

2.5.2 Properties of the Hamiltonian

Assuming $\{F(a,b,c), d_a, \gamma_a, \alpha(a,b)\}$ satisfy conditions (2.18) and (2.19), the Hamiltonian has many nice properties. The first property is that the Hamiltonian is Hermitian as long as $a_{s^*} = a_s^*$. This result follows from the identity

$$(B_p^s)^\dagger = B_p^{s^*} \tag{2.34}$$

which we derive in appendix A.6.

The second property is that the Q_I and B_p^s operators commute with each other:

$$[Q_I, Q_J] = 0 \ , \ [Q_I, B_p^s] = 0 \ , \ [B_p^s, B_{p'}^{s'}] = 0. \tag{2.35}$$

The first two equalities follow easily from the definitions of Q_I, B_p^s. The third equation is less trivial. We give an algebraic derivation of this identity in appendix A.5.

Equations (2.35) tell us that every term in the Hamiltonian (2.27) commutes with every other term so that the model is exactly soluble. This exact solubility holds for any value of the coefficients a_s. However, in what follows, we will focus on a particular value for these coefficients, for which the mathematical structure of the model is especially simple. In particular, we consider the case where

$$a_s = \frac{d_s}{|G|}. \tag{2.36}$$

It can be shown that $d_{s^*} = d_s^*$ so that this choice of a_s is compatible with the requirement $a_s^* = a_{s^*}$.

The third property of the Hamiltonian (which holds for the above choice of a_s) is that the Q_I and B_p are projection operators – i.e. they have eigenvalues $0, 1$. It is easy to derive this result for Q_I; the derivation for B_p is given in appendix A.6.

Putting these results together, we can now derive the low energy properties of H. Let

$|q_I, b_p\rangle$ denote the simultaneous eigenstates of Q_I, B_p:

$$Q_I|q_I, b_p\rangle = q_I|q_I, b_p\rangle \ , \ B_p|q_I, b_p\rangle = b_p|q_I, b_p\rangle \tag{2.37}$$

Then the corresponding energies are

$$E = -\sum_I q_I - \sum_p b_p. \tag{2.38}$$

Since the eigenvalues q_I, b_p can be either $0, 1$, it is clear that the ground state(s) have $q_I = b_p = 1$ for all I, p, while the excited states have $q_I = 0$ or $b_p = 0$ for at least one site I or plaquette p. In particular, we see that there is a finite energy gap separating the ground state(s) from the excited states. All that remains is to determine the ground state degeneracy. This degeneracy depends on the global topology of our system. In appendix A.8, we show that for a disk-like geometry with open boundary conditions (see Fig. A.4), there is a unique state with $q_I = b_P = 1$. In other words, the ground state is non-degenerate. On the other hand, in a periodic torus geometry, we find that there are $|G|^2$ degenerate ground states. This degeneracy on a torus is a consequence of the topological order in our system.[93, 94, 24]

The final property of our model which we establish in appendix A.6 is that the (unique) ground state of the lattice model in a disk geometry, $|\Phi_{latt}\rangle$, obeys the local rules (2.2 - 2.4) and (2.6 - 2.15). Therefore, since the local rules determine the ground state wave function uniquely, we conclude that $|\Phi_{latt}\rangle$ is identical to the continuum wave function Φ, restricted to string-net configurations on the honeycomb lattice. In other words, we have successfully constructed an exactly soluble Hamiltonian whose ground state is $|\Phi\rangle$. From now on, we will use $|\Phi\rangle$ to denote both the lattice ground state and the continuum wave function, since the two are effectively identical.

2.6 Quasiparticle excitations

In this section, we will derive the topological properties of the quasiparticle excitations of the string-net Hamiltonian (2.27). In particular, we will find all the topologically distinct types of quasiparticles and compute their braiding statistics with one another. Similarly to Ref. [65], our analysis proceeds in two steps: first, we construct "string" operators that create the quasiparticle excitations, and then we use the commutation algebra of the string operators to derive the quasiparticle braiding statistics.

2.6.1 *String operator picture*

Previously, it has been argued that quasiparticle excitations with nontrivial braiding statistics cannot be created by applying local operators to the ground state. Instead, these excitations are naturally created using extended *string-like* operators.[63] The basic picture is as follows. For each topologically distinct quasiparticle excitation α, there is a corresponding string operator. We denote this string operator by $W_\alpha(P)$ where P is the path along which the string operator acts. In general, $W_\alpha(P)$ is defined for both open and closed paths P; in the former case, we refer to $W_\alpha(P)$ as an open string operator, while in the latter case, we say that $W_\alpha(P)$ is a closed string operator.

The string operator $W_\alpha(P)$ is characterized by several properties. First, if P is an open path, then when $W_\alpha(P)$ is applied to the ground state $|\Phi\rangle$, the result is

$$W_\alpha(P)|\Phi\rangle = |\Phi_{ex}\rangle \tag{2.39}$$

where $|\Phi_{ex}\rangle$ is an excited state containing a quasiparticle α at one end of P, and the antiparticle of α at the other end of P. Second, the excited state created by an open string operator does not depend on the path of the string:

$$W_\alpha(P)|\Phi\rangle = W_\alpha(P')|\Phi\rangle \tag{2.40}$$

for any two paths P, P' that have the same endpoints. Third, if P is a closed path, then $W_\alpha(P)$ does not create any excitations at all: $W_\alpha(P)|\Phi\rangle \propto |\Phi\rangle$.

Physically, one may think of an open string operator as describing a process in which a particle-antiparticle pair is created out of the ground state and the two particles are brought to the two ends of the string. Likewise, a closed string operator describes a process in which a pair of quasiparticles is created, and then one of them is moved around the path of the string until it returns to its original position, where it annihilates its partner. Note that throughout this discussion, we assume that the system is defined in a topologically trivial geometry, such as a disk. In topologically non-trivial geometries, there are additional complications coming from the existence of multiple degenerate ground states, which we will not discuss here.

2.6.2 Constructing the string operators

We now construct string operators that create each of the different quasiparticle excitations of the string-net Hamiltonian (2.27). We follow the same strategy as Ref. [65]. First, we describe a particular ansatz for defining string operators in terms of certain data. Next we search for the special choices of data that lead to string operators satisfying the path independence condition (2.40). Finally, we argue that the set of string operators that we find is complete in the sense that it allows us to create *all* of the topologically distinct quasiparticle types.

We begin by describing our ansatz for constructing string operators. This ansatz allows us to build a string operator $W(P)$ given some data $(s, \omega, \bar{\omega})$, where $s \in G$, and ω, $\bar{\omega}$ are two complex-valued functions defined on the group G with $\omega(0) = \bar{\omega}(0) = 1$. Here we suppress the string label α until later discussion of the quasiparticles. First, suppose that P is a closed path. In order to define $W(P)$ we need to specify how $W(P)$ acts on each string-net configuration. Here, we find it convenient to define the action of $W(P)$ on a bra $\langle X|$ rather than describing its action on a ket $|X\rangle$. We describe the action of $W(P)$ using a graphical representation. More specifically, when $W(P)$ is applied to a string-net state $\langle X|$, it simply adds a “dashed” string along the path P “under” the preexisting string-nets:

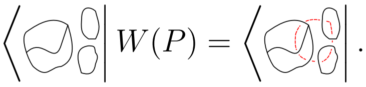

(2.41)

We then replace the dashed string with a type-s string, and we replace every crossing using the rules

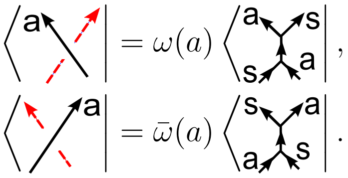

(2.42)

After making these replacements, the end result is a new string-net state $\langle X'|$, multiplied by a product of complex numbers $\omega(a)$, $\bar{\omega}(a)$ – one for each crossing. This construction defines the action of the operator $W(P)$. That is, if $\langle X|$ is the initial string-net state then $\langle X|W(P) = c\langle X'|$ where $\langle X'|$ is the final string-net state obtained by adding a dashed string using the above rules and c is a product of the $\omega(a)$ and $\bar{\omega}(a)$ factors along the path P.

The above ansatz allows us to define string operators in the continuum; we now explain how to define the string operators on the *lattice*. Let P be a closed path on the honeycomb lattice. The corresponding string operator $W(P)$ is defined as follows. First, we shift the path P slightly so that it no longer lies exactly on the honeycomb lattice. The way in which the path P is shifted is not especially important, but for concreteness, we follow a particular prescription for shifting the path P, shown in Fig. 2.6. The action of the operator $W(P)$ can then be described by a four step process. In the first three steps, we add a dashed string along the path P, replace the dashed string with a type-s string, and replace each crossing using the rules (2.42). In the final step, we use the local rules (2.2 - 2.4) and (2.6 - 2.15) to “fuse” the string s onto the links along the path P. In the above discussion, we have implicitly assumed that the initial string-net state $\langle X|$ obeys the branching rules at all the vertices along the path P; if $\langle X|$ does not obey the branching rules at any of these vertices,

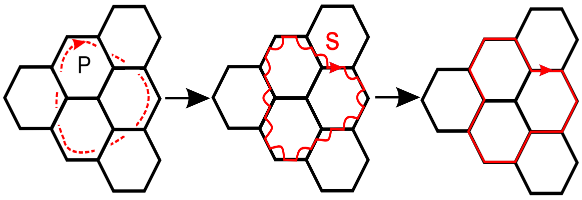

Figure 2.6: The action of the string operator $W(P)$ along a path P on the honeycomb lattice. First, the $W(P)$ operator adds a dashed line along the path P under the preexisting string-nets. Then we replace the dashed line with a type-s string and use (2.42) to resolve the crossings. Finally, we use the local rules (2.2 - 2.4) and (2.6 - 2.15) to fuse the string s onto the links along the path P.

then we define $\langle X|W(P) = 0$.

The reader may notice that the definition of the closed string operators is very similar to the graphical representation of the plaquette term in Hamiltonian, B_p^s (2.33). [3] Just like B_p^s, it is possible to construct an explicit algebraic formula for the matrix elements of $W(P)$. We will not write out the explicit formula here, but the basic structure is very similar to B_p^s: one finds that the string operator $W(P)$ only affects the spin states along the path P, and the matrix elements between these spin states are a function of the spins on the edges adjacent to P.

We can also define *open* string operators on the lattice. We use a graphical representation very similar to the closed string case: the action of an open string operator $W(P)$ is defined by adding a dashed string along the path P (shifted slightly) and then using the local rules (2.2 - 2.4) and (2.6 - 2.15), (2.42) to resolve crossings and fuse the string onto the links along P. There is some arbitrariness in defining the action of the string operator near the endpoints of P since the local rules are not defined for string-net configurations that violate the branching rules. However, it does not matter how exactly we define the action of the string operator near its endpoints, since this choice only affects the *local* properties of the quasiparticle excitation created by $W(P)$, and does not affect the *topological* properties which are our main concern here.

---

[3] In fact, B_p^s can be thought of as a special case of a closed string operator where the string runs along the boundary of a single plaquette p.

2.6.3 Path independence constraint

The above ansatz allows us to define a string operator $W(P)$ for each choice of $(s, \omega, \bar{\omega})$. However, we are only interested in the special class of string operators that create deconfined quasiparticle excitations when we apply them along an open path. As discussed above, these string operators must satisfy path independence (2.40): $W(P)|\Phi\rangle = W(P')|\Phi\rangle$ for any two paths P, P' that have the same endpoints. Below we search for the special values of $(s, \omega, \bar{\omega})$ that lead to path independent string operators.

To this end, we note that the path independence condition can be equivalently written as

$$\langle X|W(P)|\Phi\rangle = \langle X|W(P')|\Phi\rangle \tag{2.43}$$

where $\langle X|$ is an arbitrary string-net state. Furthermore, we observe that we only need to check path independence for "elementary" deformations $P \to P'$, since larger deformations can be built out of elementary ones. In this way, we can see that W will satisfy path independence if and only if

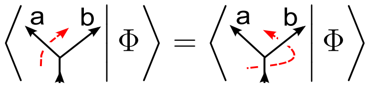

(2.44)

for any a, b and

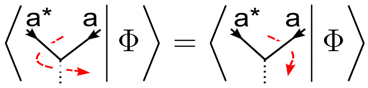

(2.45)

for any a. (The reason that the above two elementary deformations are sufficient to establish general path independence is that any vertex with any set of orientations can be built out of the above two vertices according to (2.11), (2.12), (2.13); thus the above two conditions imply path independence with respect to every vertex).

To proceed further, we translate the above graphical relations (2.44-2.45) into algebraic conditions on $(s, \omega, \bar{\omega})$ using the local rules (2.2 - 2.4), (2.6 - 2.15) and (2.42). The result is (see appendix A.9):

$$\omega(a)\omega(b) = \omega(a+b)\cdot\frac{F_{abs}F_{sab}}{F_{asb}}\frac{F_{s(a+b)(a+b)^*}}{F_{saa^*}F_{sbb^*}}, \tag{2.46}$$

$$\bar{\omega}(a) = \omega(a)^{-1}\cdot F^{-1}_{ass^*}F^{-1}_{saa^*}. \tag{2.47}$$

Next, we define

$$\mathbf{w}(a)=\omega(a)F(s,a,a^*) \quad , \quad \bar{\mathbf{w}}(a)=\bar{\omega}(a)F(a,s,s^*),$$

$$c_s(a,b)=\frac{F(a,b,s)F(s,a,b)}{F(a,s,b)}. \tag{2.48}$$

The above relations can then be written in the simple form

$$\mathbf{w}(a)\mathbf{w}(b)=c_s(a,b)\mathbf{w}(a+b), \tag{2.49}$$

$$\bar{\mathbf{w}}(a)=\mathbf{w}(a)^{-1}. \tag{2.50}$$

We wish to find all complex valued functions $\mathbf{w},\bar{\mathbf{w}}: G\to\mathbb{C}$ that satisfy (2.49), (2.50). Clearly, it is sufficient to find $\mathbf{w}$ satisfying (2.49), as $\bar{\mathbf{w}}$ can be obtained immediately from Eq. (2.50).

To solve Eq. (2.49), we observe that the self-consistency condition (2.18a) implies that $c_s(a,b)$ obeys the identity

$$c_s(a,b)c_s(a+b,c)=c_s(b,c)c_s(a,b+c). \tag{2.51}$$

Equation (2.51) means that $c_s(a,b)$ is a well-known mathematical object, namely the “factor system” of a projective representation.[17] From this point of view, the problem of solving equation (2.49) is equivalent to the problem of finding a (1D) projective representation $\mathbf{w}: G\to\mathbb{C}$ corresponding to the factor system $c_s(a,b)$.

There are two cases to consider: $c_s(a,b)$ may be symmetric in a,b or it may be non-symmetric. First, suppose $c_s(a,b)$ is non-symmetric. In this case, we can see that Eq. (2.49) has no nonzero solutions, since the left-hand side is manifestly symmetric in a,b while the right-hand side is non-symmetric. Hence, our ansatz does not yield any path independent string operators of type s. To build a path independent string operator, we have to use a more general ansatz[65] where the parameters $\mathbf{w}, \bar{\mathbf{w}}$ are *matrices* rather than scalars. Equivalently, we need to look for higher dimensional projective representations with factor system $c_s(a,b)$. We will not discuss this construction here since the resulting particles have *non-abelian* statistics,[76] and our focus is on models with purely abelian statistics. In fact, throughout this chapter we will restrict to choices of $F(a,b,c)$ such that $c_s(a,b)$ is symmetric for all s.

If $c_s(a,b)$ is symmetric, Eq. (2.49) can be solved as follows. Since every finite abelian group is isomorphic to a direct product of cyclic groups, we can assume without loss of generality that the group is $G = \mathbb{Z}_{N_1} \times ... \times \mathbb{Z}_{N_k}$. Let $a_1, a_2, ..., a_k$ be the generators of G. Once we find the value of $\mathbf{w}(a_k)$ for each generator a_k, then $\mathbf{w}$ is fully determined by equation (2.49). To find the value of $\mathbf{w}(a_k)$, we first rewrite equation (2.49) as

$$\frac{\mathbf{w}(a)\mathbf{w}(b)}{\mathbf{w}(a+b)} = c_s(a,b). \tag{2.52}$$

Setting $a = a_k$ and $b = ya_k$ where y is some integer, we obtain

$$\frac{\mathbf{w}(a_k)\mathbf{w}(ya_k)}{\mathbf{w}((y+1)a_k)} = c_s(a_k, ya_k). \tag{2.53}$$

We then take the product of the above equations over $y = 0, 1, ..., N_k - 1$. After canceling terms on the left hand side, and using the fact that $N_k a_k = 0$, we find

$$\mathbf{w}(a_k)^{N_k} = \prod_{y=0}^{N_k-1} c_s(a_k, ya_k). \tag{2.54}$$

We can see that $\mathbf{w}(a_k)$ can take N_k different values for each k. Hence, there are $\prod_k N_k = |G|$ solutions to Eqs. (2.49), (2.50) for each choice of s. The parameter s can also take $|G|$

different values, so altogether we find $|G|^2$ solutions, corresponding to $|G|^2$ path independent string operators.

At this point we have constructed $|G|^2$ string operators. Since these string operators satisfy path independence, we know that when we apply them to the ground state (along an open path) they will create quasiparticle excitations at the ends of the string. Thus, the above operators will allow us to construct $|G|^2$ different quasiparticle excitations. The next question is to determine whether this set of excitations is complete, i.e. whether it contains every topologically distinct quasiparticle. To address this question, we recall that the ground state degeneracy of the model on a torus is $|G|^2$, and hence by general arguments we expect that the system supports a total of $|G|^2$ topologically distinct excitations. Furthermore, we will show later that the above quasiparticle excitations are all topologically distinct. Putting these two facts together, we conclude that the above set of quasiparticles is indeed complete.

2.6.4 Labeling scheme for quasiparticle excitations

Having constructed all the quasiparticle excitations, we now describe a scheme for labeling these excitations. To begin, we note that it is sufficient to define a labeling scheme for the solutions to Eq. (2.49) since these solutions are in one-to-one correspondence with the different excitations. Next, we recall that Eq. (2.49) has $|G|$ different solutions $\mathbf{w}$ for each string type $s \in G$. Thus, an obvious way to label the different solutions is to use a string type index $s \in G$, together with an integer index that runs over $1, ..., |G|$, e.g. $\mathbf{w}_{(s,1)}, \mathbf{w}_{(s,2)}, ..., \mathbf{w}_{(s,|G|)}$.

While the above labeling scheme is perfectly adequate, we will see below that it is actually more natural to label the solutions to Eq. (2.49) by a string type index $s \in G$ together with an index m that runs over the different $1D$ linear representations of G. We note that this alternative scheme is sensible since every abelian group has exactly $|G|$ different $1D$ representations.

Following the latter approach, we will label each type-s solution to Eq. (2.49) by an ordered pair $\alpha = (s, m)$ where $s \in G$ and m is a $1D$ representation of G. We will denote this solution by $\mathbf{w}_\alpha$. Similarly we will denote the corresponding string operator by W_α, and we will refer to the quasiparticle excitation created by W_α as α.

In order to make this labeling scheme well-defined, we need to specify a particular type-s solution $\mathbf{w}_{(s,m)}$ to Eq. (2.49) for each ordered pair (s, m). We begin with the special case where $s = 0$. In this case, equation (2.49) takes a simple form since $c_0(i, j) = 1$ (by Eqs. (2.48),(2.18b)):

$$\mathbf{w}(a)\mathbf{w}(b) = \mathbf{w}(a + b). \tag{2.55}$$

We can see that the above equation is precisely the condition for $\mathbf{w}$ to be a $1D$ linear representation of G. Hence, there is a very natural way to define a solution $\mathbf{w}_{(0,m)}$ for each m: we simply define

$$\mathbf{w}_{(0,m)} = \rho_m \tag{2.56}$$

where ρ_m is the $1D$ representation corresponding to m.

Next we explain how $\mathbf{w}_{(s,m)}$ is defined when $s \neq 0$. Here, we proceed in two steps. In the first step, we choose some arbitrary type-s solution to Eq. (2.49) and we define $\mathbf{w}_{(s,0)}$ to be this solution; the particular solution we choose is a matter of convention – we will give some examples of conventions in sections 2.7.1,2.7.2. After choosing $\mathbf{w}_{(s,0)}$, we then define

$$\mathbf{w}_{(s,m)} = \mathbf{w}_{(s,0)} \cdot \rho_m. \tag{2.57}$$

To understand why this definition is sensible, note that $\mathbf{w}_{(s,0)} \cdot \rho_m$ will always solve Eq. (2.49) if $\mathbf{w}_{(s,0)}$ solves Eq. (2.49). Hence, (2.57) gives a complete parameterization of the different type-s solutions to Eq. (2.49).

At this point, it is useful to introduce some terminology. We will call the $(s, 0)$ excitations "fluxes" and the $(0, m)$ excitations "charges." Likewise, we will think of a general excitation (s, m) as a composite of a flux and a charge. We think of the parameter s as describing the amount of flux carried by the excitation, while m describes the amount of charge. The

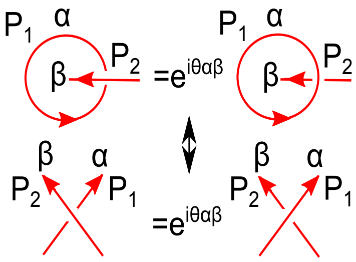

Figure 2.7: Computation of mutual statistics from string operators. On the top, we compare the action of $W_\beta(P_2)W_\alpha(P_1)$ with its reverse action $W_\alpha(P_1)W_\beta(P_2)$. The phase difference between the two products is equal to the mutual statistics $e^{i\theta_{\alpha\beta}}$ between the two quasiparticles created by W_α, W_β. In the bottom, we zoom in around the intersection point since the commutation algebra only depends on the properties of the string operators near the intersection point.

motivation for this terminology is that the mutual statistics between the $(s, 0)$ and $(0, m)$ excitations is identical to the mutual statistics between fluxes and charges in lattice gauge theory, as we will demonstrate in sections 2.7.1,2.7.2. (Note that our definitions of fluxes and charges are reversed with respect to Ref. [65]. The reason that we use a different terminology from Ref. [65] is that in this chapter, we prefer to think of our models as gauge theories on the dual triangular lattice, while Ref. [65] considered the string-net models as gauge theories on the honeycomb lattice).

In this language, the basic idea behind our labeling scheme is to define the "pure" charge excitations $(0, m)$ using Eq. (2.56), and to define the pure fluxes $(s, 0)$ in some arbitrary way – the definition of the pure fluxes is a matter of convention. All the other excitations can then be labeled as a composite of a charge and a flux, as in Equation (2.57).

2.6.5 *Braiding statistics of quasiparticles*

In the previous section, we constructed a string operator W_α for each ordered pair $\alpha = (s, m)$ where $s \in G$, and m is a 1D representation of G. We argued that these $|G|^2$ string operators serve as creation operators for $|G|^2$ different quasiparticle excitations, which we label by α. In this section, we will compute the braiding statistics of these quasiparticle excitations. More specifically, we will compute the mutual statistics $\theta_{\alpha\beta}$ for every pair of quasiparticles α, β, as well as the exchange statistics θ_α for every quasiparticle α. Here we use the convention that $\theta_{\alpha\beta}$ and θ_α are associated with clockwise braiding of particles.

To begin, we review the general relationship between braiding statistics and the string operator algebra in abelian topological phases. First we explain how the mutual statistics $\theta_{\alpha\beta}$ is encoded in the string algebra; afterwards, we will discuss the exchange statistics θ_α. Let α, β be two (abelian) quasiparticle excitations with mutual statistics $\theta_{\alpha\beta}$, and let W_α, W_β be the corresponding string operators. Then, for any two paths P_1, P_2 that intersect one another as in Fig. 2.7, the corresponding string operators $W_\alpha(P_1), W_\beta(P_2)$ obey the commutation algebra[46, 63, 65]

$$W_\beta(P_2)W_\alpha(P_1)|\Phi\rangle = e^{i\theta_{\alpha\beta}}W_\alpha(P_1)W_\beta(P_2)|\Phi\rangle \tag{2.58}$$

where $|\Phi\rangle$ denotes the ground state of the system. A simple way to derive this result is to consider the case where P_2 is an open path, and P_1 forms a closed loop (see Fig. 2.7. In this case, the two string operators $W_\alpha(P_1)$, $W_\beta(P_2)$ have different physical interpretations. The operator $W_\beta(P_2)$ describes a process in which β and its antiparticle are created and then moved to opposite endpoints of the path P_2. On the other hand, $W_\alpha(P_1)$ describes a three step physical process in which (1) α and its antiparticle are created out of the ground state $|\Phi\rangle$, (2) α is moved all the way around the closed loop P_1, and then finally (3) α and its antiparticle are annihilated. Given these interpretations, we can see that the left hand side of (2.58) describes a process in which α is first moved around P_1 and then β and its antiparticle are moved to the endpoints of P_2, while the right hand side describes a process in which β and its antiparticle are first moved to the endpoints of P_2 and then α is moved around P_1. By the definition of mutual statistics, we know that these two processes differ by the statistical Berry phase $e^{i\theta_{\alpha\beta}}$, thus implying Eq. (2.58). More generally, one can argue that Eq. (2.58) holds for *any* two paths P_1, P_2 that intersect each other once, since the commutation algebra depends only on the properties of the string operators near the intersection point.

The exchange statistics θ_α is also encoded in the string operator algebra. In the most

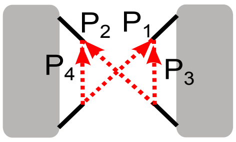

Figure 2.8: A "local" vacuum state $|0_{\text{loc}}\rangle$ with four strings ending at the four endpoints of P_1, P_2 or P_3, P_4. The shaded regions represent arbitrary string-net configurations.

general case, θ_α can be extracted by examining the commutation relations between three string operators, as discussed in Ref. [63]. However, the calculation of θ_α can be simplified, using the fact that W_α obeys the path independence conditions (2.44-2.45), and that $W_\alpha(P \cup P') = W_\alpha(P)W_\alpha(P')$ for any two paths P, P' that share an endpoint. Using these properties, it can be shown that $W_\alpha(P_1), W_\alpha(P_2), W_\alpha(P_3), W_\alpha(P_4)$ obey the algebra

$$W_\alpha(P_2)W_\alpha(P_1)|\Phi\rangle = e^{i\theta_\alpha}W_\alpha(P_4)W_\alpha(P_3)|\Phi\rangle \tag{2.59}$$

for any four paths P_1, P_2, P_3, P_4 with the geometry of Fig. 2.9 (See appendix A.10 for a derivation).

With the above relations in hand, we are now ready to compute the statistics of the quasiparticle excitations in our model. We begin with the exchange statistics. Let $\alpha = (s, m)$ be any quasiparticle excitation. We wish to find the exchange statistics of α. The first step is to multiply both sides of Eq. (2.59) by the "no-string" (vacuum) state $\langle 0|$:

$$\langle 0|W_\alpha(P_2)W_\alpha(P_1)|\Phi\rangle = e^{i\theta_\alpha}\langle 0|W_\alpha(P_4)W_\alpha(P_3)|\Phi\rangle. \tag{2.60}$$

(More precisely, instead of multiplying by the global vacuum state $\langle 0|$, we should multiply by a *local* vacuum state $\langle 0_{\text{loc}}|$ which contains four strings ending at the four endpoints of P_1, P_2 or P_3, P_4 as shown in Fig. 2.8. This choice ensures that the matrix elements in (2.60) are nonzero, which will be important below. In the following discussion, we will use $\langle 0|$ as a shorthand for $\langle 0_{\text{loc}}|$).

Next, we note that the graphical definition of W_α tells us that the action of $W_\alpha(P_2)$ on

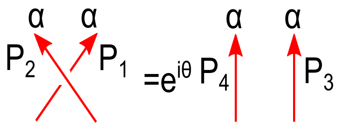

Figure 2.9: Computation of exchange statistics from string operators. The commutation relation of string operators $W_\alpha(P_2)W_\alpha(P_1) = e^{i\theta}W_\alpha(P_4)W_\alpha(P_3)$ gives the exchange statistics of quasiparticle α provided W_α is path independent and $W_\alpha(P \cup P') = W_\alpha(P)W_\alpha(P')$.

$\langle 0|$ is simply to add a type-s string along the path P_2 (there are no additional phase factors since $\omega_\alpha(0) = 1$ by assumption). The same is true for $W_\alpha(P_4)$, so we obtain:

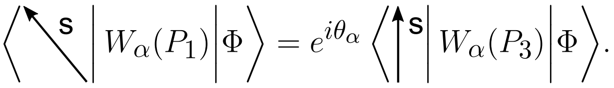

(2.61)

Applying the definition of W_α once more, we derive

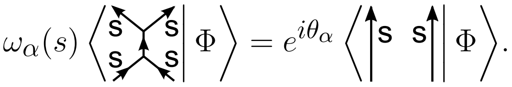

(2.62)

At the same time, using the local rules (2.4), we have

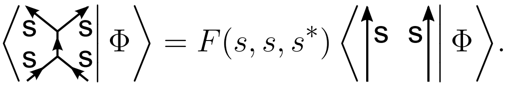

(2.63)

We conclude that

$$
\begin{aligned}
e^{i\theta_\alpha} &= \omega_\alpha(s)F(s, s, s^*) \\
&= \mathbf{w}_\alpha(s). \qquad (2.64)
\end{aligned}
$$

Next, we find the mutual statistics between two excitations $\alpha = (s, m)$, $\beta = (t, n)$. Similarly to above, the first step is to multiply both sides of Eq. (2.58) by the ket $\langle 0|$:

$$\langle 0|W_\beta(P_2)W_\alpha(P_1)|\Phi\rangle = e^{i\theta_{\alpha\beta}}\langle 0|W_\alpha(P_1)W_\beta(P_2)|\Phi\rangle. \qquad (2.65)$$

Evaluating the action of the string operators on both sides as above, we derive

$\Big\langle$ 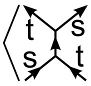

$\Big| \, \Phi \Big\rangle \omega_\alpha(t) = e^{i\theta_{\alpha\beta}} \bar{\omega}_\beta(s) \Big\langle$ 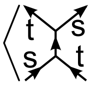

$\Big| \, \Phi \Big\rangle . \qquad (2.66)$

We conclude that

$$\begin{aligned} e^{i\theta_{\alpha\beta}} &= \frac{\omega_\alpha(t)}{\bar{\omega}_\beta(s)} \\ &= \frac{\mathbf{w}_\alpha(t)}{\bar{\mathbf{w}}_\beta(s)} \\ &= \mathbf{w}_\beta(s)\mathbf{w}_\alpha(t). \end{aligned} \qquad (2.67)$$

As a consistency check, note that when $\alpha = \beta$, the above expression simplifies to

$$e^{i\theta_{\alpha\alpha}} = \mathbf{w}_\alpha(s)^2 = e^{2i\theta_\alpha} \qquad (2.68)$$

as it should.

The above formulas (2.64), (2.67) allow us to compute the complete set of quasiparticle braiding statistics given any solution to the self-consistency conditions, $(F(a,b,c), d_a, \alpha(a,b), \gamma_a)$. The computation requires several steps. First, we need to compute $c_s(a,b)$ from $F(a,b,c)$. Second, we need to solve Eq. (2.49). Third, we need to define our labeling scheme by specifying which solutions we label by $\mathbf{w}_{(s,0)}$. Finally, after taking these steps, we can obtain the exchange statistics of $\alpha = (s,m)$ and the mutual statistics between $\alpha = (s,m)$ and $\beta = (t,n)$ using Eqs. (2.64) and (2.67).

In sections 2.7.1,2.7.2, we will follow the above procedure to find the complete quasiparticle braiding statistics for every abelian string-net model. However, before proceeding to the general case, it is illuminating to consider a few special cases where the quasiparticle braiding statistics are particularly simple. We begin with the exchange statistics of the charge excitations $(0,m)$. From equation (2.64) we can see that the exchange statistics of

$\alpha = (0, m)$ is given by

$$\exp(i\theta_{(0,m)}) = \mathbf{w}_{(0,m)}(0) = \rho_m(0) = 1 \qquad (2.69)$$

where the second equality follows from equation (2.56). We conclude that the charge excitations are all *bosons*.

It is also simple to derive the mutual statistics between two charge excitations $\alpha = (0, m)$, $\beta = (0, n)$. From equation (2.67) we have

$$\exp(i\theta_{(0,m)(0,n)}) = \mathbf{w}_{(0,n)}(0)\mathbf{w}_{(0,m)}(0) = 1 \qquad (2.70)$$

implying that the charge excitations are *mutually bosonic*.

Finally, it is easy to compute the mutual statistics between a charge excitation $\alpha = (0, m)$ and a flux excitation $\beta = (t, 0)$:

$$\exp(i\theta_{(0,m)(t,0)}) = \mathbf{w}_{(t,0)}(0)\mathbf{w}_{(0,m)}(t) = \rho_m(t) \qquad (2.71)$$

where the second equality follows from equation (2.56). The above result (2.71) is exactly equal to the Aharonov-Bohm phase associated with braiding a charge m around a flux t in conventional lattice gauge theory. This similarity is not a coincidence, since these models are in fact realizations of the topological lattice gauge theories of Dijkgraaf and Witten[23], as discussed in the introduction.

The results (2.69), (2.70), and (2.71) reveal an important feature of the quasiparticle statistics in abelian string-net models: we can see that both the mutual/exchange statistics of the charges (2.69), (2.70), and the mutual statistics between fluxes and charges (2.71), depend only on the group G. In other words, these quantities depend only on the branching rules, not on the parameters $(F(a, b, c), d_a, \alpha(a, b), \gamma_a)$ that describe the more detailed structure of the string-net condensate. Hence, these quantities are not useful for distinguishing different types of string-net condensates with the same branching rules; to make these distinctions, we need to examine the exchange/mutual statistics of the *flux* excitations $(s, 0)$.

2.6.6 Expressing braiding statistics in terms of $F(a, b, c)$

In this section, we obtain formulas that directly relate the quasiparticle braiding statistics to $F(a, b, c)$. In some cases, these formulas may provide the easiest approach for computing the quasiparticle statistics. In other cases, it may be more convenient to use the more indirect approach outlined below equation (2.68).

To begin, we derive a formula for the exchange statistics of a pure flux quasiparticle $\alpha = (s, 0)$. To obtain the exchange statistics of $\alpha = (s, 0)$, we need to find $\mathbf{w}_\alpha(s)$. Following the same steps as in the derivation of Eq. (2.54), it is easy to show that

$$(\mathbf{w}_\alpha(s))^p = \prod_{y=0}^{p-1} c_s(s, ys) = \prod_{y=0}^{p-1} F(s, ys, s) \tag{2.72}$$

where p is the smallest positive integer such that $p \cdot s = 0$. Applying the formula for exchange statistics (2.64), we conclude that

$$\exp(pi\theta_{(s,0)}) = \prod_{y=0}^{p-1} F(s, ys, s). \tag{2.73}$$

Naively, one might think that the above result (2.73) only provides *partial* information about the exchange statistics since it only tells us $\theta_{(s,0)}$ modulo $2\pi/p$. However this partial information is the best we can hope for, unless we specify a particular convention for which quasiparticle is labeled by $(s, 0)$. To see this, note that Eq. (2.57) implies that

$$\exp(i\theta_{(s,m)}) = \exp(i\theta_{(s,0)}) \cdot \rho_m(s) \tag{2.74}$$

where ρ_m is the $1D$ representation corresponding to m. It is not hard to show that as m runs over the set of $1D$ representations, $\rho_m(s)$ runs over the set of pth roots of unity, $e^{2\pi i k/p}$.

Therefore if we change our labeling convention so that $(s, 0) \to (s, m)$, the exchange statistics $\theta_{(s,0)}$ can shift by any multiple of $2\pi/p$.

In light of this observation, we can see that equations (2.73) and (2.74) actually give us complete information about the exchange statistics of every quasiparticle excitation. To compute the exchange statistics, we simply set $e^{i\theta_{(s,0)}}$ equal to one of the pth roots of $\prod_{y=0}^{p-1} F(s, ys, s)$ for each s. We can choose whatever pth root of unity that we like – different choices correspond to different definitions of what constitutes a "pure" flux $(s, 0)$. Once we have $e^{i\theta_{(s,0)}}$, we can then compute $e^{i\theta_{(s,m)}}$ for any m using Eq. (2.74).

Like the exchange statistics, it is also possible to express the mutual statistics $\theta_{\alpha\beta}$ directly in terms of $F(i, j, k)$. The simplest way to do this is to use the relationship between mutual statistics and exchange statistics, namely

$$\theta_{\alpha\beta} = \theta_\gamma - \theta_\alpha - \theta_\beta \tag{2.75}$$

where γ is the quasiparticle obtained by fusing α with β.

2.7 Quasiparticle statistics of general abelian string-net models

So far we have derived a general framework for constructing abelian string-net models and computing their quasiparticle braiding statistics. We now use this machinery to derive the quasiparticle statistics of all possible abelian string-net models. First, in section 2.7.1, we find the quasiparticle statistics for the simplest class of models, namely the models corresponding to the group $G = \mathbb{Z}_N$. Then, in section 2.7.2, we will analyze the general case $G = \mathbb{Z}_{N_1} \times ... \times \mathbb{Z}_{N_k}$.

2.7.1 $\mathbb{Z}_N$ string-net models

We begin by analyzing the abelian string-net models with group $G = \mathbb{Z}_N$. We note that a similar analysis of $\mathbb{Z}_N$ string-net models, using a different formalism, was given in Ref. [56].

Also an analysis of $\mathbb{Z}_N$ string-net models with parity invariance was given in Ref. [39].

To begin, we recall that in the $\mathbb{Z}_N$ models, the string type a can be thought of as group element $a \in \mathbb{Z}_N$ or equivalently integers $a \in \{0, 1, ..., N-1\}$. The dual string type is defined by $a^* = -a \pmod N$, while the allowed branchings are the triplets (a, b, c) that satisfy $a + b + c = 0 \pmod N$.

The first step is to construct all possible string-net models with the above $\mathbb{Z}_N$ structure. To do this, we need to find all solutions to the self-consistency equations (2.18), (2.19). In fact, it suffices to find all solutions to (2.18), (2.19) *up to* gauge transformations, since gauge equivalent solutions correspond to string-net models in the same quantum phase.

Given this freedom to make gauge transformations, we can assume without loss of generality that $d_a \equiv 1$ since we can clearly gauge transform any solution to (2.18c) to $d_a = 1$ using a g-gauge transformation (2.21) with $g(a) = d_a^{-1}$. It is then clear that $\gamma_a, \alpha(a, b)$ are fully determined by F according to (2.18d), (2.18e):

$$\begin{aligned} d_a = 1 \quad , \quad \gamma_a = F(a^*, a, a^*) \quad , \\ \alpha(a, b) = F(a, b, (a+b)^*)\gamma_{a+b}. \end{aligned} \tag{2.76}$$

The only remaining parameter is F, so our problem reduces to finding all $\{F(a, b, c)\}$ satisfying

$$F(a+b, c, d)F(a, b, c+d) = \tag{2.77}$$
$$F(a, b, c)F(a, b+c, d)F(b, c, d),$$
$$F(a, b, c) = 1 \quad \text{if } a \text{ or } b \text{ or } c = 0 \tag{2.78}$$

modulo the gauge transformation

$$\tilde{F}(a, b, c) = F(a, b, c) \cdot \frac{f(a, b+c)f(b, c)}{f(a, b)f(a+b, c)} \tag{2.79}$$

where $|f(a,b)| = 1$.

Fortunately, the problem of finding all solutions to equation (2.77), modulo the gauge transformations (2.79) is a well-known mathematical question from the subject of group cohomology[76, 17, 70]. In the context of group cohomology, the solutions to equation (2.77) are known as "3-cocycles", while the ratio $\frac{f(a,b+c)f(b,c)}{f(a,b)f(a+b,c)}$ is known as a "3-coboundary." The question of finding all cocycles modulo coboundaries is exactly the problem of computing the cohomology group $H^3(G, U(1))$.

In this section we are interested in the special case $G = \mathbb{Z}_N$. In this case, it is known that $H^3(\mathbb{Z}_N, U(1)) = \mathbb{Z}_N$. In particular, it is known that there are N distinct solutions to (2.77) up to gauge transformations. In addition, an explicit form for the N distinct solutions is known[76, 70]:

$$F(a,b,c) = e^{2\pi i \frac{pa}{N^2}(b+c-[b+c])}. \tag{2.80}$$

Here, the integer parameter $p = 0 \dots N-1$ labels the different solutions. The arguments a, b, c can take values in the range $0, 1, ..., N-1$ and the square bracket $[b+c]$ denotes $b+c$ (mod N) with values also taken in the range $0, 1, ..., N-1$. Notice that all of these solutions satisfy the additional constraint (2.78).

For each of the above N solutions, we can construct a corresponding string-net model, namely the exactly soluble lattice Hamiltonian defined in Eq. (2.27). Our next task is to derive the topological properties of these lattice models. In particular, we would like to determine the braiding statistics of the quasiparticle excitations in these models. To this end, let us recall that for a general abelian group G, the corresponding string-net model has $|G|^2$ topologically distinct quasiparticle excitations. These excitations can be labeled by ordered pairs $\alpha = (s, m)$ where s runs over the group elements $s \in G$, and m runs over the $1D$ representations of G. In the case of $G = \mathbb{Z}_N$, the group elements $s \in G$ can be parameterized by integers $s = 0, 1, ..., N-1$ and the $1D$ representations can also be parameterized by integers $m = 0, 1, ..., N-1$, where the representation $\rho_m : G \to \mathbb{C}$ is defined by

$$\rho_m(a) = e^{2\pi i \frac{ma}{N}}.$$

We now compute the braiding statistics of the quasiparticle excitations $\alpha = (s, m)$. We follow the approach outlined below Eq. (2.67). First, we compute $c_s(a, b)$:

$$c_s(a,b) = \frac{F(a,b,s)F(s,a,b)}{F(a,s,b)} = e^{2\pi i \frac{ps}{N^2}(a+b-[a+b])}.$$

Next, we solve Eq. (2.49) for each s. By inspection, we can see that one solution of Eq. (2.49) is given by $\mathbf{w}(a) = \exp(2\pi i \frac{psa}{N^2})$. We choose the convention where the above solution is labeled by $\alpha = (s, 0)$, i.e., we define

$$\mathbf{w}_{(s,0)}(a) = e^{2\pi i \frac{psa}{N^2}}.$$

Then, by Eq. (2.57) we have

$$\mathbf{w}_{(s,m)}(a) = e^{2\pi i \left(\frac{psa}{N^2} + \frac{ma}{N}\right)}. \tag{2.81}$$

We are now ready to derive the exchange statistics and braiding statistics of the quasiparticle excitations. Substituting (2.81) into (2.64), we find that the exchange statistics of $\alpha = (s, m)$ is given by

$$\theta_{(s,m)} = 2\pi \left(\frac{ps^2}{N^2} + \frac{ms}{N}\right). \tag{2.82}$$

Evidently there are two contributions to the exchange statistics of (s, m) quasiparticle: the first term can be interpreted as coming from flux-flux exchange statistics while the second term can be thought of charge-flux Aharonov-Bohm phase.

Similarly, substituting (2.81) into (2.67), we find that the mutual statistics of $\alpha = (s, m)$ and $\beta = (t, n)$ is

$$\theta_{(s,m)(t,n)} = 2\pi \left(\frac{2pst}{N^2} + \frac{ns+mt}{N}\right). \tag{2.83}$$

Again, we can see that there are two contributions to the statistics: one coming from the flux-flux statistics and the other from moving s and t fluxes around n and m charges respectively.

2.7.2 $\mathbb{Z}_{N_1} \times \cdots \times \mathbb{Z}_{N_k}$ string-net models

We now generalize the discussion to abelian string-net models with group $G = \mathbb{Z}_{N_1} \times \cdots \times \mathbb{Z}_{N_k}$. Since every finite abelian group is isomorphic to a direct product of cyclic groups, this case is sufficiently general to cover all abelian string-net models.

To begin, let us recall the structure of these models. In these models, the strings are labeled by group elements $a \in \mathbb{Z}_{N_1} \times \cdots \times \mathbb{Z}_{N_k}$. Equivalently, the string types can be parameterized by k-component integer vectors $a = (a_1, a_2, ..., a_k)$ where $0 \leq a_i \leq N_i - 1$. The dual string is defined by $a_i^* = -a_i \pmod{N_i}$ for each i, while the allowed branchings are the triplets (a, b, c) that satisfy $a_i + b_i + c_i = 0 \pmod{N_i}$ for each i.

The next step is to find all possible $\mathbb{Z}_{N_1} \times \cdots \times \mathbb{Z}_{N_k}$ string-net models. As in the $\mathbb{Z}_N$ case discussed above, the latter problem reduces to finding all $F(a, b, c)$ satisfying (2.77), (2.78) modulo the gauge transformation (2.79). This problem is closely related to the problem of computing the cohomology group $H^3(\prod_i \mathbb{Z}_{N_i}, U(1))$. This cohomology group has been calculated previously and is given by[76, 70]

$$\begin{aligned} H^3\left(\prod_i \mathbb{Z}_{N_i}, U(1)\right) &= \prod_i \mathbb{Z}_{N_i} \cdot \prod_{i<j} \mathbb{Z}_{(N_i,N_j)} \\ &\cdot \prod_{i<j<k} \mathbb{Z}_{(N_i,N_j,N_k)} \end{aligned} \tag{2.84}$$

where (N_i, N_j) denotes the greatest common divisor of N_i and N_j, and similarly for (N_i, N_j, N_k).

Now, as explained in section 2.6.3, it is important to distinguish between two types of solutions to (2.77), (2.78): solutions with $c_s(a, b) = c_s(b, a)$, and solutions with $c_s(a, b) \neq c_s(b, a)$ where c_s is defined as in Eq. (2.48). In the former case, the corresponding string-net model has only abelian quasiparticle excitations, while in the latter case, the model supports non-abelian excitations.[76] In this chapter, we focus entirely on models with abelian excitations, so we will restrict ourselves to solutions that satisfy $c_s(a,b) = c_s(b,a)$. It is known[76] that the solutions with this property are classified by a subgroup of the cohomology group $H^3(\prod_i \mathbb{Z}_{N_i}, U(1))$, namely $\prod_i \mathbb{Z}_{N_i} \prod_{i<j} \mathbb{Z}_{(N_i,N_j)}$. In particular, the total number of gauge inequivalent solutions to (2.77) is

$$\mathcal{N} = \prod N_i \cdot \prod_{i<j} (N_i, N_j). \tag{2.85}$$

An explicit form for the $\mathcal{N}$ distinct solutions is known:[76, 70]

$$F(a,b,c) = e^{2\pi i a^T \mathbf{N}^{-1} \mathbf{P} \mathbf{N}^{-1} (b+c-[b+c])}. \tag{2.86}$$

Here, the arguments a, b, c are k component integer vectors with $0 \leq a_i \leq N_i - 1$ for each i, and the square bracket $[b+c]$ denotes a vector whose i-th component is $(a_i + b_i) \pmod{N_i}$ with values taken in the range $0, 1, ..., N_i - 1$. The matrix $\mathbf{N}$ is the $k \times k$ diagonal matrix $\mathbf{N} = diag(N_1, ..., N_k)$ and $\mathbf{P}$ is a $k \times k$ upper-triangular integer matrix that parameterizes the different solutions. The diagonal elements of $\mathbf{P}$ are restricted to the range $0 \leq \mathbf{P}_{ii} \leq N_i - 1$, while the elements above the diagonal are restricted to the range $0 \leq \mathbf{P}_{ij} \leq (N_i, N_j) - 1$. As in the $\mathbb{Z}_N$ case, we can see that the $F(a,b,c)$ not only obey (2.77), but also satisfy the additional constraint (2.78).

The $\mathcal{N}$ solutions defined in (2.86) can be used to construct $\mathcal{N}$ different lattice models. Our next task is to determine the braiding statistics of the quasiparticle excitations in these models. These excitations can be labeled by ordered pairs $\alpha = (s, m)$ where s runs over the group elements $s \in G$, and m runs over the $1D$ representations of G. In the case of $G = \mathbb{Z}_{N_1} \times \cdots \times \mathbb{Z}_{N_k}$, the group elements $s \in G$ can be parameterized by k component integer vectors $s^T = (s_1, s_2, \ldots, s_k)$ with $0 \leq s_i \leq N_i - 1$, and the $1D$ representations can also be parameterized by k component integer vectors $m^T = (m_1, m_s, \ldots, m_k)$ with

$0 \leq m_i \leq N_i - 1$. In this parameterization, the representation $\rho_m : G \to \mathbb{C}$ is defined by

$$\rho_m(b) = e^{2\pi i m^T \mathbf{N}^{-1} b}.$$

To find braiding statistics of the quasiparticle excitations $\alpha = (s, m)$, we follow the same steps as in the $\mathbb{Z}_N$ case. First, we compute $c_s(a, b)$:

$$c_s(a, b) = e^{2\pi i s^T \mathbf{N}^{-1} \mathbf{P} \mathbf{N}^{-1} (a+b-[a+b])}.$$

Next, we solve Eq. (2.49) for each s. By inspection, we can see that one solution of Eq. (2.49) is given by $\mathbf{w}(a) = \exp(2\pi i s^T \mathbf{N}^{-1} \mathbf{P} \mathbf{N}^{-1} a)$. We choose the convention where the above solution is labeled by $\alpha = (s, 0)$, i.e., we define

$$\mathbf{w}_{(s,0)}(a) = e^{2\pi i s^T \mathbf{N}^{-1} \mathbf{P} \mathbf{N}^{-1} a}.$$

Then, by Eq. (2.57) we have

$$\mathbf{w}_{(s,m)}(a) = e^{2\pi i (s^T \mathbf{N}^{-1} \mathbf{P} \mathbf{N}^{-1} a + m^T \mathbf{N}^{-1} a)}. \tag{2.87}$$

We are now ready to derive the exchange statistics and braiding statistics of the quasiparticle excitations. Substituting (2.87) into (2.64), we find that the exchange statistics of $\alpha = (s, m)$ is given by

$$\theta_{(s,m)} = 2\pi (s^T \mathbf{N}^{-1} \mathbf{P} \mathbf{N}^{-1} s + m^T \mathbf{N}^{-1} s). \tag{2.88}$$

Similarly, substituting (2.87) into (2.67), we find that the mutual statistics of $\alpha = (s, m)$

and $\beta = (t, n)$ is

$$\begin{aligned}\theta_{(s,m)(t,n)} &= 2\pi(s^T\mathbf{N}^{-1}(\mathbf{P}+\mathbf{P}^T)\mathbf{N}^{-1}t \\ &+ n^T\mathbf{N}^{-1}s + m^T\mathbf{N}^{-1}t). \end{aligned} \tag{2.89}$$

2.8 Chern-Simons description

So far we have derived the basic topological properties of abelian string-net models, including their quasiparticle braiding statistics and their ground state degeneracy on a torus. It is natural to wonder: can these properties be described by some low energy effective theory? In this section, we find a field theoretic description in terms of multicomponent $U(1)$ Chern-Simons theory.

Before explaining this effective field theory description, we first (briefly) review the basic formalism of $U(1)$ Chern-Simons theory.[94, 93, 89] It is believed that the topological properties of any abelian gapped many-body system can be described by some M component $U(1)$ Chern-Simons theory of the form

$$L = \frac{K_{IJ}}{4\pi}\varepsilon^{\mu\nu\lambda}a_{I\mu}\partial_\nu a_{J\lambda} \tag{2.90}$$

where K is an $M \times M$ symmetric, non-degenerate integer matrix. In this formalism, the different quasiparticle excitations are described by coupling L to bosonic particles that carry integer gauge charge q_I for each gauge field a_I. Hence, the quasiparticles are parameterized by M component integer vectors q. The mutual statistics between two quasiparticles q and q' is

$$\theta_{qq'} = 2\pi q^T K^{-1} q' \tag{2.91}$$

while the exchange statistics of quasiparticle q is $\theta_q = \frac{1}{2}\theta_{qq}$. Two quasiparticles q and q' are said to be "topologically equivalent" if $q - q' = K\Lambda$ where Λ is an integer M component vector. The number of topologically distinct quasiparticles is given by $|\det K|$, as is the ground state degeneracy on the torus.

With this background, we are now ready to give a Chern-Simons description for the abelian string-net models. Recall that in the previous section, we explicitly constructed all possible abelian string-net models. These models are parameterized by two pieces of data: (1) a finite abelian group $G = \mathbb{Z}_{N_1} \times \ldots \mathbb{Z}_{N_k}$, and (2) a $k \times k$ upper triangular integer matrix $\mathbf{P}$ with $0 \leq \mathbf{P}_{ii} \leq N_i - 1$ and $0 \leq \mathbf{P}_{ij} \leq (N_i, N_j) - 1$. Our basic task is to find a K-matrix for each choice of G and $\mathbf{P}$ that captures the topological properties of the associated abelian string-net model. We will argue that the following K-matrix does the job:

$$K = \begin{pmatrix} \mathbf{0} & \mathbf{N} \\ \mathbf{N} & \tilde{\mathbf{P}} \end{pmatrix}. \tag{2.92}$$

Here, $\mathbf{N}$ is a $k \times k$ diagonal matrix, $\mathbf{N} = diag(N_1, ..., N_k)$, and $\tilde{\mathbf{P}}$ is a $k \times k$ symmetric, integer matrix defined by $\tilde{\mathbf{P}} = -\mathbf{P} - \mathbf{P}^T$. The '$\mathbf{0}$' is meant to denote $k \times k$ matrix with vanishing elements. Thus, K has dimension $2k \times 2k$.

To show that the abelian string-net models (2.86) are described by the above Chern-Simons theory (2.92), we need to establish a one-to-one correspondence between the quasiparticle excitations of each system. In the abelian string-net model, the quasiparticle excitations are parameterized by ordered pairs (s, m), where s, m are k component integer vectors with $0 \leq s_i, m_i \leq N_i - 1$ for each i. On the other hand, in the Chern-Simons theory (2.92), the topologically distinct quasiparticles are parameterized by $2k$ component integer vectors q (modulo $K\mathbb{Z}^{2k}$). Thus, we need a one-to-one correspondence between ordered pairs (s, m) and $2k$ component integer vectors q. It is easy to see that the following mapping does the job:

$$q = \begin{pmatrix} s \\ m \end{pmatrix} \quad (\text{modulo } K\mathbb{Z}^{2k}). \tag{2.93}$$

In fact, not only is this mapping a one-to-one correspondence, but it also preserves exchange statistics: i.e. the exchange statistics of q in the Chern-Simons theory is the same as the exchange statistics of (s, m) in the abelian string-net model. To see this, note that

$$\begin{aligned}
\theta_q &= \pi q^T K^{-1} q \\
&= \pi \begin{pmatrix} s & m \end{pmatrix} \cdot \begin{pmatrix} -\mathbf{N}^{-1}\tilde{\mathbf{P}}\mathbf{N}^{-1} & \mathbf{N}^{-1} \\ \mathbf{N}^{-1} & \mathbf{0} \end{pmatrix} \cdot \begin{pmatrix} s \\ m \end{pmatrix} \\
&= \pi(-s^T\mathbf{N}^{-1}\tilde{\mathbf{P}}\mathbf{N}^{-1}s + 2s^T\mathbf{N}^{-1}m) \\
&= \theta_{(s,m)}
\end{aligned} \tag{2.94}$$

where the last line follows from (2.88). Likewise, the mapping preserves mutual statistics: letting $q = \begin{pmatrix} s \\ m \end{pmatrix}$ and $q' = \begin{pmatrix} t \\ n \end{pmatrix}$, we have

$$\begin{aligned}
\theta_{qq'} &= 2\pi q^T K^{-1} q' \\
&= 2\pi \begin{pmatrix} s & m \end{pmatrix} \cdot \begin{pmatrix} -\mathbf{N}^{-1}\tilde{\mathbf{P}}\mathbf{N}^{-1} & \mathbf{N}^{-1} \\ \mathbf{N}^{-1} & \mathbf{0} \end{pmatrix} \cdot \begin{pmatrix} t \\ n \end{pmatrix} \\
&= 2\pi(-s^T\mathbf{N}^{-1}\tilde{\mathbf{P}}\mathbf{N}^{-1}t + s^T\mathbf{N}^{-1}n + m^T\mathbf{N}^{-1}t) \\
&= \theta_{(s,m)(t,n)}
\end{aligned} \tag{2.95}$$

where the last line follows from (2.89). We conclude that the quasiparticle braiding statistics of the Chern-Simons theory (2.92) exactly agree with the statistics of the abelian string-net model.

In addition to quasiparticle statistics, there is one other topological quantity we need to compare to be sure that the string-net models are described by the Chern-Simons theory (2.92).[45] This quantity is the thermal Hall conductance[42] (also known as the "chiral central charge"[47]). In general, the thermal Hall conductance of a multicomponent $U(1)$ Chern-Simons theory is given by the signature of the K matrix.[42] It is easy to check that the signature of (2.92) is 0, so we conclude that (2.92) has vanishing thermal Hall conductance.

At the same time, we know that the abelian string-net model has vanishing thermal Hall conductance, since the Hamiltonian is a sum of commuting projectors[4]. Thus, the thermal Hall conductances also match.

In summary, we have shown that the Chern-Simons theory (2.92) correctly captures the quasiparticle statistics and thermal Hall conductance of the abelian string-net model (2.86). In this sense, (2.92) provides a good low energy effective theory for the string-net model (2.86).

2.9 Characterizing the phases that can be realized by string-net models

Having systematically constructed all the abelian string-net models, we are faced with an important question: which topological phases can be realized by abelian string-net models, and which phases cannot be realized? In this section, we answer this question in three different ways: we describe three different criteria for characterizing the set of topological phases that can be realized by abelian string-net models. The first criterion is based on braiding statistics, the second based on the K-matrix formalism, and the third based on properties of the edge.

2.9.1 Braiding statistics and K-matrix characterizations

Our first criterion for determining whether a phase is realizable is based on braiding statistics and thermal Hall conductance. Specifically, we will show that an abelian topological phase is realizable if and only if (i) it has a vanishing thermal Hall conductance, and (ii) it has a least one *Lagrangian subgroup*. Here, a "Lagrangian subgroup"[45] $\mathcal{M}$ is a subset of quasiparticles with two properties. First, all the quasiparticles in $\mathcal{M}$ are bosons and have trivial mutual statistics with one another: $e^{i\theta_m} = e^{i\theta_{mm'}} = 1$ for all $m, m' \in \mathcal{M}$. Second, if

---

[4] see footnote 1

l is a quasiparticle that is not contained in $\mathcal{M}$, then it has nontrivial mutual statistics with at least one quasiparticle $m \in \mathcal{M}$: $e^{i\theta_{lm}} \neq 1$.

Before deriving the above result, we find it useful to explain another criterion for characterizing the set of realizable phases. We will then show that the two criteria are equivalent and prove them both simultaneously. The second criterion is based on the Chern-Simons K-matrix formalism. Here, the starting point for our analysis is the statement that every abelian topological phase can be described by a multicomponent $U(1)$ Chern-Simons theory with a symmetric, non-degenerate integer matrix K. The only constraint on K is that it must have even elements on the diagonal if the corresponding topological phase is built out of bosons, as we assume here.

Given this Chern-Simons framework, we should be able to find a criterion that tells us which K-matrices can be realized by abelian string-net models and which K-matrices cannot be realized. Naively, one might think that the answer to the question follows from equation (2.92): one might think that the realizable K-matrices are exactly the matrices of the form (2.92). However, this is not quite correct. The problem is that the correspondence between K-matrices and topological phases is not one-to-one: multiple K-matrices can correspond to the same topological phase. For example, if K, K' differ by a change-of-basis transformation of the form $K' = W^T K W$, where W is an integer matrix with determinant ± 1, then K, K' describe the same topological phase. [5] Given this equivalence between different K-matrices, we have to work a little bit harder to derive a criterion that distinguishes the realizable K-matrices from the non-realizable K-matrices. We will show that the following criterion does the job: a K-matrix is realizable if and only if it has even dimension, $2k \times 2k$, and there exist k linearly independent integer vectors $\Lambda_1, \dots, \Lambda_k$ such that

$$\Lambda_i^T K \Lambda_j = 0 \tag{2.96}$$

---

[5] One way to see that K, K' describe the same phase is to note that the corresponding Chern-Simons theories can be mapped onto one another by a field redefinition $a'_I = W_{IJ} a_j$.

for all i, j. The Λ_i are known as "null vectors."

We prove these results in three steps. First, we show that the braiding statistics and K-matrix criteria are equivalent to one another. Next, we show that the braiding statistics criterion is *necessary* for a phase to be realizable. Finally, we show that the K-matrix criteria are *sufficient* for a phase to be realizable. Once we establish these three claims, both results follow immediately.

The first claim — i.e. the fact that the braiding statistics and K-matrix criteria are equivalent to one another — follows immediately from Ref. [60]. Indeed, that work showed explicitly that a K-matrix satisfies (2.96) if and only if it satisfies conditions (i), (ii). Next, consider the second claim, namely the statement that the braiding statistics criteria are necessary for a phase to be realizable. To establish this result, it suffices to show that every string-net model obeys conditions (i) and (ii). This can be done straightforwardly: indeed, we know that all string-net models have a vanishing thermal Hall conductance, since their Hamiltonians are sums of commuting projectors[6]. Also, it is easy to see that the set of charge excitations $\{(0, m)\}$ always constitutes a Lagrangian subgroup (see Eqs. (2.69), (2.70), and (2.71)).

To complete the argument, we now show that the K-matrix criterion is sufficient for a phase to be realizable. In other words, we show that every K matrix that obeys (2.96) can be realized by an appropriate abelian string-net model. Our strategy will be to show that every K-matrix that obeys (2.96) can be written in the form (2.92) after making an appropriate change-of-basis transformation $K \to W^T K W$, where W is an integer matrix with determinant ±1. To this end, we observe that any K-matrix that obeys (2.96) can be written in the form

$$K = \begin{pmatrix} \mathbf{0} & \mathbf{A} \\ \mathbf{A}^T & \mathbf{B} \end{pmatrix}$$

after a suitable change of basis (see appendix A1b of Ref. [84] for a detailed proof). Next, we

---

[6] see footnote 1

use the Smith normal form to find matrices $\mathbf{S}, \mathbf{T}$ with unit determinant such that $\mathbf{SAT} = \mathbf{N}$, where $\mathbf{N}$ is a diagonal matrix, $\mathbf{N} = diag(N_1, \ldots, N_k)$. We then make the change of basis $K \to K' = W_1^T K W_1$, where

$$W_1 = \begin{pmatrix} \mathbf{S}^T & \mathbf{0} \\ \mathbf{0} & \mathbf{T} \end{pmatrix}.$$

After this change of variables, we have

$$K' = \begin{pmatrix} \mathbf{0} & \mathbf{N} \\ \mathbf{N} & \mathbf{B}' \end{pmatrix}$$

where $\mathbf{B}' = \mathbf{T}^T \mathbf{B} \mathbf{T}$. To complete the argument, we make one more change of basis: we define $K'' = W_2^T K' W_2$, where

$$W_2 = \begin{pmatrix} \mathbf{1} & \mathbf{U}^T \\ \mathbf{0} & \mathbf{1} \end{pmatrix}.$$

The result is

$$K'' = \begin{pmatrix} \mathbf{0} & \mathbf{N} \\ \mathbf{N} & \tilde{\mathbf{P}} \end{pmatrix} \tag{2.97}$$

where $\tilde{\mathbf{P}} = \mathbf{B}' + \mathbf{UN} + \mathbf{NU}^T$. It is not hard to see that we can always choose $\mathbf{U}$ so that $\tilde{\mathbf{P}}$ obeys the inequalities $0 \leq -\tilde{\mathbf{P}}_{ii} \leq 2(N_i - 1)$ and $0 \leq -\tilde{\mathbf{P}}_{ij} \leq (N_i, N_j) - 1$. This completes the argument.

2.9.2 *Examples of realizable and non-realizable phases*

We now describe a few representative examples of realizable and non-realizable phases. A simple example of a realizable phase is the phase corresponding to the K-matrix

$$K_1 = \begin{pmatrix} 0 & 2 \\ 2 & 0 \end{pmatrix}. \tag{2.98}$$

To see that K_1 is realizable, note that it has a null vector $\Lambda_1^T = \begin{pmatrix} 1 & 0 \end{pmatrix}$ and it has dimension 2×2, so it satisfies the two conditions from section 2.9.1. This Chern-Simons theory can equivalently be thought of as Z_2 gauge theory.[54]

More generally, it is easy to see that any K-matrix of the form $\begin{pmatrix} \mathbf{0} & \mathbf{N} \\ \mathbf{N} & \mathbf{0} \end{pmatrix}$ is realizable where $\mathbf{N} = diag(N_1, \ldots, N_k)$. Like K_1, these Chern-Simons theories are equivalent to discrete gauge theories where the gauge group is $G = \mathbb{Z}_{N_1} \times \cdots \times \mathbb{Z}_{N_k}$.

Another example of a realizable phase is:

$$K_2 = \begin{pmatrix} 2 & 0 \\ 0 & -2 \end{pmatrix}. \tag{2.99}$$

Again, it is easy to see that K_2 is realizable, since it has a null vector $\Lambda_1^T = (1, 1)$. This phase is an example of a "doubled Chern-Simons theory": it is a sum of two Chern-Simons theories with opposite chiralities. It is easy to see that general doubled Chern-Simons theories of the form $\begin{pmatrix} \mathbf{A} & \mathbf{0} \\ \mathbf{0} & -\mathbf{A} \end{pmatrix}$ are also realizable. Here, $\mathbf{A}$ is a symmetric, integer, non degenerate matrix, with even elements on the diagonal.

A third example of a realizable phase is given by

$$K_3 = \begin{pmatrix} 2 & 0 \\ 0 & -8 \end{pmatrix}. \tag{2.100}$$

Here, an appropriate null vector is given by $\Lambda_1^T = (2, 1)$. On other other hand, an example of a phase that is not realizable is

$$K_4 = \begin{pmatrix} 2 & 0 \\ 0 & -4 \end{pmatrix}. \tag{2.101}$$

One way to see this is to note that K_4 does not have any null vectors since the equation $2x^2 - 4y^2 = 0$ does not have any (nonzero) integer solutions.

The K_3, K_4 examples are interesting because they show that the simplest expectations for which topological phases can and cannot be realized by string-net models are incorrect. For example, an optimist might have guessed that the string-net models can realize all phases with vanishing thermal Hall conductance: indeed, this scenario is the best one could hope for since ground states of Hamiltonians which are sums of commuting projectors always have vanishing thermal Hall conductance, as discussed in the introduction. The K_4 example disproves this conjecture: K_4 has vanishing signature and therefore vanishing thermal Hall conductance, yet it apparently cannot be realized by any string-net model. Similarly, a pessimist might have guessed that the string-net models can only realize phases that are compatible with time-reversal symmetry since all the models realized in Ref. [65] were compatible with time-reversal symmetry. The K_3 example disproves this conjecture as well. To see this, note that the phase corresponding to K_3 is manifestly incompatible with time-reversal symmetry: indeed, this phase contains a particle with exchange statistics $\theta = -\pi/8$, but it does not contain any particle with the opposite exchange statistics, $+\pi/8$. We conclude that the set of realizable phases lies somewhere in between the pessimistic and optimistic scenarios: the string-net models can realize more than just the time-reversal symmetric phases, but they cannot realize all the phases with vanishing thermal Hall conductance.

2.9.3 Characterization in terms of gapped edges

In light of the K_3, K_4 examples discussed above, it is clear that the difference between realizable and non-realizable phases can be quite subtle. Thus, it is natural to wonder whether there is a *simple physical property* that distinguishes the two types of phases. Remarkably, such a property does exist: it is possible to show that an abelian topological phase is realizable if and only if the boundary between the phase and the vacuum can be fully gapped by suitable edge interactions. In other words, the realizable phases are exactly the phases that support *gapped edges*.

To derive this edge state characterization of realizable phases, we again make use of the results of Ref. [60]. In particular Ref. [60] proved that an abelian phase can support a gapped edge if and only if (i) it has a vanishing thermal Hall conductance and (ii) it has at least one Lagrangian group. In other words, the results of Ref. [60] imply that the edge state characterization is *equivalent* to the braiding statistics and K-matrix characterizations from section 2.9.1. Therefore, since we have already established the braiding statistics and K-matrix results (2.96), the edge state characterization follows immediately.

Before concluding, we would like to point out that it is actually quite easy to see that all realizable phases support a gapped edge: indeed in appendix A.7, we explicitly construct interactions that gap the boundary of a general abelian string-net model. Thus, we really only need Ref. [60] to prove the converse statement — i.e. to prove that all abelian phases with a gapped edge are realizable.

The above result has a number of interesting implications. One implication is that we can now show that even if we generalized our string-net construction to other types of branching rules, we would not realize any new abelian topological phases beyond those that we have realized here. To see this, we note that quite generally, *all* string-net models support a gapped edge, independent of their branching rules. Indeed, in appendix A.7, we construct explicit interactions that gap the edge of abelian string-net models. An identical construction can be used to gap the edge of general string-net models. [48] This construction means that the only topological phases that are accessible to string-net models are those that support gapped edges. Thus, since we have already realized every abelian phase with a gapped edge, we cannot possibly realize any new abelian phases, even if we consider other branching rules. (In fact, we believe that other types of branching rules always give *non-abelian* topological phases, though we do not have a proof of this conjecture).

2.10 Examples

In this section, we work out some illustrative examples, namely $\mathbb{Z}_2$, $\mathbb{Z}_3$, $\mathbb{Z}_4$ and $\mathbb{Z}_2 \times \mathbb{Z}_2$ string-net models. For each example, we determine whether α and γ can be gauged away by f and g gauge transformations. For the $\mathbb{Z}_2$ and $\mathbb{Z}_4$ models, we find a gauge where all $\gamma = \alpha = 1$. On the other hand, we find that for some of the $\mathbb{Z}_3$ models, every gauge has at least one $\alpha \neq 1$, while for some of the $\mathbb{Z}_2 \times \mathbb{Z}_2$ models, every gauge has at least one $\gamma \neq 1$. Thus, these examples show that the dot and null string structures are essential to realizing some, but not all, string-net models.

2.10.1 $\mathbb{Z}_2$ string-net model

First we specify the Hilbert space of the $\mathbb{Z}_2$ string-net models. The string types are labeled by $\mathbb{Z}_2$ group elements $\{0, 1\}$. The dual string types are $0^* = 0$, $1^* = 1$ (since $-1 \equiv 1 \pmod 2$). The branching rules are $\{(0, 0, 0), (0, 1, 1)\}$ which requires the strings form closed loops. Thus the Hilbert space is the set of all possible closed loops.

Next we construct the Hamiltonians and wave functions for the different $\mathbb{Z}_2$ string-net models. To do this, we have to solve the self-consistency conditions (2.18-2.19) for $\{F, d, \gamma, \alpha\}$. According to the general solution given in (2.80),(2.76), there are two distinct solutions, parameterized by an integer $p = 0, 1$:

$$\begin{aligned}
&F(1,1,1) = (-1)^p, \quad \gamma_1 = \alpha(1,0) = \alpha(0,1) = (-1)^p, \\
&\text{other } F, d, \gamma, \alpha = 1.
\end{aligned}$$

While the above solutions are perfectly sufficient for constructing exactly soluble models, it is desirable to have solutions with as many γ's and α's equal to 1 as possible, since this will lead to simpler models with more symmetry and topological invariance. Therefore, we now discuss how to simplify these solutions using the f, g gauge transformations (2.20, 2.21).

The first step in this simplification process is to choose a g-gauge transformation to make as many γ's equal to 1 as possible. In the above case, we can make every $\gamma = 1$ using $g(0) = 1, g(1) = (-1)^p$. After this gauge transformation we have

$$\begin{aligned} &F(1,1,1) = (-1)^p, \quad d_1 = (-1)^p, \\ &\text{other } F, d, \gamma, \alpha = 1. \end{aligned} \tag{2.102}$$

The second step in the simplification process is to use an f-gauge transformation to make as many α's equal to 1 as possible. However, in Eq. (2.102), we already have all $\alpha = 1$ and thus there is no need for an f-gauge transformation. We can see that in the above gauge, $\gamma = \alpha = 1$ so null strings and dots are irrelevant. Thus, the resulting solutions (2.102) can be constructed using the original formalism of Ref. [65].

With the solutions (2.102) in hand, we can construct the wave functions and Hamiltonian using (2.2 - 2.4), (2.6 - 2.15) and (2.27). For the $p = 0$ solution, the wave function is

$$\Phi(X) = 1 \tag{2.103}$$

for any closed string-net configuration X. The corresponding Hamiltonian is the toric code.[46, 65] On the other hand, for the $p = 1$ solution, the wave function is

$$\Phi(X) = (-1)^{\text{loop}(X)} \tag{2.104}$$

with loop(X) meaning the total number of closed loops in the configuration X. The corresponding Hamiltonian is the "doubled semion model." [65]

What if we work in other gauge, say $g(0) = 1, g(1) = -(-1)^p$? After this gauge transformation, we will get the solutions

$$\begin{aligned} &F(1,1,1) = (-1)^p, \ d_1 = -(-1)^p, \\ &\gamma_1 = \alpha(1,0) = \alpha(0,1) = -1, \ \text{others} = 1. \end{aligned}$$

In this gauge, we need to keep track of the null strings as well as the dot structure. However, for simplicity let us consider an orientation configuration on the honeycomb lattice where the orientations chosen so that there are no vertices with 3 incoming or 3 outgoing strings. In this case, there are no dots in the lattice model, and α can be safely ignored. The wave function for the $p = 0$ case can then be written as

$$\Phi(X) = (-1)^{\text{loop}(X)}(-1)^{(\text{null-in}(X)-\text{null-out}(X))/2}. \tag{2.105}$$

Here "null-in(X)" means the total number of vertices along the loops in X in which (1) two oppositely oriented strings and a null string meet one another, and (2) the null string lies on the *inside* of the loop. The quantity "null-out(X)" is similar except it counts vertices where the null string is on the outside of the loop. Similarly, the wave function for the $p = 1$ solution becomes

$$\Phi(X) = (-1)^{(\text{null-in}(X)-\text{null-out}(X))/2}. \tag{2.106}$$

We can see that the wave functions (2.105, 2.106) are more complicated than they are for the other gauge choice (2.103, 2.104). This motivates our efforts to gauge away γ and α as much as possible. That being said, we would like to mention that for some special orientation configurations, different gauges can lead to identical lattice wave functions. For example, for the honeycomb lattice with the orientations shown in Fig. 2.5, the g-gauge transformation does not change the wave function at all (see appendix A.3).

Independent of the gauge choice, the $p = 0, 1$ models each have $|G|^2 = 4$ distinct types of quasiparticles which are labeled by ordered pairs (s, m) with $s, m = 0, 1$. The braiding statistics of these particles can be read off from (2.82,2.83). Alternatively, we can describe these braiding statistics by an appropriate $U(1)$ Chern-Simons theory. In particular, according to the general result (2.92), these models are described by $U(1) \times U(1)$ Chern-Simons theories with K-matrix

$$K = \begin{pmatrix} 0 & 2 \\ 2 & -2p \end{pmatrix}.$$

2.10.2 $\mathbb{Z}_3$ string-net model

The $\mathbb{Z}_3$ models have three types of strings $\{0,1,2\}$ with dual strings $0^* = 0, 1^* = 2, 2^* = 1$. The branching rules are $\{(0,0,0),(0,1,2),(1,1,1),(2,2,2)\}$. Thus the Hilbert space consists of all possible string-nets with the above string types and branching rules.

To construct the Hamiltonians and wave functions for the $\mathbb{Z}_3$ models, we have to solve the self-consistency conditions for $\{F, d, \gamma, \alpha\}$. According to the general solution given in (2.80),(2.76), there are three distinct solutions, parameterized by an integer $p = 0, 1, 2$:

$$\begin{aligned}
&F(1,1,2) = F(1,2,1) = F(1,2,2) = e^{i2\pi p/3}, \\
&F(2,1,2) = F(2,2,1) = F(2,2,2) = e^{-i2\pi p/3}, \\
&\gamma_1 = e^{-i2\pi p/3}, \ \ \gamma_2 = e^{i2\pi p/3}, \\
&\alpha(1,0) = \alpha(0,1) = e^{-i2\pi p/3}, \\
&\alpha(2,0) = \alpha(0,2) = \alpha(1,1) = \alpha(2,2) = e^{i2\pi p/3}, \\
&\text{others } = 1.
\end{aligned}$$

As in the previous example, we now try to simplify this solution as much as possible using appropriate gauge transformations. First, we choose a g-gauge transformation (2.21) to make $\gamma = 1$. By choosing $g(a) = e^{i2\pi pa/3}$, we have

$$\begin{aligned}
&F(1,1,2) = F(1,2,1) = F(1,2,2) = e^{i2\pi p/3}, \\
&F(2,1,2) = F(2,2,1) = F(2,2,2) = e^{-i2\pi p/3}, \\
&d_1 = e^{i2\pi p/3}, \ d_2 = e^{-i2\pi p/3}, \\
&\alpha(2,2) = e^{-i2\pi p/3}, \ \text{others } = 1.
\end{aligned} \tag{2.107}$$

Next we look for an f-gauge transformation (2.20) to make $\alpha = 1$. However, when $p = 1, 2$ no such f exists. In fact, no combination of f, g can gauge away α completely. To see this, notice that if $a + a + a = 0$, the quantity $\alpha(a, a) \cdot \alpha(a^*, a^*)$ is gauge invariant under both f and g transformations. Hence, if this quantity is not equal to unity, then we have no hope of gauging away α. In the above case, we have $\alpha(1, 1) \cdot \alpha(2, 2) \neq 1$, so it is indeed not possible to find a gauge where $\alpha = 1$. We note that since α cannot be gauged away, the above $p = 1, 2$ solutions are not accessible to the original string-net construction of Ref. [65]. Thus, we have an explicit example of a string-net model that requires the dot structure to be realized.

As for the low energy excitations, the $p = 0, 1, 2$ models each have $|G|^2 = 9$ distinct quasiparticles labeled by ordered pairs (s, m) with $s, m = 0, 1, 2$. The quasiparticle statistics are described by the $U(1) \times U(1)$ Chern-Simons theory (2.92) with K-matrix

$$K = \begin{pmatrix} 0 & 3 \\ 3 & -2p \end{pmatrix}.$$

2.10.3 $\mathbb{Z}_4$ string-net model

As discussed in section 2.3.2, the Hilbert space for the $\mathbb{Z}_4$ models involves four string types labeled by $\{0, 1, 2, 3\}$. The dual string types are $0^* = 0, 1^* = 3, 2^* = 2, 3^* = 1$. The branching rules are $\{(0, 0, 0), (0, 1, 3), (0, 2, 2), (1, 1, 2), (3, 3, 2)\}$.

To construct the Hamiltonians and wave functions for the $\mathbb{Z}_4$ models, we solve the self-consistency conditions for $\{F, d, \gamma, \alpha\}$. As in the previous examples, we use the general solution (2.80),(2.76), which tells us that there are 4 solutions labeled by $p = 0, 1, 2, 3$. We then try to gauge away γ and α as much as possible using f, g. Interestingly we find a combination of gauge transformations which makes all $\gamma = \alpha = 1$ (more generally, such a gauge exists for any $\mathbb{Z}_N$ string-net model where N is not divisible by 3). To accomplish this, we first apply a g-gauge transformation (2.21) with $g(a) = i^{pa}$ followed by an f-gauge transformation with $f(3,2) = (-i)^p$, $f(3,3) = (-1)^p$. The result is:

$$\begin{aligned}
&F_{113} = F_{331} = F_{232} = F_{212} = F_{131} = i^p, \\
&F_{133} = F_{311} = F_{123} = F_{321} = F_{313} = (-i)^p, \\
&F_{122} = F_{231} = F_{223} = F_{312} = F_{222} = F_{333} = (-1)^p, \\
&d_1 = i^p,\ d_2 = (-1)^p,\ d_3 = (-i)^p,\ \text{others } = 1.
\end{aligned} \tag{2.108}$$

Since $\alpha = \gamma = 1$, these models can be defined without worrying about dots or null strings, as in Ref. [65]. (However, the reflection symmetry constraint in Ref. [65] $d_s = d_{s^*}$ suppresses the $p = 1, 3$ solutions.) As a result, the local rules are simple and highly symmetric. For example, the nontrivial local rules corresponding to F are given by:

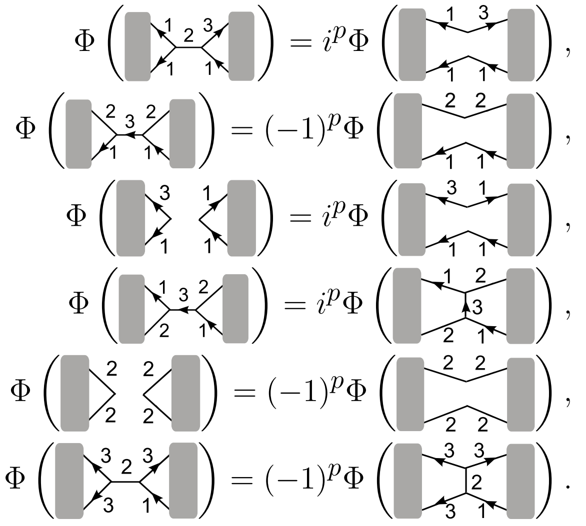

Here, each rule summarizes a group of nontrivial F which are related by 90, 180 and 270 degree rotational symmetry.

Each of these models have $|G|^2 = 16$ distinct quasiparticles which are labeled by ordered pairs (s, m) with $s, m = 0, 1, 2, 3$. The braiding statistics are described by the $U(1) \times U(1)$

Chern-Simons theory (2.92) with K-matrix

$$K = \begin{pmatrix} 0 & 4 \\ 4 & -2p \end{pmatrix}.$$

Interestingly, the $p = 1, 3$ phases break time-reversal symmetry. To see this, note that the $p = 1$ phase has a quasiparticle $(1, 0)$ with exchange statistics $\theta = \pi/8$, but no quasiparticle with statistics $-\pi/8$. Similarly, the $p = 3$ phase has a quasiparticle with statistics $\theta = -\pi/8$, but no quasiparticle with statistics $\pi/8$. (In fact, the $\mathbb{Z}_3$ string-net models with $p = 1, 2$ also break time-reversal symmetry by the same reasoning). Thus, we can see explicitly that string-net models can realize time-reversal breaking topological phases.

2.10.4 $\mathbb{Z}_2 \times \mathbb{Z}_2$ *string-net model*

Our final example is the two-component $\mathbb{Z}_2 \times \mathbb{Z}_2$ string-net model. These models have four string types $\{(0, 0), (1, 0), (0, 1), (1, 1)\}$ and we abbreviate them as $\{0, r, b, g\}$. Each string is self-dual, $0 = 0^*, r = r^*, b = b^*, g = g^*$, and the branching rules are

$$\{(0, r, r), (0, b, b), (0, g, g), (r, g, b)\}.$$

To construct the wave functions and Hamiltonians for these models, we have to solve the self-consistency conditions for $\{F, d, \gamma, \alpha\}$. To this end, we use the general solution (2.86),(2.76), which tells us that there are eight different solutions, with each solution labeled by a 2×2 upper triangular matrix

$$\mathbf{P} = \begin{pmatrix} p & q \\ 0 & r \end{pmatrix}. \tag{2.109}$$

with $p, q, r = 0, 1$. The solutions corresponding to $q = 0$ are less interesting since they give rise to models that are products of two decoupled $\mathbb{Z}_2$ string-net models. Therefore, here we focus on the case where $q=1$. More specifically, we focus on the case $q=1, p=r=0$ as this illustrates the basic features of the $q=1$ solutions. In this case, (2.86) gives

$$\begin{aligned}
&F_{rbb}=F_{rbg}=F_{rgb}=F_{rgg}=-1, \\
&F_{gbb}=F_{gbg}=F_{ggb}=F_{ggg}=-1, \\
&\gamma_g=-1,\ \alpha(0,g)=\alpha(g,0)=\alpha(r,g)=-1, \text{others } =1.
\end{aligned}$$

We can gauge away α using an appropriate f-gauge transformation, $f(b,r)=f(g,b)=-1$. The result is

$$\begin{aligned}
&F_{rbr}=F_{rbg}=F_{rgr}=F_{rgg}=F_{brr}=F_{brg}=F_{bbr}= \\
&F_{bbg}=F_{grr}=F_{grg}=F_{ggr}=F_{ggg}=-1, \\
&\gamma_g=-1, \text{others } =1.
\end{aligned}$$

Ideally, we would also like to gauge away γ. However, γ cannot be gauged away using any combination of f and g gauge transformations. One way to see this is to note that for any abelian string-net model and any $a=a^*, b=b^*$, the quantity $\gamma(a)\gamma(b)\gamma(a^*+b^*)$ is gauge invariant under f,g gauge transformations. Thus if this quantity is different from unity, then we can never gauge away γ. In the above case, we have $\gamma(r)\gamma(b)\gamma(g)=-1$, so there is no gauge where $\gamma=1$. Since γ cannot be gauged away, we have an example of a string-net model that requires our more careful treatment of the null string to be realized.

Each of the $\mathbb{Z}_2\times\mathbb{Z}_2$ string-net models has $|G|^2=16$ quasiparticles, which are labeled by ordered pairs (s,m) where $s=(s_1,s_2), m=(m_1,m_2)$, and $s_i,m_i=0,1$. The quasiparticle statistics are described by the four-component $U(1)$ Chern-Simons theory (2.92) with K-

matrix

$$K = \begin{pmatrix} 0 & 0 & 2 & 0 \\ 0 & 0 & 0 & 2 \\ 2 & 0 & -2p & -q \\ 0 & 2 & -q & -2r \end{pmatrix}.$$

2.11 Conclusion

In this chapter, we have derived several criteria for determining which abelian topological phases can and cannot be realized by string-net models. The simplest of these criteria states that an abelian topological phase can be realized by a string-net model if and only if it supports a gapped edge. This result is interesting because it shows that the string-net models realize the most general abelian phases that one could possibly hope for: indeed one could never expect string-net models to realize a phase with a protected gapless edge, since we can show explicitly that the edge of these models can be gapped by suitable interactions (see appendix A.7).

One direction for future work would be to extend our analysis to the non-abelian case. A natural conjecture is that the realizable phases are exactly the phases with gapped edges, just like in the abelian case:

Conjecture *A general 2D topological phase can be realized by a string-net model if and only if it supports a gapped edge.*

As in the abelian case, it is easy to establish the "only if" direction in this conjecture, since it can be shown explicitly that string-net models always support a gapped edge.[48] Proving the other direction — i.e. proving that the string-net models realize *all* topological phases with a gapped edge — requires more work. In particular, this result seems to require a complete characterization of which topological phases support a gapped edge; currently such a characterization only exists in the abelian case.[60, 45] Several works[51, 30] have proposed abstract classifications of gapped edges, though it has not been shown that these classifications include every possible gapped edge that can occur in microscopic models. That being said, these proposals seem to be consistent with the above conjecture.

Another motivation for considering the non-abelian case is to develop the most general possible formulation of string-net models. As we mentioned in the introduction, our construction of abelian string-net models is more general than the original construction of Ref. [65], due to two new ingredients, γ, α, which are related to the $\mathbb{Z}_2$ and $\mathbb{Z}_3$ Frobenius-Schur indicators respectively. It would interesting to understand how to incorporate γ, α into the construction of general (non-abelian) string-net models. Other generalizations of Ref. [65], such as those described in Refs. [52] - [56], have avoided including γ, α, at the cost of breaking the rotational symmetry of the lattice models. Our alternative formulation involving γ, α, preserves as much symmetry and topological invariance as possible, and therefore may give simpler models in some cases.

A final question is to determine whether string-net models can be generalized further. In particular, are there any 2D commuting projector spin Hamiltonians that realize topological phases beyond the reach of string-net models? An example of such a Hamiltonian (or a proof that no such Hamiltonian exists) would advance our understanding of both exactly soluble models and topological phases.

CHAPTER 3

3D TOPOLOGICAL PHASES AND EXACTLY SOLUBLE LATTICE MODELS

3.1 Introduction

The discovery of quantum Hall states and more recently, topological insulators[36, 77], has taught us that there are many different types of gapped quantum many body systems. In order to understand the relationship between these systems, it is useful to divide them into classes in such a way that the members of each class share the same qualitative properties. Typically these classes are defined as follows: two gapped Hamiltonians H and H' are assigned to the same class if they can be adiabatically connected to one another — that is, if there exists a one parameter family of interpolating Hamiltonians $H(s)$ with (1) $H(0) = H$, $H(1) = H'$ and (2) a finite energy gap for all s, $0 \leq s \leq 1$. The different classes of Hamiltonians are then called "gapped phases."

The precise definition of gapped phases depends on what type of systems we wish to consider. For example, if we are interested in systems with particular symmetries, then it is natural to assign H and H' to the same phase if there exists an interpolating Hamiltonian $H(s)$ which is *both* gapped and invariant under the relevant symmetries. Including such symmetry constraints typically leads to a finer classification of gapped phases, as illustrated by the example of topological and conventional insulators.[36, 77]

In this chapter, we consider the coarsest possible classification scheme: that is, we do not impose any symmetry constraints and we say that two gapped Hamiltonians H and H' belong to the same phase if they can be adiabatically connected by *any* interpolating Hamiltonian $H(s)$ with local interactions. Our starting point is a basic question: how can we tell whether or not two gapped Hamiltonians belong to the same phase?

This question has an appealing answer in the case of two dimensional (2D) systems[1].

---

[1] The 1D case is less interesting, since it is known that in the absence of symmetry all 1D bosonic

To determine whether two gapped 2D Hamiltonians belong to the same phase, one can simply compare the braiding statistics [2] of their quasiparticle excitations. If the braiding statistics data do not match, then the two Hamiltonians must belong to different phases since braiding statistics cannot change under an adiabatic deformation. Conversely, if the braiding statistics do match, then we can *almost* conclude that the two Hamiltonians belong to the same phase. To reach this conclusion, we simply need to compare one other quantity, namely the thermal Hall conductance[42]. Indeed, according to a plausible (but unproven) conjecture, if two Hamiltonians have the same braiding statistics and the same thermal Hall conductance, then they must be adiabatically connected to one another in the absence of any symmetry constraints.

In the 3D case, our understanding is much more limited. One way to attack the classification problem is to try to generalize the concept of quasiparticle braiding statistics to the 3D case. The simplest generalization begins with the observation that many 3D Hamiltonians support *loop-like* excitations in addition to particles. Given this observation, we can consider several different types of braiding statistics. First, we can look at the exchange statistics of particle-like excitations. These exchange statistics can take only one of two values for each particle: every particle must be either bosonic or fermionic.[3] Second, we can consider the statistical phase associated with braiding a particle around a loop.[1, 3, 55, 75] Finally, we can look at the statistical phase associated with braiding one loop excitation around another (Fig. 3.1a).[4, 2, 6] If we combine all of these types of braiding statistics, we can indeed distinguish many different 3D gapped phases.

Interestingly, however, this data is incomplete: Refs. [85, 41] argued that we also need to consider the statistical phase associated with a *three-loop* braiding process. In this process,

---

systems belong to the same phase[74, 19, 20, 81, 26, 73] while all 1D fermionic systems belong to one of two phases.[26]

[2] Here, when we say braiding statistics, we mean the complete set of algebraic data for anyon systems, including quantum dimensions and fusion rules. For more details, see e.g. Appendix E of Ref. [47].

[3] Here, we implicitly exclude 3D layered systems, like a stack of fractional quantum Hall states, from our discussion.

one loop is braided around another loop while both are linked to a third loop (Fig. 3.1b). It is unclear whether the three-loop braiding data is the last piece of the puzzle or whether there exist further distinctions between 3D gapped phases that can only be seen if we consider other braiding processes or other types of probes. However, either way, three-loop braiding statistics has already proven to be useful in certain cases. [88, 40, 86, 16]

One weakness of previous studies of three-loop braiding statistics is that this quantity has only been calculated using indirect and abstract arguments. For example, Ref. [85] computed the three-loop braiding statistics of 3D Dijkgraaf-Witten gauge theories using a dimensional reduction argument which relates the braiding statistics of loops in 3D Dijkgraaf-Witten models to the braiding statistics of particles in 2D Dijkgraaf-Witten models[23]. The approaches of Refs. [41, 88] were also indirect: Refs. [41, 88] computed loop braiding statistics by relating this quantity to modular transformations on a three dimensional torus.

In this chapter, we study three-loop braiding statistics using a more concrete approach. We focus on two exactly soluble lattice models and we compute their three-loop braiding statistics by explicitly implementing the loop braiding process on the lattice. Our approach is similar to how quasiparticle braiding statistics is commonly calculated in 2D lattice models[46, 63, 65]: we construct membrane operators that create and move loop-like excitations, and then we extract the three-loop statistics from the commutation algebra of these operators.

The two spin models that we analyze provide an explicit demonstration of the importance of three-loop braiding statistics for distinguishing 3D gapped phases. Indeed, we show that the models share the same particle exchange statistics as well as the same particle-loop and loop-loop braiding statistics. The only difference between the models is that they have different three-loop braiding statistics. Thus, it is only this quantity that reveals that the two models belong to different phases.

The models that we study are not completely new and have appeared previously in the literature in different forms. In particular, the first model is essentially identical to the 3D

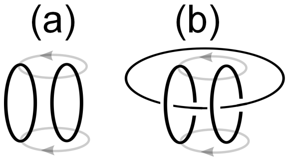

Figure 3.1: (a) Two-loop braiding process. (b) Three-loop braiding process. The gray curves show the paths of two points on the moving loop.

generalized toric code model[46, 35, 65, 15] corresponding to the group $\mathbb{Z}_2 \times \mathbb{Z}_2$. Thus, the low energy properties of this model are similar to that of conventional $\mathbb{Z}_2 \times \mathbb{Z}_2$ gauge theory[50]. The second model can be thought of as a different type of $\mathbb{Z}_2 \times \mathbb{Z}_2$ gauge theory. More specifically, this model can be obtained by starting with the spin model in Ref. [22] which describes a nontrivial symmetry-protected topological phase[32, 74, 26, 19, 20, 81, 17] with $\mathbb{Z}_2 \times \mathbb{Z}_2$ symmetry, and then coupling this system to a $\mathbb{Z}_2 \times \mathbb{Z}_2$ lattice gauge field[50]. We will explain this connection in more detail in chapter 4. In addition to its connection with the spin model in Ref. [22], we believe that the second model belongs to the same phase as one of the exactly soluble $\mathbb{Z}_2 \times \mathbb{Z}_2$ Dijkgraaf-Witten models.[23, 83] This conjecture is based on the fact that the braiding statistics in the two systems seem to match one another.

The connection between our models and symmetry-protected topological phases is not accidental: we specifically designed our models to be equivalent to gauged symmetry-protected topological phases, because according to the results of Ref. [85, 41], such gauge theories can support different types of three-loop braiding statistics. The reason that we chose to gauge the spin model from Ref. [22] is that this is one of the simplest known models for a 3D symmetry-protected topological phase with unitary symmetry group.

The rest of the chapter is organized as follows. In section 3.2 we introduce the two exactly soluble 3D spin models that we will analyze. In section 3.3, we study the particle-like and loop-like excitations of these models by explicitly constructing the string and membrane operators that create and move these excitations. We then compute the braiding statistics of these particles and loops in section 3.4. Some technical details can be found in the appendices.

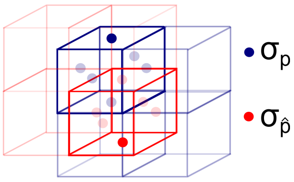

Figure 3.2: Both models are built out of two species of spins. The blue spins σ_p live on the plaquettes p of the cubic lattice while the red spins $\sigma_{\hat{p}}$ live on the plaquettes $\hat{p}$ of the dual cubic lattice.

3.2 Models

3.2.1 Hilbert space for the models

The models that we will discuss are spin-1/2 systems made up of two species of spins: "blue spins" and "red spins." The blue spins live on the plaquettes p of the cubic lattice and will be denoted by σ_p while the red spins live on the plaquettes $\hat{p}$ of the dual cubic lattice and will be denoted by $\sigma_{\hat{p}}$ (Fig. 3.2). In this notation, the S^z eigenstates $|\{\sigma^z_p, \sigma^z_{\hat{p}}\}\rangle$ provide a complete basis for the Hilbert space.

We will often find it convenient to describe spin states using an alternative language based on "membranes." In the membrane language, each S^z eigenstate $|\{\sigma^z_p, \sigma^z_{\hat{p}}\}\rangle$ corresponds to a spatial configuration of red and blue membranes on the cubic lattice and dual cubic lattice. The dictionary between spin states and membrane configurations is as follows: if $\sigma^z_p = -1$ we say that the plaquette p is occupied by a blue membrane, while if $\sigma^z_p = +1$ we say that the plaquette p is empty. Similarly, if $\sigma^z_{\hat{p}} = -1$ then $\hat{p}$ is occupied by a red membrane while if $\sigma^z_{\hat{p}} = +1$, then $\hat{p}$ is empty. In this way, each spin state can be equivalently described as a membrane state. We will label our membrane states as $|X_b, X_r\rangle$ where X_b denotes the subset of plaquettes that are occupied by blue membranes, and X_r denotes the subset of plaquettes occupied by red membranes.

3.2.2 Ground state wave functions

The two models that we will discuss have been engineered to have particular ground states. These ground states are easiest to describe if we assume an infinite (non-periodic) geometry. In such a geometry, the ground state of the first model is

$$|\Psi_0\rangle = \sum_{\text{closed } X_b, X_r} |X_b, X_r\rangle \tag{3.1}$$

where the sum runs over all *closed* membrane states $|X_b, X_r\rangle$. Here, by a closed membrane state, we mean a membrane configuration (X_b, X_r) in which all the blue and red membranes form closed surfaces, i.e. surfaces without boundaries. More precisely, a closed membrane state is defined to be a state in which every edge l in the cubic lattice and every edge $\hat{l}$ in the dual cubic lattice is adjacent to an *even* number of occupied plaquettes.

The ground state of the second model has a similar form

$$|\Psi_1\rangle = \sum_{\text{closed } X_b, X_r} (-1)^{N_g(X_b, X_r)} |X_b, X_r\rangle \tag{3.2}$$

where again the sum runs over all possible closed membrane states $|X_b, X_r\rangle$. The quantity $N_g(X_b, X_r)$ is defined as follows: for each closed membrane configuration (X_b, X_r), the intersections between the red and blue membranes $X_b \cap X_r$ form a collection of disconnected closed curves, which we will call “green loops.” The quantity $N_g(X_b, X_r)$ is defined to be the number of the green loops in $X_b \cap X_r$. As discussed in the introduction, the ground state $|\Psi_1\rangle$ is closely related to the ground state of the spin model in Ref. [22] which describes a nontrivial symmetry-protected topological phase with $\mathbb{Z}_2 \times \mathbb{Z}_2$ symmetry.

3.2.3 Sheared cubic lattice

The reader may notice that there is a technical problem with the above definition of $N_g(X_b, X_r)$: the problem is that the closed membrane condition allows for membrane configurations in

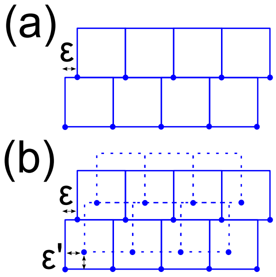

Figure 3.3: (a) The sheared square lattice is formed by shifting the corners of the square plaquettes (the blue dots) according to $(i, j) \rightarrow (i + \epsilon j, j)$ with $\epsilon > 0$. (b) Top view of the sheared cubic lattice. The solid/dashed squares denote cubes on two neighboring layers. The sheared cubic lattice is formed by shifting the corners of the cubes according to $(i, j, k) \rightarrow (i + \epsilon j + \epsilon' k, j + \epsilon' k, k)$ with $\epsilon' > \epsilon' > 0$.

which an edge l is adjacent to four occupied plaquettes. Geometrically such configurations correspond to the case where two blue membranes touch one another along the edge l. This membrane touching is problematic because it means that the "green loops" defined by the intersections of red and blue membranes can also touch one another at corners. As a result, there is some ambiguity in determining the number of disconnected green loops corresponding to a membrane configuration (X_b, X_r).

To deal with this issue, we now describe a way to infinitesimally deform the cubic lattice so as to eliminate membrane touching. Before describing this deformation, we first warm up with an analogous deformation of the square lattice. The basic idea is to think of the square plaquettes that make up the square lattice as rigid blocks that can be shifted around. The deformation we have in mind corresponds to shifting the position of the square plaquettes so that their corners move from $(i, j) \rightarrow (i + \epsilon j, j)$. The resulting lattice, which we call the *sheared* square lattice is shown in Fig. 3.3(a).

We are now ready to consider the cubic lattice. In this case, we think of the cubes that make up the cubic lattice as rigid blocks and we shift these cubes so that their corners move from

$$(i, j, k) \rightarrow (i + \epsilon j + \epsilon' k, j + \epsilon' k, k) \tag{3.3}$$

where $\epsilon' > \epsilon > 0$. The resulting *sheared* cubic lattice is shown in Fig. 3.3(b).

Now let us imagine performing the same shearing deformation to both the original cubic lattice and the dual cubic lattice. We can then deform an arbitrary closed membrane configuration (X_b, X_r) on the cubic lattice (and dual cubic lattice) to a membrane configuration on the sheared cubic lattice (and sheared dual cubic lattice). The result is a closed membrane configuration without any membrane touching of any kind. In what follows, we will always think of membrane configurations as living on the sheared cubic lattice rather than the cubic lattice so we don't have to worry about membrane touching.

3.2.4 Hamiltonians

H_0 model

We are now ready to write down the Hamiltonians for the two models. The Hamiltonian for the first membrane model is a sum of four terms,

$$H_0 = -\sum_l A_l - \sum_{\hat{l}} A_{\hat{l}} - \sum_c B_c^0 - \sum_{\hat{c}} B_{\hat{c}}^0 \tag{3.4}$$

where the indices $l, \hat{l}$ run over the links of the cubic lattice and dual cubic lattice respectively, while $c, \hat{c}$ run over the "cubes" of the cubic lattice and dual cubic lattice. To define the operators $A_l, A_{\hat{l}}, B_c, B_{\hat{c}}$, it suffices to explain how they act on the membrane basis states $|X_b, X_r\rangle$. The $A_l, A_{\hat{l}}$ operators are given by

$$A_l = \frac{1}{2}(1 + \mathscr{A}_l) \quad , \quad A_{\hat{l}} = \frac{1}{2}(1 + \mathscr{A}_{\hat{l}}) \tag{3.5}$$

where

$$\begin{aligned} \mathscr{A}_l |X_b, X_r\rangle &= (-1)^{N_l} |X_b, X_r\rangle, \\ \mathscr{A}_{\hat{l}} |X_b, X_r\rangle &= (-1)^{N_{\hat{l}}} |X_b, X_r\rangle. \end{aligned} \tag{3.6}$$

Here N_l and $N_{\hat{l}}$ are defined to be the number of occupied plaquettes adjacent to l and $\hat{l}$ respectively. The $B_c^0, B_{\hat{c}}^0$ operators are defined by

$$B_c^0 = \frac{1}{2}(1 + \mathcal{B}_c^0) \quad , \quad B_{\hat{c}}^0 = \frac{1}{2}(1 + \mathcal{B}_{\hat{c}}^0) \tag{3.7}$$

where

$$\begin{aligned} \mathcal{B}_c^0 |X_b, X_r\rangle &= |X_b + c, X_r\rangle, \\ \mathcal{B}_{\hat{c}}^0 |X_b, X_r\rangle &= |X_b, X_r + \hat{c}\rangle. \end{aligned} \tag{3.8}$$

Here the notation $X_b + c$ is meant to denote a kind of $\mathbb{Z}_2$ addition on membrane configurations. More specifically, given the membrane configuration X_b, the configuration $X_b + c$ is obtained by flipping the occupation numbers of the six plaquettes of the cube c: that is, one changes the plaquettes from unoccupied to occupied and vice versa.

There is a simple physical picture for the A and B in terms of the membrane language: the A terms favor *closed* membrane configurations, while the B terms provide an amplitude for the membranes to fluctuate. Together these terms ensure that the ground state is a superposition of many different closed membrane configurations.

Alternatively, we can express the A and B operators in the spin language:

$$A_l = \frac{1}{2}(1 + \prod_{p \in l} \sigma_p^z) \quad , \quad A_{\hat{l}} = \frac{1}{2}(1 + \prod_{\hat{p} \in \hat{l}} \sigma_{\hat{p}}^z) \tag{3.9}$$

where these products run over the four plaquettes adjacent to $l, \hat{l}$ respectively. Similarly,

$$B_c = \frac{1}{2}(1 + \prod_{p \in c} \sigma_p^x) \quad , \quad B_{\hat{c}} = \frac{1}{2}(1 + \prod_{\hat{p} \in \hat{c}} \sigma_{\hat{p}}^x) \tag{3.10}$$

where these products run over the six plaquettes adjacent to $c, \hat{c}$ respectively.

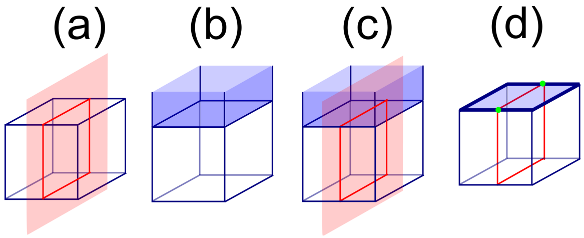

Figure 3.4: (a) A blue cube intersects a red membrane; their intersection consists of a single red loop. (b) A blue cube intersects/overlaps with a blue membrane; their intersection consists of a single blue region. (c) A blue cube intersects with both a red membrane and a blue membrane; their intersection consists of one red loop and one blue region. (d) For the membrane configuration shown in (c), the integer $m_c = 1$ because there is *one* red loop while $n_c = 2$ because there are *two* intersections (denoted by green dots) between the red loop and the boundary of the blue region (thick blue line).

H_1 model

The Hamiltonian for the second membrane model is similar:

$$H_1 = -\sum_l A_l - \sum_{\hat{l}} A_{\hat{l}} - \sum_c B_c^1 - \sum_{\hat{c}} B_{\hat{c}}^1. \tag{3.11}$$

The first two terms are defined as above, while the last two terms are defined by

$$B_c^1 = \frac{1}{2}(1 + \mathcal{B}_c^1) \cdot P_c \quad , \quad B_{\hat{c}}^1 = \frac{1}{2}(1 + \mathcal{B}_{\hat{c}}^1) \cdot P_{\hat{c}}. \tag{3.12}$$

Here P_c is a projector that projects onto states obeying the closed membrane constraint in the neighborhood of the cube c. More specifically,

$$P_c = \prod_{l \in c} A_l \cdot \prod_{\hat{l} \perp c} A_{\hat{l}} \tag{3.13}$$

where the first product runs over the twelve edges l of c and the second product runs over the six edges $\hat{l}$ that are perpendicular to the six plaquettes of the cube c. Similarly,

$$P_{\hat{c}} = \prod_{\hat{l} \in \hat{c}} A_{\hat{l}} \cdot \prod_{l \perp \hat{c}} A_l. \tag{3.14}$$

The $\mathcal{B}_c^1$ and $\mathcal{B}_{\hat{c}}^1$ operators have a similar structure as (3.8), but their matrix elements have some additional phase factors:

$$\begin{aligned}\mathcal{B}_c^1 |X_b, X_r\rangle &= (-1)^{m_c} i^{n_c} |X_b + c, X_r\rangle, \\ \mathcal{B}_{\hat{c}}^1 |X_b, X_r\rangle &= (-1)^{m_{\hat{c}}} i^{n_{\hat{c}}} |X_b, X_r + \hat{c}\rangle. \end{aligned} \tag{3.15}$$

Here $m_c, m_{\hat{c}}, n_c, n_{\hat{c}}$ are integer-valued functions of (X_b, X_r), which we will now define. In fact, we will only define m_c, n_c for membrane states (X_b, X_r) that satisfy $P_c = 1$, and we will only define $m_{\hat{c}}, n_{\hat{c}}$ for states with $P_{\hat{c}} = 1$; it suffices to discuss these subsets of states since the projectors $P_c, P_{\hat{c}}$ ensure that the matrix elements of B_c^1 and $B_{\hat{c}}^1$ vanish for all other states.

We begin with m_c. To define the value of m_c for some (X_b, X_r), consider the intersection between the set of red membranes X_r and the cube c . This intersection defines a collection of closed loops that live on the surface of the cube c (Fig. 3.4a). (The fact that the loops are closed follows from the closed membrane constraint $P_c = 1$). We will call these loops "red loops." The integer m_c is defined to be the number of these red loops, i.e.,

$$m_c(X_b, X_r) = \#\{\text{red loops on } c\} \tag{3.16}$$

(See Fig. 3.4d for an example).

To define the value of n_c for some (X_b, X_r), consider the intersection between the set of blue membranes X_b and the cube c. Because the blue membranes X_b and the cube c both live on the same cubic lattice, the intersection $X_b \cap c$ consists of 2D *regions* instead of loops.

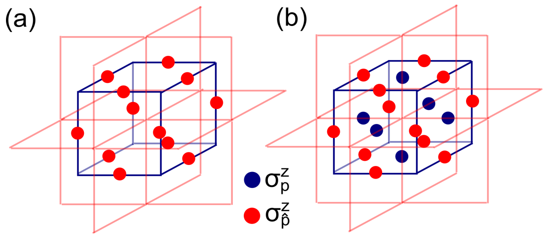

Figure 3.5: (a) The integer m_c is a function of the 12 spins $\sigma^z_{\hat{p}}$ that are closest to the cube c. (b) The integer n_c is a function of the 6 blue spins σ^z_p and 12 red spins $\sigma^z_{\hat{p}}$ around the cube c.

These 2D regions live on the surface of the cube c (Fig. 3.4b). Consider the boundary of these 2D regions. This boundary consists of a collection of closed loops. We will call these loops "blue loops." The integer n_c is defined to be the number of intersections between the blue loops and the red loops defined above:

$$n_c(X_b, X_r) = \#\{\text{blue-red intersections on } c\} \tag{3.17}$$

(See Fig. 3.4d for an example). Notice that n_c is always even.

The integers $m_{\hat{c}}$ and $n_{\hat{c}}$ are defined in an identical way but with the colors reversed:

$$m_{\hat{c}}(X_b, X_r) = \#\{\text{blue loops on } \hat{c}\} \tag{3.18}$$

and

$$n_{\hat{c}}(X_b, X_r) = \#\{\text{red-blue intersections on } \hat{c}\} \tag{3.19}$$

Here, the blue loops are defined by the intersection between the blue membranes X_b and the red cube $\hat{c}$, while the red loops are the boundaries of the intersections between the red membranes X_r and the cube $\hat{c}$.

Alternatively, we can express $m_c, m_{\hat{c}}, n_c, n_{\hat{c}}$ in the spin language. In this language, the operator m_c can be written as a function of the twelve spins $\sigma^z_{\hat{p}_1}, ..., \sigma^z_{\hat{p}_{12}}$ that are closest to

c (Fig. 3.5a), and similarly for $m_{\hat{c}}$:

$$m_c = f(\sigma^z_{\hat{p}_1}, \sigma^z_{\hat{p}_2}, \ldots, \sigma^z_{\hat{p}_{12}}),$$
$$m_{\hat{c}} = f(\sigma^z_{p_1}, \sigma^z_{p_2}, \ldots, \sigma^z_{p_{12}}). \tag{3.20}$$

Here f is a finite polynomial, but the explicit form of f is not illuminating so we do not show it here. Likewise, we can write n_c as a function of the 6 blue spins $\sigma^z_{p_1}, ..., \sigma^z_{p_6}$ and 12 red spins, $\sigma^z_{\hat{p}_1}, ..., \sigma^z_{\hat{p}_{12}}$ surrounding the cube c (Fig. 3.5b), and similarly for $n_{\hat{c}}$:

$$n_c = g(\{\sigma^z_p\}, \{\sigma^z_{\hat{p}}\}),$$
$$n_{\hat{c}} = g(\{\sigma^z_{\hat{p}}\}, \{\sigma^z_p\}). \tag{3.21}$$

As above, the expression for g is complicated so we do not show it here.

While the Hamiltonian H_0 is essentially identical to the well-known 3D toric code model[46, 35, 65, 15], some readers may be curious about the origin of the Hamiltonian H_1. As we mentioned previously, this Hamiltonian has been designed to have a particular ground state — namely, $|\Psi_1\rangle$. The state $|\Psi_1\rangle$ is in turn motivated by the ground state of the spin model in Ref. [22] which describes a nontrivial symmetry-protected topological phase with $\mathbb{Z}_2 \times \mathbb{Z}_2$ symmetry. Thus, the main question is how to design an exactly soluble Hamiltonian with a particular ground state, $|\Psi_1\rangle$. One way to do this is to follow a similar approach to the string-net construction of Ref. [65]. We recall that the string-net models of Ref. [65] can written as a sum of two types of operators — a Q operator and a B operator. The Q operator prefers closed string configurations and the B operator creates a closed loop. While the form of the Q operator is simple and intuitive, the B operator is more complicated, and its matrix elements are obtained by fusing a closed loop onto the lattice using 2D local rules. The Hamiltonian H_1 can be constructed using a similar approach: in this case the Hamiltonian is built out of A operators which prefer closed membrane configurations and B operators which create a cube. Similarly to the string-net models, the precise form of the

B operator can be obtained by writing down local rules obeyed by $|\Psi_1\rangle$, and then fusing a cube onto the lattice using 3D local rules. This is one way to obtain H_1. Another way is to use membrane operators: as we will see in section 3.3.3, the $B_c, B_{\hat{c}}$ are examples of spherical membrane operators (3.35,3.38).

3.2.5 Properties of the Hamiltonians

The two Hamiltonians H_0, H_1 have many nice properties. One property is that all the operators $\{A_l, A_{\hat{l}}, B_c^0, B_{\hat{c}}^0, B_c^1, B_{\hat{c}}^1\}$ are Hermitian so that H_0 and H_1 are also Hermitian. Indeed, the Hermiticity of $\{A_l, A_{\hat{l}}, B_c^0, B_{\hat{c}}^0\}$ is clear from the definitions (3.9,3.10), while the Hermiticity of B_c^1 and $B_{\hat{c}}^1$ can be seen by noting that the matrix elements of B_c^1 and $B_{\hat{c}}^1$, as defined in (3.15), are both symmetric and real.

Another important property is that all the terms in H_0, H_1 commute with one another, so that the two models are exactly soluble. For the case of H_0, the fact that $\{A_l, A_{\hat{l}}, B_c^0, B_{\hat{c}}^0\}$ all commute with one another follows easily from the definitions (3.9,3.10) of these operators. For the case of H_1, more work is required to verify this commutativity: while simple algebra shows that

$$[A_l, A_{l'}] = [A_{\hat{l}}, A_{\hat{l}'}] = 0 \tag{3.22}$$

and

$$[A_l, B_c^1] = [A_{\hat{l}}, B_c^1] = [A_l, B_{\hat{c}}^1] = [A_{\hat{l}}, B_{\hat{c}}^1] = 0, \tag{3.23}$$

the fact that

$$[B_c^1, B_{c'}^1] = [B_{\hat{c}}^1, B_{\hat{c}'}^1] = [B_c^1, B_{\hat{c}'}^1] = 0 \tag{3.24}$$

is not obvious. We leave the derivation of the latter identity (3.24) to Appendix B.1.

A third property of H_0, H_1 is that the operators $\{A_l, A_{\hat{l}}, B_c^0, B_{\hat{c}}^0, B_c^1, B_{\hat{c}}^1\}$ have eigenvalues 0 or 1:

$$a_l, a_{\hat{l}}, b_c^0, b_{\hat{c}}^0, b_c^1, b_{\hat{c}}^1 = 0, 1. \tag{3.25}$$

(The first two eigenvalue spectra can be derived from $A_l^2 = A_l$, etc.). A final property of these models is that $|\Psi_0\rangle$ is an simultaneous eigenstate of $\{A_l, A_{\hat{l}}, B_c^0, B_{\hat{c}}^0\}$ with

$$a_l = a_{\hat{l}} = b_c^0 = b_{\hat{c}}^0 = 1. \tag{3.26}$$

Similarly, $|\Psi_1\rangle$ is a simultaneous eigenstate of $\{A_l, A_{\hat{l}}, B_c^1, B_{\hat{c}}^1\}$ with

$$a_l = a_{\hat{l}} = b_c^1 = b_{\hat{c}}^1 = 1. \tag{3.27}$$

A derivation of the relations (3.26) and (3.27) is given in Appendix B.1.

3.2.6 Solving the models

In this section, we show that H_0 and H_1 are gapped, and that $|\Psi_0\rangle$ and $|\Psi_1\rangle$ are ground states of these Hamiltonians. We begin with H_0. To find the energy spectrum of H_0, recall that the operators $\{A_l, A_{\hat{l}}, B_c^0, B_{\hat{c}}^0\}$ commute with one another and can therefore be simultaneously diagonalized. Let us label these simultaneous eigenstates by $|a_l, a_{\hat{l}}, b_c^0, b_{\hat{c}}^0\rangle$ where $a_l, a_{\hat{l}}, b_c^0, b_{\hat{c}}^0$ denote the eigenvalues. It is clear that these states are energy eigenstates with energy

$$E = -\sum_l a_l - \sum_{\hat{l}} a_{\hat{l}} - \sum_c b_c^0 - \sum_{\hat{c}} b_{\hat{c}}^0. \tag{3.28}$$

Now, since the eigenvalues $\{a_l, a_{\hat{l}}, b_c^0, b_{\hat{c}}^0\}$ take values in $0, 1$, it follows that the ground state(s) of H_0 have $a_l = a_{\hat{l}} = b_c^0 = b_{\hat{c}}^0 = 1$, while the excited states have at least one $a_l, a_{\hat{l}}, b_c^0, b_{\hat{c}}^0$ equal to 0. We conclude that there is a finite energy gap, $\Delta = 1$, separating the ground state(s) and excited states. Furthermore, we can see that $|\Psi_0\rangle$ is a ground state of H_0 since it obeys (3.26). All that remains is to determine the ground state degeneracy of H_0. This degeneracy depends on the global topology of the system on which H_0 is defined. In an infinite non-periodic geometry, one can show that H_0 has a unique ground state — namely, $|\Psi_0\rangle$. On the other hand, in periodic (3D torus) geometry, it can be shown that the ground state degeneracy is $4^3 = 64$. These degenerate ground states are characterized by different parities of noncontractible red and blue membranes along the x, y and z directions of the 3D torus.

Now let us consider Hamiltonian H_1. Similarly to H_0, we can simultaneously diagonalize $\{A_l, A_{\hat{l}}, B_c^1, B_{\hat{c}}^1\}$ and label their eigenstates as $|a_l, a_{\hat{l}}, b_c^1, b_{\hat{c}}^1\rangle$. Following the same reasoning as above, we conclude that there is a finite energy gap, $\Delta = 1$, separating the ground state(s) and excited states. Furthermore, we can see that $|\Psi_1\rangle$ is a ground state of H_1 since it obeys (3.27). Like H_0, it can be shown that H_1 has a unique ground state in an infinite non-periodic geometry ($|\Psi_1\rangle$), and the ground state degeneracy is 64 in a 3D torus geometry.

3.2.7 *Particle-like and loop-like excitations*

If we examine equation (3.28), we can see that H_0 supports both particle-like and loop-like excitations. An example of a particle-like excitation is a point defect where b_c^0 or $b_{\hat{c}}^0$ is equal to 0 instead of the ground state value of 1. Likewise, an example of a loop-like excitation is a line defect along which a_l or $a_{\hat{l}}$ is equal to 0 instead of the ground state value of 1. These line-like defects always form closed loops: to see this, note that the quantum numbers a_l and $a_{\hat{l}}$ obey the local constraints

$$\prod_{l \in s}(1 - 2a_l) = 1 \quad , \quad \prod_{\hat{l} \in \hat{s}}(1 - 2a_{\hat{l}}) = 1 \tag{3.29}$$

for every site s in the cubic lattice and $\hat{s}$ in the dual cubic lattice. Here, the first product runs over the six edges l that are adjacent to s and similarly for the second product. The above constraints guarantee that each site s is adjacent to an even number of line-line defects, so that the defects always form closed loops. (To derive these constraints, note that they follow from the corresponding operator identities, $\prod_{l \in s}(1-2A_l) = \prod_{\hat{l} \in \hat{s}}(1-2A_{\hat{l}}) = 1$ which in turn follow from the definition (3.9)). In exactly the same way, one can see that the Hamiltonian H_1 supports particle-like excitations with b_c^1 or $b_{\hat{c}}^1$ is equal to 0, and loop-like excitations where a_l or $a_{\hat{l}}$ is equal to 0 along some closed loop.

Below we will see that in both models, these particle-like and loop-like excitations have nontrivial braiding statistics with one another and have similar properties to the charges and vortex loops in $\mathbb{Z}_2 \times \mathbb{Z}_2$ gauge theories. In view of this connection, we will refer to the particle-like excitations with b_c^0 or b_c^1 equal to 0 as "blue charges" and the excitations with $b_{\hat{c}}^0$ or $b_{\hat{c}}^1$ equal to 0 as "red charges." Similarly, we will refer to the loop-like excitations with $a_l = 0$ as "blue vortex loops" and the excitations with $a_{\hat{l}} = 0$ as "red vortex loops." In the following, we will study these charge and vortex-loop excitations in more detail, with a focus on their topological properties.

3.3 Excitations and the associated creation operators

In this section, we find operators that create the charge and vortex loop excitations of H_0 and H_1. These operators are useful because their commutation algebra contains information about the braiding statistics of the associated particles and loops.

3.3.1 General picture for string and membrane operators

In general, topologically nontrivial particle excitations cannot be created using local operators. Instead, the easiest way to create these excitations is to use string-like operators. In the following sections we will find string-like creation operators for each topologically distinct charge excitation α in H_0 and H_1. We will denote these operators by $W_\alpha(P)$ where P is the path along which the string operator acts. These operators satisfy two key properties.

First, if P is an *open* path, then when $W_\alpha(P)$ is applied to the ground state $|\Psi\rangle$, it creates an excited state $|\Psi_{ex}\rangle$ with two charge excitations α at the two ends of P:

$$W_\alpha(P)|\Psi\rangle = |\Psi_{ex}\rangle.$$

(Here the excited state $|\Psi_{ex}\rangle$ only depends on the endpoints of P and not on the choice of path). Second, if P is a *closed* path, then $W_\alpha(P)$ does not create any excitation at all: $W_\alpha(P)|\Psi\rangle \propto |\Psi\rangle$.

In addition to these string operators, which create charge excitations, we will also find membrane operators that create vortex loop excitations. That is, for each topologically distinct vortex loop excitation α in H_0 and H_1, we will find a corresponding membrane creation operator, which we will denote by $M_\alpha(S)$ with S being the surface where the membrane operator acts. These membrane operators satisfy similar properties to the string operators. First, if S is a *cylindrical* surface, then when $M_\alpha(S)$ is applied to the ground state $|\Psi\rangle$ it creates an excited state with two loop excitations at the ends of the cylinder:

$$M_\alpha(S)|\Psi\rangle = |\Psi_{ex}\rangle.$$

(Similarly to before, the excited state $|\Psi_{ex}\rangle$ only depends on the two boundaries of S and not on the choice of surface that joins them). Second, if S is a *toroidal* surface, then $M_\alpha(S)$ does not create any loop excitations at all: $M_\alpha(S)|\Psi\rangle \propto |\Psi\rangle$.

We can also consider membrane operators with other topologies beyond the cylinder and torus case: for example, later we will discuss *spherical* membrane operators. However, the structure of membrane operators is different for different topologies[4] and thus each case has to be treated separately. Here we will focus on cylindrical and toroidal cases as they are sufficient for our purposes.

---

[4] For example, toroidal operators can be decorated by string operators that encircle the torus while spherical membrane operators cannot be decorated in this way. See section 3.3.3 for more details.

The string and membrane operators have simple physical interpretations: the string operator $W_\alpha(P)$ describes a process in which a pair of charge excitations is created and then moved to the two ends of the path P. Likewise, the membrane operator $M_\alpha(S)$ describes a process in which a pair of loops is created and then moved to the two ends of the cylinder S. On the other hand, if P is a closed path then $W_\alpha(P)$ describes a process in which a pair of charge excitations is created and then moved around P and annihilated with each other. Similarly, if S is a toroidal surface then $M_\alpha(S)$ describes a process in which a loop-antiloop pair is created, moved around S and annihilated with one another.

3.3.2 String and membrane operators for H_0

String operators

It is easy to find string operators W_b^0, W_r^0 that create the blue and red charge excitations of H_0. These operators are given by

$$W_b^0(P) = \prod_{p \perp P} \sigma_p^z, \quad W_r^0(P) = \prod_{\hat{p} \perp P} \sigma_{\hat{p}}^z \tag{3.30}$$

where P is a path on the dual cubic lattice in the first expression, and a path in the cubic lattice in the second expression. The two products run over plaquettes that are perpendicular to these two paths. Equivalently, in the membrane representation, W_b^0 and W_r^0 are given by:

$$\begin{aligned} W_b^0(P)|X_b, X_r\rangle &= (-1)^{N_b}|X_b, X_r\rangle, \\ W_r^0(P)|X_b, X_r\rangle &= (-1)^{N_r}|X_b, X_r\rangle \end{aligned} \tag{3.31}$$

where N_b and N_r are the number of blue and red membranes that cross the path P.

Let us now verify that when P is an open path, $W_b^0(P)$ creates blue charge excitations at the two endpoints of P. From the definitions (3.30), it is easy to see that $W_b^0(P)$ commutes with all the terms in the Hamiltonian H_0 except for $\mathcal{B}^0_{c_1}$ and $\mathcal{B}^0_{c_2}$ where c_1 and c_2 are the two cubes at the endpoints of P. These two operators *anticommute* with $W^0_b(P)$ rather than commute. We conclude that $W^0_b(P)|\Psi_0\rangle$ is a simultaneous eigenstate of $A_l, A_{\hat{l}}, B^0_p, B^0_{\hat{p}}$ with eigenvalues $b^0_{c_1} = b^0_{c_2} = 0$ and all other eigenvalues equal to 1. Hence, $W^0_b(P)|\Psi_0\rangle$ contains two blue charge excitations at the endpoints of P. A similar argument shows that W^0_r also creates red charge excitations at the endpoints of P.

Membrane operators

It is also easy to find membrane operators M^0_b, M^0_r that create the blue and red vortex excitations of H_0. These operators are given by

$$M^0_b(S) = \prod_{p \in S} \sigma^x_p, \quad M^0_r(S) = \prod_{\hat{p} \in S} \sigma^x_{\hat{p}} \tag{3.32}$$

where S is a surface made up of plaquettes p living in the cubic lattice in the first expression, and a surface consisting of plaquettes $\hat{p}$ in the dual cubic lattice in the second expression. Equivalently, we can express M^0_b and M^0_r in the membrane representation as:

$$\begin{aligned} M^0_b(S)|X_b, X_r\rangle &= |X_b + S, X_r\rangle, \\ M^0_r(S)|X_b, X_r\rangle &= |X_b, X_r + S\rangle \end{aligned} \tag{3.33}$$

where $X_b + S$ denotes the $\mathbb{Z}_2$ addition operation defined below equation (3.8).

We now check that when S is a cylindrical surface, $M^0_b(S)$ creates blue loop excitations at the two ends of S. To establish this fact, we note that $M^0_b(S)$ commutes with all the terms in the Hamiltonian H_0 except for $\mathscr{A}_l$ when l lies along the two boundaries of S. These $\mathscr{A}_l$ operators anticommute with $M^0_b(S)$ rather than commute. It then follows that $M^0_b(S)|\Psi_0\rangle$ is an eigenstate of $A_l, A_{\hat{l}}, B^0_p, B^0_{\hat{p}}$ with eigenvalues $a_l = 0$ along the boundaries of S, and all other eigenvalues equal to 1. This establishes the claim. The same argument applies to

$M_r^0(S)$.

It should be noted that the excitations created by M_b^0 and M_r^0 are *not* the most general possible vortex loop excitations. In fact, the H_0 model supports three other types of blue vortex loops and three other types of red vortex loops. These excitations can be obtained by attaching either a red charge, a blue charge, or both a red charge and a blue charge, to the vortex loops created by M_b^0 and M_r^0. We will label the four types of blue vortex loops by (b, q_b, q_r), and the four types of red vortex loops by (r, q_b, q_r) where q_b, q_r take values in $0, 1$. In this labeling scheme, the excitations created by M_b^0 and M_r^0 are denoted by $(b, 0, 0)$ and $(r, 0, 0)$, with the other excitations labeled according to the amount of charge attached to them. As we will see later, these loop excitations are all topologically distinct from one another in the sense that they have different braiding statistics.

It is easy to find membrane operators that create these more general vortex loop excitations. For example, consider the operator $M_b^0(S)$ in the case where S is a cylinder. When this operator is applied to the ground state $|\Psi_0\rangle$, it creates two vortex loops of type $(b, 0, 0)$ at the two ends of the cylinder. We can modify this operator to create other vortex loops (b, q_b, q_r) by multiplying $M_b^0(S)$ by the string operators $W_b^0(P)$ or $W_r^0(P')$ or $W_b^0(P) \cdot W_r^0(P')$ where the paths P, P' run along the length of the cylinder. In the same way, we can construct membrane creation operators for the red vortex loops (r, q_b, q_r) by multiplying $M_r^0(S)$ by appropriate string operators.

Before concluding, we should mention that there is yet another type of vortex loop excitation which we have not discussed, namely a *composite* of a red and blue vortex loop. This type of loop excitation can be obtained by fusing together a red and blue loop, and again it comes in four subtypes which we can denote by (rb, q_b, q_r). In what follows, we will generally ignore this additional kind of vortex loop excitation since its braiding statistics properties are completely determined by the properties of the individual red and blue loops.

3.3.3 String and membrane operators for H_1

In this section, we construct string and membrane operators for the Hamiltonian H_1. The string operators are relatively easy: following the same analysis as above, it is simple to check that the same string operators that create the blue and red charge excitations in the H_0 model can also be used to create the charge excitations in the H_1 model. That is, just as in (3.31), we can set

$$\begin{aligned} W_b^1(P)|X_b, X_r\rangle &= (-1)^{N_b}|X_b, X_r\rangle, \\ W_r^1(P)|X_b, X_r\rangle &= (-1)^{N_r}|X_b, X_r\rangle \end{aligned} \tag{3.34}$$

where N_b and N_r are the number of blue and red membranes that cross the path P.

We will need to do more work to construct membrane operators for H_1. The rest of this section is devoted to this problem.

Cylindrical membrane operators for blue vortex loops

We begin by finding a membrane operator $M_b^1(S)$ that creates blue vortex loops. To proceed, it is convenient to work in the membrane basis. Let S be a cylindrical surface made up of plaquettes p living in the cubic lattice. We need to define the action of $M_b^1(S)$ on a general membrane state $|X_b, X_r\rangle$. A natural guess, inspired by (3.33), is that $M_b^1(S)$ should act as

$$M_b^1(S)|X_b, X_r\rangle = f_b(X_b, X_r, S)|X_b + S, X_r\rangle \tag{3.35}$$

for some complex-valued function $f_b(X_b, X_r, S)$. Indeed, it is easy to see that any operator of this type has the property that it anticommutes with the $\mathscr{A}_l$ terms that lie along the two boundaries of S and it commutes with every other $\mathscr{A}_l$ and $\mathscr{A}_{\hat{l}}$ term. Hence, any operator of this type has the property that if we apply it to the ground state $|\Psi_1\rangle$, it will create blue vortex loop excitations at the boundaries of S. The problem is that most of these operators

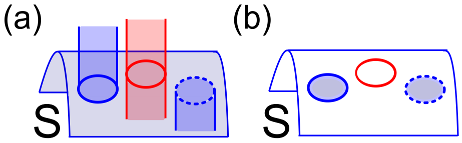

Figure 3.6: (a) A blue cylinder S intersects with a red membrane and two blue membranes (only part of S is shown for clarity). One of the blue membranes is incident from above S and the other from below. (b) We represent the intersections as a picture drawn on the cylinder S. In this case, the picture consists of a red loop, and two blue regions — one with a solid boundary and one with a dotted boundary.

also create many other excitations along the surface S since most of these operators do *not* commute with B_c^1 and $B_{\hat{c}}^1$. Thus, our task is to choose f_b appropriately so that $M_b^1(S)$ does not create any excitations except at the boundaries of S.

We now describe one choice of f_b that does the job. Below, we will just present the definition of f_b without any motivation. Later, in section 3.3.3, we will explain why this choice works and we will provide some motivation as to where it comes from.

First, we set $f_b(X_b, X_r, S) = 0$ if the membrane configuration (X_b, X_r) violates the closed membrane constraint anywhere in the neighborhood of S. More precisely, $f_b = 0$ if any link $l, \hat{l}$ that touches or intersects S is adjacent to an odd number of occupied plaquettes. On the other hand, if every such link is adjacent to an *even* number of occupied plaquettes, then $f_b(X_b, X_r, S)$ is defined in terms of the two intersections $X_b \cap S$ and $X_r \cap S$. The dependence of f_b on $X_b \cap S$ and $X_r \cap S$ is complicated, and in order to explain it, we first describe a way to represent $X_b \cap S$ and $X_r \cap S$ as a picture drawn on the surface of the cylinder S. The picture we will draw consists of a collection of red lines and blue regions with the red lines denoting the places where membranes in X_r intersect S, and the blue regions denoting the places where membranes in X_b intersect/overlap with S. We note that the boundaries of the blue regions correspond to places where a membrane in X_b is incident upon the surface S. If this membrane is incident upon S from above, we will draw the corresponding boundary as a solid line, while if it is incident from below, we will draw the boundary as a dotted line (Fig. 3.6). (Note that for this step to be well-defined, one needs to specify a convention for

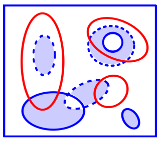

Figure 3.7: A typical picture representing the intersections of an unlinked blue cylinder with red and blue membranes. Here we draw the cylinder as a rectangle with top and bottom identified and the left and right being the two ends of the cylinder.

what side of S is defined as “above” S and what side is defined as “below” S. Equivalently, one needs to choose a normal vector to S). Putting this all together, the intersections $X_b \cap S$ and $X_r \cap S$ can be represented by a picture, drawn on the cylinder S, of the form shown in Fig. 3.7.

The value of $f_b(X_b, X_r, S)$ is completely determined by the corresponding picture. Thus, f_b can be thought of as a complex-valued function defined on pictures. All that remains is to specify this function. For reasons that will become clear later on, it is most natural to describe f_b implicitly, through local constraint equations, rather than providing an explicit formula. More specifically, we define f_b in terms of the constraint equations

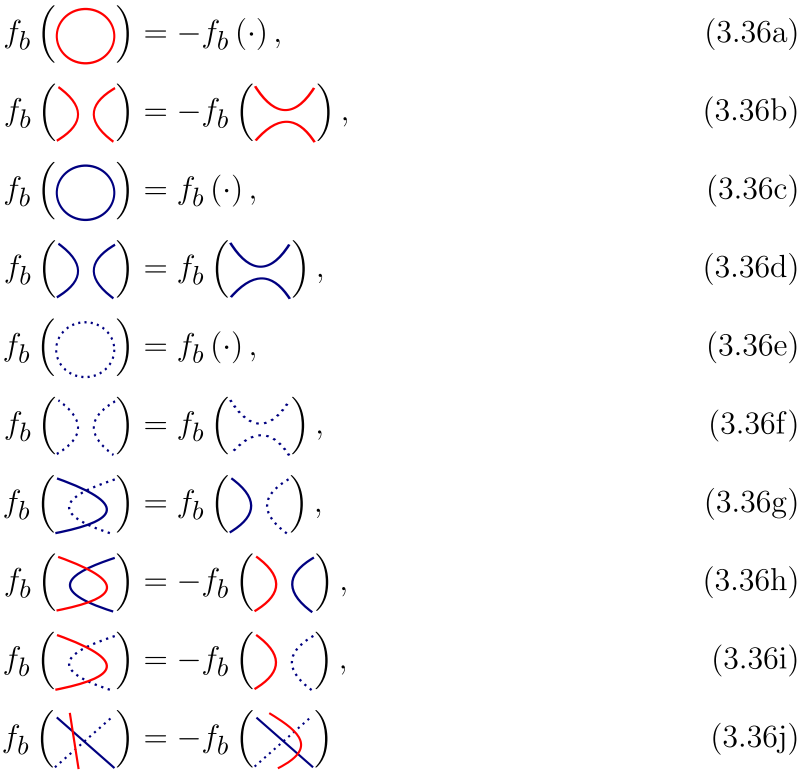

where it is understood that the value of f_b depends only on the *topology* of the picture. That is, any two pictures that can be smoothly deformed into one another have the same value of f_b. The meaning of the above constraint equations is as follows. The first equation (3.36a) states that the value of f_b for a picture with a closed red loop is equal to the value of f_b for the same picture, without the loop, up to a factor of -1. Equation (3.36b) states that two pictures that differ by the recoupling of red curves have values of f_b that differ by a factor of -1. The remaining equations have a similar meaning.

In the above constraint equations, we have left out the shading of the blue regions. But it should be understood that the blue regions are shaded in a consistent way on both sides

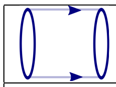	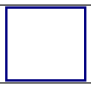	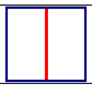	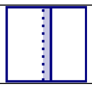	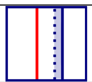
f_b	1	$-e^{i\pi q_r}$	$e^{i\pi q_b}$	$-e^{i\pi(q_r+q_b)}$

Table 3.1: The function f_b that defines the (unlinked) blue cylinder operator is completely determined by its values on four basic pictures that are drawn on the surface of the cylinder. Here the blue cylinder is represented by a rectangle with upper and lower edges identified and with the left and right being the two ends of the cylinder. The corresponding values of f_b are shown below the pictures. The integers $q_r, q_b = 0, 1$ define four different functions f_b and therefore four different cylinder operators.

of the equations. For example, (3.36d) represents two constraints with different shadings

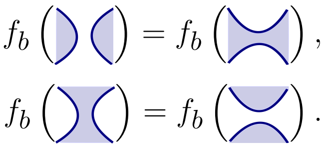

Similarly, (3.36j) also represents two constraints with different shadings

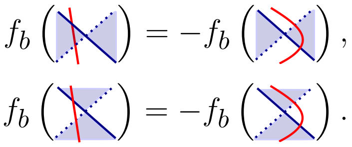

To complete the definition, we impose a boundary condition on f_b which states that $f_b = 0$ if any of the red lines or blue regions touch the boundaries of S. With this boundary condition and the above constraint equations, the value of f_b on any picture can be related to one of the four "basic" pictures shown in Table 3.1. Thus, once we specify the value of f_b on these basic pictures, we will have completely specified f_b and therefore $M_b^1(S)$.

The values for f_b on the basic pictures are shown in the bottom row of Table 3.1. These values are parameterized by two integers $q_b, q_r \in \{0, 1\}$. Hence our construction actually defines four different membrane operators. In principle, we should label these operators by $M^1_{(b,q_b,q_r)}$ to make the dependence on q_b, q_r explicit. However, this notation is cumbersome so we will denote the membrane operators by M_b^1 with the understanding that M_b^1 is not fully defined until we specify q_b, q_r. Similarly to the H_0 model, these four different blue membrane operators create four different types of blue vortex loops. These vortex loops differ from one another by the amount of charge that they carry and we will label them by (b, q_b, q_r).

At this point, we have fully defined the membrane operator $M_b^1(S)$. All that remains is to show that this membrane operator has the required properties. That is, we need to show that $M_b^1(S)$ creates blue vortex loops at its two boundaries and nothing else. We will establish this fact in section 3.3.3.

Cylindrical membrane operators for red vortex loops

To construct cylindrical membrane operators that create *red* vortex loops, we follow exactly the same recipe as above but with the roles of "red" and "blue" reversed. First, we define

$$M_r^1(S)|X_b, X_r\rangle = f_r(X_b, X_r, S)|X_b, X_r + S\rangle \tag{3.37}$$

where $f_r(X_b, X_r, S)$ is a complex-valued function. We then define $f_r(X_b, X_r, S)$ in terms of the two intersecting sets $X_b \cap S$ and $X_r \cap S$. As in the definition of f_b, we represent $X_b \cap S$ and $X_r \cap S$ in terms of a picture drawn on the surface of the cylinder S, and we think of f_r as a function defined on such pictures. In this case, each picture consists of a collection of *blue* lines and *red* regions, where the blue lines denote the intersection $X_b \cap S$, and the red regions denote the intersection $X_r \cap S$. We define the value of f_r on each picture using local constraint equations which are identical to Eqs. (3.36), but with the red and blue colors reversed. With these constraint equations, the value of f_r on any picture can be related to one of the four basic pictures shown in Table 3.1 (with the colors reversed). We then define the value of f_r on these basic pictures, just as in Table 3.1 but with the colors reversed and q_b and q_r exchanged. This procedure completely specifies f_r and therefore M_r^1. Note that, like M_b^1, this construction actually gives four different membrane operators that are parameterized by two integers $q_b, q_r \in \{0, 1\}$. These membrane operators create four different types of red vortex loops, which we denote by (r, q_b, q_r).

Cylindrical membrane operators for linked loops

We now have all the tools we need to create an excited state with a pair of vortex loops: to do this we simply apply one of the above cylindrical operators to the ground state $|\Psi_1\rangle$. But what if we want to build a state with more than two vortex loops? One might try to make such a state by applying multiple cylinder operators to the ground state. This approach will work fine if the state we are trying to build does not contain any linked loops. However, it will fail if any of the loops are linked: the above membrane operators are simply incapable of creating excited states with *linked* loops. To see this, imagine we first apply a cylindrical membrane operator $M_b^1(S)$ to the ground state, obtaining $M_b^1(S)|\Psi_1\rangle$. This state contains two blue vortex loop excitations located at the two boundaries of the cylinder S. Now, suppose we apply another cylinder operator $M_b^1(S')$ where S' is linked with one of these loops. One might hope that the result would be a state with linked vortex loops. Unfortunately, however, $M_b^1(S')$ simply annihilates this state: $M_b^1(S')M_b^1(S)|\Psi_1\rangle = 0$. To see this, note that $M_b^1(S)|\Psi_1\rangle$ is a superposition of membrane states $|X_b, X_r\rangle$, where all the membranes in X_b and X_r form closed surfaces, except at the two boundaries of S, where a blue membrane terminates. Since S' is linked with one of the boundaries of S, it follows that each of the two boundaries of S' must intersect with blue membranes an odd number of times. In particular, each boundary must have at least one intersection with a blue membrane. But if we look back at the boundary conditions for f_b, we see that any state of this kind has $f_b(X_b, X_r, S') = 0$, so any state of this kind is annihilated by $M_b^1(S')$.

We therefore need to find another set of membrane operators to create linked loops. We now define such membrane operators. Before doing this, we first need to explain the basic idea behind these operators. In general, we will be interested in excited states containing a collection of vortex loops that are all linked with a single "base loop" which can be either blue or red. We will build such states with the help of two different cylindrical membrane

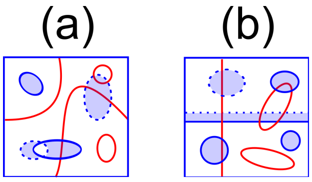

Figure 3.8: Two typical pictures representing the intersections between linked blue cylinders and red and blue membranes. Here we draw the cylinder as a rectangle with top and bottom identified. Panel (a) shows a typical picture for a blue cylinder linked with a red base loop. Panel (b) shows a typical picture for a blue cylinder linked with a blue base loop.

operators — one for each type of base loop. The operator associated with the blue base is designed to be applied to states containing a blue loop that links with the cylinder S: when the operator is applied to such a state, it creates two vortex loops at the ends of the cylinder S which are linked with the original blue loop. On the other hand, when it is applied to states that do not contain a blue loop that links with the cylinder S, it simply annihilates them. The operator associated with the red base has a similar property. This structure is reminiscent of the cylinder operators constructed in the previous two sections. In fact, the previously constructed operators can be thought of as cylindrical membrane operators associated with a *trivial* base: they only create loop excitations when applied to states without any loops linked with S.

With this picture in mind, we now construct cylindrical membrane operators for a red base loop and a blue base loop. We begin by defining a cylindrical membrane operator that creates blue vortex loops that are linked to a red base loop. This operator is defined in almost exactly the same way as the blue membrane operator $M_b^1(S)$ defined above. The only difference is that we change the boundary condition on f_b so that it only takes nonzero values on pictures in which a single red line touches the boundary of S at a fixed position y_0, and no blue regions touch the boundary. (See Fig. 3.8a for a typical picture of this type). Given this boundary condition and the constraint equations (3.36) we can reduce any such picture to one of the four basic pictures shown in the top panel of Table 3.2. We can therefore completely specify the membrane operator once we specify the value of f_b on these

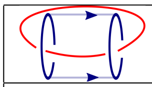	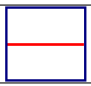	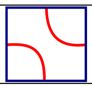	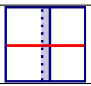	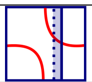
f_b	1	$i \cdot e^{i\pi q_r}$	$i \cdot e^{i\pi q_b}$	$-e^{i\pi(q_r+q_b)}$

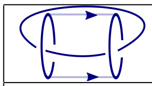	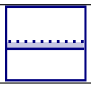	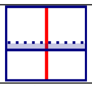	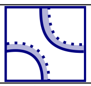	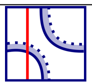
f_b	1	$e^{i\pi q_r}$	$e^{i\pi q_b}$	$e^{i\pi(q_r+q_b)}$

Table 3.2: The function f_b that defines the linked blue cylinder operator is completely determined by its values on four basic pictures that are drawn on the surface of the cylinder. The top panel shows the four basic pictures for a blue cylinder linked to a red base loop, while the bottom panel shows the pictures for a cylinder linked to a blue base loop. The corresponding values of f_b are shown below the pictures. Here $q_r, q_b = 0, 1$ define four different functions f_b and therefore four different cylinder operators for each panel.

four basic pictures. The values we choose are shown in Table 3.2.

We next describe a cylindrical membrane operator which creates a blue vortex loop which is linked to a blue base loop. Here, we choose a boundary condition on f_b so that it only takes nonzero values on pictures in which a single thin blue region touches the boundary of S at a fixed position y_0, and no red lines touch the boundary. (See Fig. 3.8b for a typical picture of this type). Given this boundary condition and the constraint equations (3.36), we can reduce any such picture to one of the four pictures shown in the bottom panel of Table 3.2. The value of f_b on these four pictures is shown in Table 3.2.

To complete the discussion, we need to explain how to construct cylindrical membrane operators that create *red* vortex loops linked to a blue or red base loop. These operators are defined exactly like the two operators described above, but with the roles of "red" and "blue" reversed.

Before concluding, we make one comment about our notation: we will use the same symbol $M_b^1(S)$ to denote all of the blue membrane operators whether they are associated with a red base (top panel of Table 3.2), a blue base (bottom panel of Table 3.2), or no base at all (Table 3.1). Similarly, we will denote all the red membrane operators by $M_r^1(S)$ independent of what base they are associated with. This abuse of notation will not introduce confusion since it will always be clear from context which operator we have in mind.

Toroidal and spherical membrane operators

So far we have only discussed cylindrical membrane operators. We now discuss how to construct membrane operators with other topologies — in particular, toroidal and spherical operators. We begin with the toroidal operators. Roughly speaking, these operators can be obtained by connecting the two ends of our cylinder operators. More precisely, we define toroidal operators exactly like the cylindrical operators, with only one modification: we replace the cylindrical boundary conditions on f_b and f_r with *periodic* boundary conditions in both directions of the torus.

Like cylindrical operators, we can build different torus operators for different base loops. The blue torus operator for a trivial base loop is defined by the values of f_b shown in Table 3.1 while the blue torus operator for a red base loop is defined by the values shown in the top panel of Table 3.2. Finally, the blue torus operator for a blue base loop is defined by the values of f_b shown in the bottom panel of Table 3.2. Red torus operators for various base loops can be defined in the same way but with the red and blue colors exchanged.

It is important to keep in mind that the two coordinates that describe the torus are *not* equivalent. One coordinate parameterizes the movement of the loop in space, while the other coordinate parameterizes the loop itself. Thus to define a torus operator, we not only have to specify the torus S, but we also have to specify which coordinate has which meaning.

Let us now discuss spherical membrane operators. We can define blue spherical operators following the same recipe as the blue cylindrical operators. The only difference is that in the spherical topology, every picture can be reduced to the vacuum or (empty) picture by application of the constraints (3.36) — in contrast with the cylindrical case where every picture can be reduced to one of the four pictures shown in Table 3.1 or Table 3.2. Thus, in the spherical case it suffices to define the value of f_b on the vacuum picture. Here we define $f_b(\text{vacuum}) = 1$. Note that there is only one type of blue spherical operator — unlike the cylindrical or toroidal case where there are four types of operators parameterized by $q_r, q_b \in \{0, 1\}$.

In fact, we already encountered spherical membrane operators in the definition of the Hamiltonian H_1: the operators $\mathcal{B}_c^1$ and $\mathcal{B}_{\hat{c}}^1$ (3.15) can be thought of small spherical membrane operators associated with a unit blue cube $S = c$ or unit red cube $S = \hat{c}$. To see that $\mathcal{B}_c^1$ is a spherical membrane operator, note that the picture drawn on the surface of the blue unit cube has the property that the boundaries of the blue regions are always solid lines —that is, there are no boundaries that are dotted lines. The reason this is so is that all membranes in X_b are incident on the cube from the outside, rather than the inside. Now, since the picture on the surface of the cube does not contain any dotted blue lines, the local constraints (3.36) simplify considerably: in fact, we can throw out equations (3.36e) - (3.36g) and (3.36i-3.36j). The resulting equations can be solved explicitly, leading to the following formula for f_b:

$$\begin{aligned} f_b(X_b, X_r, S) = (-1)^{\#\{\text{red loops on } c\}} \\ \cdot\, i^{\#\{\text{blue-red intersections on } c\}}. \end{aligned} \tag{3.38}$$

We can see that this formula, together with the definition (3.35) agrees exactly with the definition of $\mathcal{B}_c^1$.

Showing that the membrane operators have the required properties

Having defined the membrane operators $M_b^1(S)$ and $M_r^1(S)$, we now show that they have the required properties. We will focus on one case, namely blue membrane operators $M_b^1(S)$ that create *unlinked* loop excitations. The arguments for the linked case are similar.

To begin, we show that if S is a *torus* then $M_b^1(S)$ does not create any excitations at all. That is, we show

$$M_b^1(S)|\Psi_1\rangle \propto |\Psi_1\rangle. \tag{3.39}$$

To establish this result, we first rewrite (3.39) in a more convenient form. Multiplying both sides by $\langle X_b, X_r|$ gives:

$$\langle X_b, X_r|M_b^1(S)|\Psi_1\rangle \propto \langle X_b, X_r|\Psi_1\rangle. \tag{3.40}$$

Next, using the definition of $M_b^1(S)$ (3.35), we can rewrite this as

$$f_b^*(X_b, X_r, S) \cdot \Psi_1(X_b + S, X_r) \propto \Psi_1(X_b, X_r). \tag{3.41}$$

To proceed further, we observe that Eq. (3.41) is equivalent to the relation

$$\frac{f_b^*(X_b, X_r, S) \cdot \Psi_1(X_b + S, X_r)}{f_b^*(X_b', X_r', S) \cdot \Psi_1(X_b' + S, X_r')} = \frac{\Psi_1(X_b, X_r)}{\Psi_1(X_b', X_r')} \tag{3.42}$$

for any two closed membrane configurations X_b, X_r and X_b', X_r'. Finally, we use the fact that f_b is a pure phase to rewrite this equation as

$$\frac{f_b(X_b', X_r', S)}{f_b(X_b, X_r, S)} = \frac{\Psi_1(X_b, X_r)\Psi_1(X_b' + S, X_r')}{\Psi_1(X_b', X_r')\Psi_1(X_b + S, X_r)}. \tag{3.43}$$

Our task is now to prove equation (3.43). First, we claim that it suffices to prove (3.43) for the case where (X_b', X_r') and (X_b, X_r) only differ locally — i.e. only differ in some small region. The reason it is enough to consider this case is that we can get from any membrane configuration (X_b, X_r) to any other configuration (X_b', X_r') by a series of local changes:

$$(X_b, X_r) \to (X_{b1}, X_{r1}) \to (X_{b2}, X_{r2}) \cdots \to (X_b', X_r').$$

If (3.43) holds for each pair (X_{bi}, X_{ri}),$(X_{b(i+1)}, X_{r(i+1)})$ then once we multiply these relations together, we see that it automatically holds for (X_b', X_r') and (X_b, X_r).

There are two cases to consider: the region where (X_b', X_r') and (X_b, X_r) differ may overlap S or not overlap S. In the second case, it is easy to see that (3.43) holds. Indeed, in this case the left hand side of (3.43) is equal to 1 since f_b only depends on the membrane configuration in the neighborhood of S and hence $f_b(X_b', X_r', S) = f_b(X_b, X_r, S)$. Similarly, the right hand side of (3.43) is also equal to 1 since the ratio $\Psi_1(X_b', X_r')/\Psi_1(X_b, X_r)$ only depends on the membrane configuration in the region where (X_b', X_r') and (X_b, X_r) differ

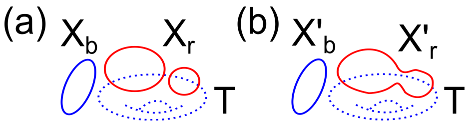

Figure 3.9: A blue torus operator $M_b(S)$ acts on two slightly different membrane configurations (a) (X_b, X_r) and (b) (X'_b, X'_r). Here, $X_b = X'_b$ is a blue sphere, while X_r consists of two red spheres and X'_r consists of a bigger red sphere obtained by merging the two red spheres in X_r.

from one another.

All that remains is the case where (X'_b, X'_r) and (X_b, X_r) differ in a small region that overlaps S. In this case, the ratio on the left hand side of (3.43) is directly determined by the local constraint equations (3.36) for f_b. The key point is that these constraint equations were chosen specifically so that a solution to these equations will automatically obey (3.43). This is easiest to see by example. Consider a blue torus operator $M_b^1(S)$ acting on the two configurations (X_b, X_r) and (X'_b, X'_r) shown in Fig. 3.9. Here $X_b = X'_b$ consists of a single blue sphere, while X_r consists of two red spheres and X'_r consists of single red sphere obtained by merging together the two spheres in X_r. In this case

$f_b(X_b, X_r, S) = f_b\Big($ 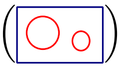 $\Big)$,

$f_b(X'_b, X'_r, S) = f_b\Big($ 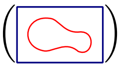 $\Big)$

so that

$\dfrac{f_b(X'_b, X'_r, S)}{f_b(X_b, X_r, S)} = \dfrac{f_b\Big(\text{ 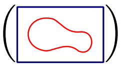 }\Big)}{f_b\Big(\text{ 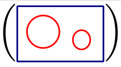 }\Big)} = -1$ (3.44)

according to (3.36b). On the other hand, it is easy to see that

$$\frac{\Psi_1(X_b, X_r)}{\Psi_1(X'_b, X'_r)} = 1, \quad \frac{\Psi_1(X_b + S, X_r)}{\Psi_1(X'_b + S, X'_r)} = -1$$

using the explicit formula for Ψ_1 (3.2). We conclude that

$$\frac{\Psi_1(X_b, X_r)\Psi_1(X_b' + S, X_r')}{\Psi_1(X_b', X_r')\Psi_1(X_b + S, X_r)} = -1 \tag{3.45}$$

so that equation (3.43) is satisfied in this case.

The above example serves two purposes. First it demonstrates, in at least one case, that f_b obeys equation (3.43). Second, it reveals where the constraint equation (3.36b) comes from: it should be clear that we chose the factor of -1 in this equation specifically to ensure that (3.43) was satisfied. Similarly, one can check that the other constraint equations (3.36) ensure that f_b obeys (3.43) in other cases.

This concludes our argument showing that the torus operator $M_b^1(S)$ does not create any excitations when applied to the ground state. Next, we need to show that the *cylinder* operator $M_b^1(S)$ does not create any excitations except at the two boundaries of S. This claim can be established using a similar argument to the torus case, but we will not repeat the derivation here. Instead we simply observe that the cylinder and torus operators look identical except near the two boundaries of the cylinder. Therefore it is intuitively clear that since the torus operator does not create any excitations, the same must be true of the cylinder operator away from its boundaries.

At this point, we have argued that the cylinder operator $M_b^1(S)$ creates blue loop excitations at its two boundaries and no other excitations anywhere else. However, we are not quite finished: we still need to verify one more property of the cylinder operator $M_b^1(S)$. Recall that H_1 supports four topologically distinct types of blue loop excitations (b, q_b, q_r) which differ from one another by attaching red and blue charges (see section 3.3.2). We need to check that $M_b^1(S)$ creates exactly one of these excitations, and not a linear superposition of different types of excitations. In other words, we need to check that $M_b^1(S)$ creates loop excitations that are *eigenstates* of braiding measurements.

To see that M_b^1 creates braiding eigenstates, we make use of a result from appendix

B.2. In that appendix, we show that the cylinder operators $M_b^1(S)$ are guaranteed to create braiding measurement eigenstates provided that f_b is multiplicative in the sense that

$$f_b(X_b, X_r, S \cup S') = f_b(X_b, X_r, S) \cdot f_b(X_b, X_r, S') \tag{3.46}$$

for any two cylinders S and S' that share a common boundary and any membrane configuration (X_b, X_r) whose intersection with the common boundary obeys the appropriate cylinder operator boundary condition.

In view of this result, we only have to show that f_b obeys condition (3.46). We go through this calculation in appendix B.2, and we show that f_b does indeed obey (3.46) provided that the values of f_b on the four basic pictures are those shown in Table 3.1. In fact, this is why we picked the particular values shown in that table: we chose those values to ensure that f_b obeys equation (3.46).

To summarize, we have shown that the cylinder operators $M_b^1(S)$ create blue loop excitations at their two boundaries and no other excitations anywhere else. We have also shown that these blue loop excitations are eigenstates of braiding measurements. This establishes that the cylinder operators have all the required properties.

3.3.4 Labeling scheme for loop excitations

In this section, we discuss some subtleties related to the labeling of loop excitations. As we have emphasized previously, both the H_0 and H_1 models support four different kinds of blue loop excitations and four different kinds of red loop excitations. We label the former by (b, q_b, q_r) and the latter by (r, q_b, q_r) where $q_b, q_r = 0, 1$. In practice, we first assign labels to the membrane operators; we then assign labels to the loop excitations according to which membrane operator creates them.

Now, an important question is how we choose which loop excitations are labeled by $(b, 0, 0)$ and $(r, 0, 0)$. We will call these excitations *neutral* loops. Once we decide which blue and red loops should called neutral, the labeling of all the other excitations is naturally fixed: for example, we assign the label (b, q_b, q_r) to the loop that is obtained by attaching q_b blue charge and q_r red charge to the neutral loop, $(b, 0, 0)$.

For the case of *unlinked* loops, there is a natural choice for which loop should be called neutral: the neutral loop is the unique loop that can be shrunk down to a point and annihilated by a local operator. Thus, for the case of unlinked loops there is a canonical labeling scheme. This is the labeling scheme we use here. Indeed, in the case of H_0, we assign $(b, 0, 0)$ to the loop created by the operator (3.32), and one can readily verify that this loop is the unique blue loop that can be annihilated locally. Similarly, in the case of H_1, we assign $(b, 0, 0)$ to the loop created by the membrane operator defined in Table 3.1 with $q_b = q_r = 0$ and one can also check that this loop can be annihilated locally. (One way to see this is to note that if we shrink the two ends of the cylinder to make a sphere, the operator defined by Table 3.1 reduces to the spherical membrane operator defined by (3.38)).

In contrast, for *linked* loops, there is no canonical way to define which loops are neutral. Therefore, we make this assignment *arbitrarily.* In other words, for each base loop, we arbitrarily choose one of the blue linked loops and one of the red linked loops, and we call them neutral. In the case of H_1, this arbitrary choice enters in how we parameterize the values in Table 3.2 which define the membrane operators and hence define the loop excitations. As we show in appendix B.2, the values in Table 3.2 are obtained by solving certain algebraic equations. These equations have four different solutions, which define four different membrane operators. All four are on an equal footing, but we simply picked one and labeled it by $q_b = 0, q_r = 0$. The labeling of the other solutions is then completely fixed. We could replace $q_b \to q_b + 1$ or $q_r \to q_r + 1$, for either the top or bottom panel of Table 3.2, and the resulting table would define an equally valid labeling convention.

The arbitrariness of our labeling scheme has an important consequence: because we picked the labels in an arbitrary way, there is no sense in which an unlinked loop of type (b, q_b, q_r) is the "same" type as a linked loop of type (b, q_b, q_r). More generally, we cannot

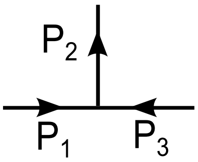

Figure 3.10: The exchange statistics of the charge excitations can be computed from the commutation algebra (3.47) of three string operators acting on three paths P_1, P_2, P_3 that share a common endpoint.

sensibly compare loops that are linked with different base loops. Each base loop effectively defines its own universe of excitations.

3.4 Braiding statistics of excitations

In the previous section, we constructed operators that create charges and vortex loops for the H_0, H_1 models. In this section, we will use these operators to compute the braiding statistics of these excitations. We consider four types of processes: (1) processes involving two charges, (2) processes involving a charge and a vortex loop, (3) processes involving two vortex loops, and finally (4) "three-loop processes" involving two vortex loops that are both linked with a third loop. We find that the two models have the same braiding statistics except for the last process; when we investigate the three-loop braiding process we find a distinction between the two models which implies that they belong to distinct topological phases.

3.4.1 Braiding two charges

To compute the statistics of the charge excitations, we use the "hopping operator algebra" derived in Ref. [63]. This algebra relates the exchange statistics of particle excitations to the commutation properties of the string operators that create these particles. To see how this works, let us consider the blue charge excitations in the H_0 model. According to the hopping operator algebra, the exchange statistics of these excitations can be read off from

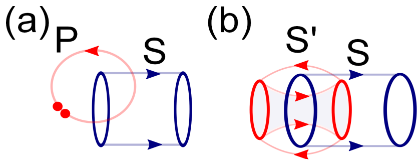

Figure 3.11: (a) The statistical phase associated with braiding a charge around a loop can be computed from the commutation algebra (3.48) of a string operator acting along a path P, and a membrane operator acting along a cylinder S. (b) The phase associated with braiding two loops around one another can be computed from the commutation algebra (3.49) of two membrane operators, one acting on a cylinder S, and the other acting on a torus S'.

the phase factor in the commutation relation

$$\begin{aligned} W_b^0(P_1)W_b^0(P_2) \quad W_b^0(P_3) \quad |\Psi_0\rangle = \\ e^{i\theta} \cdot \quad W_b^0(P_3) \quad W_b^0(P_2)W_b^0(P_1)|\Psi_0\rangle \end{aligned} \tag{3.47}$$

where P_1, P_2, P_3 are three paths arranged in the geometry of Fig. 3.10 and $|\Psi_0\rangle$ is the ground state of H_0. That is, if $\theta = 0$, then the blue charges are bosons, while if $\theta = \pi$, the blue charges are fermions. (Other values of θ are not possible in 3D). If we examine the form of the string operators, we can see that $\theta = 0$ since the string operators $W_b^0(P_1), W_b^0(P_2), W_b^0(P_3)$ (3.30) all commute with one another. We conclude that the blue charges are bosons in the H_0 model. Using identical reasoning, we can see that the blue and red charges are bosons in both models.

3.4.2 Braiding a charge and a vortex loop

Next, we compute the statistical Berry phase associated with braiding a charge around a vortex loop. More specifically, let us consider the H_0 model and imagine braiding a blue charge around a blue vortex loop. The statistical phase θ for such a process can be read off from the commutation algebra of the corresponding string operator and membrane operator

$$M_b^0(S)W_b^0(P)|\Psi_0\rangle = e^{i\theta} \cdot W_b^0(P)M_b^0(S)|\Psi_0\rangle \tag{3.48}$$

where P is a closed path and S is a cylindrical surface, arranged as in Fig. 3.11a. To see where this relation comes from, note that the operator $M_b^0(S)$ describes a process in which two vortex loops are created and moved to the ends of the cylinder S, while the operator $W_b^0(P)$ describes a three-step process in which two charges are created out of the vacuum, one of them is braided around the path P, and then the two annihilated with one another. With this interpretation, the right hand side of (3.48) describes a process in which two vortex loops are created and then a charge is braided around P, while the left hand side describes a process in which a charge is braided around P first, and then two vortex loops are created. Clearly the phase difference between these two processes is the statistical phase associated with braiding a charge around a vortex loop.

Remembering the definition of $M_b^0(S)$ and $W_b^0(P)$, we can see that these operators anticommute with each other. We conclude that braiding a blue charge around a blue vortex loop results in a statistical phase of π. Similarly, we can see that $M_r^0(S)$ and $W_r^0(P)$ anticommute with each other so braiding a red charge around a red vortex loop gives a phase of π. On the other hand, if one braids a red charge around a blue vortex loop or a blue charge around a red vortex loop, the statistical phase vanishes since these operators commute with one another.

A similar calculation for the H_1 model gives identical results. Thus the two models share the same statistics between charges and vortex loops. We note that these statistical phases agree with the Aharonov-Bohm phases associated with braiding a charge around a vortex loop in $\mathbb{Z}_2 \times \mathbb{Z}_2$ gauge theory. This is not a coincidence: as we mentioned in the introduction, the two models can be viewed as two different types of $\mathbb{Z}_2 \times \mathbb{Z}_2$ gauge theories.

3.4.3 Braiding two vortex loops

H_0 model

We now consider, for the H_0 model, the statistical phase associated with braiding a vortex loop around another vortex loop (Fig. 3.1a). For example, let us consider braiding a blue vortex loop around another blue vortex loop. Similarly to Eq. (3.48), the statistical phase θ^0_{bb} can be computed from the commutation relation

$$M^0_b(S')M^0_b(S)|\Psi_0\rangle = e^{i\theta^0_{bb}} \cdot M^0_b(S)M^0_b(S')|\Psi_0\rangle \qquad (3.49)$$

where S is a cylinder and S' is a torus, arranged as in Fig. 3.11b. Examining the definition of the membrane operators (3.32), we can see that they commute with one another so that $\theta^0_{bb} = 0$. Likewise, we can see that there is no statistical phase associated with braiding a red loop around a red loop or a red loop around a blue loop since the corresponding membrane operators all commute with one another.

The above results apply to the blue vortex loop and red vortex loops labeled by $(b, 0, 0)$ and $(r, 0, 0)$. One might also wonder about the braiding statistics of more general vortex loops (b, q_b, q_r) and (r, q_b, q_r). The braiding statistics of these more general vortex loops can be computed using the same approach as above. The only difference is that the membrane creation operators are slightly different in this case: they are obtained by multiplying M^0_b (or M^0_r) by one of the string operators $W^0_b(P)$, $W^0_r(P')$ or $W^0_b(P) \cdot W^0_r(P')$, where the paths P, P' run along the length of the cylinder. Substituting these modified membrane operators into Eq. (3.49), a simple calculation shows that the phase associated with braiding a blue vortex loop (b, q_b, q_r) around another blue vortex loop (b, q'_b, q'_r) is given by

$$\theta^0_{bb} = \pi(q_b + q'_b). \qquad (3.50)$$

Similarly, the phase associated with braiding a red vortex loop (r, q_b, q_r) around another red vortex loop (r, q_b', q_r') is

$$\theta^0_{rr} = \pi(q_r + q_r') \tag{3.51}$$

while the phase associated with braiding a red vortex loop (r, q_b, q_r) around a blue vortex loop (b, q_b', q_r') is

$$\theta^0_{rb} = \pi(q_b + q_r'). \tag{3.52}$$

These expressions have a natural interpretation in terms of Aharonov-Bohm phases: the first term in each formula is the statistical phase associated with braiding the charge on the first vortex loop around the flux of the second loop while the second term is the phase associated with braiding the flux of the first vortex loop around the charge on the second loop.

H_1 model

Similarly to the H_0 case, the statistical phase θ^1_{bb} associated with braiding a blue vortex loop around a blue vortex loop in the H_1 model can be read off from the commutation algebra of the corresponding membrane operators:

$$M^1_b(S')M^1_b(S)|\Psi_1\rangle = e^{i\theta^1_{bb}} \cdot M^1_b(S)M^1_b(S')|\Psi_1\rangle. \tag{3.53}$$

However the membrane operators M^1_b are more complicated than their counterparts in the H_0 model, so it is more difficult to apply Eq. (3.53). To deal with this issue, we now derive a simpler version of Eq. (3.53) which is more convenient for our purposes. The first step is to rewrite Eq. (3.53) as

$$\begin{aligned}\sum_X M^1_b(S')M^1_b(S)|X\rangle\langle X|\Psi_1\rangle = \\ e^{i\theta^1_{bb}} \sum_X M^1_b(S)M^1_b(S')|X\rangle\langle X|\Psi_1\rangle.\end{aligned}$$

where $|X\rangle \equiv |X_b, X_r\rangle$. Next, we use the fact that $M_b^1(S')M_b^1(S)|X_b, X_r\rangle \propto |X_b{+}S{+}S', X_r\rangle$, which implies that all of the states $M_b^1(S')M_b^1(S)|X\rangle$ that appear in the above sum are linearly independent from one another. It follows that the above equality must hold for each term *separately*. Hence, we must have

$$M_b^1(S')M_b^1(S)|X\rangle = e^{i\theta_{bb}^1} \cdot M_b^1(S)M_b^1(S')|X\rangle \tag{3.54}$$

for every membrane state $|X\rangle$ that has a nonzero amplitude in the state $|\Psi_1\rangle$.

We will now use (3.54) to compute the statistics of the loops in the H_1 model. To this end, we set $|X\rangle = |0,0\rangle$, the "no-membrane" state. We then define $|Y\rangle = |S,0\rangle$, $|Y'\rangle = |S',0\rangle$, and $|Z\rangle = |S+S',0\rangle$. With this notation, the left side of (3.54) can be computed as

$$\begin{aligned} M_b^1(S')M_b^1(S)|X\rangle &= M_b^1(S') \cdot f_b(X,S)|Y\rangle \\ &= f_b(Y,S')f_b(X,S)|Z\rangle. \end{aligned} \tag{3.55}$$

Similarly, the term on the right side is given by

$$\begin{aligned} M_b^1(S)M_b^1(S')|X\rangle &= M_b^1(S) \cdot f_b(X,S')|Y'\rangle \\ &= f_b(Y',S)f_b(X,S')|Z\rangle. \end{aligned} \tag{3.56}$$

Comparing these two expressions with (3.54), we derive

$$e^{i\theta_{bb}^1} = \frac{f_b(Y,S')f_b(X,S)}{f_b(Y',S)f_b(X,S')}. \tag{3.57}$$

To complete the calculation, we compute the value of f_b for each of these configurations

$f_b(X, S) = f_b \Big($ 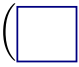 $\Big) = 1,$

$f_b(X, S') = f_b \Big($ 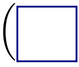 $\Big) = 1,$

$f_b(Y, S') = f_b \Big($ 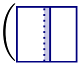 $\Big) = e^{i\pi q_{b'}},$

$f_b(Y', S) = f_b \Big($ 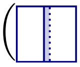 $\Big) = e^{i\pi q_b}.$ (3.58)

Substituting these values into (3.57), we find that the statistical phase associated with braiding a loop (b, q_b, q_b) around another loop (b, q_b', q_b') is

$$\theta_{bb}^{1} = \pi(q_b + q_b'). \tag{3.59}$$

We note that this result is identical to the statistical phase θ_{bb}^{0} (3.50) in the H_0 model. Similarly, it is easy to check that the phase associated with braiding two red loops around one another agrees with (3.51) while the phase associated with braiding a red loop around a blue loop agrees with (3.52). Thus, the two models share the same two-loop braiding statistics. In fact the agreement between the two models is not surprising, since the two models are equivalent to $\mathbb{Z}_2 \times \mathbb{Z}_2$ gauge theories, and in such systems the two-loop braiding statistics always has an Aharonov-Bohm form, as explained in Ref. [85].

3.4.4 Three-loop braiding

Finally, we discuss the three-loop braiding statistics in the two models. Specifically, we consider a braiding process in which a loop is braided around another loop, while both are linked to a third "base" loop (Fig. 3.1b). Unlike the other processes we have considered until now, we will see that the two models can be distinguished by their three-loop statistics.

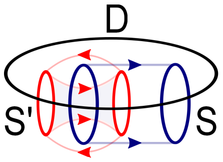

Figure 3.12: The statistical phase associated with a three-loop braiding process can be computed from the commutation algebra of two membrane operators, one acting along the cylinder S, and the other acting along the torus S'. Here both S and S' are linked with a base loop which lies along the boundary of the disk D.

H_0 model

First we compute the statistics in the H_0 model. As in the two-loop case, the three-loop braiding statistics can be read off from the commutation algebra for the membrane operators. For example, the statistical phase $\theta^0_{bb,r}$ associated with braiding a blue vortex loop around a blue vortex loop, while both are linked to a red base loop can be obtained from

$$M^0_b(S')M^0_b(S)|\Psi_{ex}\rangle = e^{i\theta^0_{bb,r}} \cdot M^0_b(S)M^0_b(S')|\Psi_{ex}\rangle \tag{3.60}$$

where S is a cylinder, S' is a torus, and $|\Psi_{ex}\rangle$ is an excited state with a red vortex loop that links with both S and S' (Fig. 3.12). Remembering that the membrane operators M^0_b all commute with each other, we deduce that $\theta^0_{bb,r} = 0$. In the same way, we can see that $\theta^0_{bb,b} = 0$.

In the above calculation we implicitly assumed loops of the form $(b, 0, 0)$. If we instead consider a process in which a general vortex loop (b, q_b, q_r) is braided around another loop (b, q'_b, q'_r) with either a red base loop or a blue base loop, then, just as in the two-loop case (3.50), one finds

$$\theta^0_{bb,r} = \theta^0_{bb,b} = \pi(q_b + q'_b). \tag{3.61}$$

Similarly, if we braid a red loop (r, q_b, q_r) around another red loop (r, q'_b, q'_r) with either base, the statistical phase is

$$\theta^0_{rr,r} = \theta^0_{rr,b} = \pi(q_r + q'_r). \tag{3.62}$$

Finally, braiding a red loop (r, q_b, q_r) around a blue loop (b, q_b', q_r') with either base gives the phase

$$\theta^0_{rb,r} = \theta^0_{rb,b} = \pi(q_b + q_r'). \tag{3.63}$$

The agreement with the two-loop statistics (3.50-3.52) is to be expected since the membrane operators $M_b^0(S)$,$M_b^0(S')$ obey the same commutation algebra independent of whether they act on the ground state $|\Psi_0\rangle$ (as in the two loop case) or an excited state $|\Psi_{ex}\rangle$ (as in the three loop case).

H_1 model

We begin by computing the statistical phase associated with braiding a blue vortex loop around another blue vortex loop, while both are linked with a red base loop. As in the H_0 case, the statistical phase $\theta^1_{bb,r}$ is given by

$$M_b^1(S')M_b^1(S)|\Psi_{ex}\rangle = e^{i\theta^1_{bb,r}} \cdot M_b^1(S)M_b^1(S')|\Psi_{ex}\rangle \tag{3.64}$$

where S is a cylinder, S' is a torus, and $|\Psi_{ex}\rangle$ is an excited state with a red vortex loop that links with both S and S' (Fig. 3.12). Following the same logic as in section 3.4.3, it is straightforward to deduce an alternative and more convenient form of equation (3.64):

$$M_b^1(S')M_b^1(S)|X\rangle = e^{i\theta^1_{bb,r}} M_b^1(S)M_b^1(S')|X\rangle \tag{3.65}$$

where $|X\rangle \equiv |X_b, X_r\rangle$ is any membrane state that has nonzero overlap with $|\Psi_{ex}\rangle$. To compute $\theta^1_{bb,r}$, we set $|X\rangle = |0, D\rangle$ where D is a disk with a boundary along the red vortex loop. We then define $|Y\rangle = |S, D\rangle$, $|Y'\rangle = |S', D\rangle$, and $|Z\rangle = |S+S', D\rangle$. With this notation, the left hand side of (3.65) can be computed as

$$M_b^1(S')M_b^1(S)|X\rangle = f_b(Y, S')f_b(X, S)|Z\rangle \tag{3.66}$$

while the expression on the right hand side can be written as

$$M_b^1(S)M_b^1(S')|X\rangle = f_b(Y',S)f_b(X,S')|Z\rangle. \tag{3.67}$$

The three-loop statistics is then given by

$$e^{i\theta_{bb,r}^1} = \frac{f_b(Y,S')f_b(X,S)}{f_b(Y',S)f_b(X,S')}. \tag{3.68}$$

To complete the calculation, we need to compute the values of f_b on each of these configurations. We have

$f_b(X,S) = f_b\Bigg($ 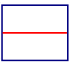 $\Bigg) = 1,$

$f_b(X,S') = f_b\Bigg($ 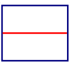 $\Bigg) = 1,$

$f_b(Y,S') = f_b\Bigg($ 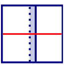 $\Bigg) = i \cdot e^{i\pi q_b'},$

$f_b(Y',S) = f_b\Bigg($ 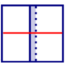 $\Bigg) = -i \cdot e^{i\pi q_b},$ (3.69)

where the '−' sign in the last equation comes from using the local rules (3.36) to reduce the picture to one of the basic pictures in Table 3.2. Substituting these values into (3.68), we find that the statistical phase associated with braiding a loop (b, q_b, q_r) around another loop (b, q_b', q_r') while both are linked to a red base loop is given by:

$$\theta_{bb,r}^1 = \pi + \pi(q_b + q_b'). \tag{3.70}$$

In a similar manner, it is easy to show that the phase associated with braiding a red loop (r, q_b, q_r) around another red loop (r, q_b', q_r'), while both are linked to a red base is:

$$\theta_{rr,r}^1 = \pi(q_r + q_r'). \tag{3.71}$$

As another example, let us compute the phase associated with braiding a red loop around a blue loop, with a red base. The analogue of equation (3.65) in this case is

$$M_r^1(S')M_b^1(S)|X\rangle = e^{i\theta^1_{rb,r}} \cdot M_b^1(S)M_r^1(S')|X\rangle \tag{3.72}$$

where $|X\rangle \equiv |X_b, X_r\rangle$ is any state that has nonzero overlap with $|\Psi_{ex}\rangle$ and $|\Psi_{ex}\rangle$ is an excited state with a red vortex loop that links with both S and S'. Letting $|X\rangle = |0, D\rangle$, $|Y\rangle = |S, D\rangle$, $|Y'\rangle = |0, D + S'\rangle$, and $|Z\rangle = |S, D + S'\rangle$, we derive

$$e^{i\theta^1_{rb,r}} = \frac{f_r(Y, S')f_b(X, S)}{f_b(Y', S)f_r(X, S')}. \tag{3.73}$$

Proceeding as before, we find

$f_b(X, S) = f_b \Bigg($ 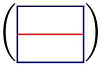 $\Bigg) = 1,$

$f_r(X, S') = f_r \Bigg($ 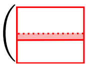 $\Bigg) = 1,$

$f_r(Y, S') = f_r \Bigg($ 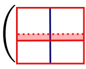 $\Bigg) = e^{i\pi q'_b},$

$f_b(Y', S) = f_b \Bigg($ 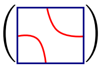 $\Bigg) = i \cdot e^{i\pi q_r}.$ (3.74)

Substituting these values into (3.73), we conclude that the statistical phase associated with braiding a loop (r, q_b, q_r) around another loop (b, q'_b, q'_r) while both are linked to a red base loop is

$$\theta^1_{rb,r} = -\frac{\pi}{2} + \pi(q_b + q'_r). \tag{3.75}$$

So far we have only discussed braiding processes involving a red base loop. We can find the braiding statistics associated with a *blue* base loop, by simply switching the roles of "red" and "blue":

$$\begin{aligned}\theta^1_{rr,b} &= \pi + \pi(q_r + q_r'), \\ \theta^1_{bb,b} &= \pi(q_b + q_b'), \\ \theta^1_{br,b} &= -\frac{\pi}{2} + \pi(q_r + q_b'). \end{aligned} \tag{3.76}$$

Putting together equations (3.70),(3.71),(3.75) and (3.76), we have found all the three-loop braiding statistics of the H_1 model. (Actually, one quantity that we have not computed is the *exchange* statistics of the loops. However, this quantity is not necessary for our purposes, since the mutual statistics computed above is sufficient to distinguish the two models).

Before concluding this section, we would like to mention that the three-loop statistics for H_1 appears to be identical to the three-loop statistics of one of the $\mathbb{Z}_2 \times \mathbb{Z}_2$ Dijkgraaf-Witten models[23, 83]. To see this, we follow the notation of Ref. [85, 86] and we summarize the three-loop statistics for H_1 in terms of the quantity $\Theta_{ij,k} \equiv 2\theta^1_{ij,k}$ where the indices $i, j, k \in \{r, b\}$, and $\Theta_{ij,k}$ is defined modulo 2π. Translating equations (3.70),(3.71), (3.75) and (3.76) into the Θ variables gives:

$$\begin{aligned}\Theta_{bb,r} &= \Theta_{rr,r} = \Theta_{rr,b} = \Theta_{bb,b} = 0 \\ \Theta_{rb,r} &= \Theta_{br,b} = \pi, \end{aligned} \tag{3.77}$$

If we compare this data to the results of Ref. [85], we can see that it matches the three-loop statistics for the $\mathbb{Z}_2 \times \mathbb{Z}_2$ Dijkgraaf-Witten model labeled by $(p_1 = 1, p_2 = 1)$. Based on this fact, we conjecture that H_1 belongs to the same phase as this Dijkgraaf-Witten model. [5]

---

[5] In fact, if our conjecture is correct then H_1 also belongs to the same phase as the Dijkgraaf-Witten models labeled by $(1, 0)$ and $(0, 1)$, since the three Dijkgraaf-Witten models labeled by $(1, 1)$, $(1, 0)$ and $(0, 1)$ all belong to the same phase, when viewed as spin models rather than gauge theories.

Comparing the three-loop statistics in the two models

With the above results, we now show that the H_0 and H_1 models have distinct three-loop statistics. To see an example of a difference between the two models, consider the formula for $\theta^1_{rb,r}$ (3.75). This formula implies that, in the H_1 model, if we braid a red loop around a blue loop, while both are linked to a red loop the resulting phase is $\pm\pi/2$ depending on what type of red and blue loops are being braided. In contrast, in the H_0 model, we can see from (3.61), (3.62), (3.63) that if we braid *any* two loops around one another, the resulting phase is always 0 or π, independent of the choice of base loop or what loops are being braided.

For another example of a difference, consider the formula for $\theta^1_{bb,r}$ (3.70) for the case where the two blue loops (b, q_b, q_r), (b, q'_b, q'_r) are *identical*, i.e. $q_b = q'_b$ and $q_r = q'_r$. In this case, $\theta^1_{bb,r} = \pi$. This means that if we braid two identical blue loops around one another while they are both linked to a red loop, the resulting statistical phase is π in the H_1 model. On the other hand, in the H_0 model, we can see from (3.61), (3.62), (3.63) that if we braid *any* two identical loops around one another the resulting phase is always 0, independent of which loops or base loops are involved.

From the above examples, it is clear that there is no way to map the loop excitations of H_0 onto the loop excitations of H_1 in such a way that the corresponding loops have the same statistics. Importantly, we can rule out *all* possible mappings between the two sets of loop excitations including those that change the "colors" or "charges" of the loop, e.g. that map the excitation $(b, 1, 0)$ in H_0 onto $(r, 0, 1)$ in H_1. (This generality is important because the "colors" and "charges" of the loops have no physical meaning in this context except as a scheme for labeling excitations). We conclude that the two models have physically distinct three-loop statistics, and hence must belong to different phases.

3.5 Conclusion

In this chapter, we have presented an explicit computation of the three-loop braiding statistics of two spin models, H_0, H_1. The key step in our analysis was our construction of membrane operators that create and move loop excitations. With the help of these operators, we were able to implement the three-loop braiding process on the lattice and find the associated statistical phase in each of the models. While technically complicated, this membrane operator approach has the advantage that it is more direct than previous calculations based on dimensional reduction[85] or modular transformations on a 3D torus.[41, 88] An additional feature of our results is that they provide a concrete demonstration of the utility of three-loop braiding statistics for distinguishing 3D gapped phases: indeed, we have shown that the two models H_0 and H_1 share the same particle exchange statistics and the same particle-loop and loop-loop braiding statistics. The only way to see that these models belong to distinct phases is to examine their three-loop braiding statistics.

The discussion in this chapter raises an important question, namely whether three-loop braiding statistics, together with particle exchange statistics and particle-loop braiding statistics, provides enough data to uniquely distinguish all 3D gapped phases. The existence of the 3D cubic code model[33] suggests that the answer to this question may be ‘no’ in general. Indeed, the cubic code model does not support deconfined particle-like and loop-like excitations like the models studied in this chapter, so it is not clear whether one can define particle or loop braiding statistics for this system. In light of this example, a more natural question may be whether the above braiding statistics data is sufficient to distinguish an appropriate subset of 3D gapped phases, such as the “gapped quantum liquids” defined in Ref. [98]. As far as we know, this is an open question: we are not aware of any counterexamples or arguments one way or the other.

One direction for future work would be to investigate the implications of our results for symmetry protected topological (SPT) phases. Indeed, as discussed in the introduction, both H_0 and H_1 can be thought of as $\mathbb{Z}_2 \times \mathbb{Z}_2$ gauge theories obtained by gauging the

$\mathbb{Z}_2 \times \mathbb{Z}_2$ symmetry of two different spin models. The H_1 model comes from a spin model[22] belonging to a nontrivial SPT phase, while H_0 comes from a spin model in a trivial SPT phase. Following the same approach as in Ref. [62], it should be possible to derive bulk and surface properties of the two SPT phases from the braiding statistics in the associated gauge theories H_0, H_1. Results of this kind will be discussed in chapter 4

Another direction would be to construct exactly soluble lattice models that can realize more general types of 3D gapped phases. For example, since the two models H_0, H_1 are built out of two species of intersecting membranes, it may be possible to build more general models by considering more species of membranes or by allowing membranes to *branch* — in analogy with the string-net models of Ref. [65]. Given our suspicion that H_0, H_1 belong to the same phase as $\mathbb{Z}_2 \times \mathbb{Z}_2$ Dijkgraaf-Witten models, a key question is whether such a construction can realize any phases that cannot be realized by previously known exactly soluble models, such as the 3D Dijkgraaf-Witten models[23, 83] or 3D string-net models[65].

CHAPTER 4

3D SPT PHASES AND EXACTLY SOLUBLE LATTICE MODELS

4.1 Introduction

Symmetry protected topological (SPT) phases[32, 19, 20, 21, 17, 73, 74, 81, 27] are generalization of topological insulators[44, 43, 79, 29, 71, 36]. They are quantum phases of gapped many-body systems in any spatial dimension with arbitrary symmetry. A quantum many-body system which realizes a nontrivial SPT phase is characterized by the following properties. First, the Hamiltonian is gapped in the bulk. Second, the system is invariant under a certain set of symmetries, none of which are broken spontaneously. Third, the ground state can be adiabatically connected to a trivial state if one or more of the symmetries are broken during the process. By a “trivial state”, we mean a product state (in the boson/spin case) or an atomic insulator (in the fermion case); by “adiabatically connected” we mean connected by varying a parameter in the Hamiltonian without closing the energy gap. Finally, the ground state cannot be adiabatically connected to a trivial state without breaking one or more of the symmetries.

The most important physical property of SPT phases is that they typically have robust gapless boundary modes. In one dimension, it was shown[19, 20] that when a nontrivial SPT phase is put on an open chain, there would be ground state degeneracy at each end of the chain. This degeneracy is stable as long as the symmetry of the system is not broken. A famous example is the Haldane spin-1 chain[32, 73, 74]. This spin chain supports a dangling spin-1/2 at each of two ends, which leads to 4-fold ground state degeneracy protected by $SO(3)$ symmetry. In two dimensions, it is known that the boundary of nontrivial SPT phases must either be gapless or break the symmetry. This statement was proven for group cohomology models with any unitary symmetry in [21].

Our understanding of three dimensional SPT phases is, however, limited. The existence of protected surface states has been established for topological insulators[61, 29] and for topological superconductors[87, 69, 25] but little is known about more general 3D SPT phases.

Since our understanding of surface states of 3D SPT phases is case by case, thus it is desired to have a general way to to understand the surface states for 3D SPT phases. Thus our starting point is the following question: Given a microscopic model in 3D, how can one tell if it has protected surface states or not?

The analogous question in 2D was answered in Ref. [62]. They showed that the nontrivial braiding statistics of vortex excitations after gauging the symmetry leads to the protected edge modes in 2D. Thus the edges must either be gapless or break a symmetry for 2D SPT phases since these phases are characterized by nontrivial braiding statistics of vortex excitations. It is natural to wonder whether there is a similar result involving the protected surface states of 3D SPT phases. Thus we arrive the question: what is the analogous bulk-boundary correspondence in 3D SPT phases?

In this chapter, we answer this question for a particular 3D exactly soluble lattice model, but the arguments apply more generally. Specifically, we construct two exactly soluble spin models with $\mathbb{Z}_2 \times \mathbb{Z}_2$ symmetry which belong to two distinct SPT phases. One model realizes the usual two copies of 3D Ising paramagnets. The other model realized a new paramagnet with a $\mathbb{Z}_2 \times \mathbb{Z}_2$ symmetry. In both cases, the particle excitations are bosons, and the particle and loop excitations have the same mutual braiding statistics. The key difference between the two models is that the new paramagnet is characterized by nontrivial three-loop braiding statistics after gauging the symmetry while the other model is not. By three-loop braiding statistics[85], we refer to a process involving braiding one vortex loop around another while both are linked with a third loop.

We prove that the new paramagnet model has protected surface states using the fact that the vortex loop excitations in the bulk have non-trivial three-loop braiding statistics. Here by "protected" surface states, we mean that the surface states are either gapless, symmetry-breaking or carries topological order. Our arguments can apply to general SPT phases in 3D. Thus the bulk-boundary correspondence for 3D SPT phases will be the statement that nontrivial three-loop braiding statistics in the bulk leads directly to the protected surface states for 3D SPT phases.

The chapter is organized as follows. In section 4.2, we introduce two exactly soluble 3D spin models with $\mathbb{Z}_2 \times \mathbb{Z}_2$ symmetry. In section 4.3, we couple the two models to the $\mathbb{Z}_2 \times \mathbb{Z}_2$ gauge field. We discuss the excitations in the gauged spin models and the associated creation operators in section 3.3. We then show that the two spin models can be distinguished by the braiding statistics of vortex loop excitations in section 3.4. In section 4.6, we prove that the nontrivial three-loop braiding statistics in the bulk implies that the surface state is either gapless, symmetry breaking or carries topological order. Some technical details can be found in the appendices.

4.2 Two kinds of paramagnets with $\mathbb{Z}_2 \times \mathbb{Z}_2$ symmetry

In this section, we construct two exactly soluble lattice spin models with $\mathbb{Z}_2 \times \mathbb{Z}_2$ symmetry. We denote the Hamiltonians for these models by H_0 and H_1 and we will show that H_0 and H_1 belong to two different SPT phases with $\mathbb{Z}_2 \times \mathbb{Z}_2$ symmetry. More specifically, we show that H_1 belongs to a nontrivial SPT phase while H_0 belongs to a trivial SPT phase.

4.2.1 Hilbert space for the models

The two spin models are built out of two types of spins: “blue” spins and “red” spins. The blue spins, which we will denote by τ_c, live on the centers of the cubes c of the cubic lattice, while the red spins, which we will denote by $\tau_{\hat{c}}$, live on the centers of the cubes $\hat{c}$ of the dual cubic lattice (see Fig. 4.1).

Working in the $|\{\tau_c^z, \tau_{\hat{c}}^z\}\rangle$ basis, these models support two different kinds of domain walls: “blue domain walls” which separate neighboring blue spins with opposite values of τ_c^z, and

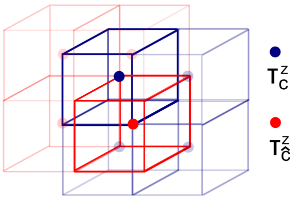

Figure 4.1: Both models are built out of two species of spins. The blue spins τ_c live on the centers c of the cubic lattice while the red spins $\tau_{\hat{c}}$ live on the centers $\hat{c}$ of the dual cubic lattice.

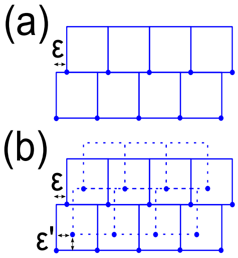

Figure 4.2: The sheared square lattice is formed by shifting the corners of the square plaquettes (the blue dots) according to $(i, j) \to (i + \epsilon j, j)$ with $\epsilon > 0$. (b) Top view of the sheared cubic lattice. The solid/dash squares denote cubes no two neighboring layers. The sheared cubic lattice is formed by shifting the corners of the cubes according to $(i, j, k) \to (i + \epsilon j + \epsilon' k, j + \epsilon' k,)$ with $\epsilon' > \epsilon > 0$.

"red domain walls" which separate neighboring red spins with opposite values of $\tau^z_{\hat{c}}$. The blue domain walls live on the plaquettes p of the cubic lattice while the red domain walls live on the plaquettes $\hat{p}$ of the dual cubic lattice.

4.2.2 Sheared cubic lattice

For the purpose of defining the Hamiltonians and the wave functions, we need to compute the number of intersecting loops between red and blue domain walls for a given configuration of red and blue domain walls. There is a technical problem when four blue domain walls meet at an edge l and intersect with one red domain wall. In that case, intersecting loops between red and blue domain walls touch one another at the edge l. Thus, it is ambiguous to determine the number of disconnected intersecting loops.

To resolve this issue, we deform the lattice infinitesimally to eliminate domain wall touching. To see how it works, let us first consider the analogous deformation of the square lattice in $2D$. The basic idea is to think of the square plaquettes which compose the square lattice as rigid blocks that can be shifted around. Then the deformation corresponds to shifting the position of the square plaquettes so that their corners move from $(i,j) \to (i+\epsilon j, j)$. The resulting lattice, which we call the *sheared* square lattice is shown in Fig. 4.2(a).

Now let us consider the cubic lattice. In the same manner, we can think of the cubes that compose the cubic lattice as rigid blocks that can be shifted around. Then we shift these cubes so that their corners move from

$$(i,j,k) \to (i+\epsilon j+\epsilon' k, j+\epsilon' k, k) \tag{4.1}$$

with $\epsilon' > \epsilon > 0$. The resulting *sheared* cubic lattice is shown in Fig. 4.2(b).

Finally, let us perform the same shearing deformation to both the original cubic lattice and the dual cubic lattice. In this way blue domain walls and red domain walls on the sheared cubic lattice and dual cubic lattice will intersect with disconnected loops without any domain wall touching. In the following, we will always think of domain walls as living on the sheared cubic lattice so we do not have to worry about domain wall touching.

4.2.3 Definition of models

The Hamiltonians for the two models are defined by

$$H_0 = -\sum_c B_c^0 - \sum_{\hat{c}} B_{\hat{c}}^0, \tag{4.2}$$

$$H_1 = -\sum_c B_c^1 - \sum_{\hat{c}} B_{\hat{c}}^1, \tag{4.3}$$

where

$$B_c^0 = \frac{1}{2}(1+\tau_c^x), \quad B_{\hat{c}}^0 = \frac{1}{2}(1+\tau_{\hat{c}}^x) \tag{4.4}$$

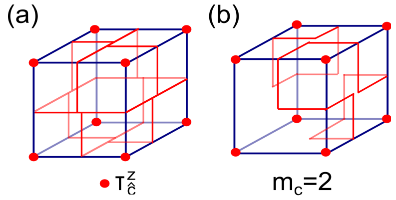

Figure 4.3: (a) The intersection between the red domain walls and the cube c in the sheared cubic lattice. (b) The configuration contains two red domain walls on the cube c and thus $m_c = 2$.

and

$$
\begin{aligned}
B^1_c &= \frac{1}{2}(1 + \tau^x_c \cdot (-1)^{m_c} \cdot i^{n_c}), \\
B^1_{\hat{c}} &= \frac{1}{2}(1 + \tau^x_{\hat{c}} \cdot (-1)^{m_{\hat{c}}} \cdot i^{n_{\hat{c}}}).
\end{aligned} \tag{4.5}
$$

Here $c, \hat{c}$ run over the cubes of the cubic lattice and dual cubic lattice, and $m_c, m_{\hat{c}}, n_c, n_{\hat{c}}$ are integer-valued functions of $\{\tau^z_c, \tau^z_{\hat{c}}\}$, which are defined as follows. First, consider m_c. To define the value of m_c for some spin configuration $\{\tau^z_c, \tau^z_{\hat{c}}\}$, consider the intersection between the set of red domain walls in $\{\tau^z_c, \tau^z_{\hat{c}}\}$ and the cube c. This intersection defines a collection of closed loops that live on the surface of the cube c (here, we draw the domain walls in the sheared cubic lattice as in section 4.2.2 (see Fig. 4.3(a))). The integer m_c is defined to be the number of these domain wall loops, i.e.,

$$
m_c = \#\{\text{red domain wall loops on } c\}. \tag{4.6}
$$

Fig. 4.3(b) shows an example of m_c for a particular membrane configuration. The integer $m_{\hat{c}}$ is defined in the same way:

$$
m_{\hat{c}} = \#\{\text{blue domain wall loops on } \hat{c}\}. \tag{4.7}
$$

To define the value of n_c, consider the intersection between the set of blue domain walls

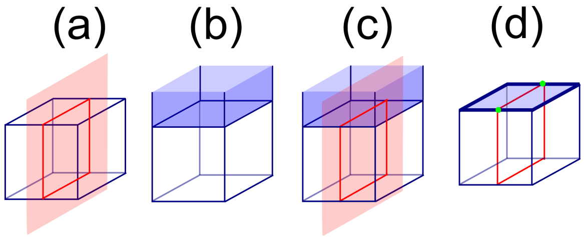

Figure 4.4: (a) A blue cube intersects a red domain wall. Their intersection consists of a single red loop. (b) A blue cube intersects/overlaps with a blue domain wall. Their intersection consists of a single blue region. (c) A blue cube intersects with both a red and a blue domain wall. Their intersection consists of one red loop and one blue region. (d) For the domain wall configuration shown in (c), the integer $m_c = 1$ because there is one red loop while $n_c = 2$ because there are two intersections (denoted by green dots) between the red loop and the boundary of the blue region (thick blue line).

and the cube c. These intersections define a collection of 2D regions that live on the surface of the cube c. Consider the boundary of these regions. This boundary will consist of a collection of closed loops which we will call "blue loops." The integer n_c is defined to be the number of intersections between the blue loops and the red domain wall loops defined above:

$$n_c = \#\{\text{blue-red intersections on } c\} \tag{4.8}$$

(See Fig. 4.4 for an example). The $n_{\hat{c}}$ operator is defined in an identical way:

$$n_{\hat{c}} = \#\{\text{red-blue intersections on } \hat{c}\}. \tag{4.9}$$

Notice that n_c and $n_{\hat{c}}$ are always an even integer.

If we wish to be more explicit, we can write m_c as a function of the relative orientations of the 8 red spins $\tau^z_{\hat{c}_1}, ..., \tau^z_{\hat{c}_8}$ that live at the 8 corners of the cube c:

$$m_c = f(\tau^z_{\hat{c}_i}\tau^z_{\hat{c}_j}, \ldots, \tau^z_{\hat{c}_k}\tau^z_{\hat{c}_l}).$$

Here, f is a finite polynomial, but its explicit form is not illuminating so we do not show it here. The arguments of f, $\tau^z_{\hat{c}_i}\tau^z_{\hat{c}_j}$, etc. run over the 12 edges of the cube c (see Fig. 4.5(a)).

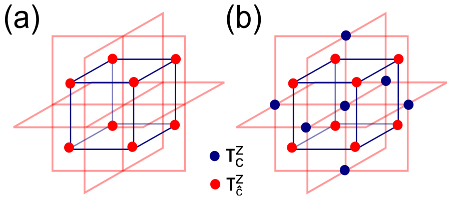

Figure 4.5: (a) The integer m_c is a function of the 8 spins $\tau^z_{\hat{c}}$ at eight corners of the cube c. (b) The integer n_c is a function of 7 blue spins τ^z_c and 8 red spins $\tau^z_{\hat{c}}$ around the cube c.

Similarly, $m_{\hat{c}}$ is a function of the 8 blue spins $\tau^z_{c_1}, ..., \tau^z_{c_8}$ that live at the eight corners of the cube $\hat{c}$:

$$m_{\hat{c}} = f(\tau^z_{c_i}\tau^z_{c_j}, \ldots, \tau^z_{c_k}\tau^z_{c_l}).$$

Likewise, n_c is a function of τ^z_c, along with the 7 blue spins $\tau^z_{c_1}, ..., \tau^z_{c_7}$ and 8 red spins, $\tau^z_{\hat{c}_1}, ..., \tau^z_{\hat{c}_8}$ surrounding the cube c (see Fig. 4.5(b))

$$n_c = g(\{\tau^z_{c_i}\tau^z_{c_j}\}, \{\tau^z_{\hat{c}_i}\tau^z_{\hat{c}_j}\})$$

while

$$n_{\hat{c}} = g(\{\tau^z_{\hat{c}_i}\tau^z_{\hat{c}_j}\}, \{\tau^z_{c_i}\tau^z_{c_j}\}).$$

As above, the expression for g is complicated so we do not show it here.

4.2.4 Properties of models

The two spin models H_0 and H_1 have several interesting properties. First, the Hamiltonians H_0 and H_1 are invariant under the two Ising symmetry transformations

$$S_b = \prod_c \tau^x_c, \quad S_r = \prod_{\hat{c}} \tau^x_{\hat{c}}. \tag{4.10}$$

Thus these models have a $\mathbb{Z}_2 \times \mathbb{Z}_2$ symmetry.

Second, the $\mathbb{Z}_2 \times \mathbb{Z}_2$ symmetry is not broken spontaneously by either H_0 and H_1. One way to see this is to note that the ground states of these Hamiltonians are gapped and unique. For the case of H_0, this is obvious: the unique ground state of H_0 is clearly $|\Psi_0\rangle = |\tau^x_c = \tau^x_{\hat{c}} = 1\rangle$ and the energy gap is $\Delta = 1$. For the case of H_1, we have to do a bit more work to establish this fact. First we observe that the operators $\{B^1_c, B^1_{\hat{c}}\}$ commute with one another and have eigenvalues 0 and 1. [1] We then label the simultaneous eigenstates by $|b^1_c, b^1_{\hat{c}}\rangle$, where $b^1_c, b^1_{\hat{c}} = 0, 1$ denote the eigenvalues. These states are energy eigenstates of H_1 with energy

$$E = -\sum_c b^1_c - \sum_{\hat{c}} b^1_{\hat{c}}. \tag{4.11}$$

From this expression, we see that the ground state(s) of H_1 have $b^1_c = b^1_{\hat{c}} = 1$, while the excited states have at least one $b^1_c, b^1_{\hat{c}}$ equal to 0. Hence there is a finite energy gap $\Delta = 1$ separating the ground state(s) from the excited states. All that remains is to show that the ground state is *unique*. To prove this, we note that the degeneracy of the $b^1_c = b^1_{\hat{c}} = 1$ eigenspace is given by $\mathrm{Tr}(\prod_c B^1_c \prod_{\hat{c}} B^1_{\hat{c}})$. If we then substitute the expressions (4.5) into this trace, and we assume a 3D torus geometry so that the number of spins is equal to the number of B^1_c and $B^1_{\hat{c}}$ operators, it is easy to see that this trace is equal to 1 (see Appendix C.1). We conclude that the ground state $|\Psi_1\rangle = |b^1_c = b^1_{\hat{c}} = 1\rangle$ is both gapped and unique, which implies that H_1 does not break the $\mathbb{Z}_2 \times \mathbb{Z}_2$ symmetry spontaneously.

We can easily write down the ground state wave functions for H_0 and H_1. The ground state wave function for H_0 in the τ^z basis is simply

$$\Psi_0(\{\tau^z_c, \tau^z_{\hat{c}}\}) = 1 \tag{4.12}$$

---

[1] One quick way to see that $\{B^1_c, B^1_{\hat{c}}\}$ commute with one another is by mapping the operators to the membrane cubic operators in chapter 3 where the cubic operators are shown to commute with one another.

while the ground state wave function for H_1 is

$$\Psi_1(\{\tau^z_c, \tau^z_{\hat{c}}\}) = (-1)^{N_g}. \tag{4.13}$$

Here, to define N_g we consider the blue and red domain walls in the spin configuration $\{\tau^z_c, \tau^z_{\hat{c}}\}$. The quantity N_g is defined to be the total number of loops formed by intersections of red and blue domain walls. Notice that Ψ_1 is the same as the wave function constructed in Ref. [22] for the nontrivial $\mathbb{Z}_2 \times \mathbb{Z}_2$ SPT phase although they did not write down the Hamiltonian explicitly.

Another important property of H_0 and H_1 is that their ground states $|\Psi_0\rangle$ and $|\Psi_1\rangle$ are both short-range entangled — that is, they can be transformed into a product state by a local unitary transformation. For $|\Psi_0\rangle$, this is obvious, since it is already a product state. To see that $|\Psi_1\rangle$ is short-range entangled requires more work, and we refer the reader to Appendix C.2 for a derivation of this result.

Putting everything together, we have shown that H_0 and H_1 have gapped, short-range entangled ground states which are invariant under a $\mathbb{Z}_2 \times \mathbb{Z}_2$ symmetry. Thus, according to the definition, the spin models H_0 and H_1 belong to $\mathbb{Z}_2 \times \mathbb{Z}_2$ SPT phases. To further distinguish the two phases, we will gauge the symmetry, that is, couple the system to $\mathbb{Z}_2 \times \mathbb{Z}_2$ gauge fields and show the two models are characterized by distinct statistics of vortex loop excitations and thus belong two distinct phases in the following section.

4.3 Coupling the Ising models to $\mathbb{Z}_2 \times \mathbb{Z}_2$ gauge field

In this section, we promote the $\mathbb{Z}_2 \times \mathbb{Z}_2$ global symmetry in H_0 and H_1 to a local symmetry by coupling H_0 and H_1 to a $\mathbb{Z}_2 \times \mathbb{Z}_2$ gauge field. We see that the gauging procedure introduces a new kind of loop-like excitations which we call vortex loops to the original spin models H_0, H_1. In the later section, we will show that vortex loops in the two models have distinct braiding statistics and thus it implies that H_0 and H_1 describe different quantum phases.

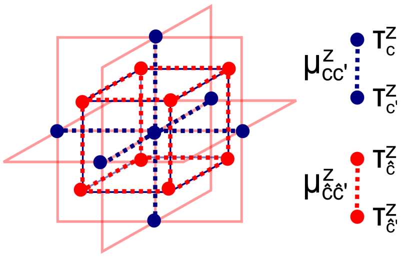

Figure 4.6: Coupling the spin models to a $\mathbb{Z}_2 \times \mathbb{Z}_2$ gauge field: $\mu^z_{\hat{c}\hat{c}'}$ lives on the links of the cubic lattice and $\mu^z_{cc'}$ lives on the links of the dual cubic lattice. The operator O_c defined in (4.15) contains a product of projectors to the zero flux state in 12 plaquettes in the dual lattice (the red plaquettes) and 6 plaquettes in the cubic lattice (the blue plaquettes).

Coupling the spins systems to a $\mathbb{Z}_2 \times \mathbb{Z}_2$ gauge field requires a few steps. First, we introduce two $\mathbb{Z}_2$ gauge fields $\mu^z_{cc'}$ and $\mu^z_{\hat{c}\hat{c}'}$, where $\mu^z_{\hat{c}\hat{c}'}$ lives on the links of the cubic lattice and $\mu^z_{cc'}$ lives on the links of the dual cubic lattice (see Fig. 4.6). Here $\mu^z_{cc'}$ is the gauge field corresponding to the symmetry S_b, while $\mu^z_{\hat{c}\hat{c}'}$ is the gauge field corresponding to the symmetry S_r. Second, we use the standard minimally coupling procedure to replace

$$\tau^z_c \tau^z_{c'} \to \tau^z_c \mu^z_{cc'} \tau^z_{c'}, \quad \tau^z_{\hat{c}} \tau^z_{\hat{c}'} \to \tau^z_{\hat{c}} \mu^z_{\hat{c}\hat{c}'} \tau^z_{\hat{c}'} \tag{4.14}$$

for each nearest neighbor spin interaction in the Hamiltonian. Further neighbor couplings can always be written as a product of nearest neighbor couplings, e.g.

$$\tau^z_c \tau^z_{c''} = (\tau^z_c \tau^z_{c'})(\tau^z_{c'} \tau^z_{c''}).$$

Next, in order to make the coupling to the gauge field unambiguous and ensure the gauged Hamiltonian is Hermitian, we multiply each term B^0_c or $\tilde{B}^1_c$ by the operator

$$\begin{aligned} O_c &= \prod_{\langle c c_1 c_2 c_3 \rangle} \frac{1 + \mu^z_{cc_1} \mu^z_{c_1 c_2} \mu^z_{c_2 c_3} \mu^z_{c_3 c}}{2} \\ &\cdot \prod_{\langle \hat{c}_1 \hat{c}_2 \hat{c}_3 \hat{c}_4 \rangle} \frac{1 + \mu^z_{\hat{c}_1 \hat{c}_2} \mu^z_{\hat{c}_2 \hat{c}_3} \mu^z_{\hat{c}_3 \hat{c}_4} \mu^z_{\hat{c}_4 \hat{c}_1}}{2} \end{aligned} \tag{4.15}$$

where the first product runs over the 12 plaquettes in the dual lattice that contain c, while the second term runs over the 6 plaquettes in the cubic lattice that make up the cube centered at c (see Fig. 4.6). Similarly, we multiply each term $B^0_{\hat{c}}$ or $\tilde{B}^1_{\hat{c}}$ by the operator

$$\begin{aligned} O_{\hat{c}} &= \prod_{\langle \hat{c}_1\hat{c}_2\hat{c}_3\hat{c}_4\rangle} \frac{1+\mu^z_{\hat{c}_1\hat{c}_2}\mu^z_{\hat{c}_2\hat{c}_3}\mu^z_{\hat{c}_3\hat{c}_4}\mu^z_{\hat{c}_4\hat{c}_1}}{2} \\ &\cdot \prod_{\langle c_1c_2c_3c_4\rangle} \frac{1+\mu^z_{\hat{c}_1c_2}\mu^z_{\hat{c}_2c_3}\mu^z_{\hat{c}_3c_4}\mu^z_{\hat{c}_4c_1}}{2} \end{aligned} \tag{4.16}$$

where the first product runs over the 12 plaquettes in the cubic lattice that contain $\hat{c}$, while the second term runs over the 6 plaquettes in the dual lattice that make up the cube centered at $\hat{c}$.

The last step is to add a gauge field energy term to the Hamiltonian of the form:

$$\begin{aligned} H_{gauge} &= -\sum_{\langle c_1c_2c_3c_4\rangle} \mu^z_{c_1c_2}\mu^z_{c_2c_3}\mu^z_{c_3c_4}\mu^z_{c_4c_1} \\ &- \sum_{\langle \hat{c}_1\hat{c}_2\hat{c}_3\hat{c}_4\rangle} \mu^z_{\hat{c}_1\hat{c}_2}\mu^z_{\hat{c}_2\hat{c}_3}\mu^z_{\hat{c}_3\hat{c}_4}\mu^z_{\hat{c}_4\hat{c}_1}. \end{aligned}$$

This term ensures that the state with vanishing $\mathbb{Z}_2 \times \mathbb{Z}_2$ flux everywhere has the lowest energy. Combining these terms, the gauged spin models are given by

$$\tilde{H}_0 = -\sum_c B^0_c O_c - \sum_{\hat{c}} B^0_{\hat{c}} O_{\hat{c}} + H_{gauge}, \tag{4.17}$$

$$\tilde{H}_1 = -\sum_c \tilde{B}^1_c O_c - \sum_{\hat{c}} \tilde{B}^1_{\hat{c}} O_{\hat{c}} + H_{gauge} \tag{4.18}$$

where

$$\begin{aligned} \tilde{B}^1_c &= \frac{1}{2}(1+\tau^x_c \cdot (-1)^{\tilde{m}_c} \cdot i^{\tilde{n}_c}), \\ \tilde{B}^1_{\hat{c}} &= \frac{1}{2}(1+\tau^x_{\hat{c}} \cdot (-1)^{\tilde{m}_{\hat{c}}} \cdot i^{\tilde{n}_{\hat{c}}}) \end{aligned}$$

and

$$\begin{aligned}
\tilde{m}_c &= f(\tau^z_{\hat{c}_i}\mu^z_{\hat{c}_i\hat{c}_j}\tau^z_{\hat{c}_j},\dots,\tau^z_{\hat{c}_k}\mu^z_{\hat{c}_k\hat{c}_l}\tau^z_{\hat{c}_l}),\\
\tilde{m}_{\hat{c}} &= f(\tau^z_{c_i}\mu^z_{c_ic_j}\tau^z_{c_j},\dots,\tau^z_{c_k}\mu^z_{c_kc_l}\tau^z_{c_l}),\\
\tilde{n}_c &= g(\{\tau^z_{c_i}\mu^z_{c_ic_j}\tau^z_{c_j}\},\{\tau^z_{\hat{c}_i}\mu^z_{\hat{c}_i\hat{c}_j}\tau^z_{\hat{c}_j}\}),\\
\tilde{n}_{\hat{c}} &= g(\{\tau^z_{\hat{c}_i}\mu^z_{\hat{c}_i\hat{c}_j}\tau^z_{\hat{c}_j}\},\{\tau^z_{c_i}\mu^z_{c_ic_j}\tau^z_{c_j}\}),
\end{aligned}$$

where the integer-valued functions f and g are defined in section 4.2.3.

The Hilbert space of the gauged spin models consists of gauge invariant states, i.e. all states which satisfy Gauss's law

$$\prod_{c'}\mu^x_{cc'} = \tau^x_c, \quad \prod_{\hat{c}'}\mu^x_{\hat{c}\hat{c}'} = \tau^x_{\hat{c}} \tag{4.19}$$

where the first product runs over the 6 nearest neighbors of c', and the second product runs over the 6 nearest neighbors of $\hat{c}'$. These constraints can be thought of as two $\mathbb{Z}_2$ analogs of Gauss' law: $\nabla \cdot E = 4\pi\rho$.

The gauged spin models have some interesting properties. First, the gauged spin models are exactly soluble because each term in $\tilde{H}_0, \tilde{H}_1$ commutes. Second, both models have energy gap. Third, there are two types of excitations. One is the particle-like excitation which we call "charges" and the other is a loop-like excitation which we call "vortex loops". The charge excitations come in two types corresponding to the blue and red spins. We denote these two types of charges by e_b, e_r respectively. The charge e_b at the site c corresponds to $B^0_c = 0$ in $\tilde{H}_0$ and $\tilde{B}^1_c = 0$ in $\tilde{H}_1$, while e_r at the site $\hat{c}$ corresponds to $B^0_{\hat{c}} = 0$ in $\tilde{H}_0$ and $\tilde{B}^1_{\hat{c}} = 0$ in $\tilde{H}_1$. Likewise, the vortex loops come in two types, corresponding to the blue and red gauge fields. We denote these two types of vortex loops by m_b, m_r respectively. The vortex m_b at the link l corresponds to $\prod_{p\in l}\mu^z_p = -1$ and m_r at the link $\hat{l}$ corresponds to $\prod_{\hat{p}\in\hat{l}}\mu^z_{\hat{p}} = -1$. Here the product in m_b runs over four links $p = cc'$ encircling the link l in the cubic lattice and the product in m_r runs over four links $\hat{p} = \hat{c}\hat{c}'$ encircling the link $\hat{l}$ in the dual cubic lattice. An important point is that these vortex excitations m_b, m_r always form closed loops. To see this, note that $\mu^z_p, \mu^z_{\hat{p}}$ obey the local constraints

$$\prod_{l \in s} \prod_{p \in l} \mu^z_p = 1, \quad \prod_{\hat{l} \in \hat{s}} \prod_{\hat{p} \in \hat{l}} \mu^z_{\hat{p}} = 1 \tag{4.20}$$

for every site s in the cubic lattice and $\hat{s}$ in the dual cubic lattice. In the first expression, the product runs over the 6 edges l adjacent to the site s and 4 links $p = cc'$ encircling l while in the second expression the product runs over the 6 edges $\hat{l}$ adjacent to the site $\hat{s}$ and 4 links $\hat{p} = \hat{c}\hat{c}'$ encircling $\hat{l}$. The constraints ensure that there are even number of line defects adjacent to each site $s, \hat{s}$ and thus the defects form closed loops.

In fact, there are four types of m_b vortex loops, which differ by the addition of the charges e_b, e_r : $\{m_b, m_b \cdot e_b, m_b \cdot e_r, m_b \cdot e_b \cdot e_r\}$. Similarly, there are also four types of m_r vortex loops obtained by attaching e_b and e_r.

In the Appendix C.3, we establish the mapping between the gauged spin models (4.17,4.18) and the membrane models (3.4,3.11) constructed in chapter 3. Since we have the exact mapping between the two sets of models, we will cite some results from chapter 3 without repeating the derivation and refer the readers to that chapter for details.

4.4 Excitations and the associated creation operators

In this section, we find the operators which create the charge and the vortex loop excitations in $\tilde{H}_0$ and $\tilde{H}_1$. These creation operators are closely related to the string and membrane operators constructed in chapter 3 by the mapping discussed in the Appendix C.3. These operators allow us to compute the braiding statistics of the associated particles and loop excitations. For readers who are curious about how we construct these operators, we refer them to chapter 3 for the detailed construction.

4.4.1 String and membrane operators for $\tilde{H}_0$

String operators

Let us start with constructing operators that create excitations for the $\tilde{H}_0$ model. We begin with the particle-like excitations: the charges e_b, e_r. These charges can be created by extended stringlike operators. If we apply these stringlike operators to the ground state, the result is an excited state with a pair of charges at two ends of the string. For the $\tilde{H}_0$ model, the creation operators of e_b, e_r are

$$W_b^0(P) = \tau^z_{c_1}\tau^z_{c_2}\prod_{p\perp P}\mu^z_p, \quad W_r^0(P) = \tau^z_{\hat{c}_1}\tau^z_{\hat{c}_2}\prod_{\hat{p}\perp P}\mu^z_{\hat{p}}. \tag{4.21}$$

Here P is a path on the dual cubic lattice which ends at the two cubes c_1, c_2 in the first expression, and a path in the cubic lattice which ends at the two cubes $\hat{c}_1, \hat{c}_2$ in the second expression. The product runs over the plaquettes p or $\hat{p}$ penetrated by the path P. We call these operators $W_b^0(P), W_r^0(P)$ the string operators.

We can verify that $W_b^0(P)$ creates two charges at the two endpoints c_1, c_2 of P by noting that $W_b^0(P)$ commutes with all terms in $\tilde{H}_0$ except for $\mathcal{B}^0_{c_1}$ and $\mathcal{B}^0_{c_2}$ which anticommute with $W_b^0(P)$. Also notice that this property does not depend on the choice of the path P, but only on the endpoints of P. This is a general feature of string operators. Hence, the state $W_b^0(P)|\Psi_0\rangle$ contains two blue charges e_b at two endpoints of P. A similar argument shows that $W_r^0(P)$ also creates two red charges e_r at the endpoints of P.

Membrane operators

Next, we want to construct the creation operators for the line-like excitations: the vortex loops m_b, m_r. The vortex loops can be created by an extended membranelike operator. If we apply these membranelike operators to the ground state, the result is an excited state with vortex loops at the boundary of the membrane. For the case of $\tilde{H}_0$, one can show that the following operators do the job

$$M_b^0(S) = \prod_{p \in S} \mu_p^x, \quad M_r^0(S) = \prod_{\hat{p} \in S} \mu_{\hat{p}}^x. \tag{4.22}$$

Here S is a surface made up of plaquettes p living in the cubic lattice in the first expression, and a surface made up of plaquettes $\hat{p}$ in the dual cubic lattice in the second expression. The products run over the plaquettes p or $\hat{p}$ on the surface S. We call these operators the membrane operators.

One can also check that when S is a cylindrical surface, $M_b^0(S)$ create blue vortex loops m_b at the two ends of S. To see this, we note that $M_b^0(S)$ commutes with all the terms in $\tilde{H}_0$ except for the flux terms $\prod_{p \in l} \mu_p^z$ with l at the boundary of S which anticommute with $M_b^0(S)$. Again, this property does not depend on the choice of region S, but only on the boundary of S. This is a general feature of membrane operators. Hence, the state $M_b^0(S)|\Psi_0\rangle$ contains two blue vortex loops m_b at two ends of S. A similar argument shows that $M_r^0(S)$ also creates two red vortex loops m_r at two ends of S.

As mentioned in the previous section, there are four types of m_b and four types of m_r vortex loops which differ by attaching e_b, e_r excitations. Let us label the four types of m_b by (b, q_b, q_r) and four types of m_r by (r, q_b, q_r) where q_b, q_r are the amount of attached e_b, e_r charges and take values in $0, 1$. In this labeling scheme, the operators M_b^0 and M_r^0 in (4.22) create the $(b, 0, 0)$ and $(r, 0, 0)$ excitations. To create (b, q_b, q_r) excitations, we can modify M_b^0 by multiplying $M_b^0(S)$ by the string operators $W_b^0(P)$ or $W_r^0(P')$ or $W_b^0(P) \cdot W_r^0(P')$ where the paths P, P' run along the length of the cylinder. Similarly, we can construct membrane operators which create (r, q_b, q_r) vortex loops by multiplying $M_r^0(S)$ by appropriate string operators.

4.4.2 String and membrane operators for $\tilde{H}_1$

In this section, we construct the string operators for $\tilde{H}_1$ model. The membrane operators for $\tilde{H}_1$ are more complicated and have been constructed explicitly in chapter 3. Thus we refer the readers to chapter 3 for details. Instead, we discuss the general structure and properties of the membrane operators for $\tilde{H}_1$ which is relevant for our purpose in the later section.

String operators

The string operators that create the blue and red charge excitations in the $\tilde{H}_1$ model are exactly the same as the string operators in the $\tilde{H}_0$ model:

$$W_b^1(P) = \tau_{c_1}^z \tau_{c_2}^z \prod_{p \perp P} \mu_p^z, \quad W_r^1(P) = \tau_{\hat{c}_1}^z \tau_{\hat{c}_2}^z \prod_{\hat{p} \perp P} \mu_{\hat{p}}^z. \tag{4.23}$$

Following the same analysis as above, one can see that $W_b^1(P), W_r^1(P)$ commutes with $\tilde{H}_1$ except for the two ends of P and thus create blue and red charges at two endpoints of P.

Membrane operators

The membrane operators for $\tilde{H}_1$ are more complicated and they are explicitly constructed in chapter 3. We will not repeat the construction here. Instead, we mainly discuss the general picture of the membrane operators for $\tilde{H}_1$.

Let S be a cylindrical surface made up of plaquettes p living in the cubic lattice. The membrane operator which creates blue vortex loops has the form

$$M_b^1(S) = \prod_{p \in S} \mu_p^x f_b(\{\tau_{c_i}^z \mu_{c_i c_j}^z \tau_{c_j}^z\}, \{\tau_{\hat{c}_i}^z \mu_{\hat{c}_i \hat{c}_j}^z \tau_{\hat{c}_j}^z\}) P_b. \tag{4.24}$$

Here the products run over the plaquettes p on the surface S. The factor f_b is some complex-valued function of spins and gauge variables on S. The function f_b is properly designed so that $M_b^1(S)$ only creates the blue vortex loops at the two boundaries and nothing else. The projector P_b acting on the boundary of S which specifies the boundary condition of the membrane operator.

In general, we can define different membrane operators for different projectors P_b. Specifically, we are interested in three types of membrane operators. The first type of operator is the membrane operator which creates a pair of unlinked blue loops. In this case, P_b projects to the states without any loop which links with the cylinder S. Thus it creates two unlinked blue loops at the ends of S when the operator is applied to such a state. Otherwise it annihilates the state. The second type of operator is the membrane operator which creates a pair of blue loops which link with a blue base loop. In this case, P_b projects to the excited states with a blue loop which links with the cylinder S. Thus when the operator is applied to such a state, it creates two blue loops at the ends of S which are linked with the original blue loop. On the other hand, when it is applied to states without a blue loop that links with S, it simply annihilates them. The third type of membrane operator which creates a pair of blue loops which link with a red base loop has a similar property.

Furthermore, for each type of membrane operators discussed above, we can construct four different membrane operators which create vortex loops carrying a certain amount of charges $q_b, q_r \in \{0,1\}$ by modifying the function f_b. These vortex loops differ from one another by the amount of charge that they carry and we label them by (b, q_b, q_r) where q_b, q_r take values in $0, 1$.

The cylindrical membrane operator which creates red vortex loops has a similar form but with the roles of “red” and “blue” reversed:

$$M_r^1(S) = \prod_{\hat{p} \in S} \mu^x_{\hat{p}} f_r(\{\tau^z_{\hat{c}_i} \mu^z_{\hat{c}_i \hat{c}_j} \tau^z_{\hat{c}_j}\}, \{\tau^z_{c_i} \mu^z_{c_i c_j} \tau^z_{c_j}\}) P_r. \tag{4.25}$$

Here S is a surface made up of plaquettes $\hat{p}$ in the dual cubic lattice. The products run over the plaquettes $\hat{p}$ on the surface S. The function f_r and the projector P_r are defined similarly as in the M_b^1 operator with the roles of red and blue reversed.

Like M_b^1, we can define three types of red membrane operators which create unlinked red loops, linked red loops with a blue base loop or a red base loop respectively corresponding to different projectors P_r. Furthermore, for each type of membrane operators, there are four different membrane operators that are parametrized by two integers $q_b, q_r \in \{0, 1\}$. These membrane operators create four different red vortex loops labeled by (r, q_b, q_r) which differ by the amount of charges attached to the flux loops.

Finally, we can also construct membrane operators with other topology such as toroidal and spherical operators. Roughly speaking, the toroidal operators can be obtained from the cylinder operators by connecting the two ends while spherical operators can be obtained from the cylinder operators by closing each of the two ends. Thus only a few modifications are needed to define the toroidal and spherical operators from the cylinder operators. We refer the readers to chapter 3 for details.

4.5 Braiding statistics of excitations

In this section, we discuss the braiding statistics of excitations in the gauged spin models $\tilde{H}_0, \tilde{H}_1$. The two gauged models contain two types of excitations: particle-like charge excitations and string-like vortex loop excitations. In both models the particle excitations are bosons and the particle and loop excitations have the same mutual braiding statistics. The two models can only be distinguished by recently proposed three-loop braiding statistics[85] in which one loop is braided around another while both are linked to a third loop. Thus the two models $\tilde{H}_0, \tilde{H}_1$ belong to distinct phases and accordingly the ungauged spin models H_0, H_1 describe different quantum phases.

Let us first show that the two models share the same exchange statistics of charges and the mutual braiding statistics of charges and flux loops. First, we see that the charge excitations are bosons

$$\theta_b = \theta_r = 0. \tag{4.26}$$

This follows from the fact that charges are the excitations of the original short-range entangled boson models H_0, H_1 and thus must be bosons. Second, by the definition of $\mathbb{Z}_2 \times \mathbb{Z}_2$ gauge theory, if we braid a charge e_α around a vortex loop m_β with $\alpha, \beta \in \{b, r\}$, the resulting statistical phase $\theta_{\alpha,\beta}$ is π if the charge and flux loop are of the same color and is 0 otherwise

$$\theta_{b,b} = \theta_{r,r} = \pi, \quad \theta_{b,r} = \theta_{r,b} = 0. \tag{4.27}$$

Finally, to analyze the braiding statistics of two unlinked loops, we use the following fact about the unlinked loops: any flux loop can be obtained from a subset of neutral loops by attaching a proper amount of charge. The neutral loops are the flux loops which can be shrunk to a point and annihilated by local gauge invariant operators. Thus, we can see that the braiding statistics of two neutral loops m_α, m_β is trivial $\theta_{\alpha\beta} = 0$ with $\alpha, \beta \in \{b, r\}$ since the braiding process can be smoothly deformed into another process in which α is braided around the vacuum. Furthermore, general flux loops m_α, m_β carrying charges can be thought of as neutral loops with some charges. The corresponding mutual statistics of m_α, m_β will be a sum of the braiding phase of two neutral loops and the braiding phase of the charge on one loop around the other loop. As a result, the statistical phase $\theta_{\alpha\beta}$ for braiding a flux loop $m_\alpha = (\alpha, q_b, q_r)$ around the other $m_\beta = (\beta, q_b', q_r')$ has the Aharonov-Bohm form

$$\begin{aligned} \theta_{bb} &= \pi(q_b + q_b'), \\ \theta_{rr} &= \pi(q_r + q_r'), \\ \theta_{rb} &= \pi(q_b + q_r'). \end{aligned} \tag{4.28}$$

The first term is the statistical phase associated with braiding the charge on the first flux loop around the flux of the second loop while the second term is the phase associated with braiding the flux of the first loop around the charge on the second loop. Thus we see that the particles and loop excitations in the two Hamiltonians $\tilde{H}_0, \tilde{H}_1$ share the same particle-loop and loop-loop mutual braiding statistics.

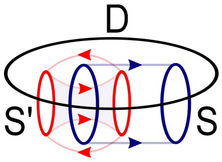

Figure 4.7: The statistical phase associated with a three-loop braiding process can be computed from the commutation algebra of two membrane operators, one acting along the cylinder S, and the other acting along the torus S'. Here both S and S' are linked with a base loop which lies along the boundary of the disk D.

All that remains is to examine the braiding statistics of linked loops. It has been proposed recently[85] that one important piece of data to distinguish 3D SPT phases is the three-loop braiding process. It is a process involving three loops, say $m_\alpha, m_\beta, m_\gamma$, in which m_α is braided around m_β both of which are linked with m_γ. To obtain the statistical phases, we use the fact that the statistical phases associated with different braiding processes of excitations are encoded in the commutation algebra of the corresponding string and membrane operators which create these excitations. Thus the statistical phases $\theta_{\alpha\beta,\gamma}$ associated with three-loop braiding can be read off from

$$M_\beta(S')M_\alpha(S)|\Psi_{ex}\rangle = e^{i\theta_{\alpha\beta,\gamma}} M_\alpha(S)M_\beta(S')|\Psi_{ex}\rangle \tag{4.29}$$

where S is a cylinder, S' is a torus, and $|\Psi_{ex}\rangle$ is an excited state

$$|\Psi_{ex}\rangle = M_\gamma(D)|\Psi_0\rangle \tag{4.30}$$

which contains a flux loop m_γ at the boundary of a disk D that links with both S and S' (Fig. 4.7).

The three-loop statistical phases has been computed in chapter 3 by plugging the explicit form of membrane operators into (4.29,4.30). Thus we only cite the results and refer the reader to chapter 3 for details. For the Hamiltonian $\tilde{H}_0$, the three-loop braiding statistics is the same as two-loop braiding statistics since the commutation algebra of two membrane operators is independent of which states they act. Thus for the $\tilde{H}_0$ model, we have the three-loop braiding statistical phases $\theta_{\alpha\beta,\gamma}$ for $m_\alpha = (\alpha, q_b, q_r), m_\beta = (\beta, q_b', q_r'), m_\gamma = (\gamma, q_b'', q_r'')$ with $\alpha, \beta, \gamma \in \{r, b\}$:

$$\begin{aligned}
\theta^0_{bb,r} &= \theta^0_{bb,b} = \pi(q_b + q_b'), \\
\theta^0_{rr,r} &= \theta^0_{rr,b} = \pi(q_r + q_r'), \\
\theta^0_{rb,r} &= \theta^0_{rb,b} = \pi(q_b + q_r').
\end{aligned} \tag{4.31}$$

Note that the three-loop braiding phases are independent of the amount of charges on the base loop m_γ. On the other hand, for the Hamiltonian $\tilde{H}_1$, the three-loop braiding phases are

$$\begin{aligned}
\theta^1_{bb,r} &= \pi + \pi(q_b + q_b'), & \theta^1_{bb,b} &= \pi(q_b + q_b'), \\
\theta^1_{rr,r} &= \pi(q_r + q_r'), & \theta^1_{rr,b} &= \pi + \pi(q_r + q_r'), \\
\theta^1_{rb,r} &= -\frac{\pi}{2} + \pi(q_b + q_r'), & \theta^1_{rb,b} &= -\frac{\pi}{2} + \pi(q_b + q_r').
\end{aligned} \tag{4.32}$$

Now, it is apparent that the flux loops in $\tilde{H}_0, \tilde{H}_1$ are characterized by distinct three-loop braiding statistics. It then follows that the gauged spin models $\tilde{H}_0, \tilde{H}_1$ are physical distinct in the sense that they can not be continuously connected to one another without breaking the $\mathbb{Z}_2 \times \mathbb{Z}_2$ symmetry or closing the gap.

4.5.1 Implication of three-loop braiding statistics

We now argue that the H_0, H_1 models belong to *distinct* SPT phases: in other words, H_0 and H_1 cannot be continuously connected with one another by varying some parameter in the Hamiltonian without closing the gap or breaking the $\mathbb{Z}_2 \times \mathbb{Z}_2$ symmetry. Our argument is based on the relationship between the spin models H_0, H_1 and the gauged spin models $\tilde{H}_0, \tilde{H}_1$. One important property of our gauging procedure is that it maps a gapped spin model to the other gapped gauged spin model. With this property, it is easy to see that H_0 and H_1 belong to distinct SPT phases. Indeed, if H_0 and H_1 could be continuously connected by some interpolating Hamiltonian H_s, $0 \leq s \leq 1$, then by coupling H_s to a $\mathbb{Z}_2 \times \mathbb{Z}_2$ lattice gauge field, we could construct an interpolation between the gauged models $\tilde{H}_0$ and $\tilde{H}_1$. Importantly, this interpolation is guaranteed to be gapped as long as H_s is gapped since our gauging prescription maps gapped spin models to gapped gauge theories (in fact, the low energy spectrum of the gauge theory is identical to that of the spin model). But we know that a gapped interpolation between $\tilde{H}_0$ and $\tilde{H}_1$ is not possible since they have different three-loop statistics (discrete invariants). Hence, we conclude that a gapped, symmetric interpolation between H_0 and H_1 is also impossible: these Hamiltonians must belong to distinct SPT phases. Clearly H_0 belongs to a trivial SPT phase, so H_1 must belong to a nontrivial SPT phase.

4.6 Protected surface modes and the three-loop braiding statistics

In this section, we sketch an argument showing that H_1 has gapless surface modes which are protected in a certain sense that will be explained below. This result provides an important physical distinction between the two models, since it is clear that H_0 does not have protected surface modes.

We now explain the precise statement that we will prove. Let us consider the spin model H_1, defined in the upper half space $z \geq 0$ with a Hamiltonian of the form

$$H = H_{bulk} + H_{surf}, \quad H_{bulk} = -\sum_c B_c^1 - \sum_{\hat{c}} B_{\hat{c}}^1 \tag{4.33}$$

where $B_c^1, B_{\hat{c}}^1$ are defined as in (4.5) and where the surface Hamiltonian H_{surf} can be any $\mathbb{Z}_2 \times \mathbb{Z}_2$ symmetric Hamiltonian with local interactions which has support near the $z = 0$ boundary. Let $|\Psi\rangle$ be the ground state of H (or one of the ground states of H, if there is a ground state degeneracy). What we will show is that $|\Psi\rangle$ cannot be both $\mathbb{Z}_2 \times \mathbb{Z}_2$ symmetric and short-range entangled. Here by a "short-range entangled" state, we mean a state that can be transformed into a product state by a local unitary transformation.

To understand the intuitive meaning of this result, note that $|\Psi\rangle$ is always symmetric and short-range entangled in the *bulk*. Hence, the above result implies that the surface always either breaks the $\mathbb{Z}_2 \times \mathbb{Z}_2$ symmetry or is a long-range entangled state. In the latter case, we expect that the surface is either gapless or a (gapped) topological ordered state. Thus, this result suggests that the surface is guaranteed to host gapless modes as long as (1) the $\mathbb{Z}_2 \times \mathbb{Z}_2$ symmetry is not broken (explicitly or spontaneously) and (2) the surface is not topologically ordered. In this sense, our argument suggests that the surface states are protected.

Our argument is a proof by contradiction: we assume that the ground state $|\Psi\rangle$ of H is $\mathbb{Z}_2 \times \mathbb{Z}_2$ symmetric and short-range entangled and we show that these assumptions lead to a logical inconsistency. The key idea is to imagine coupling H to a $\mathbb{Z}_2 \times \mathbb{Z}_2$ lattice gauge field. We will then show that the bulk and surface properties of the resulting gauged spin model — which we denote by $\tilde{H}$ — are not consistent with one another.

Bulk and surface properties of $\tilde{H}$

We first discuss the bulk and surface properties of $\tilde{H}$; afterwards we will explain why they are inconsistent. We begin with the bulk. As discussed in section 4.3, we know that $\tilde{H}$ supports two types of bulk excitations: vortex loops and charges. We also know that the vortex loop excitations obey the three-loop statistics defined in equation (4.32).

Now let us consider the surface. An important property of the *ungauged* model H is that its surface does not spontaneously break the $\mathbb{Z}_2 \times \mathbb{Z}_2$ symmetry. This property follows from our assumption that the ground state $|\Psi\rangle$ of the ungauged model is $\mathbb{Z}_2 \times \mathbb{Z}_2$ symmetric and short-range entangled: in general, short-range entangled states always obey $\lim_{|x-y|\to\infty} \langle O(x)O(y)\rangle - \langle O(x)\rangle\langle O(y)\rangle = 0$ for any local operator O and therefore these states can never spontaneously break a symmetry.

The lack of spontaneous symmetry breaking in the ungauged model H has an important implication for the gauged model $\tilde{H}$: it means that vortex lines can be *annihilated* at the surface of $\tilde{H}$. That is, if we bring a segment of a vortex loop near the $z = 0$ surface, then it is possible to absorb this segment into the surface and annihilate it by applying a suitable local gauge invariant operator. One way to see this is to note that when we move a vortex line to the surface, we effectively create a domain wall along the vortex line. As long as the ungauged model does not spontaneously break the $\mathbb{Z}_2 \times \mathbb{Z}_2$ symmetry, this domain wall is a local object and hence can be annihilated locally.

Another property of the surface is that, like the bulk, it does not support any topologically nontrivial particle-like excitations other than the charge excitations. In other words, every particle-like excitation near the surface can be transformed into either a charge excitation or the vacuum (i.e. trivial excitation) by a local operator. This property follows from our assumption that the ground state $|\Psi\rangle$ of the ungauged model is short-range entangled: in general, whenever one gauges the symmetry of a 3D short-range entangled state, the only nontrivial particle-like excitations in the resulting gauge theory are charges. To see this, note that in an *ungauged* short-range entangled state, every particle-like excitation is trivial — that is, every particle-like excitation can be created and annihilated by local operators. If one gauges the symmetry of such a system, some of these excitations remain trivial, namely those that can be created and annihilated by operators that are invariant under the symmetry. The other excitations, which are created and annihilated by local operators that transform nontrivially under the symmetry, correspond to charges.

Deriving a contradiction

We now show that the above bulk and surface properties are not consistent with one another. The argument has two parts. In the first part, we show that the bulk three loop statistical phase is equivalent to the phase associated with braiding two vortex "arches" around one another on the surface. In the second part, we show that the phase for the latter process

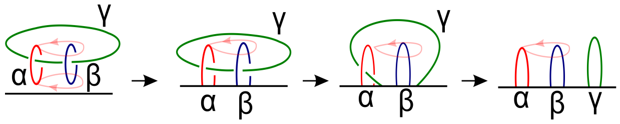

Figure 4.8: A sequence to show that three-loop braiding is equivalent to two-arch braiding.

must be either 0 or π. This leads us to a contradiction, since we know $\tilde{H}$ supports three-loop statistics different from 0 or π.

To begin, we imagine performing a three-loop braiding process in the bulk. That is, we imagine braiding a vortex loop α around another loop β, while both are linked the base loop γ (see Fig. 4.8). For concreteness, we suppose that γ lies in the xy plane while α and β lie in the yz plane. For now, α, β, γ may be vortex loops of any type (red, blue, etc.) — later we will specialize to particular cases.

Next, we imagine stretching the bottom of α and β so that they nearly touch the $z = 0$ surface. This stretching should not affect the statistical phase associated with the braiding process. More generally we expect that the statistical phase is invariant under any "smooth" deformation of the braiding process. Here, a "smooth" deformation is any sequence of small, local changes to the braiding trajectories of the loops with the property that the worldsheets swept out by the loops α and β stay far apart from one another at all times during the deformation.

We then merge the bottom of α and β into the surface, changing α and β to vortex *lines* that terminate at the surface. The resulting vortex lines have an arch-like structure so we will refer to them as "vortex arches" below. The deformed process now involves braiding the two vortex arches α, β around one another, while they are both linked to the loop γ. Again, the statistical phase should remain the same as in the original braiding process. Note that this step in the argument depends on the fact that vortex lines can be absorbed into the surface — one of the surface properties discussed above.

We now slide down the loop γ and merge a small segment of it into the surface, changing γ into a vortex line. We then unwind the γ vortex line so that it is no longer linked with α

and β. The process now involves braiding two *unlinked* arches around one another.

So far we have shown that the statistical phase associated with the three-loop braiding process is equivalent to the phase associated with braiding two arches α and β. We next argue that the latter phase must be either 0 or π. To do this, we use the second basic property of the surface — namely, that it does not support any topologically nontrivial particle-like excitations other than the charge excitations. Given this property, we know that if we shrink down either of the vortex arches α or β so that they are localized near a point, the resulting particle-like excitation is equivalent, up to a local operation, to either the vacuum excitation or a charge excitation. In the first case, we will say that the vortex arch is "neutral" and in the second case we will say that it carries charge. First suppose that α and β are both neutral. In this case, it is easy to see that the statistical phase associated with braiding α and β must vanish since the braiding process can be deformed into one in which α is braided around the vacuum (see Fig. 4.9). Now consider the more general case where α and β carry charge. In this case, we can think of α and β as neutral arches with some attached charge. The statistical phase is then a sum of two pieces, one associated with braiding the charge on α around the vortex arch β, and the other associated with braiding the charge on β around the vortex arch α. Now, we already computed all the different charge-vortex statistical phases in section 3.4, and we found that they were always either 0 or π depending on what type of charge and vortex were being braided. We conclude that the statistical phase associated with braiding α around β is always either 0 or π since it is a sum of two terms, each of which is either 0 or π.

Putting this all together, we conclude that the statistical phase associated with the original three loop braiding process must be either 0 or π. We now arrive at a contradiction, since our calculation of the three loop statistics shows that this statistical phase can be different from 0 or π. For example, if α is a red vortex loop, β is a blue vortex loop, and γ is a red vortex loop then the three-loop statistical phase is $\pm\pi/2$. This contradiction implies that our assumption must be false: that is, the ground state $|\Psi\rangle$ cannot be both short-range

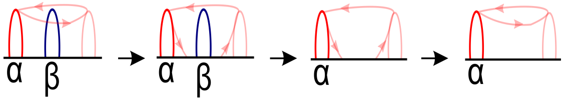

Figure 4.9: A sequence to show that two-arch braiding is trivial.

entangled and $\mathbb{Z}_2 \times \mathbb{Z}_2$ symmetric.

What can't we make the same argument for the other spin model H_0? The reason is that in that case, if we gauge the spin model, the three-loop statistical phase is always 0 or π for any vortex loops α, β, γ. As a result, there is no contradiction between bulk and surface properties of the gauged spin model and the argument breaks down. This is reassuring, of course, since H_0 doesn't have protected surface modes.

Comparing these two cases, we can see that the three-loop statistics plays a key role in our argument: as long as the bulk three-loop statistics are sufficiently nontrivial, we can deduce the existence of protected surface modes. A generalization of this argument to other SPT phases with unitary abelian symmetry groups will be presented elsewhere.

4.7 Conclusion

In this work, we addressed the question: what is the bulk-boundary correspondence in 3D SPT phases? We showed that the bulk-boundary correspondence in 3D SPT phases is the statement that nontrivial three-loop braiding statistics of vortex loop excitations in the bulk leads to the protected surface states in 3D SPT phases which can either be gapless, symmetry-breaking or carry topological order. We demonstrated this correspondence by constructing two exactly soluble 3D spin models H_0, H_1 which realize two distinct SPT phases with $\mathbb{Z}_2 \times \mathbb{Z}_2$ symmetry. Specifically, H_1 is characterized by nontrivial three-loop braiding of vortex loop excitations in the bulk while H_0 is not. We showed that H_1 has protected surface states by using the fact that the vortex loop excitations in the bulk have nontrivial three-loop braiding statistics. One the other hand, H_0 does not support protected surface states due to the trivial three-loop braiding statistics in the bulk. Although we prove the result for a particular 3D exactly soluble lattice model, the arguments apply more generally.

In this chapter, we only showed that the surface of nontrivial SPT phases can support topological order while we have not specified what possible surface topological orders are for a given SPT phase. One may expect that there is a connection between nontrivial three-loop braiding statistics in bulk of a gauged SPT phase and its compatible surface topological order. Indeed, the three-loop braiding statistics put a certain set of constraints on the possible surface topological order. The results will appear in a separate publication.

It is also interesting to construct exactly soluble surface Hamiltonians which realize certain topological order. The models would be helpful to understand the interplay between symmetry and topological order on the surface of 3D SPT phases.

CHAPTER 5

CONCLUSION

5.1 Summary of results

In this thesis, we investigated the universal properties of topological phases and SPT phase in 2D and 3D by explicitly constructing and analyzing the exactly soluble models which realize these phases.

In Chapter 2, we asked which topological phases can and cannot be realized by exactly soluble string-net models. We answered this question for the simplest class of topological phases, namely those with abelian braiding statistics. Specifically, we found that an abelian topological phase can be realized by a string-net model if and only if it supports a gapped edge. We established these results by systematically constructing all possible abelian string-net models and analyzing the quasiparticle braiding statistics in each model. An additional feature of this work is that the models we constructed are more general than the original string-net models, due to several new ingredients. As a result, we can realize topological phases that were not accessible to the original construction, including phases that break time-reversal and parity symmetry.

In Chapter 3, we constructed two exactly soluble lattice spin models that demonstrate the importance of three-loop braiding statistics for the classification of 3D gapped quantum phases. The two models are superficially similar: both are gapped and both support particle-like and loop-like excitations similar to that of charges and vortex lines in a $\mathbb{Z}_2 \times \mathbb{Z}_2$ gauge theory. Furthermore, in both models the particle excitations are bosons, and in both models the particle and loop excitations have the same mutual braiding statistics. The difference between the two models is only apparent when one considers the recently proposed three-loop braiding process in which one loop is braided around another while both are linked to a third loop. We found that the statistical phase associated with this process is different in the two models, thus proving that they belong to two distinct phases.

In Chapter 4, we constructed two spin models with $\mathbb{Z}_2 \times \mathbb{Z}_2$ global symmetry in three dimensions. We showed that one of these spin models realizes a nontrivial $\mathbb{Z}_2 \times \mathbb{Z}_2$ symmetry protected phase while the other model realizes a trivial phase. We also showed that the surface state of the nontrivial SPT phase is either gapless, symmetry-breaking or carries topological order. We established these results in two steps. First we coupled the two models to the $\mathbb{Z}_2 \times \mathbb{Z}_2$ gauge field and showed that they are characterized by distinct three-loop braiding statistics. Next we showed that the nontrivial three-loop braiding statistics directly leads to the existence of gapless or degenerate surface states. We believe that the connection between the nontrivial vortex loop braiding statistics in the bulk and the protected surface states can be extended to general three dimensional symmetry protected phases with any unitary symmetry.

5.2 Future directions

One future direction would be to develop the most general possible formulation of string-net models for the non-abelian topological phases. In chapter 2, our construction of abelian string-net models is more general than the original construction of Ref. [65], due to two new ingredients, γ, α, which are related to the $\mathbb{Z}_2$ and $\mathbb{Z}_3$ Frobenius-Schur indicators respectively. It would interesting to understand how to incorporate γ, α into the construction of general (non-abelian) string-net models. These models could help in understanding the topological properties of general topological phases and their edge properties.

Another direction would be to construct exactly soluble lattice models that can realized more general types of 3D gapped phases. For example, since the two models H_0, H_1 in chapter 3 are built out of two species of intersecting membranes, it may be possible to build more general models by considering more species of membranes or by allowing membranes to branch–in analogy with the string-net models of Ref. [65]. Given our suspicion that H_0, H_1 belong to the same phase as $\mathbb{Z}_2 \times \mathbb{Z}_2$ Dijkgraaf-Witten models, a key question is whether such a construction can realize any phases that cannot be realized by previously known exactly soluble models, such as the 3D Dijkgraaf-Witten models or 3D string-net models.

Also, it would be interesting to construct an exactly soluble surface Hamiltonian which is invariant under certain anomalous symmetry and realizes surface topological order. This model would be very helpful to understand the interplay between the symmetry and topological order on the surface of 3D SPT phases.

In addition to constructing models, there are many interesting questions associated with topological phases and SPT phases to be further investigated. To mention just a few, how do we generalize the string-net picture to realize chiral topological phases? The string-net picture is known to work only for the nonchiral phases. A related picture for the chiral phases would be very useful for understanding quantum Hall liquids. Also what is the connection between string-net models and the slave particle approach which is another way to construct 2D topological phases? In the slave particle approach, the spin operator is represented as a fermion or boson bilinear and the spin Hamiltonian is mapped to a fermion or boson Hamiltonian where fermions or bosons are coupled by a gauge field. These two approach must be connected but the precise relation is still unclear. In addition, how do we generalize three-loop braiding statistics to 3D nonabelian topological phases? At this moment, the three-loop braiding statistics works for classifying 3D abelian topological phases. To proceed to 3D nonabelian cases, it would be important to understand the three-loop braiding in the nonabelian topological phases. The answer to this question would be helpful for classifying 3D topological phases and generalizing the bulk-boundary correspondence to SPT phases with nonabelian symmetries. Finally, what is the low energy effective theory for 3D topological phases? The low energy effective theory for 2D topological phases is known as Chern-Simons theory. It is unclear what the effective theory for the 3D topological phases which can capture nontrivial three-loop braiding statistics.

Throughout the thesis, we attempt to understand a small part of the topological phases and SPT phases by the exactly soluble model approach. There are still many more mysteries left to answer and new exotic phases of matter to be explored.

APPENDIX A

APPENDICES FOR CHAPTER 2

A.1 Motivation for γ and α

In this section, we explain the motivation for introducing γ and α. Our explanation is based on the string-net formulation of lattice gauge theory[49, 8, 65] or equivalently, quantum double models[13], so we first briefly review how this string-net formulation works. Consider a quantum double model[46] associated with some finite group G (in this discussion G can be *any* finite group and need not be abelian). The string-net description of this model goes as follows: the string types are labeled by irreducible representations μ of G, and the null string is labeled by the trivial representation $\mathbf{1}$. The dual string type of μ is defined to be the dual representation $\bar{\mu}$, and the branching rules allow $\{\mu_1, \mu_2, \mu_3\}$ to meet at a vertex if and only if the tensor product $\mu_1 \otimes \mu_2 \otimes \mu_3$ contains the trivial representation $\mathbf{1}$. If the trivial representation appears more than once in this tensor product, i.e. $\mu_1 \otimes \mu_2 \otimes \mu_3 = n \cdot \mathbf{1} + ...$ then the vertex carries an additional label ν that runs over n values.

Our motivation for introducing α, γ can be seen by considering the ground state wave function Φ in these models. This wave function can be written down explicitly once we fix some conventions. In particular, for every allowed branching μ_1, μ_2, μ_3 with vertex label ν, we fix a corresponding three index tensor $T_{m_1 m_3 m_3}$ that belongs to the invariant subspace within $\mu_1 \otimes \mu_2 \otimes \mu_3$ — i.e. the subspace corresponding to the identity representation $\mathbf{1}$. Here, m_i is an index which transforms under G according to the representation μ_i. Also, m_i is an upper or lower index depending on whether the corresponding string points outward or inward.

Once we fix these invariant tensors, the wave function Φ can be computed as follows. Consider some string-net configuration X. To calculate the amplitude $\Phi(X)$, we assign tensors T to every vertex in X following the above prescription. We then contract all the indices $m_1, m_2, ...$ of these tensors along the adjoining strings (every string will have one lower index and one upper index). The complex number that results from this tensor contraction gives $\Phi(X)$.

We now carefully examine the above formula for Φ and we show that we need to introduce α and γ to make everything work out. We begin with α. The need for α appears when we consider vertices that are attached to three outgoing (or incoming) strings, each of which are labeled by the same representation μ. In this case, the associated invariant tensor T has 3 lower indices m_1, m_2, m_3 that transform under the same representation μ. The problem occurs if the tensor T is not cyclically symmetric, i.e. $T_{m_1 m_2 m_3} \neq T_{m_3 m_1 m_2}$. In this case, there is an ambiguity in our prescription for calculating $\Phi(X)$, since we don't know which index m_i should be assigned to which string. To resolve this ambiguity, we introduce a "dot" at each vertex. We then assign m_1 to the string that is adjacent to the dot in the clockwise direction, and then assign m_2 and m_3 to the remaining strings, ordered in the clockwise direction. With this convention, the value of $\Phi(X)$ depends on the position of the dot. To see how this dependence comes about, note that if we cyclically symmetrize our tensors, we can assume without loss of generality that $T_{m_1 m_2 m_3} = T_{m_3 m_1 m_2} \cdot \alpha(\mu)$ where $\alpha(\mu) = 1, \omega, \omega^2$ is a third root of unity. If we then move the dot in the clockwise direction, we have $\Phi(X) \to \Phi(X) \cdot \alpha(\mu)$ similarly to Eqs. (2.14 - 2.15).

The motivation for γ is similar. Consider a vertex that adjoins one null string and two outgoing (incoming) strings labeled with the same representation μ. Since the identity representation is one dimensional, thus we can write T as $T_{m_1 m_2}$. If T is not symmetric, i.e. $T_{m_1 m_2} \neq T_{m_2 m_1}$, then we again have an ambiguity in our prescription for calculating $\Phi(X)$. To resolve this ambiguity, we use the position of the null string to break the symmetry: we adopt the convention that m_1 is assigned to the string that is in the clockwise direction from the null string, and m_2 is assigned to the other string. In this way, the null string serves the same function as the dot. Now, by symmetrizing our tensors appropriately, we can assume without loss of generality that T is either symmetric or antisymmetric: $T_{m_1 m_2} = T_{m_2 m_1} \cdot \gamma(\mu)$ where $\gamma(\mu) = \pm 1$. If we then flip the position of the null string then $\Phi(X) \to \Phi(X) \cdot \gamma(\mu)$

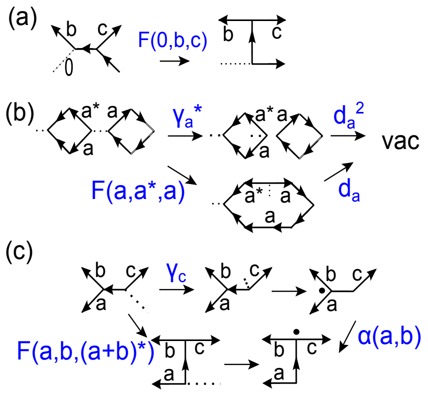

Figure A.1: Derivation of self-consistency conditions. Self-consistency in sequences (a),(b) and (c) requires the conditions (A.1b),(A.1d) and (A.1e), respectively.

similarly to Eqs. (2.8 - 2.9). With this picture, we can also motivate the rules (2.10 - 2.13): these rules correspond to conventions for how to raise and lower indices of our tensors $T_{m_1 m_2 m_3}$.

The reader may notice that the α, γ formalism in this chapter differs slightly from what we have motivated above: in this chapter, we include α factors for *all* vertices with three outgoing or incoming strings, even if they have different labels. Likewise, we include γ factors for all vertices with one null string and two incoming or outgoing strings, independent of their labels. While this observation is correct, we only use α, γ in these more general situations because it simplifies our notation: it is always possible to gauge away the α and γ factors in these cases, as discussed in section 2.4.5.

To summarize, we have shown that the α and γ factors naturally appear in the string-net formulation of quantum double models. It is this observation that motivates us to include α, γ in our construction.

A.2 Derivation of self-consistency conditions

In this section, we show that the local rules (2.2 - 2.4) and the conventions (2.6 - 2.15) are self-consistent if and only if the parameters $\{F(a,b,c), d_a, \gamma_a, \alpha(a,b)\}$ satisfy the following conditions

$$F(a+b,c,d)F(a,b,c+d) = \tag{A.1a}$$

$$F(a,b,c)F(a,b+c,d)F(b,c,d),$$

$$F(a,b,c) = 1 \text{ if } a \text{ or } b \text{ or } c = 0, \tag{A.1b}$$

$$d_a d_b = d_{a+b}, \tag{A.1c}$$

$$\gamma_a = F(a^*, a, a^*) d_a, \tag{A.1d}$$

$$\alpha(a,b) = F(a,b,(a+b)^*)\gamma_{a+b}. \tag{A.1e}$$

First, we show that the above conditions are *necessary* for self-consistency. The first condition (A.1a) was derived previously in the text (see section 2.4.4). The second condition (A.1b) can be understood by considering the rule (2.4) for the special case where $a = 0$, the null string. As shown in Fig. A.1(a), equation (A.1b) must be satisfied in order for the rule (2.4) to be consistent with the topological invariance rule (2.2) and the rule for erasing null strings (2.7). Similarly, the conditions (A.1d) and (A.1e) follow from considering the string-net configurations shown in Fig. A.1(b), and Fig. A.1(c) and demanding consistency between the two sequences of moves shown there. To derive (A.1c), we note that

$$\alpha(a,b)\alpha(b,c)\alpha(c,a) = 1 \text{ if } a+b+c = 0 \tag{A.2}$$

as can be shown by considering a sequence of three α moves as in Fig. A.2. It then follows from (A.1e) that

$$1 = \alpha_{ab}\alpha_{bc}\alpha_{ca} = \frac{F_{abc}F_{bca}F_{cab}}{F_{aa^*a}F_{bb^*b}F_{cc^*c}}\frac{1}{d_a d_b d_c}. \tag{A.3}$$

Here we use the abbreviation $F_{abc} = F(a,b,c)$ and $\alpha_{ab} = \alpha(a,b)$. To proceed further, we note that (A.1a) implies the identity

$$\frac{F_{abc}F_{bca}F_{cab}}{F_{aa^*a}F_{bb^*b}F_{cc^*c}} = 1. \tag{A.4}$$

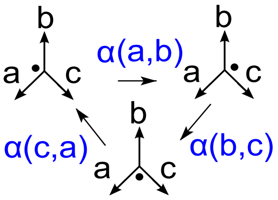

Figure A.2: A sequence of three α moves will return to the original configuration. Thus self-consistency requires $\alpha(a,b)\alpha(b,c)\alpha(b,a) = 1$ with $a+b+c=0$ as shown in (A.2).

Substituting (A.4) into (A.3), we derive (A.1c).

The above arguments show that Eqs. (A.1) are *necessary* conditions for the rules to be self-consistent. To prove that they are *sufficient*, suppose that $\{F(a,b,c), d_a, \gamma_a, \alpha(a,b)\}$ obey Eqs. (A.1). Then, using $\{F, d, \gamma, \alpha\}$, we can construct an exactly soluble lattice Hamiltonian H (2.27). The Hamiltonian H has a number of interesting properties, which are discussed in section 2.5.2 and proven in the appendices. Here we concentrate on one of these properties, namely the fact that the ground state of H satisfies the local rules (2.2 - 2.4) on the lattice:

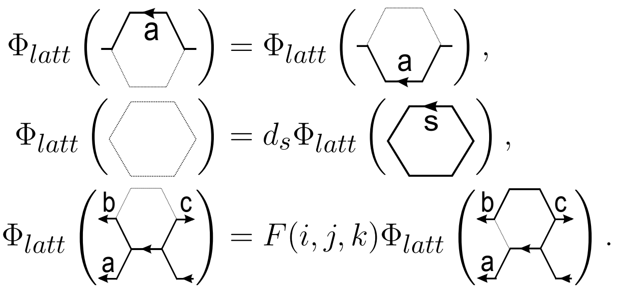

Given this fact, it is now easy to prove that the rules are self-consistent: suppose to the contrary that the rules (2.2 - 2.4) are not self-consistent. Then there exists two sequences of "moves" which relate the same initial and final (continuum) string-net states X_1, X_2, but with different proportionality constants: i.e. $\Phi(X_1) = c\Phi(X_2)$ and $\Phi(X_1) = c'\Phi(X_2)$ with $c \neq c'$. Clearly, these two sequences of moves can be adapted from the continuum to the honeycomb lattice if we make the lattice sufficiently fine. But this leads us to an immediate contradiction since the ground state Φ_{latt} of H gives an explicit example of a wave function that obeys the rules on the lattice. We conclude that our assumption is false: the rules must be self-consistent.

A.3 Local unitary transformations and gauge equivalence

In this section, we study the two gauge transformations f, g (2.20,2.21) which act on the parameters $\{F, d, \gamma, \alpha\}$. We show that both f and g can be implemented by a local unitary transformation.U[18] More precisely, we show that, for both f and g, the lattice Hamiltonians and ground state wave functions corresponding to $\{F, d, \gamma, \alpha\}$ and $\{\tilde{F}, d, \tilde{\alpha}, \tilde{\gamma}\}$ are related to one another by

$$\tilde{H} = UHU^{\dagger}, \quad |\tilde{\Phi}\rangle = U|\Phi\rangle.$$

We begin with the f-transformation. In this case, the local unitary transformation U that connects the wave functions Φ and $\tilde{\Phi}$ is defined by:

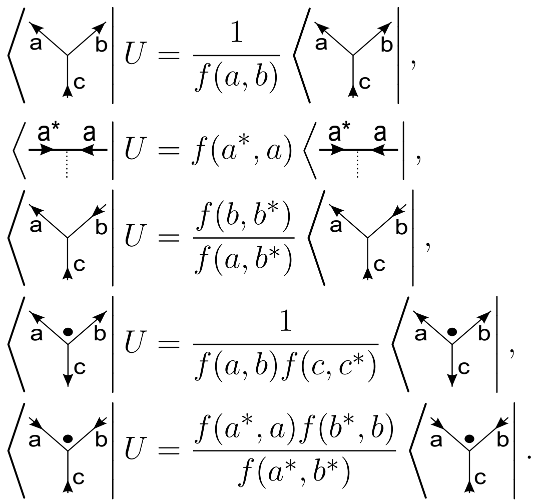

Here, by this notation, we mean that U multiplies each string-net basis state by the above phase factors for each vertex of the above form.

It is not hard to check that U transforms Φ to $\tilde{\Phi}$. Indeed, if we substitute the above transformation into the local rules (2.2 - 2.4) and (2.6 - 2.15), we can see that if $|\Phi\rangle$ obeys the local rules corresponding to $\{F, d, \gamma, \alpha\}$, then $U|\Phi\rangle$ obeys the local rules corresponding to

$\{\tilde{F}, \tilde{d}, \tilde{\gamma}, \tilde{\alpha}\}$. Therefore, since the local rules determine the wave function uniquely, we must have $U|\Phi\rangle = |\tilde{\Phi}\rangle$. Similarly, it is easy to check that the gauge transformed Hamiltonian $\tilde{H}$ is unitarily equivalent to the original Hamiltonian, i.e. $UHU^\dagger = \tilde{H}$, by applying U to (2.32), (2.28) We conclude that two solutions related by f-transformation describe the same phase since the two wave functions and Hamiltonians are connected by a local unitary transformation U.

As for the g-transformation, one can show that $\tilde{d}_s \tilde{B}_p^s = d_s B_p^s$ by substituting the transformation (2.21) into (2.32) and noting that all the factors of g cancel. It then follows that the Hamiltonian is invariant under the g-transformation, i.e. $H = \tilde{H}$. Accordingly, the wave function is also invariant under the transformation: $|\Phi\rangle = |\tilde{\Phi}\rangle$. In other words, the unitary transformation that relates the two models is simply the identity map, $U = \mathbf{1}$. We would like to mention that the triviality of the g-transformation is special to the particular orientation choice shown in Fig. 2.5: for other orientation choices, $|\Phi\rangle \neq |\tilde{\Phi}\rangle$. That being said, it is clear that $|\Phi\rangle$ and $\tilde{\Phi}\rangle$ are still related by local unitary transformations for other orientation choices. Indeed, this result follows from the fact that a change in the orientation configuration can be implemented by a local unitary transformation (made up of a product of α and γ factors).

A.4 Graphical representation of the Hamiltonian

In this section we demonstrate the graphical representation of B_p^s leads to the same matrix elements as in equation (2.31).

According to the graphical representation, the action of the operator B_p^s on the string-net state $\Bigg\langle$ 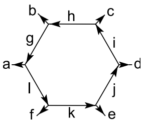

$\Bigg|$ is equivalent to adding a loop of type-s string. This allows us to obtain the matrix elements of B_p^s:

$\Big\langle$ 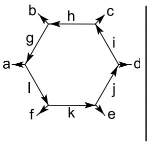

$\Big| \, B_p^s = \Big\langle$ 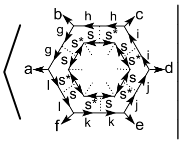

$\Big| = \prod_{x=\{g,h,i,j,k,l\}} F_{s^*sx} \Big\langle$ 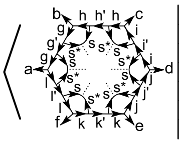

$\Big|$

$= \left(\prod_{x=\{g,h,i,j,k,l\}} F_{s^*sx} \right) F_{s^*g'b} F_{s^*h'c} F_{s^*i'd} F_{s^*j'e} F_{s^*k'f} F_{s^*l'a} \Big\langle$ 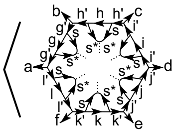

$\Big|$

$= \left(\prod_{x=\{g,h,i,j,k,l\}} F_{s^*sx} F_{s^*x'x'^*} \alpha_{sx} \gamma_{x'^*} \gamma_{s^*} d_s \right) F_{s^*g'b} F_{s^*h'c} F_{s^*i'd} F_{s^*j'e} F_{s^*k'f} F_{s^*l'a} \Big\langle$ 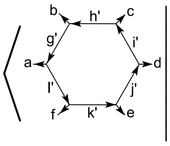

$\Big|$

$= F_{s^*g'b} F_{s^*h'c} F_{s^*i'd} F_{s^*j'e} F_{s^*k'f} F_{s^*l'a} \Big\langle$ 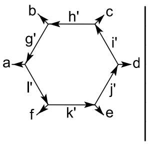

$\Big| \equiv B^{s,ghijkl}_{p,g'h'i'j'k'l'}(abcdef) \Big\langle$ 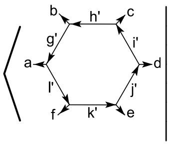

$\Big|$,

with $x' = x + s$. Here the fourth equality follows from

$\Big\langle$ 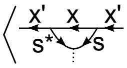

$\Big| = \alpha_{sx} \Big\langle$ 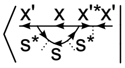

$\Big|$

$= \alpha_{sx} F_{s^*x'x'^*} \gamma_{x'^*} \gamma_{s^*} d_s \, \langle$ 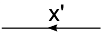

$|$

while the fifth equality follows from the identity

$$F_{s^*sx} F_{s^*x'x'^*} \alpha_{sx} \gamma_{x'^*} \gamma_{s^*} d_s = 1$$

with $x' = x + s$. This identity can be derived from the self-consistency conditions (2.18), by expressing α,γ in terms of F, and then using the pentagon identity (2.18a) together with (2.18b) to simplify the resulting expression.

Our derivation is now complete: we can see that the above expression agrees with the matrix elements of Eq. (2.31), as we wished to show.

A.5 Showing $B_{p_1}^{s_1}$ and $B_{p_2}^{s_2}$ commute

In this section we will show that the operators $B_{p_1}^{s_1}$ and $B_{p_2}^{s_2}$ commute with one another. We only have to consider the case where the two plaquettes are the same, $p_1 = p_2$, or the case where p_1 and p_2 are adjacent since it is clear that the two operators will commute if p_1 and p_2 are further apart.

The first case is when the two B_p operators act on the same plaquette, i.e. $p_1 = p_2 = p$. We need to show B_p^s and B_p^t commute. One can prove this by writing down the matrix elements of $B_p^s B_p^t$:

$$(B_p^s B_p^t)_{g''h''i''j''k''l''}^{ghijkl}(abcdef) = F_{s^*g'b}F_{s^*h'c}F_{s^*i'd}F_{s^*j'e}F_{s^*k'f}F_{s^*l'a}F_{t^*g''b}F_{t^*h''c}F_{t^*i''d}F_{t^*j''e}F_{t^*k''f}F_{t^*l''a}$$

where $x' = x + s$ and $x'' = x' + t$ with $x \in \{g, h, i, j, k, l\}$. Using the pentagon identity, $F_{s^*,x',y}F_{t^*x''y} = F_{(s+t)^*x''y}F_{s^*t^*(x''+y)}/F_{s^*t^*x''}$, the above expression can be rewritten as

$$\begin{aligned}(B_p^s B_p^t)_{g''h''i''j''k''l''}^{ghijkl}(abcdef) &= F_{(s+t)^*g''b}F_{(s+t)^*h''c}F_{(s+t)^*i''d}F_{(s+t)^*j''e}F_{(s+t)^*k''f}F_{(s+t)^*l''a} \\ &= (B_p^{s+t})_{g''h''i''j''k''l''}^{ghijkl}(abcdef).\end{aligned}$$

We conclude that

$$B_p^s B_p^t = B_p^t B_p^s = B_p^{s+t}. \tag{A.5}$$

proving commutativity when $p_1 = p_2 = p$.

The second case is when the two B_p operators act on two adjacent plaquettes p_1, p_2. We want to show $B_{p_1}^t B_{p_2}^s = B_{p_2}^s B_{p_1}^t$ (see Fig. A.3). To prove this, we use (2.32) to write down the matrix elements of operators on each side and then show they are equal.

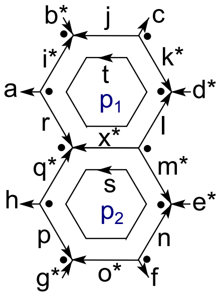

Figure A.3: Two plaquette operators $B^t_{p_1}$ and $B^s_{p_2}$ act on two adjacent plaquettes and add two loops in two different orders. If we apply $B^s_{p_2}$ first and then $B^t_{p_1}$, the resulting matrix elements are (A.6). Conversely, if we apply $B^t_{p_1}$ first and then $B^s_{p_2}$, we will get (A.7).

The matrix elements of $B^s_{p_2}B^t_{p_1}$ are

$$\begin{aligned} &B^{s,qx^*mnop}_{p_2,q'x^{*'}m'n'o'p'}(hr^*lefg) \times \\ &B^{t,ijkl(x-s)r}_{p_1,i''j''k''l''(x-s)''r''}(abcdm'^*q'). \end{aligned} \tag{A.6}$$

Here we use the notation $y' = y + s$ and $y'' = y + t$ for any string type-y. Similarly, the matrix elements of $B^t_{p_1}B^s_{p_2}$ are

$$\begin{aligned} &B^{t,ijklxr}_{p_1,i''j''k''l''x''r''}(abcdm^*q) \times \\ &B^{s,q(x+t)^*mnop}_{p_2,q'(x+t)^{*'}m'n'o'p'}(hr''^*l''efg). \end{aligned} \tag{A.7}$$

Writing out (A.6) and (A.7) explicitly using (2.32), we see that many of the factors of F, α, γ are the same in both expressions. Thus, to prove $(A.6) = (A.7)$, it is sufficient to compare the factors which are different. Specifically, we need to show the product

$$\begin{aligned} &F_{s^*q'r^*}F_{s^*x^{*'}l}F_{t^*l''m'^*}F_{t^*(x+t-s)q'} \times \\ &\alpha_{x^{*'}l}\alpha_{x''^*l''}\alpha_{xq}\alpha_{(x+t-s)q'}\gamma_{x+t}\gamma_{x-s} \end{aligned} \tag{A.8}$$

which appears in (A.6) is equal to the product

$$F_{s^*q'r''^*}F_{x^*(x+t-s)^*l''}F_{t^*l''m^*}F_{t^*x''q} \times$$
$$\alpha_{(x+t-s)^*l''}\alpha_{x^*l}\alpha_{(x-s)q'}\alpha_{x''q}\gamma_x\gamma_{x+t-s} \tag{A.9}$$

which appears in (A.7).

Equivalently, we need to show that the ratio of (A.8) and (A.9) is equal to unity. To this end, we divide the F, α factors in the ratio $(A.8)/(A.9)$ into two groups which are associated with the left and right ends of the common link, respectively. Combining all the factors from the left end of the link gives

$$C_L \equiv \frac{F_{s^*q'r^*}F_{t^*(x+t-s)q'}\alpha_{xq}\alpha_{(x+t-s)q'}}{F_{s^*q'r''^*}F_{t^*x''q}\alpha_{(x-s)q'}\alpha_{x''q}}.$$

Similarly, the factors from the right end of the link give

$$C_R \equiv \frac{F_{s^*x^{*\prime}l}F_{t^*l''m'^*}\alpha_{x^{*\prime}l}\alpha_{x''^*l''}}{F_{x^*(x+t-s)^*l''}F_{t^*l''m^*}\alpha_{(x+t-s)^*l''}\alpha_{x^*l}}.$$

Showing $(A.8)/(A.9) = 1$ is then equivalent to proving that

$$C_L C_R \cdot \frac{\gamma_{x+t}\gamma_{x-s}}{\gamma_x\gamma_{x+t-s}} = 1. \tag{A.10}$$

We notice that C_L and C_R are related by $C_R = C_L^{-1}(x \to -x, s \leftrightarrow t, q \to l, r \to m)$.

The next step is to express all the α factors in C_1, C_2 in terms of F using (2.18e) and then simplify the resulting expressions using the pentagon identity (2.18a). The result is:

$$C_L = \frac{F_{xs^*x^{*\prime}}}{F_{t^*x''s^*}F_{x''s^*(x+t-s)^*}}, \tag{A.11}$$
$$C_R = \frac{F_{s^*x^{*\prime}t^*}F_{x^{*\prime}t^*(x+t-s)}}{F_{x^*t^*x''}}. \tag{A.12}$$

Furthermore, using (2.18d) (2.18c), we derive

$$\frac{\gamma_{x+t}\gamma_{x-s}}{\gamma_x\gamma_{x+t-s}} = \frac{F_{(x+t)(x+t)^*(x+t)}F_{(x-s)(x-s)^*(x-s)}}{F_{xx^*x}F_{(x+t-s)(x+t-s)^*(x+t-s)}}. \tag{A.13}$$

In the final step, we take the product of (A.11),(A.12),(A.13). The expression on the right hand side can then be reduced to 1, using the pentagon identity (2.18a) together with (2.18b). This establishes the identity (A.10) and completes the proof that the B_p^s terms commute with one each other.

A.6 Properties of the Hamiltonian (2.27)

In this section, we will establish the following properties of the Hamiltonian (2.27):

1. $(B_p^s)^\dagger = B_p^{s^*}$.
2. B_p is a projection operator, that is $B_p^2 = B_p$.
3. The ground state wave function on the honeycomb lattice satisfies the local rules (2.2 - 2.4).

Let us show them in order. To prove the first result, we use the pentagon identity (2.18a) and (2.18b) to derive

$$\begin{aligned} F_{sx'y}F_{s^*xy} &= F_{0xy}F_{ss^*(x+y)}/F_{ss^*x} \\ &= F_{ss^*(x+y)}/F_{ss^*x} \end{aligned} \tag{A.14}$$

where $x' = x + s$. We then set $x = g, h, i, j, k, l$ and $y = b, c, d, e, f, a$, and take the product of these six equations, thereby deriving

$$B^{s,g'h'i'j'k'l'}_{p,ghijkl}(abcdef)^{-1} = B^{s^*,ghijkl}_{p,g'h'i'j'k'l'}(abcdef). \tag{A.15}$$

Finally, we use $F_{ijk}^{-1} = F_{ijk}^{*}$ (2.19) to rewrite (A.15) as

$$B_{p,ghijkl}^{s,g'h'i'j'k'l'}(abcdef)^* = B_{p,g'h'i'j'k'l'}^{s^*,ghijkl}(abcdef). \tag{A.16}$$

This establishes the first property.

To prove the second result, we use the identity (A.5) established in appendix A.5 to derive

$$B_p^2 = \sum_{s,t} \frac{d_s d_t}{|G|^2} B_p^s B_p^t = \sum_{s,t} \frac{d_s d_t}{|G|^2} B_p^{s+t}. \tag{A.17}$$

We then use the self-consistency condition (2.18c) to write $d_s d_t = d_{s+t}$. Changing variables to $s' = s + t$, we derive

$$B_p^2 = \sum_{s'} \frac{d_{s'}}{|G|} B_p^{s'} = B_p. \tag{A.18}$$

Finally we show that the ground state Φ_{latt} of H obeys the local rules (2.2 - 2.4). To see this, we use the fact that $B_p|\Phi_{latt}\rangle = |\Phi_{latt}\rangle$ together with the following relations:

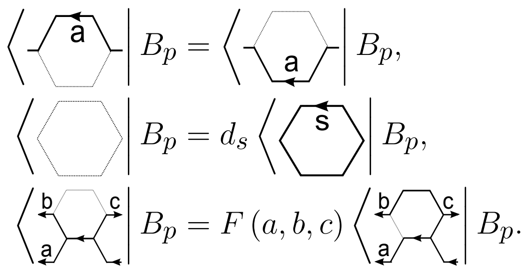

(A.19)

Multiplying these equations by the ground state ket $|\Phi_{latt}\rangle$, we can immediately see that the ground state wave function $\Phi_{latt}(X) = \langle X|\Phi_{latt}\rangle$ satisfies the local rules (2.2 - 2.4).

The relations (A.19) can be proved using the expression for the matrix elements of B_p^s in (2.31) together with the pentagon identity. For example, to prove the last equation, we expand out the left hand side as

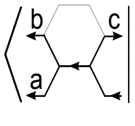

$$B_p = \sum_s \frac{d_s}{|G|}$$

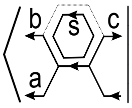

$$= \sum_s \frac{d_s}{|G|} \alpha^{-1}_{(a+b)^* a} \alpha_{(a+b)c} \gamma_{b^*} \gamma_{(a+b)^*}$$

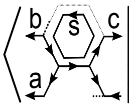

$$= \sum_s \frac{d_s}{|G|} \alpha^{-1}_{(a+b)^* a} \alpha_{(a+b)c} \gamma_{b^*} \gamma_{(a+b)^*} \times$$

$$B^{s,000c(a+b)^* b^*}_{sssc'(a+b)^{*\prime} b^{*\prime}} (b00c(a+b+c)^* a)$$

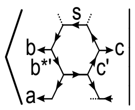

$$.$$

Here B is defined in (2.31), $x' = x + s$. Similarly, on the right hand side, we find

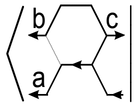

$$B^s_p = \sum_s \frac{d_s}{|G|}$$

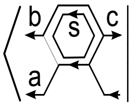

$$= \sum_s \frac{d_s}{|G|} \alpha_{a(b+c)} \gamma_{a^*} \times$$

$$B^{s,bbb(b+c)a^* 0}_{b'b'b'(b+c)'a^{*\prime} s} (b00c(a+b+c)^* a)$$

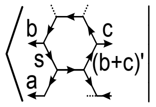

$$.$$

Changing the dummy variable s to $s+b$ in the first expression, we can see that the resulting final state is the same as the second final one. We then compute the ratio of the two corresponding amplitudes. Using (2.18), this ratio can be simplified to $F(a,b,c)$. This justifies the third equation in (A.19). In addition, by taking $a = 0, b = c^*$, we obtain the first equation. The second equation can be shown in a similar manner.

A.7 Gapped edge states

In this section, we analyze the abelian string-net models in a disk geometry, and we show that the boundary of the disk can be gapped for an appropriate choice of edge interactions. We note that a more general analysis of gapped boundaries of string-net models was given in Ref. [48].

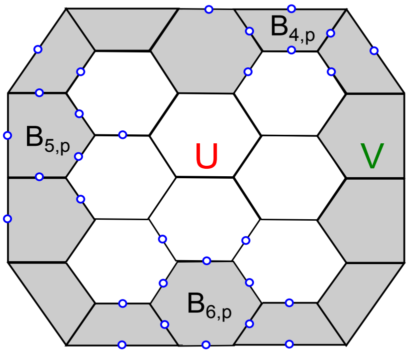

Figure A.4: The lattice spin model in a disk geometry. The gray region denotes the edge part V and the white is the bulk U. The total Hamiltonian has the form $H = H_{bulk} + H_{edge}$ where the bulk Hamiltonian H_{bulk} is defined by (A.20) and the edge Hamiltonian H_{edge} contains three kinds of spin interaction terms $B_{4,p}, B_{5,p}$, and $B_{6,p}$ defined in (A.22).

For concreteness, let us consider the geometry shown in Fig. A.4. Let us assume that in the bulk of the disk, the Hamiltonian is defined by (2.27), that is,

$$H_{bulk} = -\sum_{I \in U} Q_I - \sum_{p \in U} B_p. \tag{A.20}$$

Here the second sum runs over all plaquettes p in region U in Fig. A.4, while the first sum runs over all vertices I that are inside or on the boundary of region U.

Our task is to find an edge Hamiltonian H_{edge} acting on the spins near the boundary of the disk such that $H = H_{bulk} + H_{edge}$ has an energy gap and either a unique or finitely degenerate ground state. Once we find such an edge Hamiltonian, we will have proven explicitly that the edge of the abelian string-net models can be gapped.

Fortunately, it is easy to construct the desired H_{edge}. The key point is that, although we have focused on the string-net Hamiltonian (2.27) in the context of the honeycomb lattice, the Hamiltonian (2.27) can be readily generalized to any planar trivalent graph such as the graph shown in Fig. A.4. Hence there is a natural way to define H_{edge} that maintains the exact solubility and other properties of the bulk Hamiltonian. To be specific, we define

$$H_{edge} = -\sum_{I \in V} Q_I - \sum_{p \in V} B_{n,p} \tag{A.21}$$

where the second sum runs over all plaquettes p in region V and the first sum runs over all vertices on the boundary of the disk. Each of the plaquette terms $B_{n,p}$ is a $2n$-spin interaction term with $n = 4, 5, 6$ (see Fig. A.4). Similarly to the bulk plaquette terms B_p, we define

$$B_{n,p} = \sum_{s \in G} \frac{d_s}{|G|} \cdot B^s_{n,p} \tag{A.22}$$

where

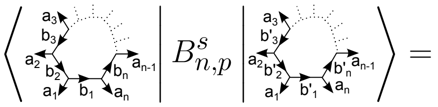

$$B^{s,b_1 b_2 \dots b_n}_{n,p,b'_1 b'_2 \dots b'_n}(a_1 a_2 \dots a_n)$$

and

$$B^{s,b_1 b_2 \dots b_n}_{n,p,b'_1 b'_2 \dots b'_n}(a_1 a_2 \dots a_n) = \prod_{i=1}^{n} \delta^{b_i + s}_{b'_i} \cdot \prod_{i=1}^{n} F(s^*, b'_i, a_i). \tag{A.23}$$

(Note that Eq. (A.23) only defines the plaquette operators for a particular choice of orientations. The definition of B_p for other orientations will generally include additional factors of γ and α as in Eq. (2.32).)

Now, using exactly the same arguments as in the original honeycomb lattice case (2.27), one can show that every term in $H = H_{bulk} + H_{edge}$ commutes with every other term:

$$[Q_I, B^s_{n,p}] = [B^s_p, B^s_{n,p}] = [B^s_{n,p}, B^{s'}_{n',p'}] = 0. \tag{A.24}$$

Also, one can show that every term in the Hamiltonian is a projection operator, i.e. $Q_I, B_p, B_{n,p}$ all have eigenvalues $0, 1$. Putting these facts together, we deduce that the ground state has eigenvalues $q_I = b_p = b_{n,p} = 1$, and that the lowest excited state is separated from the ground state by an energy gap of at least 1.

At this point, we have almost proven that the abelian string-net models support a gapped edge: all that remains is to show that the ground state is unique or finitely degenerate; in fact we show the ground state is *unique* on a disk. We establish this result in appendix A.8.

A.8 Ground state degeneracy

In this section, we calculate the ground state degeneracy of the string-net model (2.27). We consider two geometries: a periodic torus geometry and a disk geometry, where the latter is defined in appendix A.7. We show that the degeneracy on a torus is $D = |G|^2$, while the degeneracy on a disk is $D = 1$.

Our calculation, which is similar to that of Ref. [61], is based on the commuting projectors Q_I and B_p from Sec.2.5. Let us consider the product of these projectors over all vertices and plaquettes on a lattice. Since Q_I and B_p have eigenvalues 0 and 1, this product will select out the states with eigenvalues $q_I = b_p = 1$ for all I and p. In other words, it will select out the ground states. Hence the ground state degeneracy can be calculated by taking the trace of the product of all the projectors:

$$D = \mathrm{Tr}\left(\prod_p B_p \prod_I Q_I\right). \tag{A.25}$$

Here the trace is over all states in the Hilbert space.

We notice that the product of Q_I's constrains the trace to configurations obeying the branching rules. Thus D reduces to the trace of the product of B_p over allowed string-net configurations X. Plugging in the expression for B_p, we have

$$\begin{aligned} D &= \sum_{\text{strnet X}} \langle X| \prod_p \sum_s \frac{d_s}{|G|} B_p^s |X\rangle \\ &= \frac{1}{|G|^{N_{plaq}}} \sum_{\{s\}} \sum_X \langle X| \prod_p d_s B_p^s |X\rangle. \end{aligned} \tag{A.26}$$

Here $\{s\}$ means sets of N_{plaq} numbers which specify B_p^s over all plaquettes and N_{plaq} is the total number of plaquettes.

The next step is to calculate the expectation value $\langle X| \prod_p B_p^s |X\rangle$. Let us first consider the disk geometry. For a disk, this expectation value is nonzero only if $s = 0$ for all plaquettes. The reason is that to get a nonzero expectation value, the final state after the action of $\prod_p B_p$ has to be the same as the original state. Since the disk has a boundary, this forces $s = 0$ on the boundary and thus $s = 0$ in the interior of the disk as well. Hence, in this case, (A.26) simplifies to

$$D = \frac{1}{|G|^{N_{plaq}}} \sum_X 1 = \frac{1}{|G|^{N_{plaq}}} N_{config} \tag{A.27}$$

where N_{config} is the number of string-net configurations on a disk. To count these configurations, we can compare the number of free parameters to the number of constraints. The number of free parameters is the number of links $N_{param} = N_{link}$. As for the number of constraints, there is a constraint at each site coming from the branching rules. However, not all the branching constraints are independent because if we sum up all the constraint equations, we get an equality which is automatically satisfied. Thus, the total number of constraints is $N_{const} = N_{site} - 1$. Combining these calculations, the total number of string-net configurations on a disk is

$$N_{config} = |G|^{N_{param} - N_{const}} = |G|^{N_{link} - N_{site} + 1}. \tag{A.28}$$

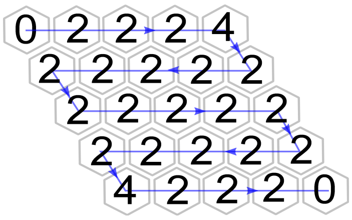

Figure A.5: A 5×5 lattice on torus. We want to apply the B_p^s operators to the whole lattice. We start by applying the B_p^s operators to the upper left hand corner and then following a zig-zag path to fill the lattice. When a B_p^s acts on each plaquette, it creates a closed loop-s around the boundary of the plaquette. Two adjacent loops will merge to a bigger loop, multiplied by a phase factor of d_{s^*}. In general, each application of B_p^s comes with a factor $d_{s^*}^{N_{ext}/2}$ with N_{ext} being the number of external legs on the boundary of the plaquette p that are occupied by strings. These numbers N_{ext} are shown above in each plaquette.

Substituting this expression into (A.27), we derive

$$D = \frac{1}{|G|^{N_{plaq}}} N_{config} = |G|^{N_{link} - N_{plaq} - N_{site} + 1}. \tag{A.29}$$

The final step is to note that a disk has an Euler characteristic of 1, so

$$N_{site} - N_{link} + N_{plaq} = 1. \tag{A.30}$$

Thus we conclude $D = 1$ on a disk.

Next we consider a torus geometry. Again, we need to calculate the expectation value $\langle X | \prod_p B_p^s | X \rangle$ and substitute into (A.26). In the case of a torus, this expectation value is nonzero for any configuration in which s is constant. This is because a torus does not have boundary and therefore as long as s is constant, each link is acted on by two adjacent B_p^s in opposite directions, so that $\prod_p B_p^s |X\rangle \propto |X\rangle$. Hence, in this case (A.26) simplifies to

$$D = \frac{d_s^{N_{plaq}}}{|G|^{N_{plaq}}} \sum_{s \in G} \sum_X \langle X | \prod_p B_p^s | X \rangle. \tag{A.31}$$

To proceed further, we use the identity

$$\langle X|\prod_p B_p^s|X\rangle = d_{s^*}^{N_{plaq}} \tag{A.32}$$

for constant s. We prove this identity in two steps. First, we note that every string-net state $|X\rangle$ can be written as $|X\rangle \propto \prod B_p^s \cdot \prod W_\alpha(P)|0\rangle$ where $|0\rangle$ denotes the vacuum state, and the product runs over some arbitrary set of plaquette operators B_p^s and closed string operators $W_\alpha(P)$. Using this fact, together with the fact that $B_p^s, W_\alpha(P)$ commute with one another, it follows that

$$\langle X|\prod_p B_p^s|X\rangle = \langle 0|\prod_p B_p^s|0\rangle. \tag{A.33}$$

We then calculate the latter expectation value by brute force. To this end, we order the plaquette operators in a particular way, starting with the upper left hand corner of Fig. A.5 and then following a zig-zag path. When we apply the first plaquette operator to the vacuum state $\langle 0|$, we get a single closed loop around the boundary of that plaquette. When we apply the second plaquette operator, the result is a larger closed loop, multiplied by a phase factor of d_{s^*}. In general, it can be shown that each plaquette operator B_p^s comes with phase factor of $d_{s^*}^{N_{ext}/2}$ with N_{ext} being the number of external legs on the boundary of the plaquette p that are occupied by strings. The values of N_{ext} for the zig-zag ordering are shown in Fig. A.5. We can see that after applying all the plaquette operators, the total number of factors of d_{s^*} is $(N_{plaq}-4)\cdot 1+2\cdot 2 = N_{plaq}$. Hence, $\langle 0|\prod_p B_p^s|0\rangle = d_{s^*}^{N_{plaq}}$. This proves the identity (A.32).

Substituting (A.32) into (A.31), and using the fact that $d_s \cdot d_{s^*} = d_0 = 1$, we derive

$$\begin{aligned} D &= \frac{1}{|G|^{N_{plaq}}}\sum_{s\in G}\sum_X 1 \\ &= \frac{|G|}{|G|^{N_{plaq}}}N_{config} \\ &= |G|^{N_{link}-N_{site}-N_{plaq}+2} \end{aligned} \tag{A.34}$$

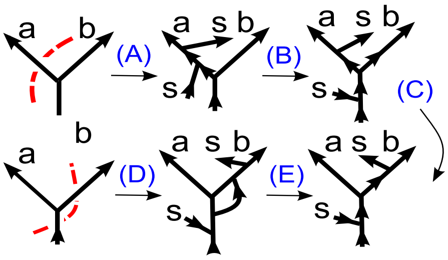

Figure A.6: The sequence to show Eq. (2.49). The arrows involve factors from local rules and resolving crossings (see (A.37)).

where the counting of string-net configurations N_{config} is identical to the disk case. Now a torus has an Euler characteristic of 0 so

$$N_{site} - N_{link} + N_{plaq} = 0. \tag{A.35}$$

Therefore, we conclude that the ground state degeneracy on a torus is $D = |G|^2$.

A.9 Derivation of Eqs. (2.46, 2.47)

In this section, we show that the string operator $W(P)$ obeys the path independence conditions (2.44) and (2.45) if and only if ω obeys Eqs. (2.46, 2.47). The main steps in the argument are shown in Figs. A.6, A.7.

We begin with Fig. A.6. Clearly the string operator $W(P)$ will satisfy (2.44) if and only if the amplitudes of the two string-net configurations on the left hand side of Fig. A.6 are equal to one another. At the same time, using the local rules (2.2 - 2.4) and (2.6 - 2.15) and (2.42) we can relate both of these amplitudes to the amplitude of the configuration shown in the bottom right hand corner of Fig. A.6. In this way, one can show that (2.44) is equivalent to the algebraic equation

$$(A)(B)(C) = (D)(E) \tag{A.36}$$

where

$$\begin{aligned}
(A) &= \omega(a), \qquad &\text{(A.37)}\\
(B) &= F_{s^*(a+s)b}\alpha^{-1}_{s^*(a+s)}\alpha_{s^*(a+b+s)}\gamma_a\gamma_{(a+b)^*},\\
(C) &= F_{asb},\\
(D) &= \bar{\omega}(b)\omega(a+b),\\
(E) &= F_{abs}F_{(b+s)s^*s}d_s^*\gamma_s.
\end{aligned}$$

Simplifying (A.36) using (2.18), we obtain

$$\omega(a) = \bar{\omega}(b)\omega(a+b)\frac{F_{abs}F_{bss^*}F_{(a+s)b(a+b)^*}}{F_{ab(a+b)^*}F_{asb}}. \tag{A.38}$$

Setting $a = 0$ and using the fact that $\omega(0) = 1$, along with (2.18b), we derive (2.47):

$$\bar{\omega}(b) = \omega(b)^{-1} \cdot F^{-1}_{bss^*}F^{-1}_{sbb^*}. \tag{A.39}$$

Substituting the above relation back into (A.38) and simplifying using the pentagon identity (2.18a) gives (2.46):

$$\omega(a)\omega(b) = \omega(a+b) \cdot \frac{F_{abs}F_{sab}}{F_{asb}}\frac{F_{s(a+b)(a+b)^*}}{F_{saa^*}F_{sbb^*}}. \tag{A.40}$$

From the above analysis, we conclude that a string operator $W(P)$ will obey the path independence condition (2.44) if and only if ω obeys Eqs. (2.46,2.47). The next question is to see whether the other path independence condition (2.45) gives any new constraints on ω. We will show that it does not.

To this end, we consider Fig. A.7. Clearly $W(P)$ will satisfy (2.45) if and only if the amplitudes of the two configurations on the left hand side of Fig. A.7 are equal. At the same time, these amplitudes can both be related to the amplitude of the configuration shown in

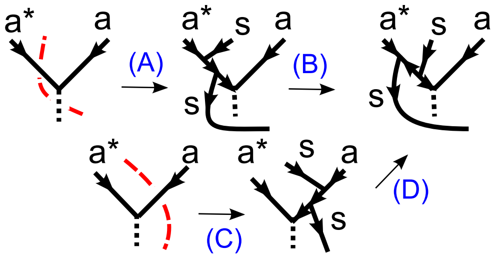

Figure A.7: The sequence to show Eq. (2.50). The arrows involve factors from local rules and resolving crossings (see (A.42)).

the top right hand corner of Fig. A.7. Thus we see that (2.45) is equivalent to the equation

$$(A)(B) = (C)(D) \tag{A.41}$$

where

$$\begin{aligned}(A) &= \omega(a^*), \qquad \text{(A.42)}\\ (B) &= F_{a^*sa},\\ (C) &= \bar{\omega}(a),\\ (D) &= \alpha^{-1}_{a^*(s+a)}\gamma_s.\end{aligned}$$

Simplifying (A.41) using (2.18) gives

$$\omega(a^*) = \bar{\omega}(a)\frac{F_{a^*as}F_{ass^*}}{F_{a^*sa}}, \tag{A.43}$$

which is exactly the relation (A.38) by setting $a \to -a$ and $b \to a$. Thus it does not give rise to new constraints. This completes the proof that the string operator $W(P)$ is path independent if only if ω obeys (2.46,2.47).

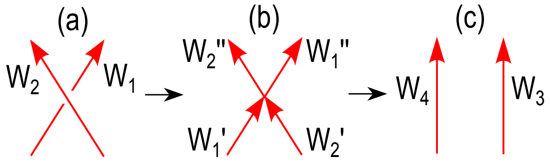

Figure A.8: There are two steps to connect the string operation in (a) and (c). First, we use piece-connectedness to decompose W_1, W_2 in (a) into four pieces W_1', W_1'', W_2', W_2'' in (b). Second, we use path independence to deform the $W_1''W_2'$ into W_3 and $W_2''W_1'$ into W_4 in (c).

A.10 Exchange statistics

In this section, we derive the string algebra (2.59) from the main text. That is, we show that the string operators $W_\alpha(P_1), W_\alpha(P_2), W_\alpha(P_3), W_\alpha(P_4)$ obey

$$W_\alpha(P_2)W_\alpha(P_1)|\Phi\rangle = e^{i\theta_\alpha}W_\alpha(P_4)W_\alpha(P_3)|\Phi\rangle \tag{A.44}$$

where θ_α is the exchange statistics of the quasiparticle α created by the string operator W_α, and P_1, P_2, P_3, P_4 are any four paths with the geometry of Fig. 2.9. We will derive the algebra (2.59) given two assumptions about the string operators:

$$\begin{aligned} W_\alpha(P)|\Phi\rangle &= W_\alpha(P')|\Phi\rangle, & \text{(A.45)} \\ W_\alpha(P_1)W_\alpha(P_2)|\Phi\rangle &= W_\alpha(P_1 \cup P_2)|\Phi\rangle. & \text{(A.46)} \end{aligned}$$

Here, the first assumption (A.45) is that the string operators satisfy *path independence*: i.e., their action on the ground state is the same for any two paths P, P' with the same endpoints. The second assumption (A.46) is that the string operator are *piece-connected*: i.e. two string operators $W_\alpha(P_1)$, $W_\alpha(P_2)$ acting on paths P_1, P_2 that share a common endpoint, can be "glued" together in the natural way. After proving (A.44), we will then show that the above two assumptions are valid.

Before proving (A.44), we first introduce some notation: we denote $W_\alpha(P_1)$ by W_1 and similarly for P_2, P_3, P_4. In this notation, (A.44) can be written as

$$W_2 W_1 |\Phi\rangle = e^{i\theta_\alpha} W_4 W_3 |\Phi\rangle. \tag{A.47}$$

The first step in the proof is to use (A.46) to decompose W_1, W_2 into two pieces, as shown in Fig. A.8(a,b):

$$W_2 W_1 |\Phi\rangle = (W_2'' W_2')(W_1'' W_1')|\Phi\rangle. \tag{A.48}$$

We then use the "hopping operator algebra" derived in Ref. [63]. This algebra connects the exchange statistics of a particle to the commutation properties of three string operators. Applying it in our case gives:

$$W_2' W_1'' W_1' |\Phi\rangle = e^{i\theta_\alpha} W_1' W_1'' W_2' |\Phi\rangle \tag{A.49}$$

where θ_α is the exchange statistics of α. Substituting this expression into (A.48), we derive

$$W_2 W_1 |\Phi\rangle = e^{i\theta_\alpha} W_2'' W_1' W_1'' W_2' |\Phi\rangle. \tag{A.50}$$

In the final step, we use path independence (A.45) to write (see Fig. A.8(c))

$$\begin{aligned} (W_2'' W_1')(W_1'' W_2')|\Phi\rangle &= (W_2'' W_1') W_3 |\Phi\rangle \\ &= W_4 W_3 |\Phi\rangle. \end{aligned} \tag{A.51}$$

Comparing (A.51) and (A.50), the claim (A.44) follows immediately.

To complete the argument we need to show that the two assumptions (A.45,A.46) are valid for the string operators $W_\alpha(P)$. The path independence assumption (A.45) certainly holds since the string operators were constructed specifically to obey this property. As for the piece-connectedness assumption (A.46), we can establish this property if we can show that the open string operators can be defined in such a way that two string operators with

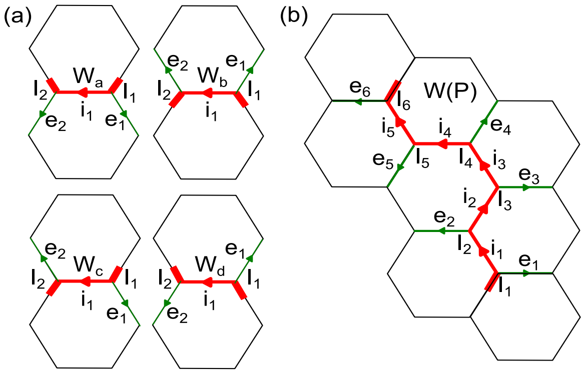

Figure A.9: (a) Four building blocks of any string operator defined on each link. W_a and W_b have ends in the same side of the link while W_c and W_d have ends in opposite sides of the link. Here i_1, e_1, e_2 denote the initial spin state in the link and two spin states on the external legs, respectively. I_1, I_2 label the vertices. Their matrix elements are given in (A.52). (b) A typical open string operator $W(P)$ along the path $P = I_1, I_2, \ldots, I_6$ (the red line). It can be decomposed into product of basic string blocks acting on each link along P. The matrix elements of $W(P)$ between an initial bra state $i'_1, i'_2, \ldots, i'_5$ and a finial bra state $i_1, i_2, \ldots, i_5$ is $W^{i_1\ldots i_5}_{i'_1\ldots i'_5}(e_1\ldots e_6) = W^{s,i_5}_{a,i'_5}(e_5e_6)W^{s,i_4}_{d,i'_4}(e_4e_5)W^{s,i_3}_{b,i'_3}(e_3e_4)W^{s,i_2}_{c,i'_2}(e_2e_3)W^{s,i_1}_{d,i'_1}(e_1e_2)$.

a common endpoint can be glued together to form a longer string. To this end, we will first introduce some basic string operators defined on each link of the honeycomb lattice and then show how to construct a general string operator from these building blocks. This construction automatically gives string operators that are piece-connected.

The basic string operators act on a single link of the honeycomb lattice. For each link, there are four types of basic operators which differ from one another at their two ends (see Fig. A.9(a)). These ends are meant to indicate how to glue two string operators together at a vertex. Specifically, two basic string operators can be connected only if their ends *match* one another. That is, the two connecting ends must lie along the same path in the lattice. Thus we can construct a general string operator $W(P)$ along a path P on the honeycomb lattice by gluing together a sequence of basic string operators that follow the path P (see Fig. A.9(b)).

Now we have to define these basic string operators in such a way that they can be glued together to form longer string operators. One way to find an appropriate definition is to start with a long string operator as defined in section 2.6.3, and then break it up into many short string operators. In general there are many ways to do this, since there are many ways of dividing the phase associated with a vertex between the two shorter string operators that share this vertex. Here, we use a symmetrical convention: we split equally the phase associated with a vertex to the two connecting ends of the basic string operators at this vertex. In this way, we obtain the following definition of the basic string operators:

$$\begin{aligned}
W^{s,i_1}_{a,i'_1}(e_1e_2) &= F(i_1^*, i_1, s)\sqrt{V_{R,s}(i_1+e_1, e_1)V_{R,s}(i_1, e_2)}, \\
W^{s,i_1}_{b,i'_1}(e_1e_2) &= F(s^*, s, i_1)\sqrt{V_{L,s}(i_1+e_1, e_1)V_{L,s}(i_1, e_2)}, \\
W^{s,i_1}_{c,i'_1}(e_1e_2) &= \bar{\omega}_{i_1 s}\sqrt{V_{R,s}(i_1+e_1, e_1)V_{L,s}(i_1, e_2)}, \\
W^{s,i_1}_{d,i'_1}(e_1e_2) &= \omega_{i_1 s}\sqrt{V_{L,s}(i_1+e_1, e_1)V_{R,s}(i_1, e_2)},
\end{aligned} \tag{A.52}$$

with

$$\begin{aligned}
V_{L,s}(a,b) &= \frac{F(s^*, a-b+s, b)}{F(s^*, s, a)}, \\
V_{R,s}(a,b) &= \frac{F(b, a-b, s)}{F(b-a, a-b, s)}.
\end{aligned}$$

Here $V_{L,s}$ and $V_{R,s}$ are the phases associated with the left and right turning of the string at each vertex, respectively. The phases F, ω and $\bar{\omega}$ are from the fusion of the string to the link without and with crossings while $V_{R,s}, V_{L,s}$ are from the fusion at the vertices.

With (A.52) at hand, we define the matrix elements for general string operators $W(P)$ by taking the product of the matrix elements of the basic string operators for each link along the path P (see Fig. A.9(b)). This prescription (A.52) satisfies $W(P_1)W(P_2)|\Phi\rangle = W(P_1 \cup P_2)|\Phi\rangle$ by construction.

We would like to mention that there is one subtlety in gluing together the basic string operators: the above matrix elements are defined for strings satisfying the branching rules at vertices, yet when we apply the first string operator to a string-net state $|X\rangle$, the branching rules will be violated at the two endpoints. To use (A.52) for the second string operator connecting to the first one, we follow a special prescription: focusing on the vertex where the two strings meet, we pretend that the link along which the first string operator acts is in the unique state that obeys the branching rules with the other two links adjoining the vertex. With this prescription, the matrix elements of the second string operator are well-defined.

APPENDIX B

APPENDICES FOR CHAPTER 3

B.1 Proving the identities (3.24,3.26,3.27)

In this section, we prove a few identities involving the operators $A_l, A_{\hat{l}}, B^0_c, B^0_{\hat{c}}, B^1_c, B^1_{\hat{c}}$ and the wave functions $|\Psi_0\rangle$ and $|\Psi_1\rangle$. We used these identities when we solved the two models, H_0 and H_1. The first set of identities state that $|\Psi_0\rangle$ and $|\Psi_1\rangle$ are eigenstates of the $A_l, A_{\hat{l}}$ operators:

$$\begin{aligned} A_l|\Psi_0\rangle &= A_{\hat{l}}|\Psi_0\rangle = |\Psi_0\rangle, \\ A_l|\Psi_1\rangle &= A_{\hat{l}}|\Psi_1\rangle = |\Psi_1\rangle. \end{aligned} \tag{B.1}$$

Similarly, the second set of identities state that $|\Psi_0\rangle$ is an eigenstate of $B^0_c, B^0_{\hat{c}}$ and $|\Psi_1\rangle$ is an eigenstate of $B^1_c, B^1_{\hat{c}}$:

$$B^0_c|\Psi_0\rangle = B^0_{\hat{c}}|\Psi_0\rangle = |\Psi_0\rangle, \tag{B.2}$$

$$B^1_c|\Psi_1\rangle = B^1_{\hat{c}}|\Psi_1\rangle = |\Psi_1\rangle. \tag{B.3}$$

The last identity states that the $B^1_c, B^1_{\hat{c}}$ operators commute with one another:

$$[B^1_c, B^1_{c'}] = [B^1_{\hat{c}}, B^1_{\hat{c}'}] = [B^1_c, B^1_{\hat{c}}] = 0. \tag{B.4}$$

We begin by deriving Eqs. (B.1). These relations are obvious since $|\Psi_0\rangle$ and $|\Psi_1\rangle$ are linear superpositions of closed membrane configurations $|X_b, X_r\rangle$, which by definition obey $A_l|X_b, X_r\rangle = A_{\hat{l}}|X_b, X_r\rangle = |X_b, X_r\rangle$. The relation (B.2) is also easy to prove: first we note

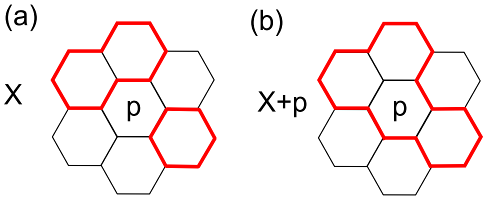

Figure B.1: An example of the 2D identity (B.8) for the case of loops living on the honeycomb lattice. Panel (a) shows a loop configuration X, while panel (b) shows the corresponding configuration $X+p$. In this example, $N_{\text{loop}}(X) = 2$ and $N_{\text{loop}}(X+p) = 1$. Also $n_p(X) = 4$, since four of the six legs adjacent to the plaquette p are occupied by strings. The identity (B.8) holds for this example, since $(-1)^{1-2} = (-1) \cdot i^4$.

that

$$\begin{aligned}
\mathcal{B}_c^0|\Psi_0\rangle &= \sum_{\text{closed } X_b, X_r} \mathcal{B}_c^0|X_b, X_r\rangle \\
&= \sum_{\text{closed } X_b, X_r} |X_b + c, X_r\rangle \\
&= \sum_{\text{closed } X_b', X_r} |X_b', X_r\rangle \\
&= |\Psi_0\rangle
\end{aligned} \tag{B.5}$$

where we made the change variables $X_b' = X_b + c$ in the third line. Then using the fact that $B_c^0 = \frac{1}{2}(1 + \mathcal{B}_c^0)$, we immediately derive the required relation $B_c^0|\Psi_0\rangle = |\Psi_0\rangle$. The same argument works for $B_{\hat{c}}^0$.

The relation (B.3) requires a little more work. First, we note that

$$\begin{aligned}
\mathcal{B}_c^1|\Psi_1\rangle &= \sum_{\text{closed } X_b, X_r} (-1)^{N_g(X_b, X_r)} \mathcal{B}_c^1|X_b, X_r\rangle \qquad \text{(B.6)} \\
&= \sum_{\text{closed } X_b, X_r} (-1)^{N_g(X_b, X_r)} (-1)^{m_c} i^{n_c} |X_b + c, X_r\rangle
\end{aligned}$$

where N_g is the number of green loops in the configuration X_b, X_r and m_c, n_c are integer valued functions of X_b, X_r which are defined in section 3.2.4. To proceed further, we use the following identity:

$$(-1)^{N_g(X_b+c,X_r)-N_g(X_b,X_r)} = (-1)^{m_c(X_b,X_r)} i^{n_c(X_b,X_r)}. \tag{B.7}$$

Here, we explicitly show the dependence of m_c and n_c on X_b, X_r, for clarity. Equation (B.7) says that when we add a blue cube, i.e. $X_b \to X_b + c$, the resulting change in the parity of the number of green loops N_g can be computed in terms of m_c and n_c. This relation is nontrivial because $(-1)^{N_g}$ depends on the *global* properties of the membrane configuration X_b, X_r, while m_c and n_c only depend on *local* properties of X_b, X_r in the neighborhood of the cube c.

To derive the above identity (B.7), we first recall an analogous, but simpler identity involving 2D loop models. The 2D identity applies to 2D loop configurations X that live on the links of a 2D planar trivalent lattice. It states that if we add a loop around the boundary of a single plaquette p to form a new loop configuration $X + p$, then

$$(-1)^{N_{\text{loop}}(X+p)-N_{\text{loop}}(X)} = (-1) \cdot i^{n_p(X)} \tag{B.8}$$

where $N_{\text{loop}}(X)$ and $N_{\text{loop}}(X+p)$ are the number of loops in the configurations X and $X+p$, and where $n_p(X)$ is the number of occupied legs of the plaquette p. (See Fig. B.1 for an example). The 2D identity (B.8) is closely related to the 2D exactly soluble double semion model of Ref. [65], and can be established using the local rules that define that model.

To derive the 3D identity (B.7) from its 2D cousin (B.8), it is helpful to think about the configuration of green loops in X_b, X_r, for a fixed red membrane configuration X_r. These green loops lie on the surfaces of the red membranes X_r. When we add a blue cube, this effectively adds a collection of green loops along all the red membranes that intersect the cube. Adding these green loops is similar to adding the loop p in the 2D identity (B.8), so when we add these loops, the change in the parity of the number of green loops can be calculated by multiplying the factors on the right hand side of (B.8) over all the additional green loops. Taking the product of these factors gives the 3D identity (B.7).

Now that we have established the identity (B.7), we can complete our derivation of (B.3): substituting (B.7) into (B.6), we obtain

$$\begin{aligned}\mathcal{B}_c^1|\Psi_1\rangle &= \sum_{\text{closed } X_b, X_r} (-1)^{N_g(X_b+c,X_r)}|X_b+c, X_r\rangle \\ &= \sum_{\text{closed } X_b', X_r} (-1)^{N_g(X_b',X_r)}|X_b', X_r\rangle \\ &= |\Psi_1\rangle \qquad \text{(B.9)}\end{aligned}$$

where we made the change of variables $X_b' = X_b + c$ in the second line. Finally, using the fact that $B_c^1 = \frac{1}{2}(1+\mathcal{B}_c^1)P_c$ and $P_c|\Psi_1\rangle = |\Psi_1\rangle$, we derive the required relation $B_c^1|\Psi_1\rangle = |\Psi_1\rangle$. The same argument works for $B_{\hat{c}}^1$.

All that remains is the third relation (B.4). In principle, one could establish (B.4) by writing out the explicit form of $B_c^1, B_{\hat{c}}^1$ and calculating their commutators. However such a calculation would be tedious and not particularly illuminating. Therefore we use a different approach to show (B.4). We make use of two properties of the operators $\mathcal{B}_c^1$. The first property is the relation

$$\mathcal{B}_c^1|\Psi_1\rangle = |\Psi_1\rangle \qquad \text{(B.10)}$$

which we just established above. The second property is that, for any closed membrane configuration (X_b, X_r),

$$\mathcal{B}_c^1|X_b, X_r\rangle = e^{i\theta(X_b,X_r,c)}|X_b+c, X_r\rangle \qquad \text{(B.11)}$$

where $e^{i\theta(X_b,X_r,c)}$ is a phase factor that depends on X_b, X_r, c. The latter property follows immediately from the definition of $\mathcal{B}_c^1$.

Using the above two properties (B.10) and (B.11), we will now show that the two operators $\mathcal{B}_c^1, \mathcal{B}_{c'}^1$ commute with one another when acting on closed membrane states. The argument is simple. From property (B.11), we compute

$$\begin{aligned}\mathcal{B}^1_{c'}\mathcal{B}^1_c|X_b, X_r\rangle &= \mathcal{B}^1_{c'} \cdot e^{i\theta(X_b,X_r,c)}|X_b + c, X_r\rangle \\ &= e^{i\theta(X_b+c,X_r,c')} \cdot e^{i\theta(X_b,X_r,c)}|X_b + c + c', X_r\rangle\end{aligned} \tag{B.12}$$

On the other hand, if we reverse the order we find

$$\begin{aligned}\mathcal{B}^1_c\mathcal{B}^1_{c'}|X_b, X_r\rangle &= \\ e^{i\theta(X_b+c',X_r,c)} &\cdot e^{i\theta(X_b,X_r,c')}|X_b + c + c', X_r\rangle\end{aligned} \tag{B.13}$$

We need to show that the expressions on the right hand sides of (B.12) and (B.13) are equal. To this end, we note that property (B.10) implies that

$$\langle X_b, X_r|B^1_c|\Psi_1\rangle = \langle X_b, X_r|\Psi_1\rangle. \tag{B.14}$$

Then, using property (B.11), we can write this as

$$e^{-i\theta(X_b,X_r,c)}\langle X_b + c, X_r|\Psi_1\rangle = \langle X_b, X_r|\Psi_1\rangle \tag{B.15}$$

so that

$$e^{i\theta(X_b,X_r,c)} = \frac{\langle X_b + c, X_r|\Psi_1\rangle}{\langle X_b, X_r|\Psi_1\rangle}. \tag{B.16}$$

We now substitute (B.16) into equation (B.12). The result is

$$\mathcal{B}^1_{c'}\mathcal{B}^1_c|X_b, X_r\rangle = \frac{\langle X_b + c + c', X_r|\Psi_1\rangle}{\langle X_b, X_r|\Psi_1\rangle}. \tag{B.17}$$

Likewise, if we substitute (B.16) into equation (B.13), we obtain the same expression:

$$\mathcal{B}^1_c\mathcal{B}^1_{c'}|X_b, X_r\rangle = \frac{\langle X_b + c + c', X_r|\Psi_1\rangle}{\langle X_b, X_r|\Psi_1\rangle}, \tag{B.18}$$

implying that $\mathcal{B}_c^1$ and $\mathcal{B}_{c'}^1$ commute when acting on closed membrane states.

Now that we know that $\mathcal{B}_c^1$ and $\mathcal{B}_{c'}^1$ commute when acting on closed membrane states, we can immediately deduce that the combinations $\mathcal{B}_c^1 P_c$ and $\mathcal{B}_{c'}^1 P_{c'}$ commute when acting on *arbitrary* membrane states, since the operators P_c and $P_{c'}$ project onto states that are closed in the neighborhood of c and c'. It then follows that the operators B_c^1 and $B_{c'}^1$ commute with one another, since B_c^1 is a linear combination of $\mathcal{B}_c^1 P_c$ and P_c.

We have shown that $[B_c^1, B_{c'}^1] = 0$ for any cubes c, c' in the cubic lattice. This establishes the first identity in Eq. (B.4). The other two identities in Eq. (B.4) can be proven in exactly the same way.

B.2 Showing that the cylinder operators create braiding eigenstates

In this section we show that the blue cylinder operator $M_b^1(S)$ creates loop excitations which are eigenstates of braiding measurements. Our argument consists of two parts. In the first part, we show that as long as f_b obeys condition (3.46), then the loop excitations are guaranteed to be eigenstates of braiding measurements. In the second part, we check that f_b does in fact obey (3.46). The second part can also be thought of as a derivation of Table 3.1 and Table 3.2, since we will see that the values in those tables are completely fixed by the requirement that f_b obey equation (3.46).

B.2.1 Connection between equation (3.46) and braiding eigenstates

In this section we show that if f_b obeys condition (3.46) then the blue cylinder operator is guaranteed to create loop excitations which are braiding eigenstates. We reprint equation (3.46) below for convenience:

$$f_b(X_b, X_r, S_1 \cup S_2) = f_b(X_b, X_r, S_1) \cdot f_b(X_b, X_r, S_2). \tag{B.19}$$

Here S_1 and S_2 can be any two cylinders that share a common boundary while (X_b, X_r) can be any membrane configuration whose intersection with the common boundary obeys the relevant cylinder operator boundary condition.

To begin, it is helpful to consider an example. Let $|\Psi_{ex}\rangle$ be an excited state with a single red loop. We will call this red loop the "base loop." Let $M_b^1(S)$ be a blue cylinder operator that is linked with the base loop. Consider the state $M_b^1(S)|\Psi_{ex}\rangle$. This state contains two blue loops at the two ends of the cylinder S, both of which are linked with the red base loop. Now, what we want to show is that these blue loops are eigenstates of braiding measurements. That is, we want to show that if we braid any other loop around one of these loops, the system returns to its original state multiplied by a complex number (in fact, a phase factor). We now translate this claim into a mathematical equation.

Consider, for example, braiding another blue loop around one of these loops. This braiding process can be implemented by applying a blue torus operator $M_b^1(S')$ where the the torus S' encircles the loop that we wish to braid around (see Fig. 3.12 for a similar geometry). The fact that the blue loop is an eigenstate of this braiding process is equivalent to the equation

$$M_b^1(S') \cdot (M_b^1(S)|\Psi_{ex}\rangle) = (\text{const.}) \cdot M_b^1(S)|\Psi_{ex}\rangle. \tag{B.20}$$

Our task is to show that if f_b obeys (B.19) then the operators M_b^1 obey equation (B.20). To establish this result, we first rewrite (B.20) in a more convenient form. We begin by recalling that since S' is a torus operator, it does not create any excitations — in other words, $M_b^1(S')|\Psi_{ex}\rangle \propto |\Psi_{ex}\rangle$. Using this fact, the above equation can be written as

$$M_b^1(S')M_b^1(S)|\Psi_{ex}\rangle = (\text{const.}) \cdot M_b^1(S)M_b^1(S')|\Psi_{ex}\rangle.$$

Next, multiplying both sides by $\langle X_b, X_r|$ gives

$$\begin{aligned}\langle X_b, X_r|M_b^1(S')M_b^1(S)|\Psi_{ex}\rangle = \\ (\text{const.}) \cdot \langle X_b, X_r|M_b^1(S)M_b^1(S')|\Psi_{ex}\rangle.\end{aligned}$$

Using the definition of M_b^1, we rewrite the matrix elements on the left and right hand sides as:

$$\begin{aligned}\langle X_b, X_r|M_b^1(S')M_b^1(S)|\Psi_{ex}\rangle &= f_b^*(X_b, X_r, S') \\ &\cdot f_b^*(X_b + S', X_r, S) \cdot \Psi_{ex}(X_b + S + S', X_r), \\ \langle X_b, X_r|M_b^1(S)M_b^1(S')|\Psi_{ex}\rangle &= f_b^*(X_b, X_r, S) \\ &\cdot f_b^*(X_b + S, X_r, S') \cdot \Psi_{ex}(X_b + S + S', X_r).\end{aligned}$$

Therefore, what we need to prove is

$$\begin{aligned}f_b(X_b, X_r, S') \cdot f_b(X_b + S', X_r, S) = \\ (\text{const.}) \cdot f_b(X_b, X_r, S) \cdot f_b(X_b + S, X_r, S')\end{aligned}$$

or equivalently

$$\frac{f_b(X_b + S', X_r, S)}{f_b(X_b, X_r, S)} \cdot \frac{f_b(X_b, X_r, S')}{f_b(X_b + S, X_r, S')} = (\text{const.}). \tag{B.21}$$

We now prove (B.21). Focusing on the first ratio in (B.21), we note that the numerator and denominator can be represented graphically as

$f_b(X_b + S', X_r, S) \;=\; f_b\Big($ 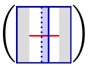 $\Big)$,

$f_b(X_b, X_r, S) \;=\; f_b\Big($ 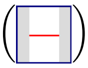 $\Big)$.

Here the thin vertical blue region corresponds to the intersection $S' \cap S$, while the gray areas on the left and on the right are meant to denote some arbitrary pictures correponding to $X_b \cap S$ and $X_r \cap S$. (We can assume without loss of generality that the pictures are of the above simple form, since we can use the path independence property, discussed below eqs. (3.36), to deform S and S' as we wish). Next we use equation (B.19) twice to break up the cylinder S into three smaller cylinders, giving us

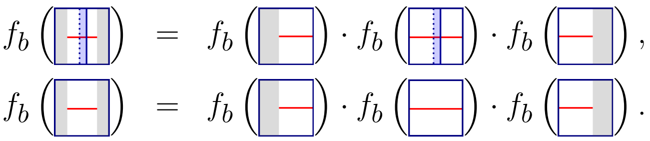

Taking the ratio of these expressions gives

$$\frac{f_b(X_b + S', X_r, S)}{f_b(X_b, X_r, S)} =$$

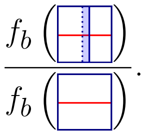

In particular, we see that $\frac{f_b(X_b+S',X_r,S)}{f_b(X_b,X_r,S)}$ is *independent* of X_b, X_r. In exactly the same way, one can show that $\frac{f_b(X_b,X_r,S')}{f_b(X_b+S,X_r,S')}$ is independent of X_b, X_r. This proves equation (B.21): both terms on the left hand side are independent of X_b, X_r, so their product must be independent of X_b, X_r as well.

So far, we have shown that (B.19) implies the braiding eigenstate property in *one* case. The case we considered was a blue loop linked to a red base loop. We showed that the blue loop is a braiding eigenstate with respect to braiding another blue loop around it. To prove the general claim, we need to establish the same braiding eigenstate property for all other cases, that is all other combinations of red and blue loops. We will not discuss the other cases here, but it should be clear that the above argument is not specific to the case considered above and applies equally well to the other cases.

B.2.2 Checking that f_b obeys equation (3.46)

In this section, we check that f_b obeys equation (3.46) — or equivalently (B.19). To begin, we note that it suffices to check (B.19) for the case where the intersections $X_b \cap S_i$ and $X_r \cap S_i$ look like one of the four basic pictures shown in Table 3.1 and Table 3.2. The reason that we only need to consider this case is that the constraint equations (3.36) that define f_b are *local*, so if (B.19) holds for basic pictures, then it automatically holds for general X_b, X_r.

Let's start with the simplest case: blue cylinder operators that create *unlinked* loops. In this case, the four basic pictures are those shown in Table 3.1. Specializing to these pictures, equation (B.19) reduces to $4^2 = 16$ different relations that we need to check. Many of these equations are redundant, so we only write the four independent ones below:

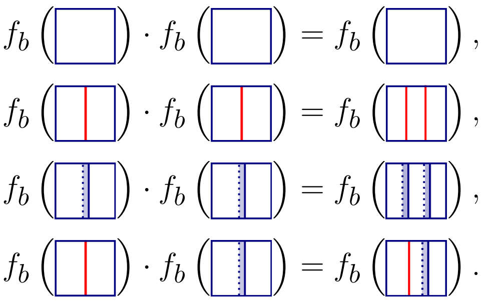

Next, we use the constraint equations (3.36) to reduce the pictures in the second and third lines to basic pictures:

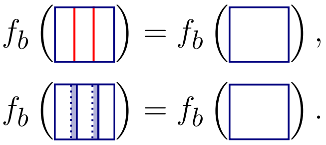

Putting this together, we have

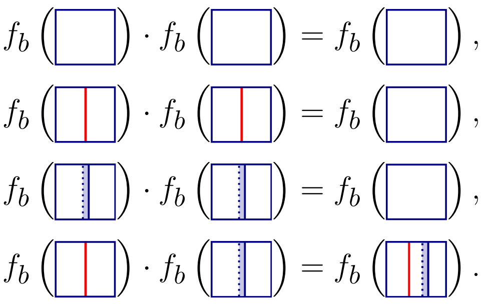

Letting

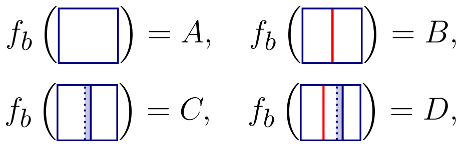

we can rewrite these equations as

$$
\begin{aligned}
A^2 &= A, \\
B^2 &= A, \\
C^2 &= A, \\
B \cdot C &= D. \qquad \text{(B.22)}
\end{aligned}
$$

Now let us compare with the values for A, B, C, D given in Table 3.1:

$$A = 1, \quad B = -e^{i\pi q_r}, \quad C = e^{i\pi q_b}, \quad D = -e^{i\pi(q_r + q_b)} \qquad \text{(B.23)}$$

where $q_b, q_r = 0$ or 1. First, we can see that the above expressions (B.23) do in fact obey equations (B.22). Thus, we have successfully verified (B.19) for the case of an unlinked blue cylinder operator. In fact, we can see that (B.23) is actually the most general possible solution to the equations (B.22). Thus, the above calculation can also be regarded as a derivation of Table 3.1.

Next, we consider the case of a blue cylinder operator linked with a red base loop. We proceed in exactly the same way as in the unlinked case. First, we note that equation (B.19) reduces to $4^2 = 16$ different relations, of which 4 are independent:

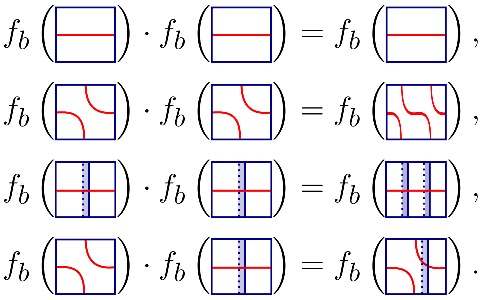

Next, we use the constraint equations (3.36) to derive:

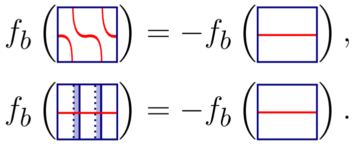

Putting this together gives

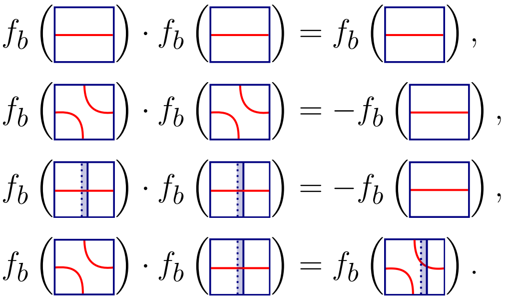

Letting

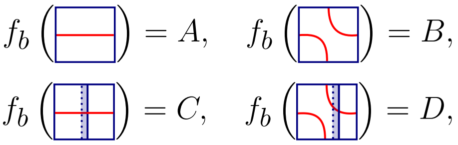

we arrive at the following algebraic equations:

$$\begin{aligned} A^2 &= A, \\ B^2 &= -A, \\ C^2 &= -A, \\ B \cdot C &= D. \end{aligned} \tag{B.24}$$

Let us compare with the values of A, B, C, D given in the top panel of Table 3.2:

$$A = 1, \quad B = i \cdot e^{i\pi q_r}, \quad C = i \cdot e^{i\pi q_b}, \quad D = -e^{i\pi(q_r+q_b)}. \tag{B.25}$$

Again, we can see that the above expressions (B.25) obey (B.24). Thus, we have proven equation (B.19) for the case of a blue cylinder operator linked to a red base loop. We can also see that the above expressions are the most general solutions to these equations. Thus, our calculation can also be thought of as a derivation of the top panel of Table 3.2.

Finally, we consider the case of a blue cylinder operator linked with a blue base loop. Proceeding in the same away, we set

$f_b\Big($ 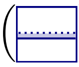 $\Big) = A,\quad f_b\Big($ 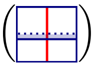 $\Big) = B,$

$f_b\Big($ 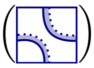 $\Big) = C,\quad f_b\Big($ 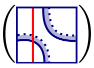 $\Big) = D.$

and we derive the algebraic equations

$$\begin{aligned} A^2 &= A, \\ B^2 &= A, \\ C^2 &= A, \\ B \cdot C &= D. \end{aligned} \tag{B.26}$$

Again, it is easy to check that the values of A, B, C, D given in the bottom panel of Table 3.2 obey equations (B.26). This establishes equation (B.19) for the case of a blue cylinder operator linked with a blue base loop.

APPENDIX C

APPENDICES FOR CHAPTER 4

C.1 Ground state degeneracy

In this section, we calculate the ground state degeneracy of the Hamiltonian H_1 on the 3D torus. We show tat the degeneracy on a 3D torus is $D = 1$.

Our calculation is based on the commuting projectors $B^1_c, B^1_{\hat{c}}$. Let us consider the product of these projectors over all cubes on a lattice. Since these operators have eigenvalues 0 and 1, this product will select out the states with eigenvalues $b^1_c = b^1_{\hat{c}} = 1$ for all c and $\hat{c}$. That is, it will select out the ground states. Hence the ground state degeneracy can be computed by taking the trace of the product of all the projectors:

$$D = Tr\left(\prod_c B^1_c \prod_{\hat{c}} B^1_{\hat{c}}\right). \tag{C.1}$$

Here the trace is over all states in the Hilbert space.

Plugging in the expressions for B^1_c and $B^1_{\hat{c}}$, we have

$$\begin{aligned} D &= \sum_X \langle X| \prod_c \frac{1+\tau^x_c f(c)}{2} \prod_{\hat{c}} \frac{1+\tau_{\hat{c}} f(\hat{c})}{2} |X\rangle \\ &= \frac{1}{2^{N_c} 2^{N_{\hat{c}}}} \sum_X \langle X|1|X\rangle = \frac{1}{2^{N_c} 2^{N_{\hat{c}}}} 2^{N_c N_{\hat{c}}} = 1. \end{aligned}$$

Here $f(c), f(\hat{c})$ denote the phase factors in (4.5), and $N_c, N_{\hat{c}}$ are the numbers of sites on the cubic lattice and the dual cubic lattice respectively. Since each $\tau^x_c, \tau^x_{\hat{c}}$ flips the spin state at site c, c', thus only contribution to the trace comes from the identity part in $B^1_c, B^1_{\hat{c}}$. As a result, we find the ground state degeneracy of H_1 on the 3D torus is 1. An identical computation applied H_0 (i.e. by setting the phase factors $f(c) = f(\hat{c}) = 1$) shows that the ground state degeneracy of H_0 on the 3D torus is 1 as well.

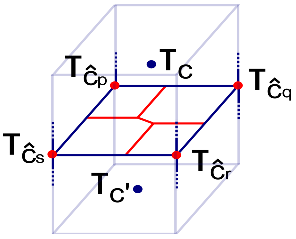

Figure C.1: The unitary operator U acts on pairs of adjacent blue spins $\tau_c, \tau_{c'}$ and four red spins $\tau_{\hat{c}_p}, \tau_{\hat{c}_q}, \tau_{\hat{c}_r}, \tau_{\hat{c}_s}$ at four corners of the plaquette shared by the cubes c, c'.

C.2 Showing that $|\Psi_1\rangle$ is short-range entangled

In this section, we show that $|\Psi_1\rangle$ and $|\Psi_0\rangle$ can be connected by a local unitary transformation. Since $|\Psi_0\rangle$ is short-range entangled, this implies that $|\Psi_1\rangle$ is short-range entangled as well.

Let us consider the unitary transformation

$$U = \prod_{\langle c,c'\rangle} \left(\frac{1-\tau_c^z\tau_{c'}^z}{2} U_{\langle \hat{c}_p\hat{c}_q\hat{c}_r\hat{c}_s\rangle} + \frac{1+\tau_c^z\tau_{c'}^z}{2}\right) \tag{C.2}$$

with

$$U_{\langle \hat{c}_p\hat{c}_q\hat{c}_r\hat{c}_s\rangle} = e^{i\frac{\pi}{24}\{3(\tau_{\hat{c}_p}+\tau_{\hat{c}_r})\tau_{\hat{c}_q}\tau_{\hat{c}_s} - \tau_{\hat{c}_p} - \tau_{\hat{c}_r} - 2\tau_{\hat{c}_q} - 2\tau_{\hat{c}_s}\}} \tag{C.3}$$

where the product runs over all pairs of nearest neighbor blue spins $\langle c, c'\rangle$ and $\langle \hat{c}_p\hat{c}_q\hat{c}_r\hat{c}_s\rangle$ are four red spins sitting on the four corners of blue plaquette shared by the cubes c, c' (see Fig. C.1). The unitary transformation U acts as $U_{\langle \hat{c}_p\hat{c}_q\hat{c}_r\hat{c}_s\rangle}$ when there is a blue domain wall between c, c' and acts as identity when there is no domain wall between them. Using this unitary transformation, one can show that

$$|\Psi_1\rangle = U|\Psi_0\rangle. \tag{C.4}$$

Since $|\Psi_0\rangle$ is a short-range entangled state and $|\Psi_1\rangle$ can be transformed into $|\Psi_0\rangle$ by the local unitary operator U, thus $|\Psi_1\rangle$ is short-range entangled as claimed.

C.3 Mapping between spin models and membrane models

In this section we establish the connection between the spin models H_0, H_1 and the membrane models constructed in chapter 3, which we denote by H_0^m, H_1^m. Via the mapping to the membrane models, we can obtain the braiding statistics of excitations in the gauged spin models easily by identifying the corresponding excitations between the membrane models and gauged spin models.

The basic idea of the mapping is to think of the domain walls for two types of spins as two kinds of membranes. More specifically, the mapping is defined by setting

$$\begin{aligned} \sigma_p^z &= \tau_c^z \mu_{cc'}^z \tau_{c'}^z, & \sigma_{\hat{p}}^z &= \tau_{\hat{c}}^z \mu_{\hat{c}\hat{c}'}^z \tau_{\hat{c}'}^z, \\ \sigma_p^x &= \mu_{cc'}^x, & \sigma_{\hat{p}}^x &= \mu_{\hat{c}\hat{c}'}^x. \end{aligned} \tag{C.5}$$

Here p is the plaquette separating the cubes c, c' and $\hat{p}$ is the plaquette separating the cubes $\hat{c}, \hat{c}'$. Substituting these expressions into $\tilde{H}_0, \tilde{H}_1$ and making use of the gauge invariance constraint (4.19), the result is exactly the two membrane models constructed in chapter 3, which we call them H_0^m, H_1^m. Both of the two membrane models are built out of two kinds of spins $\sigma_p, \sigma_{\hat{p}}$ sitting on the plaquettes p of the cubic lattice and the plaquettes $\hat{p}$ of the dual cubic lattice respectively. The Hamiltonian for the first membrane model H_0^m is

$$H_0^m = -\sum_l A_l - \sum_{\hat{l}} A_l - \sum_c B_c^{m0} - \sum_{\hat{c}} B_{\hat{c}}^{m0} \tag{C.6}$$

with

$$A_l = \frac{1}{2}(1 + \prod_{p \in l} \sigma_p^z), \quad A_{\hat{l}} = \frac{1}{2}(1 + \prod_{\hat{p} \in \hat{l}} \sigma_{\hat{p}}^z) \tag{C.7}$$

where these products run over the 4 plaquettes adjacent to the links $l, \hat{l}$ respectively and

$$B_c^{m0} = \frac{1}{2}(1 + \prod_{p \in c} \sigma_p^x), \quad B_{\hat{c}}^{m0} = \frac{1}{2}(1 + \prod_{\hat{p} \in \hat{c}} \sigma_{\hat{p}}^x) \tag{C.8}$$

where these products run over the 6 plaquettes adjacent to the cubes $c, \hat{c}$ respectively. The Hamiltonian for the second membrane model H_1^m is

$$H_1^m = -\sum_l A_l - \sum_{\hat{l}} A_{\hat{l}} - \sum_c B_c^{m1} - \sum_{\hat{c}} B_{\hat{c}}^{m1}. \tag{C.9}$$

The first two terms are defined as above while the last two terms are defined as

$$B_c^{m1} = \frac{1}{2}(1 + \mathcal{B}_c^1) \cdot P_c, \quad B_{\hat{c}}^{m1} = \frac{1}{2}(1 + \mathcal{B}_{\hat{c}}^1) \cdot P_{\hat{c}}. \tag{C.10}$$

Here $P_c, P_{\hat{c}}$ are projectors that projects to the states with the closed membrane constraint in the neighborhood of the cubes $c, \hat{c}$ respectively. More precisely,

$$P_c = \prod_{l \in c} A_l \cdot \prod_{\hat{l} \perp c} A_{\hat{l}}$$

where the first product runs over the 12 edges l of the cube c and the second product runs over the 6 edges $\hat{l}$ that are perpendicular to the 6 plaquettes of the cube c. Similarly,

$$P_{\hat{c}} = \prod_{\hat{l} \in \hat{c}} A_{\hat{l}} \cdot \prod_{l \perp \hat{c}} A_l.$$

The $\mathcal{B}_c^1$ and $\mathcal{B}_{\hat{c}}^1$ operators are

$$\mathcal{B}_c^1 = \prod_{p \in c} \sigma_p^x \cdot (-1)^{m_c'} \cdot i^{n_c'},$$

$$\mathcal{B}_{\hat{c}}^1 = \prod_{\hat{p} \in \hat{c}} \sigma_{\hat{p}}^x \cdot (-1)^{m_{\hat{c}}'} \cdot i^{n_{\hat{c}}'}$$

with

$$
\begin{aligned}
m'_c &= f(\sigma^z_{\hat{p}_1}, \sigma^z_{\hat{p}_2}, \dots, \sigma^z_{\hat{p}_{12}}),\\
m'_{\hat{c}} &= f(\sigma^z_{p_1}, \sigma_{p^z_2}, \dots, \sigma^z_{p_{12}}),\\
n'_c &= g(\{\sigma^z_p\}, \{\sigma^z_{\hat{p}}\}),\\
n'_{\hat{c}} &= g(\{\sigma^z_{\hat{p}}\}, \{\sigma^z_p\})
\end{aligned}
$$

where the functions f and g are defined in section 4.2.3

In fact, one can also map the ungauged models H_0, H_1 onto the restricted membrane models by simply identifying the domain walls as membranes

$$
\sigma^z_p = \tau^z_c \tau^z_{c'}, \quad \sigma^z_{\hat{p}} = \tau^z_{\hat{c}} \tau^z_{\hat{c}'} \tag{C.11}
$$

with the restriction that the membranes are closed surfaces, that is, they satisfy the conditions on every link l and $\hat{l}$

$$
A_l = A_{\hat{l}} = 1.
$$

Accordingly, the restricted dual membrane models which we call $H^{m'}_0, H^{m'}_1$ are

$$
\begin{aligned}
H^{m'}_0 &= -\sum_c B^{m0}_c - \sum_{\hat{c}} B^{m0}_{\hat{c}},\\
H^{m'}_1 &= -\sum_c B^{m1'}_c - \sum_{\hat{c}} B^{m1'}_{\hat{c}}
\end{aligned} \tag{C.12}
$$

with

$$
B^{m1'}_c = \frac{1}{2}(1 + \mathcal{B}^1_c), \quad B^{m1'}_{\hat{c}} = \frac{1}{2}(1 + \mathcal{B}^1_{\hat{c}}). \tag{C.13}
$$

These Hamiltonian are defined on the Hilbert space with closed membrane states.

Since the mappings are local transformations and can be thought of equivalence relation between quantum systems. Thus the gauged spin models $\tilde{H}_0, \tilde{H}_1$ are physically identical to the unrestricted membrane models H_0^m, H_1^m (the Hilbert space consists of closed and open membranes) while the ungauged spin models H_0, H_1 are physically identical to the restricted membrane models $H_0^{m'}, H_1^{m'}$ (the Hilbert space consists of only closed membranes).

The mappings are the generalization of well-known relation between 2D Ising model and 2D $\mathbb{Z}_2$ gauge theory. Here the restricted membrane models $H_0^{m'}, H_1^{m'}$ can be thought of a standard $\mathbb{Z}_2 \times \mathbb{Z}_2$ gauge theory Hamiltonian (in the zero coupling limit where the electric field terms $\sum_p \sigma_p^z, \sum_{\hat{p}} \sigma_{\hat{p}}^z$ are absent) and a twisted $\mathbb{Z}_2 \times \mathbb{Z}_2$ gauge theory Hamiltonian in 3D respectively. Thus the relation between H_0, H_1 and $H_0^{m'}, H_1^{m'}$ is a duality between two types of 3D $\mathbb{Z}_2 \times \mathbb{Z}_2$ paramagnets and two types of 3D $\mathbb{Z}_2 \times \mathbb{Z}_2$ gauge theories. On the other hand, the unrestricted membrane models H_0^m, H_1^m can be thought of two types of $\mathbb{Z}_2 \times \mathbb{Z}_2$ gauge theories coupled to a conventional $\mathbb{Z}_2 \times \mathbb{Z}_2$ paramagnet while the gauged spin models $\tilde{H}_0, \tilde{H}_1$ are two types of $\mathbb{Z}_2 \times \mathbb{Z}_2$ paramagnets coupled to a standard $\mathbb{Z}_2 \times \mathbb{Z}_2$ gauge field. Hence, the relation between $\tilde{H}_0, \tilde{H}_1$ and H_0^m, H_1^m is the self-duality of a 3D $\mathbb{Z}_2 \times \mathbb{Z}_2$ gauge theory coupled to $\mathbb{Z}_2 \times \mathbb{Z}_2$ symmetric matter.

One may also expect the dualities can be generalized to any finite unitary symmetry group G in 3D. That is, each 3D SPT phase with symmetry group G is dual to a corresponding gauge theory with gauge group G in 3D.

REFERENCES

[1] Y. Aharonov and D. Bohm. Significance of electromagnetic potentials in the quantum theory. *Phys. Rev.*, 115:485, 1959.

[2] M. G. Alford, K.-M. Lee, J. March-Russell, and J. Preskill. Quantum field theory of non-abelian strings and vortices. *Nucl. Phys. B*, 384:251, 1992.

[3] M. G. Alford and F. Wilczek. Aharonov-bohm interaction of cosmic strings with matter. *Phys. Rev. Lett*, 62:1071, 1989.

[4] C. Aneziris, A. P. Balachandran, L. Kauffman, and A. M. Srivastava. Local discrete symmetry and quantum-mechanical hair. *Int. J. Mod. Phys. A*, 06:2519, 1991.

[5] Daniel Arovas, J. R. Schrieffer, and Frank Wilczek. Fractional statistics and the quantum hall effect. *Phys. Rev. Lett.*, 53:722–723, Aug 1984.

[6] J. C. Baez, D. K. Wise, and A. S. Crans. Quantum field theory of non-abelian strings and vortices. *Adv. Theor. Math. Phys.*, 11:707, 2007.

[7] L. Balents, M. P. A. Fisher, and S. M. Girvin. Fractionalization in an easy-axis kagome antiferromagnet. *Phys. Rev. B*, 65:224412, 2002.

[8] T. Banks, R. Myerson, and John Kogut. Phase transitions in abelian lattice gauge theories. *Nucl. Phys. B*, 129:493, 1977.

[9] B. Andrei Bernevig, Taylor L. Hughes, and Shou-Cheng Zhang. Quantum spin hall effect and topological phase transition in hgte quantum wells. *Science*, 314(5806):1757–1761, 2006.

[10] B. Andrei Bernevig and Shou-Cheng Zhang. Quantum spin hall effect. *Phys. Rev. Lett.*, 96:106802, 2006.

[11] B. Blok and Xiao-Gang Wen. Effective theories of the fractional quantum hall effect: Hierarchy construction. *Phys. Rev. B*, 42:8145, 1990.

[12] Parsa Hassan Bonderson. *Non-abelian anyons and interferometry.* PhD thesis, California Institute of Technology, 2007.

[13] Oliver Buerschaper and Miguel Aguado. Mapping kitaev's quantum double lattice models to levin and wen's string-net models. *Phys. Rev. B*, 80:155136, 2009.

[14] Oliver Buerschaper, Miguel Aguado, and Guifré Vidal. Explicit tensor network representation for the ground states of string-net models. *Phys. Rev. B*, 79:085119, Feb 2009.

[15] Claudio Castelnovo and Claudio Chamon. Entanglement and topological entropy of the toric code at finite temperature. *Phys. Rev. B*, 76:184442, 2007.

[16] Xie Chen, Fiona J. Burnell, Ashvin Vishwanath, and Lukasz Fidkowski. Anomalous symmetry fractionalization and surface topological order. *arxiv:1403.6491*, 2015.

[17] Xie Chen, Zheng-Cheng Gu, Zheng-Xin Liu, and Xiao-Gang Wen. Symmetry-protected topological orders and the cohomology class of their symmetry group. *Phys. Rev. B*, 87:155114, 2013.

[18] Xie Chen, Zheng-Cheng Gu, and Xiao-Gang Wen. Local unitary transformation, long-range quantum entanglement, wave function renormalization, and topological order. *Phys. Rev. B*, 82:155138, 2010.

[19] Xie Chen, Zheng-Cheng Gu, and Xiao-Gang Wen. Classification of gapped symmetric phases in one-dimensional spin systems. *Phys. Rev. B*, 83:035107, 2011.

[20] Xie Chen, Zheng-Cheng Gu, and Xiao-Gang Wen. Complete classification of one-dimensional gapped quantum phases in interacting spin systems. *Phys. Rev. B*, 84:235128, 2011.

[21] Xie Chen, Zheng-Xin Liu, and Xiao-Gang Wen. Two-dimensional symmetry-protected topological orders and their protected gapless edge excitations. *Phys. Rev. B*, 84:235141, 2011.

[22] Xie Chen, Yuan-Ming Lu, and Ashvin Vishwanath. Symmetry-protected topological phases from decorated domain walls. *Nature Communications*, 5:3507, 2014.

[23] Robbert Dijkgraaf and Edward Witten. Topological gauge theories and group cohomology. *Comm. Math. Phys.*, 129:393, 1990.

[24] T. Einarsson. Fractional statistics on a torus. *Phys. Rev. Lett.*, 64:1995, 1990.

[25] Lukasz Fidkowski, Xie Chen, and Ashvin Vishwanath. Non-abelian topological order on the surface of a 3d topological superconductor from an exactly solved model. *Phys. Rev. X*, 3:041016, 2013.

[26] Lukasz Fidkowski and Alexei Kitaev. Effects of interactions on the topological classification of free fermion systems. *Phys. Rev. B*, 81:134509, 2010.

[27] Lukasz Fidkowski and Alexei Kitaev. Topological phases of fermions in one dimension. *Phys. Rev. B*, 83:075103, 2011.

[28] Liang Fu and C. L. Kane. Topological insulators with inversion symmetry. *Phys. Rev. B*, 76(4):045302, 2007.

[29] Liang Fu, C. L. Kane, and E. J. Mele. Topological insulators in three dimensions. *Phys. Rev. Lett.*, 98(10):106803, 2007.

[30] Jurgen Fuchs, Christoph Schweigert, and Alessandro Valentino. Bicategories for boundary conditions and for surface defects in 3-d tft. *arXiv:1203.4568*, 2012.

[31] Zheng-Cheng Gu, Zhenghan Wang, and Xiao-Gang Wen. A classification of 2d fermionic and bosonic topological orders. *arXiv:1010.1517*, 2010.

[32] Zheng-Cheng Gu and Xiao-Gang Wen. Tensor-entanglement-filtering renormalization approach and symmetry protected topological order. *Phys. Rev. B*, 80:155131, 2009.

[33] Jeongwan Haah. Local stabilizer codes in three dimensions without string logical operators. *Phys. Rev. A*, 83:042330, 2011.

[34] F. D. M. Haldane. Nonlinear field theory of large-spin heisenberg antiferromagnets: Semiclassically quantized solitons of the one-dimensional easy-axis néel state. *Phys. Rev. Lett.*, 50:1153–1156, Apr 1983.

[35] Alioscia Hamma, Paolo Zanardi, and Xiao-Gang Wen. String and membrane condensation on 3d lattices. *Phys. Rev. B*, 72:035307, 2005.

[36] M. Z. Hasan and C. L. Kane. Topological insulators. *Rev. Mod. Phys.*, 82:3045, 2010.

[37] David Hsieh, Dong Qian, Andrew L. Wray, Yuqi Xia, Yusan Hor, Robert Cava, and M. Zahid Hasan. A topological dirac insulator in a quantum spin hall phase. *Nature Letters*, 524:970, 2008.

[38] Yuting Hu, Yidun Wan, and Yong-Shi Wu. Twisted quantum double model of topological phases in two–dimension. *Phys. Rev. B*, 87:125114, 2013.

[39] Ling-Yan Hung and Yidun Wan. String-net models with z_n fusion algebra. *Phys. Rev. B*, 86:235132, 2012.

[40] Chao-Ming Jian and Xiao-Liang Qi. Layer construction of 3d topological states and string braiding statistics. *Phys. Rev. X*, 4:041043, 2014.

[41] Shenghan Jiang, Andrej Mesaros, and Ying Ran. Generalized modular transformations in (3+1)d topologically ordered phases and triple linking invariant of loop braiding. *Phys. Rev. X*, 4:031048, 2014.

[42] C. L. Kane and Matthew P. A. Fisher. Quantized thermal transport in the fractional quantum hall effect. *Phys. Rev. B*, 55:15832, 1997.

[43] C. L. Kane and E. J. Mele. $\mathbb{Z}_2$ topological order and the quantum spin hall effect. *Phys. Rev. Lett.*, 95:146802, 2005.

[44] C. L. Kane and E. J. Mele. Quantum spin hall effect in graphene. *Phys. Rev. Lett.*, 95(22):226801, 2005.

[45] Anton Kapustin and Natalia Saulina. Topological boundary conditions in abelian chern-simons theory. *Nucl. Phys. B*, 845:393, 2011.

[46] Alexei Kitaev. Fault-tolerant quantum computation by anyons. *Annals of Physics*, 303:2–30, 2003.

[47] Alexei Kitaev. Anyons in an exactly solved model and beyond. *Ann. Phys.*, 321:2, 2006.

[48] Alexei Kitaev and Liang Kong. Models for gapped boundaries and domain walls. *Commun. Math. Phys.*, 313:351, 2012.

[49] John Kogut and Leonard Susskind. Hamiltonian formulation of wilson's lattice gauge theories. *Phys. Rev. D*, 11:395, 1975.

[50] John B. Kogut. An introduction to lattice gauge theory and spin systems. *Rev. Mod. Phys.*, 51:659, 1979.

[51] Liang Kong. A mathematical theory of anyon condensation. *arXiv:1307.8244*, 2013.

[52] Liang Kong. Some universal properties of levin-wen models. In *Proceedings of XVIITH International Congress of Mathematical Physics*, page 444, 2014.

[53] Markus Konig, Steffen Wiedmann, Christoph Brune, Andreas Roth, Hartmut Buhmann, Laurens W. Molenkamp, Xiao-Liang Qi, and Shou-Cheng Zhang. Quantum spin hall insulator state in hgte quantum wells. *Science*, 318(5851):766–770, 2007.

[54] Su-Peng Kou, Michael Levin, and Xiao-Gang Wen. Mutual chern-simons theory for z_2 topological order. *Phys. Rev. B*, 78:155134, 2008.

[55] Lawrence M. Krauss and Frank Wilczek. Discrete gauge symmetry in continuum theories. *Phys. Rev. Lett.*, 62:1221, 1989.

[56] Tian Lan and Xiao-Gang Wen. Topological quasiparticles and the holographic bulk-edge relation in 2+1d string-net models. *arXiv:1311.1784*, 2013.

[57] L. Landau. On the theory of phase transitions. *Zh. Eksp. Teor. Fiz*, 7:19, 1937.

[58] R. B. Laughlin. Anomalous quantum hall effect: an incompressible quantum fluid with fractionally charged excitations. *Phys. Rev. Lett.*, 50:1395, 1983.

[59] J.M. Leinaas and J. Myrheim. On the theory of identical particles. *Il Nuovo Cimento B (1971-1996)*, 37(1):1–23, 1977.

[60] Michael Levin. Protected edge modes without symmetry. *Phys. Rev. X*, 3:021009, 2013.

[61] Michael Levin, F. J. Burnell, Maciej Koch-Janusz, and Ady Stern. Exactly soluble models for fractional topological insulators in 2 and 3 dimensions. *Phys. Rev. B*, 84:235145, 2011.

[62] Michael Levin and Zheng-Cheng Gu. Braiding statistics approach to symmetry-protected topological phases. *Phys. Rev. B*, 86:115109, 2012.

[63] Michael Levin and Xiao-Gang Wen. Fermions, strings, and gauge fields in lattice spin models. *Phys. Rev. B*, 67:245316, 2003.

[64] Michael Levin and Xiao-Gang Wen. Detecting topological order in a ground state wave function. *Phys. Rev. Lett.*, 96:110405, 2006.

[65] Michael A. Levin and Xiao-Gang Wen. String-net condensation: A physical mechanism for topological phases. *Phys. Rev. B*, 71:045110, 2005.

[66] Chien-Hung Lin and Michael Levin. Generalizations and limitations of string-net models. *Phys. Rev. B*, 89:195130, May 2014.

[67] Chien-Hung Lin and Michael Levin. Loop braiding statistics in exactly soluble three-dimensional lattice models. *Phys. Rev. B*, 92:035115, Jul 2015.

[68] Andrej Mesaros and Ying Ran. A classification of symmetry enriched topological phases with exactly solvable models. *Phys. Rev. B*, 87:155115, 2013.

[69] Max A. Metlitski, Lukasz Fidkowski, Xie Chen, and Ashvin Vishwanath. Interaction effects on 3d topological superconductors: surface topological order from vortex condensation, the 16 fold way and fermionic kramers doublets. *arXiv:1406.3032*, 2014.

[70] Gregory Moore and Nathan Seiberg. Classical and quantum conformal field theory. *Communications in Mathematical Physics*, 123:177, 1989.

[71] J. E. Moore and L. Balents. Topological invariants of time-reversal-invariant band structures. *Phys. Rev. B*, 75(12):121306, 2007.

[72] Frank Pollmann, Erez Berg, Ari M. Turner, and Masaki Oshikawa. Entanglement spectrum of a topological phase in one dimension. *Phys. Rev. B*, 81:064439, 2010.

[73] Frank Pollmann, Erez Berg, Ari M. Turner, and Masaki Oshikawa. Symmetry protection of topological phases in one-dimensional quantum spin systems. *Phys. Rev. B*, 85:075125, 2012.

[74] Frank Pollmann, Ari M. Turner, Erez Berg, and Masaki Oshikawa. Entanglement spectrum of a topological phase in one dimension. *Phys. Rev. B*, 81:064439, 2010.

[75] J. Preskill and L. M. Krauss. Local discrete symmetry and quantum-mechanical hair. *Nucl. Phys. B*, 341:50, 1990.

[76] Mark de Wild Propitius. *Topological interactions in broken gauge theories*. PhD thesis, University of Amsterdam, 1995.

[77] Xiao-Liang Qi and Shou-Cheng Zhang. Topological insulators and superconductors. *Rev. Mod. Phys.*, 83:1057, 2011.

[78] N. Read and Dmitry Green. Paired states of fermions in two dimensions with breaking of parity and time-reversal symmetries and the fractional quantum hall effect. *Phys. Rev. B*, 61:10267, 2000.

[79] Rahul Roy. Topological phases and the quantum spin hall effect in three dimensions. *Phys. Rev. B*, 79(19):195322, 2009.

[80] Shinsei Ryu. Three-dimensional topological phase on the diamond lattice. *Phys. Rev. B*, 79:075124, Feb 2009.

[81] Norbert Schuch, David Perez-Garcia, and Ignacio Cirac. Classifying quantum phases using matrix product states and projected entangled pair states. *Phys. Rev. B*, 84:165139, 2011.

[82] D. C. Tsui, H. L. Stormer, and A. C. Gossard. Two-dimensional magnetotransport in the extreme quantum limit. *Phys. Rev. Lett.*, 48:1559, 1982.

[83] Yidun Wan, Juven Wang, and Huan He. Twisted gauge theory model of topological phases in three dimensions. *arxiv:1409.3216*, 2014.

[84] Chenjie Wang and Michael Levin. Weak symmetry breaking in two dimensional topological insulators. *Phys. Rev. B*, 88:245136, 2013.

[85] Chenjie Wang and Michael Levin. Braiding statistics of loop excitations in three dimensions. *Phys. Rev. Lett.*, 113:080403, 2014.

[86] Chenjie Wang and Michael Levin. Topological invariants for gauge theories and symmetry-protected topological phases. *arxiv:1412.1781*, 2014.

[87] Chong Wang and T. Senthil. Interacting fermionic topological insulators/superconductors in three dimensions. *Phys. Rev. B*, 89:195124, 2014.

[88] Juven Wang and Xiao-Gang Wen. Non-abelian string and particle braiding in topological order: Modular sl(3,z) representation and 3+1d twisted gauge theory. *arXiv:1404.7854*, 2014.

[89] X. G. Wen and A. Zee. Classification of abelian quantum hall states and matrix formulation of topological fluids. *Phys. Rev. B*, 46(4):2290–2301, 1992.

[90] Xiao-Gang Wen. Topological orders in rigid states. *International Journal of Modern Physics B*, 04(02):239–271, 1990.

[91] Xiao-Gang Wen. Theory of the edge states in fractional quantum hall effects. *International Journal of Modern Physics B*, 06(10):1711–1762, 1992.

[92] Xiao-Gang Wen. Topological orders and edge excitations in fqh states. *Advances in Physics*, 44:405, 1995.

[93] Xiao-Gang Wen. Topological orders and edge excitations in fractional quantum hall states. *Adv. Phys.*, 44:405, 1995.

[94] Xiao-Gang Wen. *Quantum Field Theory of Many-body Systems: From the Origin of Sound to an Origin of Light and Electrons*. Oxford University Press, 2007.

[95] Xiao-Gang Wen and Q. Niu. Ground-state degeneracy of the fractional quantum hall states in the presence of a random potential and on high-genus riemann surfaces. *Phys. Rev. B*, 41:9377, 1990.

[96] Frank Wilczek. Quantum mechanics of fractional-spin particles. *Phys. Rev. Lett.*, 49:957–959, Oct 1982.

[97] Simeng Yan, David A. Huse, and Steven R. White. Spin-liquid ground state of the s = 1/2 kagome heisenberg antiferromagnet. *Science*, 332(6034):1173–1176, 2011.

[98] Bei Zeng and Xiao-Gang Wen. Stochastic local transformations, emergence of unitarity, long-range entanglement, gapped quantum liquids, and topological order. *arxiv:1406.5090*, 2014.